THESIS

# COMPOSITION AND FABRIC OF THE KUPFERSCHIEFER, SANGERHAUSEN BASIN, GERMANY AND A COMPARISON TO THE KUPFERSCHIEFER IN THE LUBIN MINING DISTRICT, POLAND

Submitted by

Brianna E. Lyons

Department of Geosciences

In partial fulfillment of the requirements

For the Degree of Master of Science

Colorado State University

Fort Collins, Colorado

Fall 2013

Master's Committee:

Advisor: Sally Sutton

John Ridley
Thomas Sale

ABSTRACT

COMPOSITION AND FABRIC OF THE KUPFERSCHIEFER, SANGERHAUSEN BASIN, GERMANY AND A COMPARISON TO THE KUPFERSCHIEFER IN THE LUBIN MINING DISTRICT, POLAND

The Kupferschiefer, or "copper shale," is a thin carbonaceous marly shale deposited during the Late Permian within the Zechstein Basin of central Europe. A classic example of a sediment hosted stratiform copper deposit, the Kupferschiefer is mineralized with Cu and other metals of economic interest such as Pb, Zn, and Ag. The unit is overlain by the Zechstein Limestone and underlain by the Weissliegend sandstone; it is most well known in Germany and Poland. Overall, the Kupferschiefer in the Sangerhausen Basin in Germany has been less studied than its counterpart in the Lubin mining district in Poland. Some previous studies compare the Kupferschiefer from the Lubin mining district, and more rarely the Sangerhausen Basin, to other stratiform copper deposits, but few compare data from both locations.

This study analyzes, compares, and contrasts geochemical, mineralogical, and petrologic data from five Sangerhausen Basin locations and four locations in the Lubin and Rudna mines of the Lubin mining district. A total of 101 samples were examined: 61 Sangerhausen samples (41 from above the Kupferschiefer-Weissliegend contact, and 20 from below the contact) and 41 Lubin mining district samples (28 from above the Kupferschiefer-Weissliegend contact, and 13 from below the contact). Of these, 62 (36 Sangerhausen and 26 Lubin mining district) were geochemically analyzed, and 65 samples were observed in thin section (35 Sangerhausen, 30 Lubin mining district).

The Sangerhausen Basin Kupferschiefer exhibits textural, geochemical, and mineralization characteristics broadly similar to those of the Lubin mining district Kupferschiefer, with a few distinct differences. Sulfide mineralization, in the form of disseminated spherules, blebs, aggregates, framboids, and bedding-parallel and -perpendicular veins, is observed in both locations on macro- and microscopic

scales. The most abundant sulfide in mineralized samples from both locations is chalcocite, followed by chalcopyrite. Sulfide mineralization is commonly associated with the presence of quartz and carbonate veins in Lubin mining district samples, while mineralization is rarely associated with these veins in Sangerhausen Basin samples. Fluorescence from hydrocarbons is observed in association with sulfide mineralization in some samples, and is generally more common in samples from the Sangerhausen Basin than in those from the Lubin mining district. Both locations show similar geochemical trends with stratigraphic depth, as the units transition from Weissliegend to Kupferschiefer to Zechstein Limestone. The Sangerhausen Basin Kupferschiefer exhibits $P_2O_5$ enrichment (averaging 0.26 wt.%) compared to Lubin mining district Kupferschiefer and average shale $P_2O_5$ values (averaging 0.13 wt.% and 0.16 wt.%, respectively). Copper concentrations are greater in samples from the Lubin mining district (~14 wt.% max, most samples above ~1 to 2 wt.%) compared to Sangerhausen samples (~10 wt.% max, most samples below 0.5 wt.%). The lower ~25 cm of the Kupferschiefer is enriched in ore metals (Cu, Ag, Pb, Zn, and U) in both locations, and in the Sangerhausen Basin, in middle rare earth elements (REEs) as well. This suggests that the reactions resulting from interaction between fluids migrating from the underlying Weissliegend and overlying Zechstein evaporates mostly occurred in the lower 20 cm of the Kupferschiefer. Assuming that the REEs were carried in the mineralizing fluids, the differences in REE patterns from Sangerhausen samples taken 7 and 8 cm above the basal contact of the Kupferschiefer suggest that even within a single basin the reactions resulting from fluid interaction did not occur at the same stratigraphic level at all locations.

The strata-form nature of the deposit suggests large scale bedding-parallel fluid flow. On a smaller scale, the orientation of sulfide, quartz, and carbonate veins and of elongated sulfide macro-blebs suggests that the local, small-scale flow direction is preferentially bedding-parallel as well, especially in the lower 20 to 30 cm of the Kupferschiefer where the matrix is primarily composed of alternating lenses of carbon- and clay-rich pods, and carbonate-rich pods. However, the presence of bedding-perpendicular sulfide blebs and carbonate and quartz veins illustrate that flow was not exclusively bedding-parallel. The Lubin mining district probably experienced at least two pulses of fluid flow, as illustrated by the presence

of veins that exhibit alternating carbonate and sulfide precipitation; similar characteristics were not observed in the Sangerhausen Basin samples. The presence of both yellow and blue fluorescence of bitumen in Sangerhausen samples, however, suggests that there were at least two pulses of hydrocarbon migration. The generally well-sorted Lubin mining district Weissliegend was more permeable than the poorly-sorted Sangerhausen Basin Weissliegend.

TABLE OF CONTENTS

# ACKNOWLEDGEMENTS

The completion of this masters thesis would not have been possible without my committee: Drs. Sally Sutton, John Ridley, and Thomas Sale. I am especially grateful to Sally for her patience and expertise as she kept me on track through the science and writing process, and to John for all of his assistance with the reflective and fluorescent microscopy work.

Thank you to Carl-Heinz Friedel at Sachsen-Anhalt Landesmat für Geologie und Bergwessen for providing the Sangerhausen Basin core samples; to Sabine Walther at Martin Luther University in Halle, Germany, for providing access to the Wettelrode mine; and to Zbigniew Sawłowicz for providing access to the Lubin and Rudna mines.

I would like to thank the Colorado State University Geosciences department and the Joby Adams Geosciences Graduate scholarship for helping to fund my masters thesis. To Sharyl Pierson and Sharon Gale, I would like to thank each of you for your assistance with navigating the department, and for the casual chats that made even the most hectic of days easier to get through.

I cannot express my gratitude to John Matthews (my grandfather), William Santoro, and Dr. John Madsen for initiating, sustaining, and finally cementing my love of science- and especially geology. And to my professors at the University of Delaware and Colorado State University for passing on their knowledge and love of the geosciences, in particular Drs. Ron Martin, Art Trembanis, Sue McGeary, Jim Pizzuto, Beth Weinman and Kyungsoo Yoo; and Drs. Sally Sutton, John Ridley, Sara Rathburn, Sven Egenhoff, and Kaleb Scarberry.

To my fellow CSU grads: Anne Ji, Max Jackl, Chris Hanratty, Ian Hogan, Richard Zaggle, and Nathan Marolf, quite simply: I could not have asked for better officemates.

Last but never least, thank you to the people who have helped me to grow into the person I am today; my family for your unending love and support: Mom, Dad, Kristin Emily, and Gma. My patient and loving boyfriend, Matt Hergett. My geology sisters, Kelsey Lanan and Katy Ames ("What the heck, rocks? Tell me your secrets!"). And my best non-rock friends, Deana LaRocco and Emily Manz.

LIST OF TABLES

LIST OF FIGURES

Chapter 5

# CHAPTER 1 - INTRODUCTION

## 1.1 Kupferschiefer: "Copper Shale"

The Kupferschiefer is a thin marly shale, typically ≤1 meter thick, and a classic example of a sediment hosted stratiform copper deposit. Deposited during the Late Permian within the Zechstein Basin of central Europe, it marks the transition between the continental Rotliegend unit and the marine Zechstein cycles.

The Kupferschiefer is mineralized with copper and other metals of economic interest such as Pb, Zn, Ag, V, Se, Au, Mo, Ni, Re, Ge, and Cd. Other elements of economic interest that have been recorded in the Kupferschiefer include: platinum group elements, U, As, Sb, Bi, Se, and Tl (Vaughan *et al*., 1989). The unit is most well known for its presence in Germany and Poland, though it extends as far west as England, north into the Netherlands, and as far east as Belarus. The unit was mined for copper from the medieval times until 1990 in the Sangerhausen Basin of Germany, and has been mined in the Lubin mining district of southwestern Poland since the second half of the 1900s.

## 1.2 Purpose of this Masters Thesis

The broad purpose of this master's study is to increase the available knowledge of the lithology, geochemistry, and mineralization of the Kupferschiefer within the Sangerhausen Basin in Germany, since this area has been given much less attention than the Lubin mining district in Poland. The Sangerhausen Kupferschiefer is also of interest because of its unique levels of sulfide mineralization; while it does not contain abundant ore-grade sulfides, it is still mineralized above the levels of an "average" black shale. Many of the previous studies on the Kupferschiefer focus on the types and abundances of sulfide mineralization, gold and platinum group elements, and organic carbon content. These studies occasionally compare the Kupferschiefer from the Lubin mining district, and more rarely the Sangerhausen Basin, to other units, but few compare data from both locations. Differences between the Sangerhausen Kupferschiefer and Weissliegend units and the Lubin mining district units could have important implications for the composition, flow rate, and flow path of the fluid(s) responsible for the

sulfide precipitation. Disparities in the bulk and trace geochemistry of samples from both basins could point to differences in the local depositional environment. This study aims to relate geochemistry to texture, note observable relationships between texture and mineralization, and compare and contrast data from five Sangerhausen Basin locations and four locations in the Lubin and Rudna mines. The data collected in this study will also be compared with previously published Kupferschiefer data.

### 1.3 Objectives

The goals of this masters thesis are as follows:

a) characterize the form and composition of sulfide minerals, on both macro- and microscopic scales, in Kupferschiefer samples from the Sangerhausen Basin ore zone

b) compare Sangerhausen Basin petrographic and mineralogical data to Lubin mining district data

c) examine and describe the geochemical characteristics of the Sangerhausen Basin; compare to the geochemistry of the Lubin mining district and previous studies

d) determine the relative proximity of the Sangerhausen Basin and Lubin mining district Kupferschiefer to the oxidized, barren zone ("Rote Fäule") that is closely associated with the copper-sulfide deposits

e) identify possible geochemical or petrographic indications of fluid flow through the unit and suggest the extent of reactions resulting from migration and interaction of fluids

# CHAPTER 2 - BACKGROUND

## 2.1 Kupferschiefer and Rotliegend/Zechstein Stratigraphy

The Kupferschiefer mineralization is a classic example of a sediment-hosted stratiform copper deposit. The shale is an Upper Permian black, organic-rich, fine-grained, and finely laminated (clayey) marl unit of marine origin (Jung and Knitzscheke, 1976; Vaughan *et al.*, 1989; Pancost *et al.*, 2002; Krouse *et al.*, 2006; Symons *et al.*, 2011). The unit reaches approximately 1,500 km across north-central Europe, covering an estimated 600,000 $km^2$ (Paul, 1982) from the North Sea coast of England and Northern Ireland, northeast across the Netherlands into Belarus, and south into southern Germany and Poland (Figure 2.1).

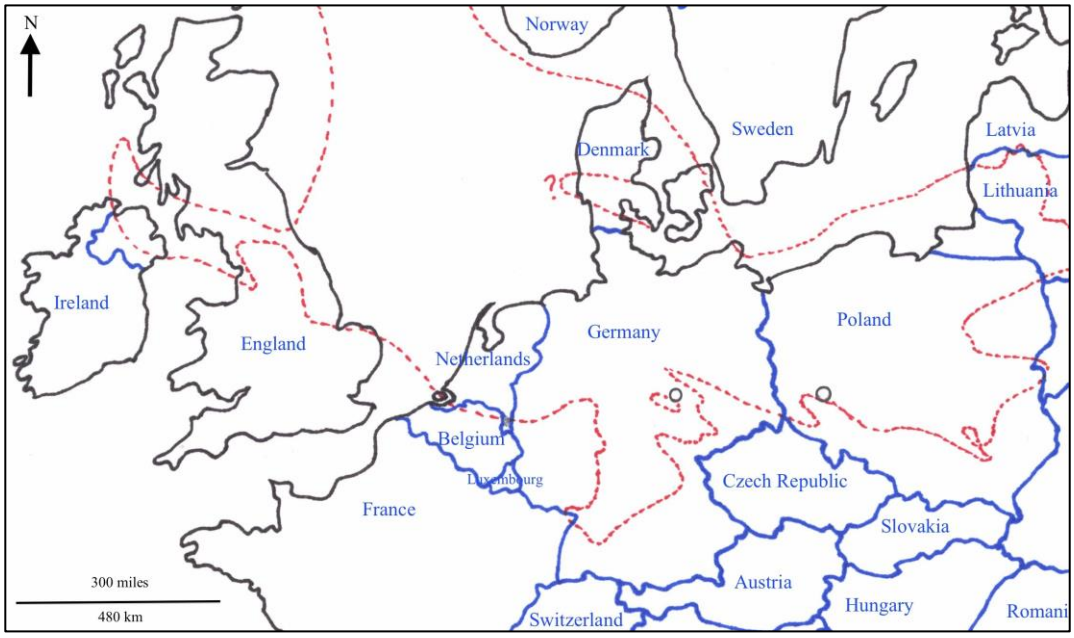


Figure 2.1: The red dashed lines represent the approximate boundary of the Zechstein basin (after Vaughan *et al.*, 1989) during the Permian. Gray circles note the approximate location of the Sangerhausen Basin in Germany and the Lubin mining district in Poland. Note how the mining districts are located near the edge of the basin.

The Kupferschiefer is part of the Middle to Late Permian Zechstein group, which is composed of multiple depositional cycles, each beginning with a marine transgression and ending with the restriction

of the basin (Ziegler, 1990). The Kupferschiefer is recognized as the basal unit of the first Zechstein cycle, at the transition between the underlying Weissliegend and Rotliegend sandstones and the overlying Zechstein limestone and Werra Anhydrite (Figure 2.2).

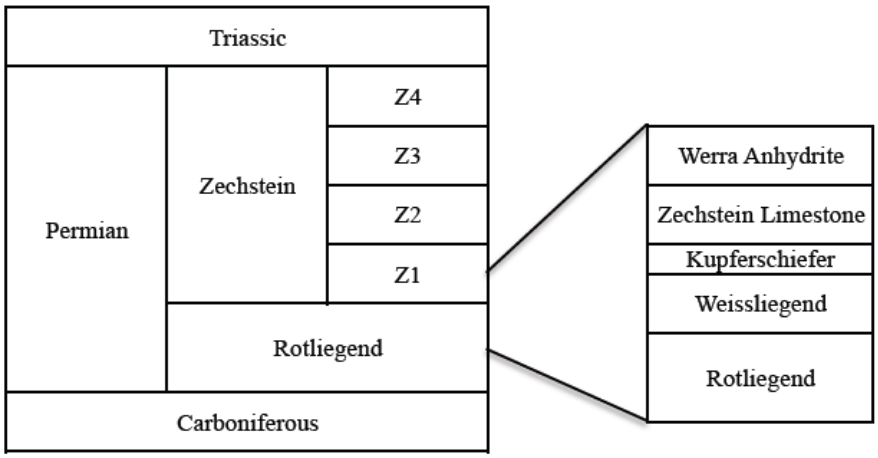


Figure 2.2: Stratigraphy of Permian sediments in Germany; relative thicknesses are not to scale. Z1-4 represent cycles within the Zechstein deposit. Figure modified from Asael (2009).

The thickness of the Kupferschiefer is, on average, approximately 1 meter, though it can vary from only a few centimeters up to 4 meters (Rentzsch, 1974; Vaughan *et al*., 1989). Some workers subdivide the Kupferschiefer into 3 or 5 subunits. These units include, from the base to the top: black shale, black bituminous marly shale, dark grey marly shale, medium grey laminated marl, and medium grey marl (Symons *et al*., 2011). The Kupferschiefer exhibits ore grade mineralization in zones a decimeter to a meter in thickness (Wedepohl *et al*., 1978) in localized areas of southern Poland and south-central Germany. Near the paleo-shores of the Zechstein basin, the lower Kupferschiefer is generally enriched in trace elements such as Pb, Zn, As, Co, Ag, and U; the ore grade areas also enriched in Cu, which can account for up to 19.88 wt% (Sun and Püttmann, 1997). It is estimated that the mass of the copper content of this unit is close to that of the African Copperbelt, but ore grade mineralization at depths that would be economical to mine is rare (Wedepohl *et al*., 1978). Pyrobitumen, sparry calcite, and arsenopyrite are also found in the relatively well-mineralized lower section. The lateral equivalent of

the Kupferschiefer is known as the Marl Slate in England; the units show strong correlation through stratigraphy and biostratigraphy (Hirst and Dunham, 1963). The Marl Slate is described as a laminated silty dolomite (Turner *et al*., 1978), and lacks the ore grade mineralization and sulfides found in other Kupferschiefer areas, though it does contain micro-spherules of pyrite (Hirst and Dunham, 1963).

The Kupferschiefer is generally described as being a carbon- and carbonate-rich shale; it is composed in part by calcite, dolomite, gypsum, anhydrite, quartz, feldspars, biotite, clay minerals, and bitumen. The clay material is mostly composed of illite, though montmorillonite, kaolinite, chlorite, and glauconite are also present (Jung and Knitzscheke, 1976; Oszczepalski and Rydzewski, 1987). Organic content can reach 10 wt.% (Kotarba *et al*., 2006; Pašava *et al*., 2010) in the lower half of the unit, and in some locations remains of plants and fishes have been preserved (Pancost *et al*., 2002). The Kupferschiefer is organic-rich at its base, and grades upwards into a carbonate-rich marl. The base of the unit occasionally exhibits discontinuous, alternating laminations of carbonate and organic material that may be flat, wavy, or lenticular in shape, and are generally hundredths to tenths of a mm thick. The light laminae are composed of a mix of clay and carbonate material, while the dark laminae are composed of clay, organics, and carbonates (Oszczepalski and Rydzewski, 1987). Cyclical deposition, possibly on the order of yearly or seasonal variations, may account for these alternating laminations (Hirst and Dunham, 1963). It is likely that the deglaciation occurring at the poles during the deposition of the Kupferschiefer probably did not affect the Zechstein basin directly, but the subsequent climatic instability may account for the increase in sedimentation rate that resulted in the decrease in lamination and organic carbon content, and the increase in clastic particles and eventually an increase in carbonate being deposited (Jung and Knitzscheke, 1976; Hitzman *et al*., 2010).

It is possible that the carbonate is the remains of micro-organisms, such as foraminifera (Hirst and Dunham, 1963), though geochemical data from a study by Wedepohl and Rentzsch (2006) suggest that the carbonates were formed through secondary solutions, and not through direct precipitation from sea water. The average Sr values found in the Kupferschiefer are lower than what would be found in carbonates that had precipitated directly from sea water (Wedepohl and Rentzsch, 2006).

Bioturbation is generally absent from the Kupferschiefer (Pancost *et al*., 2002), though at least one instance of it has been recorded (Peryt, 1989), suggesting that the depositional environment was not perpetually anoxic. Hydrocarbon studies have indicated that green sulfur bacteria were present in the Zechstein sea (Pancost *et al*., 2002); since these organisms require light and free $H_2S$, their presence is evidence of occasional photic zone euxinia during the early history of the Zechstein Sea. The Kupferschiefer thins over sand bars, sometimes pinching out entirely, indicating that deposition generally occurred in a relatively shallow marine environment (Jung and Knitzscheke, 1976). In some areas of Poland, the Kupferschiefer is composed of irregularly laminated sediments that exhibit bioturbation and lack fossils; these areas were probably deposited near normal wave base, at depths of about 10-30 m. Some sub-sections of the Kupferschiefer exhibit undisturbed laminations that probably formed below storm wave base, at depths greater than 50-60 m (Oszczepalski, 1989). The following has been cited as evidence against the generalization of basin-wide shallow water deposition: the unit is relatively continuous and extensively distributed within the basin; it is composed of fine-grained sediments, and is rich in organic carbon and clay and carbonate mud; it exhibits regular lamination, and there is an absence of sedimentary structures that would indicate current deposition, erosion, or subaerial exposure; bioturbation occurs only along the margins of the basin, and there is a dearth of skeletal fauna and burrows (Oszczepalski and Rydzewski, 1987). Furthermore, the increase in carbonate content as the shale transitions from organic- to carbonate-rich may indicate decreasing oxygenation and water energy, and an increase in water depth and/or distance from the shore (Oszczepalski, 1989).

The Kupferschiefer is directly overlain by the Zechstein Limestone (also referred to as the Zechsteinkalk), which is classified as a marly limestone. Differentiating between the two units is often difficult, since the carbonate-rich upper half of the Kupferschiefer grades smoothly into the overlying limestone. The Zechstein Limestone appears to have been deposited under more oxic conditions compared to the Kupferschiefer, likely in an open marine environment, and is composed of between 4 and 7 unique cycles (Ziegler, 1990).

The Weissliegend ("white sandstone") is a fine- to medium-grained sandstone that underlies the Kupferschiefer. It was formed when the Rotliegend ("red sandstone") was reworked by a rapid marine transgression, through a combination of rapid flooding, wave action, and soft sediment deformation (Ziegler, 1990). The Weissliegend is technically the basal unit of the first Zechstein sequence, but it is difficult to clearly differentiate between the reworked Weissliegend and the undisturbed Rotliegend. The Kupferschiefer is more easily recognizable in cores and on wire-line logs (Glennie, 1989), and is therefore regarded as the effective basal unit, especially for the purpose of hydrocarbon exploration. The Weissliegend is thought to have formed in three different depositional stages, from oldest to youngest: fluvial, aeolian (possibly coastal dunes), and shallow marine (reworked and redeposited). This unit thus shows the transition from continental Rotliegend to marine Zechstein. Evidence for reworking and redeposition includes marine fauna and trace fossils indicative of biogenic activity, erosional surfaces on a localized scale, sedimentary structures resulting from a marine environment, and well-mixed grain populations present in the grain-size distributions (Nemec and Porębski, 1977a).

In a few locations, the Kupferschiefer is separated from the Weissliegend by other, thin units which postdate the Weissliegend (Figure 2.3). The Zechstein conglomerate is found in inter-dune hollows and is only a few centimeters thick on average, though it can reach up to 5 meters (Glennie, 1989). The Boundary Dolomite, known as Mutterflöz in Mansfeld, Germany, is lens-like in nature and thus not always present below the Kupferschiefer. Where it is present, the Boundary Dolomite can vary between a few centimeters and a few decimeters in thickness, though thicknesses of up to 7 meters have been recorded (Peryt, 1989). The presence of foraminifers, brachiopods, bivalves, echinoderms, ostracods, and bryozoans within the dolomite indicate this unit was deposited in a subtidal environment (Peryt, 1989).

The Weissliegend is underlain by the Rotliegend, a red sandstone and conglomerate unit with some volcanics. It is separated into two subunits by some workers: the Upper Rotliegend, composed of sandstones and conglomerates, and the Lower Rotliegend, composed of volcanic rocks such as melaphyres, porphyries, and tuffs (the Autunian volcanics), in addition to shales and limestones (Kucha

and Pawlikowski, 1986). The red color of Rotliegend may have developed *in situ*, as a result of alteration and the breakdown of detrital iron-rich silicates and iron-oxide grains soon after deposition (Nemec and Porębski, 1977b). There does not appear to be any evidence to support the hypothesis that the Weissliegend deposit was ever red, at least in the area studied by Nemec and Porębski (1977b), though bleaching in localized areas still could have occurred. Where the Rotliegend sandstone is capped by the Zechstein salts, particularly in Germany and the Netherlands, the unit contains potentially recoverable gas reserves (Ziegler, 1990). The Rotliegend and Zechstein groups are overlain by younger Mesozoic and Cenozoic strata that can reach thicknesses up to, and sometimes exceeding, 7000 m (Ryka, 1989).

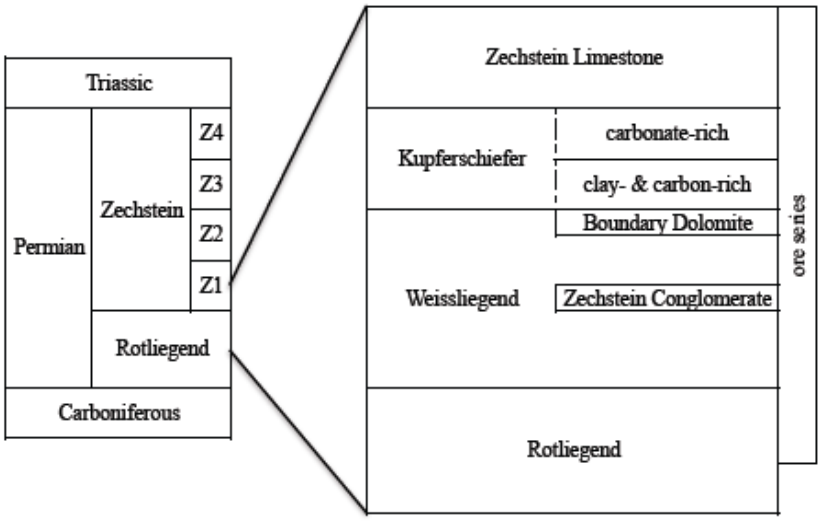


Figure 2.3: More detailed stratigraphy (compiled and modified from Oszczepalski and Rydzewski (1987) and Asael *et al*. (2009)).

The Rote Fäule ("red rot") is not a unique stratigraphic unit, but instead a zone of oxidation characterized by barren red-stained sediment that results from the epigenetic replacement of framboidal pyrite by hematite. It is present over a few thousand square kilometers in the Richelsdorf and Mansfeld-Sangerhausen areas of Germany, which is a relatively small area compared to the 10,000 square kilometers it covers in the Polish regions of Brandenburg, Lower Lusatia, and Lower Silesia. The Rote Fäule is thought to have formed approximately in the Jurassic (Bechtel and Püttmann, 1991), and may have developed over the course of 4 individual cycles (Jung and Knitzscheke, 1976). This oxidized zone

is most commonly found above paleohighs (Bechtel *et al*., 2002) and wanders in and out of the Kupferschiefer, Weissliegend, Rotliegend, and Zechstein Limestone at low angles, occasionally even reaching into the Werra Anhydrite unit that overlies the Zechstein Limestone.

The Rote Fäule is important in the study of the Kupferschiefer because of its strong association with mineral zonation (Jowett, 1986). The location of the Rote Fäule appears to relate directly to the location of mineralization within the Kupferschiefer. When the Rote Fäule is proximal (i.e. adjacent to or within the Kupferschiefer unit), mineralization is more likely to be found in the upper half of the Kupferschiefer and within the Zechstein Limestone, whereas when the Rote Fäule is relatively distal, mineralization is present in the lower half of the Kupferschiefer and the upper Weissliegend (Hammer *et al*., 1990). The presence of the Rote Fäule serves an economic purpose, as well. It can be used as an aid in prospecting, since mineral zonation is often directly associated with the Rote Fäule, radiating outward both laterally and vertically, and forming something like a series of mineralization belts (Cu and Ag, Pb, Zn) around the oxidation zone (Jowett *et al*., 1987). For example, it has been noted that copper and silver grades decrease sharply as distance from the Rote Fäule increases, leaving only the series of Pb, Zn, and iron-sulfide in the sediments (Oszczepalski, 1999).

**2.2 Geologic History**

The Kupferschiefer was deposited from the Zechstein sea during the Upper Permian, approximately 250 million years ago. A rendition of what Europe might have looked like during the Permian is shown in Figure 2.4 (Blakey, 2011). Paleontological data give an age of 255 Ma (Hitzman *et al*., 2010); Re-Os data give an age of 247±20 Ma for the Kupferschiefer (Pašava *et al*., 2010). The illite age from mineralized Kupferschiefer samples is 239 to 256 Ma, suggesting that the illite underwent recrystallization and/or chemical or thermal resetting during diagenesis, in part due to the presence of the migrating mineralizing fluid (Bechtel *et al*., 1996). Low-temperature alteration processes post-deposition, possibly as mineralizing fluid was flowing through the unit may have further obscured the dates (Pašava *et al*., 2010; Symons *et al*., 2011). The age of some of the source rocks for the Kupferschiefer unit is

estimated using clay mineralogy and K-Ar dating, which provides an age of approximately 325 Ma (Bechtel *et al*., 1996).

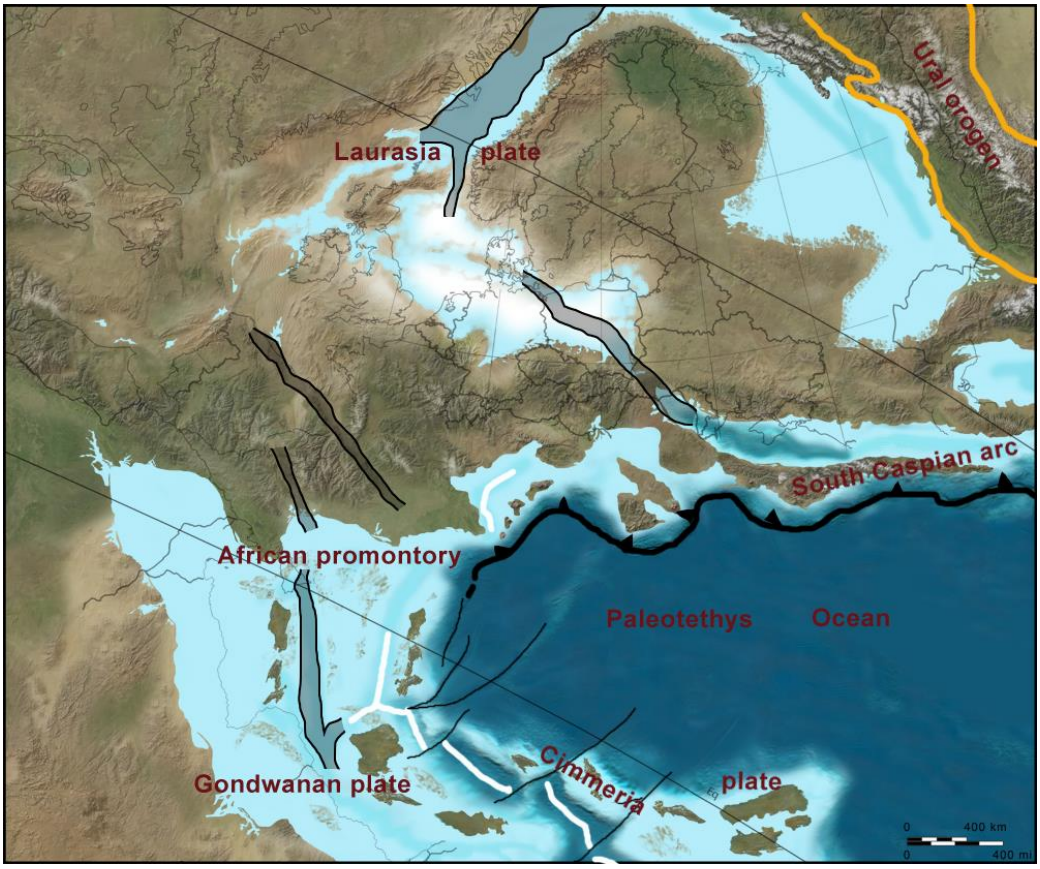

Figure 2.4: Illustration by Blakey (2011) of Europe during the Permian-Triassic period.

A study by Symons *et al.* (2011) notes that the 254±6 Ma paleomagnetic age for the Rote Fäule, determined by previous authors to be the result of the migrating fluids, is more likely to actually be the result of relict magnetization preserved within the hematite from primary deposition or early diagenesis. Symons *et al.* (2011) obtained an estimate of 149±3 Ma for the mineralization of Kupferschiefer, Zechstein, and Weissliegend sediments. The authors suggest that this age, which is significantly younger than previous estimates, may have been caused by sulphidic hydrothermal fluids during the Late Jurassic, which would have resulted in major chemical alteration or recrystallization.

Continental ice sheets were present over Antarctica and northern Siberia during the Late Permian, but by the Late Triassic ice only remained over northern Siberia. Icehouse conditions were present from the late Carboniferous to early Permian, approximately 324.5 to 292.5 million years ago. Sea level fluctuated during the Late Permian, with a global low-stand present during the transition from the Permian through to the Triassic. Eustatic sea level rose in a cyclical fashion during the Triassic, which may in part account for the different evaporate/carbonate cycles within the Zechstein formation (Ziegler, 1990).

The presence of polar ice caps during the Permian would have affected the global air-pressure belts in such a way as to cause zones of high and low pressures to exist closer to each other than is the case in modern conditions (Ziegler, 1990). Furthermore, most of the major land masses were located near the equator during the Permian (Hitzman *et al*., 2010). The compressed air pressure belts would have resulted in higher average velocities of the trade-winds, and thus higher rates of evaporation and deflation. During the Permian, the Zechstein basin (along with the rest of what is now Western and Central Europe) would have experienced desert-like conditions as a result of the strong trade-winds and the presence of the Variscan fold belt, which acted as a precipitation barrier for moisture coming from the Tethys to the south (Ziegler, 1990).

Under these arid conditions, ephemeral streams carried eroded sediments and volcanics from the highlands of the Variscan fold belt to the Northern and Southern Permian basins of Western Europe. The basins were subsiding in part due to the contraction of the lithosphere resulting from cooling, and the deposition of the material carried by the ephemeral streams resulted in the formation of the Rotliegend redbed units and halite sequences. The cooling and contraction of the lithosphere continued into the Triassic, though later on there was also extensional tectonic activity associated with the Faeroe-Rockall rift, which further contributed to basin subsidence (Ziegler, 1990).

The volcanic rocks, generally mafic or bimodal in composition, at the base of the sequence may be the source of the oxidized fluids and a potential source of copper and other metals. The volcanic rocks that underlie the late Permian sediments within southwestern Poland were produced by subaerial

volcanism that began in the Carboniferous and continued into the Permian, peaking during the Rotliegend. Three cycles (basaltic, dacitic, and rhyolitic) of bimodal volcanism occurred near the Sudeten area, resulting from mantle diapirs that formed during the collision of the West European plate and the South European plate (Ryka, 1989). The overlying shales were deposited during and after the "rift climax." In the case of the Kupferschiefer, conditions were conducive to the formation of evaporites during the rift climax through to post-rifting deposition. This resulted in carbonates in small amounts at the base of the Kupferschiefer, with increasing volumes of carbonates as the sedimentation rates decreased and less detrital (quartz) was incorporated into the unit (Hitzman *et al*., 2010).

As a result of the Permian breakup of the supercontinent Pangaea, failed rifts developed that became intracratonic basins with closed hydrologic systems well suited for the formation of redbeds. The cycles that influence supercontinent formation may also be responsible in some capacity for the formation of redbeds (Malinovsky and Gablina, 2008). Thick deposits of redbeds are generated under the same climatic conditions as those found on supercontinents, implying that they form together. Thus redbed copper deposits likely have a cyclicity comparable to the Wilson cycle, which controls the formation and breakup of supercontinents, and operates on the order of 400 to 450 million years (Legler *et al*., 2005). Redbed deposits are followed by the deposition of marine and lacustrine shales or, particularly in low latitude basins (within 20˚ to 30˚ of the equator), evaporite deposits (Hitzman *et al*., 2010). Rifting and associated tectonic instability in the basin was present through to approximately 265-260 Ma, as indicated by syndepositional faulting, gradually decreasing until it ceased completely (Ziegler, 1990).

The Southern Permian basin reaches across 1500 km, from the North Sea coast of England to Poland; the width ranges between 250 and 350km. The basin is sub-divided into the Southern North Sea/German sub-basin and the Polish sub-basin by a northeastern trending saddle roughly located along the border between Germany and Poland. The presence of these sub-basins account in part for the difference in the thickness of the Rotliegend sediments that underlie the Kupferschiefer; the Rotliegend reaches a thickness of 1500m in Germany, while it only obtains a thickness of 800m in Poland. These sandstone deposits were formed in desert-lake and/or sabkha conditions, with the cyclical flooding and

incomplete desiccation of the basin resulting in the localized deposition of an alternating sequence of evaporites and red shales with minor anhydrite composition; sulfur isotope studies and the absence of marine fauna have shown that the units were not precipitated from marine waters (Ziegler, 1990).

The Zechstein Sea, estimated to be 1700 km long and about 600 m wide (Figure 2.1), resulted from a transgression of the South Permian basin. This occurred through a combination of subsidence of the basin below sea levels, an eustatic sea level rise due to the deglaciation of Gondwana, and the breakdown of barriers that had previously isolated the basin from the Arctic seaway. Any solid physical evidence of a connection between the two water bodies was eroded after the Permian. The filling of the basin and the formation of the Zechstein Sea was rapid, and might even have been catastrophic (Ziegler, 1990), though other authors support a slow transgression and the deposition of the Kupferschiefer in shallow marine or swamp-like conditions (Jowett *et al*., 1987).

Dunes are preserved within the Rotliegend, suggesting that the transgression would have been rapid, on the order of decimeters per day; the transgression would have had to occur in conjunction with a time of atmospheric calm so that there was little or no wave action to destroy and rework the dunes (Glennie, 1989). There would have been catastrophic reworking where the water entered the basin from what was most likely the proto-Atlantic (Glennie, 1989), but on the southern shore of the basin it would have stayed very calm. Furthermore, the presence of a large desert lake within the basin could have further protected and buffered the underlying Rotliegend from being reworked by the sudden influx of water. Deformation present at the top of the dunes could be a result of air being released all at once, after having been trapped by the capillary "seal" of the water in the fine sand. It is possible that the rapid inundation of Weissliegend dune sands that had formerly been above the level of the water table is what prevented the sands from becoming reddened, and that the sands that were already below the water table had a greater chance of reddening (Glennie, 1989). The addition of land-derived nutrient-rich waters quickly resulted in high organic production within the Zechstein Sea, and thus anoxic bottom waters below the wave base. The water depth may have been between 200 and 300 m (Ziegler, 1990), with the high organic production and high evaporation rates contributing to the anoxic bottom-water conditions.

High $\delta^{18}O$ values in near-shore carbonates suggest hypersaline conditions during deposition (Bechtel and Püttmann, 1997). High V/C, Mo/C, and U/C ratios suggest that deposition rates were very slow (Wedepohl, 1994).

The Zechstein basin became larger than the underlying Rotliegend basin because of regional subsidence during the sag phase that followed the rift phase; this resulted in the Zechstein basin overstepping the margins of the Rotliegend basin. In England, for example, the Marl Slate is not underlain by the Rotliegend equivalent (Hirst and Dunham, 1963). Paleo-geographic relief played a large role in the Kupferschiefer deposition and placement of the Zechstein Limestone facies; relic highs from the Rotliegend caused the Kupferschiefer to pinch out, but the Zechstein basin eventually encroached into the Variscan highlands. The original Zechstein thickness was probably on the order of 1500 to 2000 m, though it was affected after early diagenesis by salt diapirism, erosion, and subsurface leaching (Ziegler, 1990).

It is hypothesized that Zechstein deposition took place over 5 to 8 Ma, with variable deposition rates. The Zechstein is subdivided into 4 to 7 depositional cycles; Peryt (1978) identified 5 main microfacies. Each cycle opens with a marine transgression and ends with the restriction of the basin, as evidenced by the deposition of sulfate or halite and resulting from a downward fluctuation in sea level at a local or eustatic scale. The Kupferschiefer is considered to be the beginning of the first Zechstein cycle ("Werra"), indicating a marine transgression. It is possible that the Zechstein deposits may have been connected to both the Arctic and Tethys Seas, as evidenced through the presence of specific microfauna fossils (Ziegler, 1990).

It is possible that the Jurassic extensional tectonic activity responsible for the formation of the North German Basin is also in part responsible for the mineralizing hydrothermal activity, in that it reactivated and extended basement faults up into the overlying units (Symons *et al.*, 2011). Triassic rifting could have activated thermal convection, and possibly opened up a route to the Tethys to the south, which in turn may have reduced the isolation of the Zechstein basin. The subsidence and affects of thermal anomalies are hypothesized to have moved the Rotliegend formation waters up into the overlying

sediments, and natural fractures from this tectonic activity (or coincidental natural hydrofractures) would have further permitted the movement of these fluids into and through the Kupferschiefer (Jowett *et al*., 1987).

The Zechstein sediments underwent burial during the Mesozoic (Ziegler, 1990). At least in the area of the Lower Rhine Basin in western Germany, it is thought that this depth would not have exceeded 1000 m (Bechtel and Püttmann, 1997). Temperatures due to burial or hydrothermal activity, or both, are not thought to have exceeded 130˚C for the Kupferschiefer and the Rote Fäule (Bechtel *et al*., 1995).

**2.3 Mining History**

In Germany, the Kupferschiefer was mined during medieval times through the early 1990s. Especially during the medieval period, the shale was mined despite its low grade concentration of copper largely because of the ease of access (thanks to uplift/tilting during the Harz orogeny). Mining is estimated to have begun in the 13th century, and continued in the Sangerhausen Basin of the Harz foreland until the Reunification of Germany in 1990; after Reunification the demand for copper was no longer high enough to warrant the uneconomical cost of extracting the ore. The Kupferschiefer has been mined mostly for Cu, Pb, Zn, and Ag, though V, Pt, Se, and Au have also been produced from the Mansfeld-Sangerhausen ores. There was also historic production of Mo, Ni, Re, Ge, and Cd (Rentzsch, 1974). During the eight centuries that it was in production, the Mansfeld-Sangerhausen mining district produced 2.6 Mt of copper and 14,200 tons of silver (Symons *et al*., 2011) (Figures 2.5 and 2.6).

Other locations in Central Europe where the Kupferschiefer was mined historically include: the Richelsdorfer Gebirge region, closed after 1950; the regions of Mansfeld and Eisleben in the southeastern Harz foreland, discontinued in 1970; the Mulkwitz structure at Spremberg; the region of Bolesławiec within the Inner Sudetic syncline; and the region of Zajaczek and Grodzice, which was mined at least from the 1930s through to the 1970s. The Subsudetic Monocline region of Lubin-Polkowice-Sieroszowice and Wrocław-Głogów was discovered in the 1960s, and thought to be the largest copper deposit in Europe (Jung and Knitzscheke, 1976). The Lubin mining district includes the Lubin, Rudna, Sieroszowice, and Polkowice mines; the Lubin deposit was discovered in 1957 (Oszczepalski, 1989) and

is still being mined (Jung and Knitzscheke, 1976). The Lubin mine is located south of the Rudna mine and closer to the Fore Sudetic block (Figure 2.7). Samples from the Rudna mine represent deposition in deeper basin conditions (Oszczepalski, 1989) compared to Lubin samples. Ore mineralization in Lubin mine samples is dominated mostly by copper and copper-iron sulfides (Large *et al*., 1995).

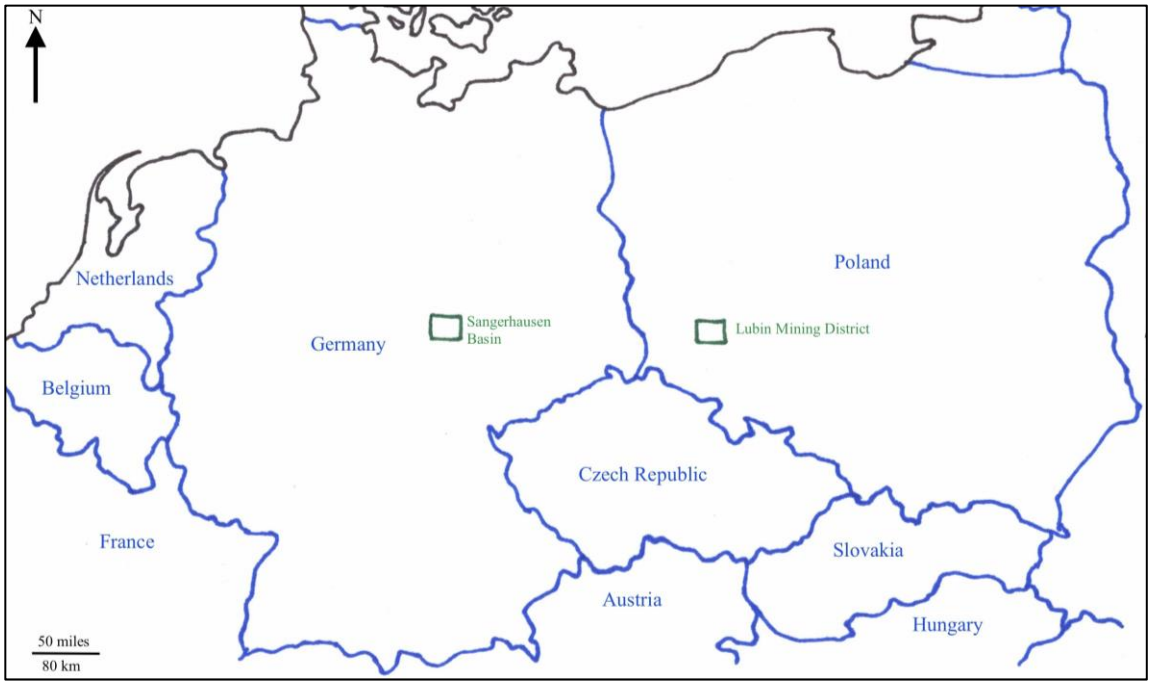


Figure 2.5: The approximate location of the Sangerhausen Basin in Germany, and the Lubin Mining District in Poland (~210 miles, or 340 km, east of Sangerhausen).

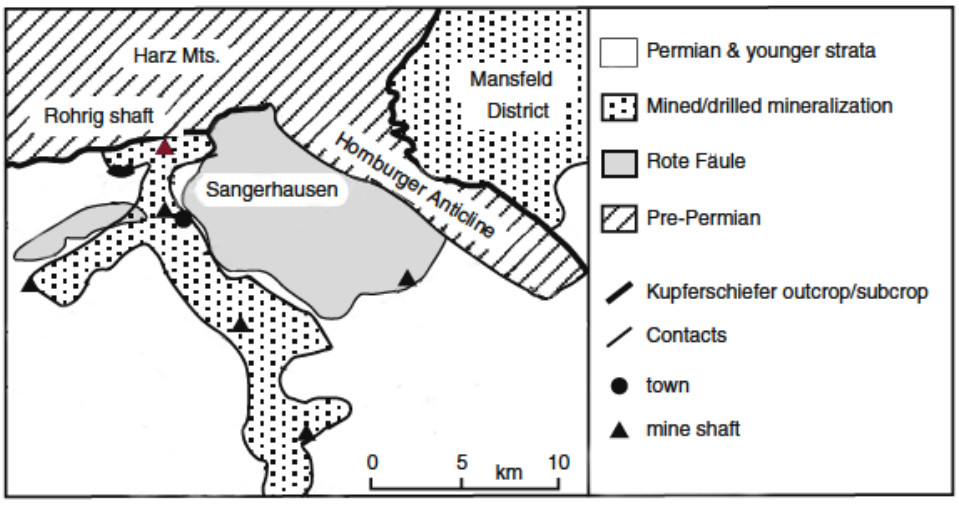


Figure 2.6: A geologic map illustrating the relationship of the Permian units and Rote Fäule within the Sangerhausen Basin, with the Rohrig mine shaft highlighted in red. Modified from Symons *et al*. (2011).

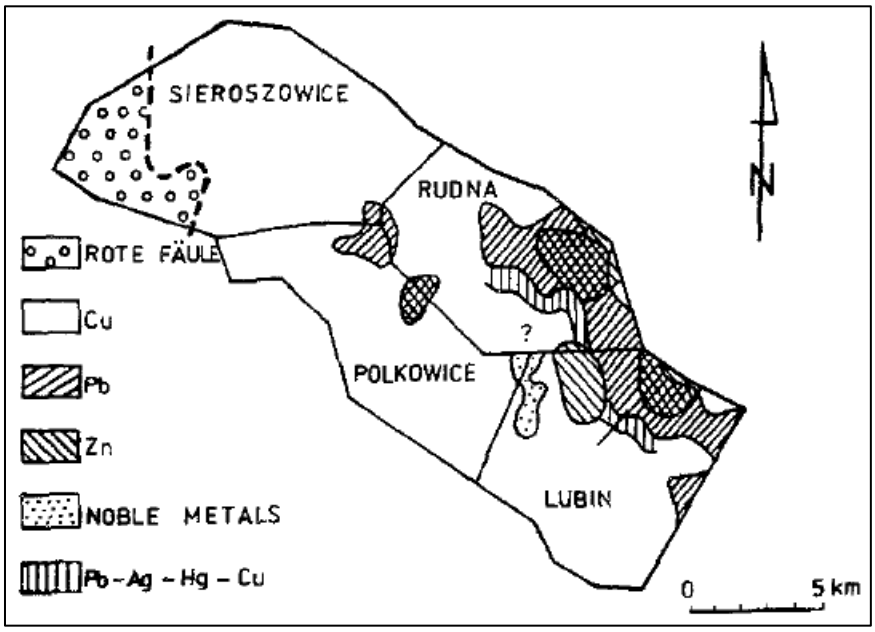


Figure 2.7: Modified from Kucha (1990) (fig. 1), showing the relative locations of the mining districts within Poland and the zones of dominant mineralization found within the Weissliegend, Kupferschiefer, and Zechstein limestone.

### 2.4 Mineralization

Of the Zechstein and Rotliegend units, the Kupferschiefer hosts the richest ore mineralization, although mineralization can also occasionally be found in the underlying sandstones and the overlying dolomites and limestones. The mineralization of the Kupferschiefer is not necessarily unusual in its thinness (~1 meter): in general, the sulfide-bearing zones of sediment-hosted stratiform copper deposits are less than 30 meters thick, though they are usually even thinner, at 3 meters or less. In other stratiform copper deposits, mineralization is approximately parallel to local sedimentary layers, though in some cases it is known to wander in and out of units at low angles (Hitzman *et al*., 2010), similar to the copper sulfide mineralization associated with the Kupferschiefer. Mineralization is generally in the form of micrometer-scale dispersed grains, and rarely as small veins or more massive forms (Krouse *et al*., 2006). Chalcocite is often the most abundant copper sulfide mineral, sometimes accounting for up to 90% of the rock (Sawłowicz, 2013). The Marl Slate only shows microspheres of pyrite ($FeS_2$), and no other iron- or copper-sulfide minerals (Hirst and Dunham, 1963).

Over much of its extent, the Kupferschiefer is not enriched in metals compared to other black shales (Vaughan *et al*., 1989). Aside from the influence of the Rote Fäule, mineralization varies in concentration and distance from the paleo-shore of the Zechstein sea. Copper mineralization (concentration ≥0.3%) is almost exclusively found in near-shore regions, and is present in approximately 1% of the estimated 600,000 $km^2$ area. Zinc mineralization is both more abundant, present in 4 to 10% of the area (concentration ≥0.3%), and more likely to be found at a distance from the shoreline. Lead mineralization is intermediate in both abundance and location relative to copper and zinc. Further than 150 km from the paleo-shore, the sediment is not enriched in Pb, Zn, or Cu, and becomes a bituminous marl enriched in V, Mo, and U as is common for black shales (Wedepohl *et al*., 1978). In the Zechstein rocks of Spessart district, Germany, there are stratabound Cu-Pb-Zn-(Ag) ores, structurally controlled Cu-As-(Ag) ores, crosscutting Co-Ni-(Bi)-As and Cu-Fe-As veins, and stratabound metasomatic Fe-Mn carbonate ores in the dolomite (Wagner *et al*., 2010).

In the Sangerhausen Basin, chalcocite ($Cu_2S$) is the main copper mineral within a zone 2 km wide, situated spatially SE of the Rote Fäule (Wedepohl and Rentzsch, 2006) (Figure 2.8). Continuing in the SE direction, eventually the chalcocite (representative of the Cu zone) is replaced by galena (Pb), which is present over a zone up to 4 km wide. Wedepohl and Rentzsch (2006) hypothesize that the migration of mineralizing fluids from the Rote Fäule into the carbonaceous clay of the Kupferschiefer resulted in an increase in pH (>3), the replacement of pyrite ($FeS_2$) by chalcocite ($Cu_2S$), and a reduction in Cu concentration within the mineralizing fluids. The Cu-depleted fluid then continued further into the shale and precipitated galena (PbS) and sphalerite ((Zn,Fe)S) in more distal zones. The authors propose that the fluids were already slightly reducing, and their slightly acidic nature was neutralized by the presence of the carbonates in the marly shale, thus allowing the precipitation of Mn, Fe, Cu, Zn, Pb, and other elements. The sequence of mineralization along proposed flow paths in their samples is listed as: bornite ($Cu_5FeS_4$), chalcopyrite ($CuFeS_2$), chalcocite ($Cu_2S$), galena (PbS), sphalerite ((Zn,Fe)S).

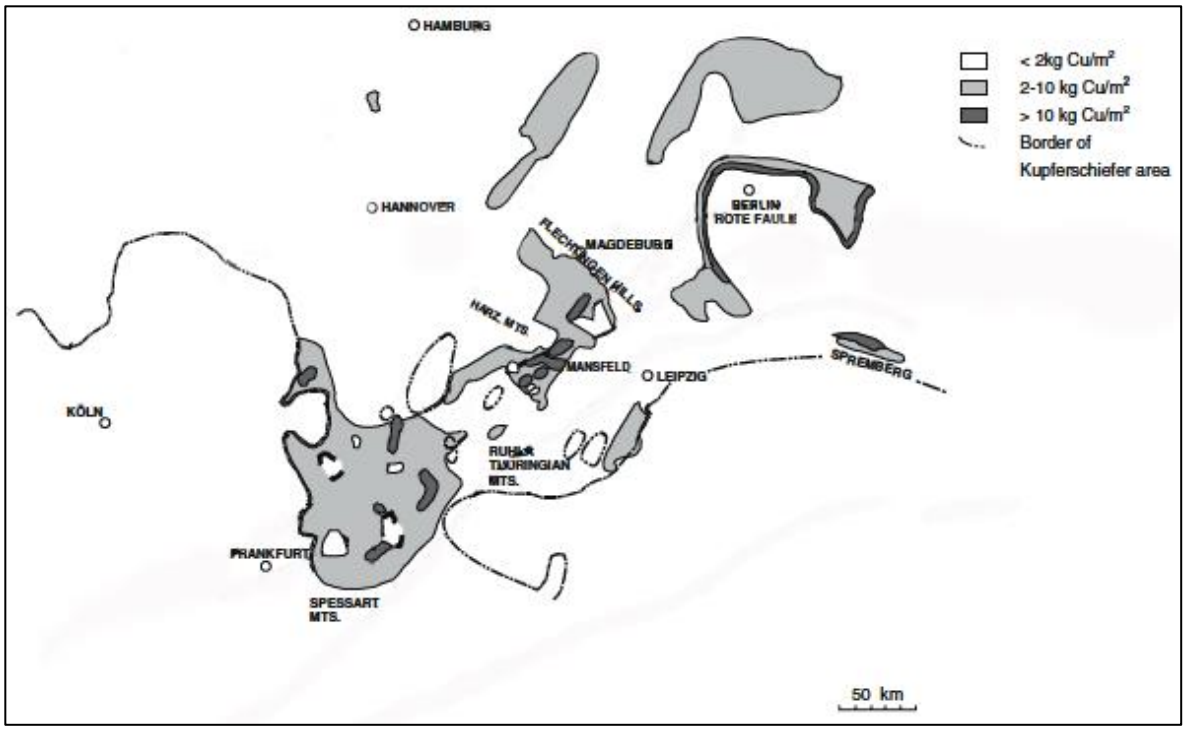


Figure 2.8: From Wedepohl and Rentzsch (2006), showing the regional distribution of high (>10 kg $C/m^2$), medium (2-10 kg $C/m^2$), and low (<2 kg $C/m^2$) copper concentrations. Two kg $Cu/m^2$ is approximately equal to 0.2% Cu. Note the location of the strongest Cu mineralization in relation to the position of the Rote Fäule.

In samples studied by Gablina & Lur'e (2001), the sequence of replacement was as follows: djurleite ($Cu_{31}S_{16}$), digenite ($Cu_9S_5$), bornite ($Cu_5FeS_4$), chalcopyrite ($CuFeS_2$), pyrite ($FeS_2$). This would require impeded, or obstructed, water exchange, since free water-exchange would result in the formation of unstable mineral associations (ex.: pyrite + djurleite, chalcopyrite + digenite) and disrupt the zonation mentioned previously (Gablina and Lur'e, 2001).

Rose (1989) lists the sequence of mineralization as hematite ($Fe_2O_3$)- (native Cu)- chalcocite ($Cu_2S$)- bornite ($Cu_5FeS_4$)- chalcopyrite ($CuFeS_2$)- (galena [PbS])- (sphalerite [(Zn,Fe)S])- pyrite ($FeS_2$). This is what would be expected to result from one of two possible situations: the progressive addition of $H_2S$ (at least some of which was produced by bacterial sulfate reduction, or BSR) to an oxidizing fluid with dissolved Cu, Fe, (Pb, Zn), or the progressive reaction between pyrite and a fluid with dissolved Cu(-Pb-Zn). The author lists all of the possible fluid sources responsible for the transportation of the metals: the underlying redbeds, seawater, river water, marine sediments, and hydrothermal fluids. Rose (1989)

notes that a marine sediment source would be problematic because if $H_2S$ was present even in trace amounts, as is common in marine sediments, Cu and Ag would be immobile. A hydrothermal fluid source is also somewhat unlikely, since the transport of Cu is uncommon at temperatures below 250˚C. If $H_2S$ was formed after the precipitation of copper, through either BSR or abiotic means, then galena, sphalerite, and Co sulfides would have been precipitated as well. The presence of digenetic pyrite after Cu has been precipitated from the fluid allows for the subsequent deposition of Pb, Zn, and Co (Rose, 1989).

Large *et al*. (1995) determined the following alteration sequence of Cu and Cu-Fe sulfides: chalcocite ($Cu_2S$), djurleite ($Cu_{31}S_{16}$), anilite ($Cu_7S_4$), geerite ($Cu_8S_5$), spionkopite ($Cu_{1.4}S$), yarrowite ($Cu_9S_8$) and bornite ($Cu_5FeS_4$), copper-poor pinkish-orange bornite, copper-poor orange bornite + chalcopyrite ($CuFeS_2$), and covellite (CuS) (Large *et al*., 1995). The presence of anilite is significant because it indicates low temperatures (<40˚C) of sulfide alteration. The authors hypothesize the mechanism of copper depletion at low temperatures to explain the mineralization present in the Lubin and Rudna mines, such as the presence of copper-poor bornites partially decomposing into covellite and chalcopyrite. The authors note that there is a difference in mineralization between the Lubin and Rudna mines: the copper and copper-iron sulfides in Lubin samples are more copper-depleted compared to the sulfides from Rudna samples. At Lubin, yarrowite, covellite, copper-poor bornite, and chalcopyrite (the most copper-depleted minerals) are often associated with veins of gypsum ($Ca(SO_4)\bullet 2H_2O$), anhydrite ($Ca(SO_4)$), and atacamite ($Cu_2Cl(OH)_3$), probably because of interaction (i.e., leaching) between saline mine waters and the sulfides. At Rudna, alteration from early diagenesis is present along horizons and is associated with bacterial sulfate reduction (BSR) activity. Possible causes of copper depletion listed by the authors include leaching by saline waters descending after interacting with the overlying Zechstein evaporites, or leaching by seawater during the time of deposition (Large *et al*., 1995).

The Cu, Pb, and Zn zones in Kupferschiefer have other metals associated with them. The Cu zone is enriched in transition metals (Ag, Ni, Co, V, Mo at concentrations of 600 to 1500 ppm); these metals are especially concentrated in the bottom section of the shale unit. Cobaltite-cemented pyrite

framboids have been found in the Lubin-Sieroszowice mining district (Large *et al*., 1999). The source of Co and As is assumed to be oxyhydroxides that can be found in the upper, oxic part of the Weissliegend, which could explain in part why the cobaltite-cemented pyrite framboids were only found within a few cm above or below the Kupferschiefer/Weissliegend contact. The cobaltite most likely precipitated in response to the changing chemical environment when it encountered the Kupferschiefer, which acted as a geochemical barrier. In the Cu zone, where it transitions into the Pb zones, other metals found include Au, platinum group metals, and U (in concentrations of trace to several hundred ppm). In the Pb zones, near the Cu-contact, Ag and Hg increase in concentration (100-1500 ppm for Ag, 5-800 ppm for Hg, with Hg averaging 61 ppm throughout the Pb zone) (Kucha, 1990).

Gold present in the Kupferschiefer is usually sub-economic, though in two boreholes from the Mansfeld/Sangerhausen district studied by Borg *et al*. (2005), gold reaches "anomalously high levels" (Au= 282 ppb, Pt= 53.5 ppb, Pd= 16.5 ppb). In other German locations, Au is present at a few ppb or less, and sometimes below detection altogether (Walther and Borg, 2010). A study by Walther and Borg (2010) compared geochemical data from the Sangerhausen Kupferschiefer to the geochemistry of a barren shale; they used the Devonian Ohio Shale (SDO-1) as a baseline. Compared to barren shale, the Sangerhausen Kupferschiefer has concentration of up to 700x Cu, Zn, Pb, and Co. The Richelsdorf District and Spessart/Rhön areas only show concentrations of up to 100x that of SDO-1 levels. The latter two do show an enrichment in As (up to 70x SDO-1), whereas Sangerhausen does not show any enrichment. When compared to other metalliferous shales, such as those found in Canada, China, and Finland, the Kupferschiefer shows lower levels of enrichment in Ni, Co, and Mo. Another unique characteristic of the Kupferschiefer is that, while other metalliferous shales generally have a clear genetic link to hydrothermal or magmatic activity, the Kupferschiefer lacks any clear connection with such activities (Walther and Borg, 2010).

Commercial levels of Au, Ag, and platinum group elements (PGE) are found in the Kupferschiefer of the Lubin-Sieroszowice district. These metals are concentrated in the oxidized sections of the Cu deposits, near the basal contact of the ore beds. Silver has been found at the chalcocite-bornite

($Cu_2S$-$Cu_5FeS_4$) transition in Poland (Oszczepalski, 1989). Using average values of 2.25 ppm Au, 0.14 ppm Pt, and 0.08 ppm Pd, it is estimated that Au resources could be as high as 50 tons, with 12 tons of Pt + Pd (Pieczonka and Piestrzyński, 2011). Over the course of 50 years of mining, more than 20 tons of Au have already been produced, at a rate of 200 to 1700 kg per year. Palladium + platinum production ranges between 30 and 100 kg per year.

Platinum group elements (PGE) occur in order of solubility in the Poland deposits, radiating out from the Rote Fäule. Platinum, the least soluble, has the highest concentrations within the Rote Fäule, while more soluble silver, copper, lead, and rhenium show the highest concentrations within the Kupferschiefer (Bechtel, Ghazi, *et al*., 2001). The authors think the brine fluids were heavy in $Cl^-$ complexes such as $PtCl_6^{2-}$, $PtCl_4^{2-}$, and $PdCl_4^{2-}$. Rare earth elements (REE) also follow the "established" base metal zonation in such a way that can be explained by differences in solubility. Eh decreased and pH increased as the fluids interacted with the reduced/anoxic Kupferschiefer, thus probably altering the solubility of the elements within the fluid and causing precipitation zones. Bechtel, Ghazi, *et al*. (2001) also note that Re, Ag, and Ir are more abundant in the Cu-rich, reduced Kupferschiefer, and as Eh decreases, these elements increase in solubility and exhibit stronger chalcophile characteristics. A study on noble metals (Au, Pt, Pd) in the Kupferschiefer in Poland found that noble metals only exhibited increased concentrations at redox boundaries (Kucha and Przybyłowicz, 1999).

Kucha and Pawlikowski (1986) describe the ore mineral textures as oriented granules, flasers, and lenses that are sometimes macroscopic in size. Disseminated sulfide grains appear to be aligned with the host bedding, though the ore minerals are intergrown with the host matrix to the extent that no relative timing relationships can be determined. Some of the mineralization has replaced calcareous algae and detrital bioclasts. Fractures discordant with the bedding alignment are present, on the order of several cm wide and a few mm thick. Concordant fractures occasionally transition into disseminated mineralization.

In a study by Oszczepalski (1989), the author determines that ~80% of the mineralization is fine grained (<50 um) and disseminated, mostly in the form of fine bands within organic rich matrix. Mineralization is also present as coarser grained aggregates and lenses (>100 um), and veinlets that can

be concordant or discordant with lamination. Laminae can be found to bend around sulfide grains, or to be completely disrupted, and some of the ore present is the result of replacement of organic matter and carbonates. Vein sulfides likely formed after the disseminated sulfides, since the former are isotopically heavier than the latter (Oszczepalski, 1989). Another study found that veinlets of calcite and copper-(iron) sulfide cross cut and are cut by sulfide replacement lenses (Jowett, 1987).

Vaughan *et al*. (1989) lists four different types or phases of mineralization that are present in the Kupferschiefer, resulting from various processes. The first, and oldest, mineralization is found in the Marl Slate. It is thought to be synsedimentary in origin, a result of the stratification of the early Zechstein sea, fluctuations in water levels, and in the location of the oxic-anoxic boundary. The average base metal content is ~100 ppm. The second type is "average" mineralization, with a base metal content of ~2,000 ppm. This mineralization is likely early diagenetic in origin, using sulfur derived from bacterial sulfate reduction (BSR), and low temperature fluids and metal content from the underlying Rotliegend. The third type of mineralization reaches ore grade, with base metal concentrations of ~3 wt.%. The mineralization is associated with the proximity of the Rote Fäule, exhibits a clear zonation, and is restricted to the margins of the basin. It is most likely late diagenetic in age, and the result of metal rich brines at temperatures of ~120˚C. Basin compaction may be responsible in part for this mineralization, with the sulfur a result of BSR. The fourth type of mineralization is post-diagenetic, structure-controlled mineralization with possible hydrothermal origin, exhibiting Co, Ni, Ba, As, and Ag phases. It is worth noting that this list of mineralization types does not include possible other, more localized mineralization types, which could represent additional phases.

Sawłowicz (1990) identified multiple types of mineralization in the Kupferschiefer. These include spherules, aggregates, clusters, large grains, framboids, dispersed mineralization, lenses, and irregular clusters. Spherules are small, rounded, and occasionally elongated, with either a smooth or rough surface. This mineralization type ranges in size from 1 to 16 μm, with a majority of spherules measuring between 2 and 8 μm (Figure 2.9). Framboids range from 5 to 10 μm in size; framboidal clusters/aggregates range from 10s to 100s of μm Figure 2.9). Framboidal clusters can be composed of

digenite, chalcocite, and occasionally covellite. Sawłowicz (1990) hypothesizes that the framboids and spherules are formed as pseudomorphs of pyrite framboids, which were probably formed while sedimentation was still taking place or during very early diagenesis. Framboids are more commonly found in the organic-rich component of the shale as opposed to the carbonate-shale; some framboids may have formed after globs of organic matter. Large grains are defined as homogeneous grains at least 50 μm in size; they do not show any framboidal-like features, are irregularly shaped, and do not encompass any voids. Cracks in the ore minerals may be a result of desiccation and the associated shrinking. Sawłowicz (1990) proposes that both the sulfide spherules and some of the large grains probably developed after passing through the metastable framboid stage, and are indicative of different stages in the evolution of framboids. The stages of evolution probably occurred more quickly for the other sulfides than for the pyrite framboids. Mineralization primarily occurred during sedimentation or early diagenesis, with remobilization and subsequent recrystallization resulting in non-framboidal textures and the current ore mineral distribution (Sawłowicz, 1990).

Some of the disseminated or framboidal mineralization that is not composed of pyrite is assumed to simply be copper sulfides that have replaced pyrite framboids. However, in a study by Alyanak and Vogel (1974) on the chalcocite framboids in the Nonesuch Shale of White Pine, Michigan, the authors find that the copper sulfide framboids are morphologically distinct from the pyrite framboids. The authors conclude that there is no evidence to support the idea that the chalcocite replaced pyrite, and therefore the chalcocite is primary in origin (Alyanak and Vogel, 1974). Sawłowicz (1990) notes that textures, chemistry, and features of the copper sulfides (digenite ($Cu_9S_5$), chalcocite ($Cu_2S$), and covellite (CuS) in the form of disseminated spherules, framboids, aggregates, etc.) that differ from pyrite framboids suggest that the former are primary precipitates. It is also possible that the copper and copper-iron sulfides replaced monosulfides and not pyrite; this hypothesis is supported by the presence of isotopically light sulfur (Sawłowicz, 1990).

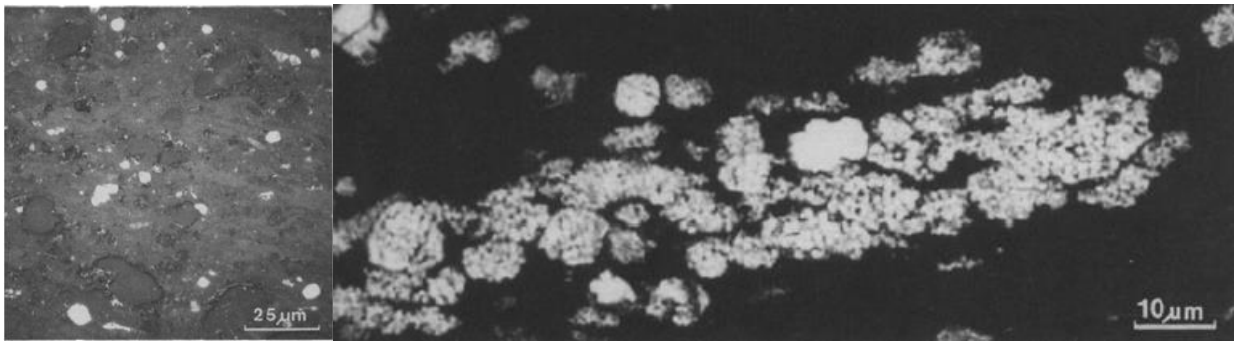

Figure 2.9: Left: An example of diffused copper sulfide mineralization from Sawłowicz (1990). Right: An example of an aggregate of digenite, composed of framboids, framboidal clusters, and spheres, from Sawłowicz (1990).

### 2.4.1 Weissliegend Sulfide Bands

Within localized areas of the Weissliegend there are sulfide bands, composed mostly of digenite ($Cu_9S_5$) and chalcocite ($Cu_2S$), with occasional djurleite ($Cu_{31}S_{16}$) and minor covellite (CuS). The sulfide in the bands acts as a cement for the sandstone; in the barren sandstone above the bands, poikilotopic calcite can be abundant (Mayer and Piestrzyński, 1990). Mayer and Piestrzyński (1990) put forward the idea the sulfides are diagenetic in origin, and a S-isotope study by Michalik and Sawłowicz (2001) indicates an early formation for the copper sulfide bands. Kucha and Pawlikowski (1986) note that there is a "surprising compatibility" between the number of dewatering pulses resulting from compaction, and the number of chalcocite laminations within the Weissliegend. It may be that each individual chalcocite laminae represents a pulse of brine expulsion (Kucha and Pawlikowski, 1986).

The bands are found 0.7-1.4 m below the basal contact of the Kupferschiefer, formed from top to bottom (Sawłowicz and Wedepohl, 1992). Two different types of sulfide bands in the Weissliegend have been recorded: single bands and rhythmic sets of bands; both are thought to be diagenetic in origin (Mayer and Piestrzyński, 1990). Single bands are generally concordant with primary sedimentary structures, whereas the bands are generally discordant when they occur in sets. Mayer and Piestrzyński (1990) hypothesize that single bands are the result of clay and fine sand grains acting as a semipermeable membrane for migrating ions. The sets of bands may have formed as a result of mass diffusion of the ions. The bands are only found to occur in association with the Kupferschiefer; they have never been

described in locations where the Weissliegend is present but the Kupferschiefer is absent (i.e., due to the presence of a sandbar).

Sets of bands are most common; they can be 0.3 to 2 meters thick, are composed of "several to several tens" of individual bands (Figure 2.10), and can sometimes be found with one or two other sets in the same profile, each being separated from the other set(s) by barren sandstone. The bands that make up the sets can reach lengths of up to 20 m, and vary in thickness from 0.5 to 2 cm, with the lowest band of the set generally being the thickest. Each band exhibits a sharp lower boundary and a gradational upper boundary (Mayer and Piestrzyński, 1990).

The Pb, Ni, Zn, and Ag contents in the sulfide bands are similar to those found in the Kupferschiefer. The pattern of increasingly heavier isotopic sulfur in lower sections of the sandstone suggests that the BSR system could have been closing as the bands were formed. Hydrogen sulfide produced by BSR could have diffused from the Kupferschiefer down into the Weissliegend and mixed with dissolved copper in the sandstones, precipitating out as roughly equidistant bands (Sawłowicz and Wedepohl, 1992).


Figure 2.10: A sample of sulfide banding within the Weissliegend from the Rudna Mine, Poland. The sample exhibits diffused upper contacts and sharper, more distinct lower contacts. Modified from Sawłowicz (1992).

### 2.4.2 Timing of Mineralization

Some of the earlier authors support the idea of a single mineralization event responsible for the formation of copper, lead, and zinc sulfides present in the Kupferschiefer (Rentzsch, 1974; Jowett, 1987).

Jowett (1987) hypothesizes that the base-metal mineralization could have formed as the result of a single event, most likely during the Triassic rifting event that coincided with the formation of the Tethys ocean. More of the later authors support the hypothesis that mineralization took place over a very long time and through multiple phases or sources, citing different types of mineralization, cross cutting relationships, and/or stable isotope geochemistry analyses as evidence (Dill, 1984; Speczik, 1995; Michalik and Sawłowicz, 2001; Schmidt Mumm and Wolfgramm, 2004).

A subtopic of the mineralization disagreement in the literature is exactly when the mineralization formed, with the options approximately separated into: syndepositional, diagenetic (Sun *et al*., 1995; Bechtel *et al*., 2000), late diagenetic (Jowett, 1986), and epigenetic mineralization. Some authors bridge multiple phases, the most common being syndepositional to early diagenetic (Wedepohl, 1980; Sawłowicz, 1989; Sawłowicz, 1990; Wedepohl, 1994) or syndepositional to epigenetic (ex., until the late Jurassic or Alpine Orogeny) mineralization (Michalik and Sawłowicz, 2001; Hitzman *et al*., 2010) and diagenetic to epigenetic (Jasinski, 1994). Still others cannot seem to pin down the timing any better than to say it was not syndepositional (Rospondek *et al*., 1994). There is also the possibility of metal remobilization to make the determination of timing more difficult, as Dill (1984) notes that Pb, Zn, and Cu could have been remobilized during late diagenesis.

Arguments for early diagenetic mineralization include the assertion that unconsolidated sediments would have been required in order for the metals to be able to migrate through the Rotliegend and Kupferschiefer, occasionally into the Zechstein Limestone (Wedepohl and Rentzsch, 2006). Wedepohl and Rentzsch (2006) break down the mineralization in such a way that diagenetic mineralization from thermal fluids (300 Mt Cu, 800 Mt Zn, 300 Mt Pb) is responsible for a greater percent of the mineralization compared to syndepositional mineralization from anoxic sea water (~40 Mt Cu, 200 Mt Zn, 5 Mt Pb). Jowett (1987) cites the presence of replacement textures and cross-cutting relationships between the zonations of different metals to support the hypothesis of late diagenetic or epigenetic mineralization.

There is at least some agreement that pyrite framboids were formed by bacterial sulfate reduction (BSR) during early diagenesis and later replaced by copper sulfides and oxide pseudomorphs (Dill, 1984; Jowett, 1992; Oszczepalski, 1999). It is thought that some of the copper sulfides were later replaced by iron oxides and covellite.

Early mineralization was most likely influenced by BSR, copper sulfide framboids, replacement of iron monosulfide framboids by copper sulfides, and Zechstein seawater acting as an oxidant and resulting in low-temperature leaching of copper from copper sulfides (Michalik and Sawłowicz, 2001). According to Hitzman *et al*. (2010), a considerable amount of the sulfide mineralization occurred early in the diagenesis, and mineralization lasted for a relatively long time, possibly intermittently, spiking in precipitation during the Alpine orogeny (65.5 to 2.6 Ma).

Studies done in the 1960s on the metals present in the Kupferschiefer favor syndepositional mineralization due to the narrow thickness of the deposit and apparent influence of paleogeography on the location and zoning of the deposit. Recrystallization during early diagenesis would be required with this model, however, to account for the larger grain sizes of the present ore compared to that of unaltered sulfides precipitated from sea water (i.e., at low temperature). Even five decades ago, BSR was thought to be responsible as the original source of sulfide. Light sulfur and carbon isotope compositions (of sulfides and carbonates, respectively) is reported as evidence for BSR within a closed, or partly closed, system (Wedepohl *et al*., 1978).

Syndepositional precipitation of the copper and zinc would require the paleo-sea water to contain high metal concentrations compared to present-day sea water chemistry, especially if there was sulfide production resulting from bacterial activity near the sediment-water interface. The exchange of Cu, Pb, and Zn between anoxic and oxic waters would have been critical to bolster, and maintain, metal concentrations.

Wedepohl *et al*. (1978) argue against a late diagenetic or epigenetic mineralization on the grounds that the sulfur isotope characteristics did not support the idea of solutions reacting with early diagenetic pyrite, and that large volumes of water would need to flow through the thin, fine grained unit. These

issues might be reconciled with the presence of a metal-rich brine, though Wedepohl *et al*. (1978) think that it would not account for the paleogeographical zonation of the mineralization or the widespread mineralization as opposed to localized "channels" resulting from the fluid flow. Wedepohl *et al*. (1978) cite the preservation of clay carbonate banding, the small grain size of the sulfides, and the lack of benthic fossils as an indicator for anoxic bottom waters, as further evidence against mineralization being a result of epigenetic mineralization.

Evidence for late mineralization includes the presence of disseminated sulfides, massive sulfides acting as cementation within the Weissliegend, the ore-mineralization that is well-separated both spatially and isotopically, and varied types of mineralization such as veins, disseminated, and massive sulfides (Michalik and Sawłowicz, 2001).

At least within the Sangerhausen Basin, Germany, some authors suggest that mineralization occurred through multiple stages: syndepositional framboidal pyrite was formed with the assistance of BSR and later replaced during diagenesis by Cu/Fe minerals and chalcocite (Sun and Püttmann, 1997). Sections with high copper mineralization (>8%) resulted from pyrite replacement followed by thermochemical sulfate reduction (TSR), and is indicated by the associated pyrobitumen and sparry calcite.

A study of noble metals (Au, Pt, Pd) in the Lubin mining district, Poland, found evidence for noble metal mineralization after Cu mineralization had taken place (Kucha and Przybyłowicz, 1999). The two types of mineralization are also separated spatially, as the noble metals are present in a separate horizon, lower than the Cu mineralization. The authors hypothesize that a downward excavating hydrothermal cell existed, and as it travelled deeper the waters would have become hotter, allowing for differences in the metal load carried by the fluids. Kucha and Przybyłowicz (1999) also propose that the redox boundary shifted upward and downward approximately four times, resulting in an increase in ore grade and the introduction of new metals. It is also possible that this shifting of the redox boundary could have resulted in the relocation of minerals and metals previously precipitated.

### 2.4.3 Small Scale Processes

Another subject of contention in literature pertaining to the mineralization system is what small scale processes were the most influential in mineralization/precipitation. Bacterial sulfate reduction (BSR) (Michalik and Sawłowicz, 2001), thermochemical sulfate reduction (TSR) (the association between oxidized organic matter and the precipitation of the sulfides due to thermochemical sulfate reduction) (Bechtel, Sun, *et al*., 2001), and pyrite replacement (the replacement of pyrite by Cu-Fe-sulfides during diagenesis) have all been put forward as possible mechanisms, with some authors advocating a mix of all three (Bechtel, Sun, *et al*., 2001).

It is possible that the bacteria had an influence on the development of the smaller (<1μm) mineral precipitates, though it would be almost impossible to discern if the sulfides had formed in the presence of the bacteria or not (Konhauser, 2007). It may be that BSR was more important for producing the reducing conditions, while the actual controls on copper isotope fractionation were abiogenic (i.e., changes in chloride activity where higher values allow Cu(I) species to become more dominant components of the brine solution) (Asael *et al*., 2009). Sulfur isotope studies indicate that BSR took place during a transition from an open system to a closed system (Sawłowicz, 1989). At the very least, BSR aided in mineralization by providing a source of sulfur (Sawłowicz and Kosacz, 1995).

Thermochemical sulfate reduction (TSR) may be responsible for up to 12% of Cu enrichment, while pyrite replacement likely accounts for less that 8% of Cu enrichment (Sun and Püttmann, 2000). As long as pyrite was present to supply sulfur, TSR would not have been the most significant metal-fixing process (Oszczepalski *et al*., 2002); instead TSR would have acted as an alteration process, induced when oxidizing fluids travelled through the unit after the main copper mineralization event. It is thought that pyrite replacement is the consequence of interaction between rising fluids and carbonates in the Kupferschiefer, resulting in a fluctuation of the pH levels and thus the destabilization of pyrite. This allowed for the replacement of pyrite with chalcopyrite and bornite (pH 3-5), and later with chalcocite, galena, and sphalerite (pH 5+) (Wedepohl and Rentzsch, 2006).

### 2.4.4 Temperature

Studies of organic matter show that mineralization temperatures were most likely at or below 130˚C (Sun *et al*., 1995). Further evidence for low temperature mineralization includes the presence of sulfur-rich bornite, which will exsolve chalcopyrite at temperatures above 75˚C in most situations, and the presence of orthorhombic chalcocite, which is only stable to temperatures of 103˚C. Textural evidence for low temperatures of formation include the preservation of cell structures in plant material that has been replaced by mineralization; this is a strong indication that the mineralization took place before the sediment was buried deep enough that it would have crushed the cells of the organic matter (Rose, 1989). There is also a lack of evidence for hydrothermal alteration or recrystallization within the Kupferschiefer mineralization, which otherwise would have indicated temperatures in the range of 100 to 150˚C. Rose (1989) claims the temperatures could have been as low as 25˚C.

## 2.5 Fluids

While there is a lot of disagreement in the literature about exactly when and how the mineralization in the lower Zechstein sediments formed, there is a general consensus that the sulfides could not have come solely from precipitation from seawater during deposition (Hirst and Dunham, 1963; Wedepohl, 1965). Pore water composition would originally have been derived from sea water (Jowett, 1992), but Wedepohl (1965) estimated that, at most, 0.1% of the mineralization could be accounted for solely from seawater precipitation. At least some of the water was meteoric, as indicated by oxygen isotope geochemistry (Hammer *et al*., 1990; Bechtel *et al*., 2000). The flow of meteoric water from the Rotliegend to the Kupferschiefer would have lasted until late diagenesis, and travelled through fractured zones. Local metal accumulation probably resulted from high flow rates and long circulation times, as the fluids would not have been able to flow through the Kupferschiefer over distances on the order of kilometers (Hammer *et al*., 1990).

It is estimated that approximately 80% of copper in solution would have occurred in the form of $CuCl_3^{2-}$ complexes (Asael *et al*., 2009). Aside from the minerals leached from Lower Permian redbeds, ore metals could have also been provided by hydrothermal sulfide mineralization in early Permian

volcanics, Variscan granitoids, crystalline Permian basement rocks, and metamorphosed Carboniferous rocks (Oszczepalski, 1989). This mix of sources was necessary to form the ore-grade deposits in the Kupferschiefer; any single source would not have provided enough metal to do anything beyond slightly increasing the concentration or influencing the localized deposition.

Hirst and Dunham (1963) caution against hydrothermal mineralization as the sole source of the mineralization due to the very large scale of the Kupferschiefer/Marl Slate unit. While there is similar mineralization in the areas where the Kupferschiefer has been studied (i.e. England, Germany, Poland), not all of these locations underwent the same tectonic influences. This is important to note because the tectonic activity and associated processes, such as hydrothermal mineralization, that might be responsible for mineralization in some locations may not have occurred in all of the mineralized sections of the unit; therefore this mechanism cannot be cited as the sole cause of mineralization. At least within the Polish basin, however, the presence and migration of hydrothermal fluids could help to explain the location and degree of mineralization; there appears to be an association between increased amounts of mineralization and higher geothermal gradients (Kucha and Pawlikowski, 1986). Hirst and Dunham (1963) favor the hypothesis that, during sedimentation, there were occasional submarine springs that introduced the metals to the system. A similar hypothesis is put forward by Blundell *et al*. (2003), with mineralization in the Lubin copper district thought to be a result of multiple short pulses of fluid, delivered to the area through the injection of hot brine into a fault-fracture system.

There are hypotheses of multistage formation which involve a combination of salt diapirism, tectonics and or thermal activity driving fluid flow, along with natural hydro-fractures from hydrocarbon generation and faults that allowed the fluid to migrate upwards through otherwise impermeable rock (Jowett, 1992; Wagner *et al*., 2010). The mix of tectonic, geothermal, and seismic activity could account for the fluid flow in Poland; the Mansfeld-Sangerhausen area is underlain by thin crust, which could have allowed for sufficient heat flow to mobilize the fluid and account for the localized mineralization found there (Blundell *et al*., 2003). The presence and thickness of the Rotliegend may also be significant, since the fluids might have been geochemically altered after migrating through the unit (Sverjensky, 1989) and

this in turn could have a direct influence on the grade of the resulting deposits. Finally, the influence of paleogeography on fluid migration should not be neglected (Speczik, 1995), as this may have played an important role in exactly where and how the fluid moved through some units and eventually up into overlying units. The importance of the presence of the Rotliegend deposits is illustrated in part by the fact that chalcocite, bornite, and chalcopyrite mineralization with more than 0.5% Cu is only found in small regions underlain by large volumes of Rotliegend rocks (Wedepohl, 1994). The presence of underlying volcanics may also be significant, as Glennie (1989) notes that the Marl Slate does not exhibit ore grade mineralization, and volcanics are absent under this section of the unit. It is possible that a portion of the Cu in the Kupferschiefer could have come directly from the underlying Rotliegend (Walker, 1989). However, no correlation has been observed between differences in mineralization and the porosity of the strata underlying the Kupferschiefer (Wedepohl *et al*., 1978).

The chemical composition of a hot brine coming up from underlying units would have exhibited variations region to region, due to regional differences in composition of the basement (Kucha and Pawlikowski, 1986). However, it is generally agreed that the oxidizing brines that carried the metals which precipitated out and formed the ore deposits were enriched in Na, sulfate (Bechtel and Püttmann, 1991), and Cl (Michalik, 1997). Warren (2000) proposes that overlying salt could be the source of the Cl brines.

Most formation hypotheses put forward by previous authors deal with how the presence of a redox front is important in facilitating metal precipitation. The processes either involve an oxidized fluid coming into contact with the reduced Kupferschiefer, or interaction between two brines. The mixing of two different brines would have most likely involved an unmineralized cold, reducing brine from the unlithified overlying evaporites, rich in Na, Ca, Cl, $SO_4$, with a pH greater than 7. The other fluid would have been a warm, oxidized brine from underlying sediments in the center of the basin, rich in Mg, K, Cl, $SO_4$, $CO_3$, with a pH of 7 or below (Kucha and Pawlikowski, 1986; Oszczepalski, 1989). During the migration of the lower hot brine, the fluid would have leached metals from the underlying units. Kucha and Pawlikowski (1986) propose that the mixing of the fluids on their own would have been enough to

result in economic levels of mineralization, but the additional presence of the shale lower boundary added extra components, such as the concentrations of noble metals. Ultimately, the black shale (Kupferschiefer) would be required for mineralization because the two brines could have been similar enough in composition that they would have needed the decaying organic matter to act as an electron donor (Kucha and Pawlikowski, 1986).

The oxidizing fluid thought to have originated in the underlying volcanic rocks or early Permian Rotliegend, perhaps in part from the formation waters of that unit, could be the source of the Rote Fäule (Bechtel, Ghazi, *et al*., 2001; Hitzman *et al*., 2010). Isotope geochemistry analyses of the Rote Fäule carbonates indicate that different redox conditions prevailed during both sedimentation and diagenesis (Hammer *et al*., 1990). Isotopic evidence was found in samples taken near the Rote Fäule for upward migration by the oxidizing brine into the Kupferschiefer (Bechtel and Püttmann, 1991). Oszczepalski *et al*. (2001) also found evidence for the presence of an ascending ore fluid: decreases in Hydrogen Indices, $C_{org}$, bitumen, and liptinite contents, and the low concentration of base metals within the oxidized rocks. The redox boundary would have migrated upward as the mineralization process continued, gradually increasing the size and grade of the ore deposits until the circulation stopped. The transition zone marks the final location of the oxidation front (Oszczepalski *et al*., 2001). When the relatively oxidized fluid reached the Kupferschiefer, the marly shale acted as a geochemical trap and assisted in the precipitation of metals from the migrating fluids due to the presence of organic carbon, which facilitated redox reactions (Bechtel and Püttmann, 1991). Abundant basement highs and a corresponding thinning or pinching out of the underlying redbeds would cause the fluids coming from the underlying units to be over-pressured in these locations and much more likely to interact with the overlying Kupferschiefer (Hitzman *et al*., 2010). This would help to explain why mineralization is found almost exclusively along the paleo-coast of the Zechstein Sea.

Fluid flow was initiated by tectonic activity during the Triassic; fluids would have been delivered to the basin in numerous short pulses, along fractures that were opened and pinched closed multiple times as a result of seismic activity. This allowed brine to enter the voids, and later be expelled upward into the

overlying Rotliegend sandstone and Kupferschiefer shale. Theoretically, multiple expulsion events would move the amount of water needed to deposit the volume of copper found in the Polish basin section of the Kupferschiefer (Borg *et al*., 2002). Blundell *et al*. (2003) estimate that fluid could be moved through the basin about 63m/year, driven by earthquakes in the area. Flow from each earthquake would last approximately a year, totaling $0.07m^3$ of fluid. Using 100-200 year intervals for the earthquakes (an average of 7,000/Ma), this could move $6{,}000km^3$ of fluid over the course of 12 Ma. If the copper concentration was about 60 ppm within the fluid, then these calculations would be sufficient to account for the mineralization seen in the SW Polish basin. Jowett (1986) calculates that with a convection velocity of 13cm per year, aided by rifting, a copper solubility of 1,000mg/kg, and 20-30% Ca-Na-Cl brines, the Lubin deposit could be formed over the course of 6 million years. If fracture permeability and a solubility of 300 mg/kg is used, less than 10 million years would be needed. This would call for 20 or more cycles of convection. The difference in thermal conductivity of the shale basin centers compared to the basement highs would have created the needed temperature gradients to drive convective fluid flow; the rifting would have given the flow the needed velocity to form the ore deposits (Jowett, 1986).

Mineralization zones usually dip away from paleo-highs towards the basin centers, suggesting convecting fluid flow as opposed to through-going flow through the basin (Jowett *et al*., 1987). Schmidt Mumm and Wolfgramm (2004) argue that the Kupferschiefer Cu-Ag deposits were formed from unicellular convection during the Triassic, with flows following changes in basement topography, and that the deposits could have formed in 5 to 10 million years. Convection cells would have been initiated by differences in thermal conductivity between basement highs and basin lows, and the increased tectonic strain and thermal activity during Triassic rifting, associated with the opening of the Tethys ocean, would have increased rates of convection and aided in ore formation. Up to 4 unique fluid phases are responsible for the mineralization in Germany, two of which took place during the Permian (Schmidt Mumm and Wolfgramm, 2004) and some of which may have partially overlapped (Bechtel, Sun, *et al*., 2001). The recirculation of fluids would have allowed multiple instances of dissolution and precipitation of copper (Cathles III *et al*., 1993). Oszczepalski *et al*. (2002) argue against convective flow, as there

does not appear to be any isotopic evidence for downward fluid flow; if the fluids were migrating during basin compaction then it would have been unlikely for the fluids to travel back down into the sediments as available pore space was decreasing (Oszczepalski *et al*., 2002).

Faults would have helped to focus the rising hydrothermal fluids, and thus the sulfides that precipitated as a result of the mixing of hydrothermal fluids from the crystalline basement with the groundwater (Jowett, 1992; Wagner *et al*., 2010). Migration could have been caused by geothermal gradients, extensional tectonics, basement configuration, block faulting concurrent with sedimentation, zones of crustal weakness (Oszczepalski, 1989). Short pulses of fluid flow could have been delivered to the area through the injection of hot brine into a fault-fracture system, and moved along by coseismic strain involving the closing of the fractures and forcing the fluid into the overlying aquifer, in this case the Rotliegend (Blundell *et al*., 2003). The presence of the Zechstein evaporites may have been important during fluid migration driven by hydrothermal convection and rifting preceding the uplift of the Harz Mountains, as the evaporite units acted as a seal. This may have been especially important because the ductile nature of the evaporites would have aided in the maintenance of the seal during basin subsidence (Schmidt Mumm and Wolfgramm, 2004).

### 2.6 Carbon/Organics/Hydrocarbons

The presence of organic matter in the Kupferschiefer is important as it could have played a role in the accumulation, preservation, and redistribution of sulfides. Hirst and Dunham (1963) put forward the idea that metals would have been adsorbed onto the organic carbon, thus fixing them so that they remained throughout the process of sedimentation and any alteration of the carbonates. The conversion of the metals to sulfides would have occurred later. Organic matter is thought to be responsible for aiding the precipitation of metals from the ascending brines through the process of thermochemical sulfate reduction, by serving as a proton donor for TSR (Bechtel, Sun, *et al*., 2001). Hydrogen sulfides generated by the hydrocarbons can also aid in the precipitation of the ore (Poplavko *et al*., 1977). Metals such as V, Ni, and noble metals can occur within organic matter as organometallic complexes, and positive correlations have been found between mineralization and total organic carbon (TOC) (Sawłowicz, 1991).

Matlakowska *et al*. (2010) shows that the organic material in the Kupferschiefer could be used by indigenous bacterial strains as a source of energy (and carbon); the growth of the bacteria resulted in chemical and textural changes to the black shale, including the release of metals from organometallic compounds. Knowledge of such bacteria could have important implications for mining from organic-rich metal-bearing black shales like the Kupferschiefer, including better metal recovery from the host rock, and bioremediation of resulting copper tailings (Matlakowska and Sklodowska, 2010).

Organic matter also assists in the determination of the depositional environment. In the case of the Sangerhausen Basin, the organic facies indicate deposition in a normal marine and euxinic environment. This differs from samples taken from Kupferschiefer locations near the Konrad and Polkowice mines, where the depositional environment is thought to have been anoxic (Sun, 1998).

Kerogen from Konrad, Polkowice, and Sangerhausen mines belongs to algal type II, though some has been altered to type III by secondary oxidation (Sun, 1998; Kotarba *et al*., 2006; Nowak, 2007). In Rudna, kerogen from the Kupferschiefer is type I-II (Sun *et al*., 1995). Hydrocarbon generation would have occurred after the burial of the deposits, which occurred from the late Permian through to the Cretaceous, during the middle Triassic to late Jurassic (Kotarba *et al*., 2006). The volume of hydrocarbons produced would be limited by the thickness of the Kupferschiefer, and thus most likely negligible. Kotarba *et al*. (2006) assert that while the Kupferschiefer would not be a source rock, it could act as a seal for gas hydrocarbons produced by the limestone and Rotliegend; Nowak (2007) disagrees, and comments that the Kupferschiefer can be regarded as a source rock for hydrocarbons.

### 2.7 Rare Earth Elements

A study by Sawłowicz (2013) looks at the geochemistry of samples from the Rote Fäule, Weissliegend, Kupferschiefer, and Zechstein limestone, taken from the Lubin-Glogow mining district in Poland. The author notes that the Weissliegend samples have strongly convex rare earth element (REE) patterns (i.e. middle REE (MREE) enriched), with positive Eu and negative Gd anomalies. The MREE enrichment is described as a light REE (LREE) depletion, with MREE enriched relative to heavy REE (HREE) (Sawłowicz, 2013). The shale and limestone samples have relatively flat REE patterns compared

to the sandstone samples, and strong negative Eu anomalies. The shales also exhibited small positive Gd anomalies. Shales from within the Cu and Pb zones exhibit MREE enrichment, but while Cu-rich shales contain weak negative Eu anomalies, shales from the Pb zone are unique from the other shales and the overlying dolomites in that they exhibit positive Eu anomalies. This difference in Eu anomaly may be the result of more oxidizing conditions during the deposition of the Pb-shales (Sawłowicz, 2013). Shales from the Zn zone exhibit flat REE patterns and strong negative Eu anomalies. Overall, the highly mineralized section shows stronger negative Eu and positive Gd anomalies, and the shale samples from this section show slight MREE enrichment. Sawłowicz (2013) notes that the transitional zone, between the Rote Fäule and the highly mineralized zones, exhibit strong MREE enrichment and no Eu anomaly compared to the mineralized shale.

While source rocks and/or depositional environment likely had some degree of influence on the REE composition, the author rules out the possibility of very strong influence of these factors on account of the small area of the study (i.e. the Lubin mining district) and the short period of Kupferschiefer deposition; a change in source rocks for such a small area and/or over a relatively short period of time is unlikely. Therefore the variation in REE patterns must be the result of diagenetic processes, possibly associated with the ore mineralization and oxidation. Sawłowicz (2013) hypothesizes that the relatively high REE contents in the lower section of the Kupferschiefer are the result of the upward migration of fluids from the Rote Fäule though the Weissliegend and into the Kupferschiefer. The author puts forward the idea that the higher HREE contents of the Weissliegend samples could be the result of greater concentrations of heavy minerals (i.e. garnet and zircon). It is also suggested that the presence of detrital and authigenic feldspars could have an influence on REE patterns, particularly (positive) Eu anomalies. The Eu anomalies observed in the Weissliegend samples could be the result of interaction between feldspars and migrating hydrothermal fluids (Sawłowicz, 2013).

A study by Bechtel, Ghazi, *et al.* (2001) also found relatively high REE concentrations in the Rote Fäule and transition zones. The authors hypothesize that the REEs were carried in the oxidizing fluids that formed the Rote Fäule, or that the REEs could have originally been within the shales and were

simply remobilized by the migration of oxidizing brines. The presence of Eu and Ce anomalies that differ from those expected to result from deposition in an anoxic environment suggests that REE redistribution during the formation of the Rote Fäule (Bechtel, Ghazi, *et al*., 2001).

# CHAPTER 3 - METHODS

## 3.1 Field Work

Kupferschiefer and Weissliegend samples (n=101) used in this study were collected from locations in Germany and Poland (Figure 2.6). The German samples (n=61) were taken from the Sangerhausen Basin, and obtained through two means. Hand samples were collected from the Röhrig shaft of the Wettelrode mine, which is now the Röhrigschacht Mining Museum. Samples were also obtained from cores currently housed at Landesamt für Geologie und Bergwesen Sachsen-Anhelt in Halle, originally taken from multiple locations within the Sangerhausen Basin (Figure 3.1). Sample collection from the mine and cores was such that the entire thickness of the Kupferschiefer was collected, and some of the lower Zechstein Limestone is included in the samples described and analyzed in this thesis. Approximate latitude and longitude locations for the German core locations are as follows: SGH133: 51°24'29.68" N, 11°25'19.18" E; SGH132: 51°20'19.60" N, 11°17'37.90" E; E-27: 51°27'34.74" N, 11°14'12.26" E; and SGH103: 51°24'40.37" N, 11°24'19.53" E. It should be noted that core locations are estimated, as they were triangulated from the map shown in Figure 3.2 in conjunction with Google Earth software. Polish hand samples (n=40) were collected from the Lubin and Rudna mines (Figure 3.2) from the Lubin mining district. Two stops were made at each mine, resulting in 4 locations: Lubin stop 1, Lubin stop 2, Rudna stop 1, and Rudna stop 2. These locations are referred to in the text and charts as Lubin 1, Lubin 2, Rudna 1, and Rudna 2. The entire thickness of the Kupferschiefer was not collected from each of the Lubin mining district locations.

Samples are labeled according to the order in which they were collected, as well as in relation to their stratigraphic distance from the basal contact of the Kupferschiefer. Positive values after the sample number indicate the distance, in centimeters, above the basal contact of the Kupferschiefer; these samples are therefore located within the bounds of the Kupferschiefer or the overlying Zechstein Limestone. Negative values indicate the distance below the contact, and are thus located within the underlying Weissliegend, or in the case of two samples from Lubin 2, within the Boundary Dolomite. The positive

or negative value following the sample number corresponds to the distance of the *center* of the sample from the basal Kupferschiefer contact. It should be noted that, especially with the longer core samples, the thin section and geochemical data from the same sample may not have come from the center, and may therefore be a few centimeters away from not only each other, but also the location recorded by the sample number. For example, sample K40+8 from core SGH132 is 12 centimeters long, and thus encompasses a range approximately 2 to 14 cm above the basal contact of the Kupferschiefer; geochemical analyses were performed on a section taken from 8 to 9 cm above the contact, and a thin section was produced from a section ranging from 9.5 to 11 cm above the contact.

It should be noted that the samples are largely referred to in this thesis according to their location (mine or core) and depth. Tables of geochemical data include the location, depth, and sample number.

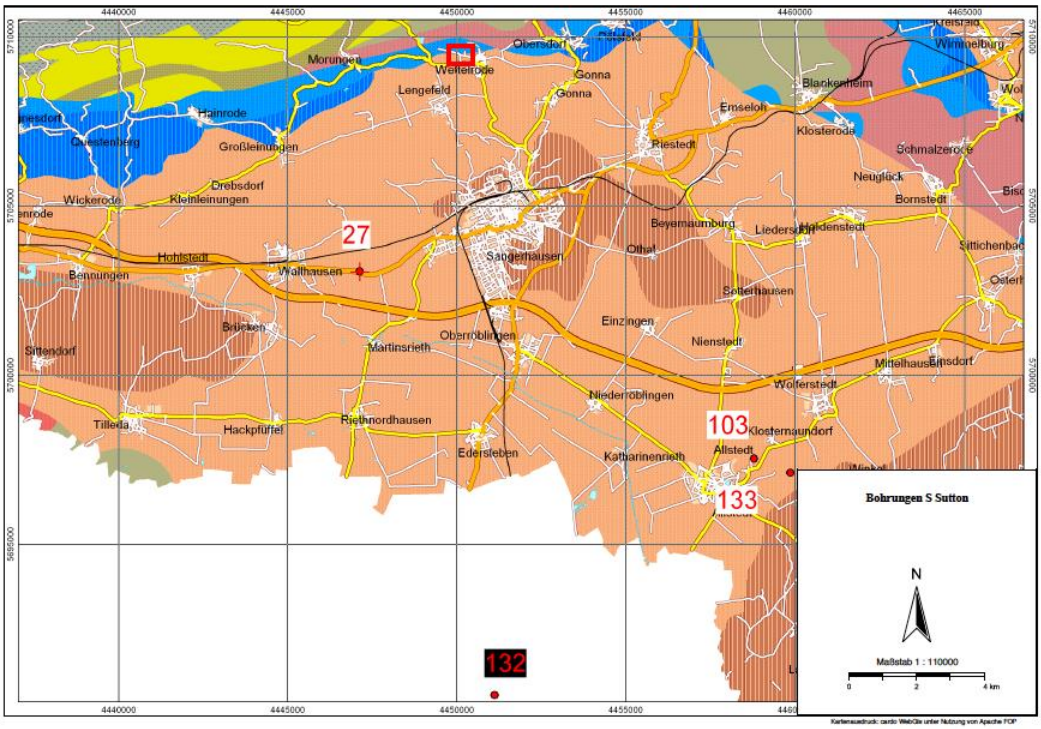


Figure 3.1 Detail of the German Kupferschiefer sample locations, as indicated by the box labeled "Sangerhausen Basin" in Figure 2.5. Location of the Wettelrode Mine, now the Röhrigschacht Mining Museum (red box). Locations of all core samples from the Sangerhausen Basin, Germany: E-27, SGH103, SGH133, and SGH132.

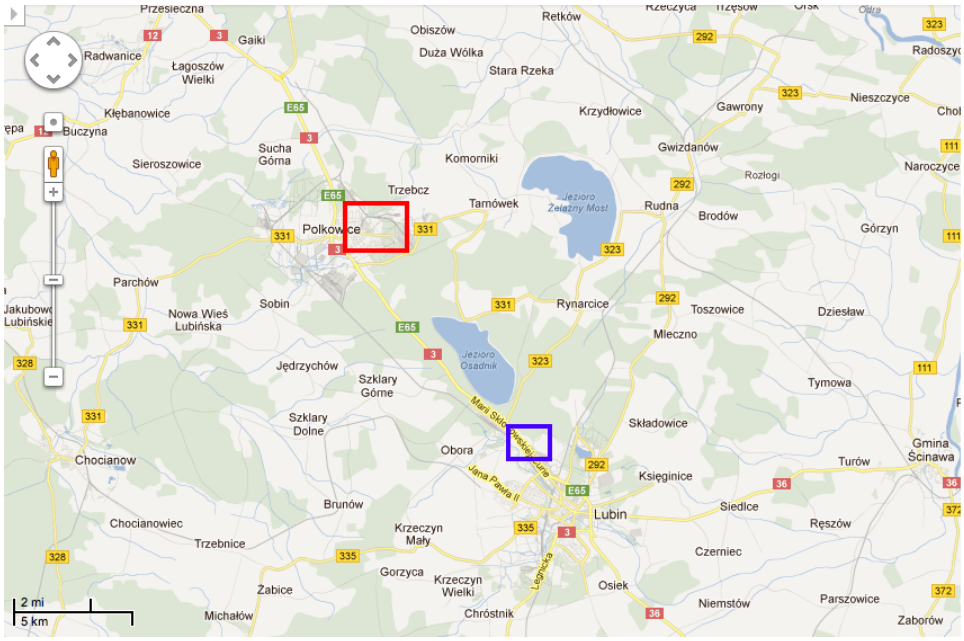


Figure 3.2: Detail of the Lubin mining district where Kupferschiefer samples were collected, as previously indicated by the box labeled "Lubin Mining District" in Figure 2.5. Approximate locations of the Rudna (red box) and Lubin (blue box) mines are indicated; samples were taken from two locations within each of the two mines. Note the close proximity of the mines.

### 3.2 Lab Work

Rock samples earmarked for thin section and geochemistry (Tables 3.1 and 3.2) were cut to size in the CSU Geosciences rock room. Thin section samples were then sent to Spectrum Petrographics Inc. in Vancouver, Washington, where they were vacuum impregnated with blue epoxy to better identify and differentiate fractures and holes from clear or cloudy minerals, then cut and polished. All samples were stained for carbonate identification using potassium ferricyanide in an acid solution. The compound produces a blue stain when the acid reacts with the carbonate and the potassium ferricyanide encounters ferrous iron. Used in the past to differentiate dolomite from calcite (the former is more likely to contain ferrous iron than the latter), it is now acknowledged that this analysis is not very reliable, as any carbonate mineral that reacts with the acid and contains ferrous iron will exhibit the stain (Dickson, 1965). Seven of the thin sections made from samples taken from the Lubin mine in Poland were also stained with alizarin red [1,2-dihyroxyanthraquinone: $C_{14}H_8O_4$] to aid in calcite identification. This dye stains calcite a pink-

red color, but does not affect dolomite, thus allowing differentiation between the two common carbonate minerals. None of the thin sections have a cover slip.

Samples for geochemistry (n=62) were sent to Activation Laboratories Ltd. (ActLabs) in Ontario, Canada. All samples were analyzed using prep code RX2 and package code 4B1; 37 of those were analyzed with package code 4LITHO-Quant, and 25 of the samples were analyzed with 4Litho. The RX2 simply delineates that all samples were rock samples, and requests sample preparation by crushing to a 1.7 mm mesh, mechanical splitting (using a riffle machine), and pulverizing with mild steel.

The 4Litho code (Lithium Metaborate/Tetraborate Fusion - whole rock ICP and trace element ICP/MS) indicates a suite of analyses for lithogeochemistry. Elements analyzed include: Ag, As, Ba, Be, Bi, Cd, Ce, Co, Cr, Cs, Cu, Dy, Er, Eu, Ga, Gd, Ge, Hf, Ho, In, La, Lu, Mo, Nb, Nd, Ni, Pb, Pr, Rb, S, Sb, Sc, Sm, Sn, Sr, Ta, Tb, Th, Tl, Tm, U, V, W, Y, Yb, Zn, Zr; $SiO_2$, $Al_2O_3$, $Fe_2O_3$(total), MnO, MgO, CaO, $Na_2O$, $K_2O$, $TiO_2$, $P_2O_5$. The fused sample was diluted and then analyzed along with three blanks and a total of five controls: three of which were analyzed before the sample, and two afterwards. The instrument used for analysis was a Perkin Elmer Sciex ELAN 6000, 6100 or 9000 ICP/MS, which was recalibrated after every 40 samples.

Code 4B1 lowers the detection limit for base metals Cu, Ni, Pb, and Zn, in addition to providing the detection of S and Cd. Using this method, the sample (0.25 grams) was digested with four different acids: hydrofluoric, a mixture of nitric and perchloric acids, and hydrochloric acid. After the digestion with the first three acids, the sample was heated until dry. Dryness is achieved by heating over the course of multiple ramping and holding cycles that are precisely controlled by a programmer. The hydrochloric acid was then used to bring the sample back into solution. ActLabs warns that this digestion process may only partially solubilize certain minerals, such as: zircon, monazite, sphene, gahnite, chromite, cassiterite, rutile, and barite. High concentrations of silver (>50 ppm) and lead (>5,000 ppm) could potentially reprecipitate, so a different analysis method may be required, and it is noted that only sulphide sulfur will be solubilized. Quality control was assured through the use of certified reference materials, or similar in-lab standards. The instrument used for analysis of the samples was a Varian Vista 735 ICP.

Code 4LITHO-Quant was required to obtain quantitative values for chalcophile elements (Ag, As, Bi, Co, Cu, Mo, Ni, Pb, Sb, Sn, W, Zn) within mineralized samples. Samples (1 gram) analyzed using this method were digested using aqua regia, and diluted to a total volume of 250 ml. The equivalent reference materials, which meet international standards, were digested in tandem with the samples. The instrument used for analysis was a Thermo Jarrell Ash ENVIRO II simultaneous and sequential ICP, Varian Vista 735 ICP, or a Thermo 6500 ICP.

The aforementioned elements, this time followed by their detection limits for the geochemical analyses used in this thesis: Ag (0.3 ppm, 0.5 ppm, and 3 ppm), As (5 ppm), Ba (3 ppm), Be (1 ppm), Bi (0.4 ppm), Cd (0.5 ppm), Ce (0.1 ppm), Co (1 ppm and 0.003 %), Cr (20 ppm), Cs (0.5 ppm), Cu (1 ppm, 10 ppm, and 0.001 %), Dy (0.1 ppm), Er (0.1 ppm), Eu (0.05 ppm), Ga (1 ppm), Gd (0.1 ppm), Ge (1 ppm), Hf (0.2 ppm), Ho (0.1 ppm), In (0.2 ppm), La (0.1 ppm), Lu (0.04 ppm), Mo (2 ppm), Nb (1 ppm), Nd (0.1 ppm), Ni (1 ppm and 20 ppm), Pb (5 ppm and 0.003 %), Pr (0.05 ppm), Rb (2 ppm), S (0.001 %), Sb (0.5 ppm), Sc (1 ppm), Sm (0.1 ppm), Sn (1 ppm), Sr (2 ppm), Ta (0.1 ppm), Tb (0.1 ppm), Th (0.1 ppm), Tl (0.1 ppm), Tm (0.05 ppm), U (0.1 ppm), V (5 ppm), W (1 ppm), Y (2 ppm), Yb (0.1 ppm), Zn (1 ppm, 30 ppm, and 0.001 %), Zr (4 ppm); $SiO_2$ (0.01 %), $Al_2O_3$ (0.01 %), $Fe_2O_3$ (0.01 %), MnO (0.001 %), MgO (0.01 %), CaO (0.01 %), $Na_2O$ (0.01 %), $K_2O$ (0.01 %), $TiO_2$ (0.001 %), $P_2O_5$ (0.01 %).

### 3.3 Hand Sample Petrography

Viewing the mineralization in the hand samples is generally facilitated by wetting the surface of the sample with water; in some cases sanding is needed to expose a clean surface. Photos of hand samples were taken using a digital camera (Canon Power Shot SD600) and with a DSLR camera (Canon Rebel Ti3). Some of the core samples from the Sangerhausen Basin required the removal of glue residue from tape used during packing and transportation; this was accomplished through the use of 220- and 150-grade garnet sandpaper and water. Descriptions of the samples were made mostly while the surface of the samples were wet, in order to better observe the features, and occasionally with the assistance of a 10x hand lens. Color descriptions were aided by the use of Munsell® color chips in a Geological Society of America Rock Color Chart.

### 3.4 Microscope Work

Thin section petrography and microlithology was studied using a petrography microscope (which could also be used as a light microscope) [Leica DM 2500 P] with a Clemex Captiva camera [L-Type DCAM, HC L3TP], and a reflecting light microscope [Leica MZ 16]. External light sources were also used [Leica 12V 100 W and NCL 150, respectively].

#### 3.4.1 Thin Section Petrography

Photos of thin sections, under both transmitted and reflected light, were used to aid in the comparison of lithology and geochemistry. Photos were taken using the Clemex Captiva camera attached to the petrography microscope, as well as with a handheld digital camera (Canon Power Shot SD600).

#### 3.4.2 Fluorescence Microscope

Thin sections were examined for the presence of oil and gas using an Olympus BX51 microscope with fluorescence. The mercury vapor lamp provides 330-385 nm excitation. Linksys32 was used for image capture.

Fluorescence in black shales generally results from the presence of hydrocarbons and/or organic matter. The wavelength, or color, of the light depends on the maturity of the hydrocarbons, and not on the reservoir environment conditions or the original source (Riecker, 1962; Chang and Huang, 2008; Zhang *et al*., 2012). The amount of light aromatics compared to heavier hydrocarbons such as aliphatic compounds depends on the length of the migration pathway, and on the abundance of active porous solids. Longer percolation distances and greater abundances of active porous solids will remove more of the fluorescing compounds through adsorbance to rock grain surfaces, and result in a shorter wavelength of fluorescence (Riecker, 1962). As asphaltic and aromatic compounds are removed from the oil, fluorescence shifts from longer wavelengths (reds and yellows) to shorter wavelengths (blue); thus yellow fluorescence generally indicates relatively abundant aromatics, while blue indicates a higher concentration of aliphatic compounds (Riecker, 1962; Zhang *et al*., 2012). Chang and Huang (2008) caution that a single oil cannot be used as a universal indicator of maturity without identification of and comparison to the original oil or kerogen source.

### 3.5 Analytical Methods

For geochemical plots where some samples registered below the detection limit, a line was plotted with the data to represent the detection limit and aid in the identification of samples that fall below the limit. Values of half the detection limit were assigned to the samples that registered below the detection limit; these artificial data points serve as place holders for the sample.

To better determine the composition of the fluids that are thought to be responsible for the mineralization of the Kupferschiefer, element cross plots are presented to illustrate potential associations between concentrations of two elements and between pairs of element ratios. Element by depth graphs are plotted for major, ore, and trace elements, and for ratios of rare earth elements. Rare earth element patterns are also presented, as are plots of REEs and elements by depth, and ratios of LREE and MREE over total rare earth element concentrations. For plots that appear to show a correlation, any possible association between the variables is double checked by fitting a linear regression line and computing an $R^2$ value.

The presence of an Eu anomaly was determined using the standard equation: $Eu/Eu^*=Eu_N/[(Sm_N)(Gd_N)]^{1/2}$. Samples with ratios of Eu/Eu* less than 0.95 were assigned a negative Eu anomaly, and those with values greater than 1.05 are assigned a positive Eu anomaly.

It should be noted that all samples, including sandstone samples, are being normalized to a shale standard for REE analyses.

Table 3.1: List of Sangerhausen Basin hand samples and thin sections.

| Location | Depth (cm) | Sample # | Geochemistry | Thin Section | Stain | |
|---|---|---|---|---|---|---|
| | | | | | Calcite | Ferrous Iron |
| Wettelrode | 54 | K14 | ✓ | ✓ | ✓ | ✓ |
| | 35 | K13 | | | | |
| | 31 | K12 | | | | |
| | 26 | K2 | ✓ | ✓ | ✓ | ✓ |
| | 24 | K3 | | | | |
| | 22 | K1 | | | | |
| | 20 | K4 | | | | |
| | 14 | K5 | ✓ | ✓ | | |
| | 10 | K6 | ✓ | ✓ | | |
| | 8 | K7 | ✓ | | | |
| | 0 | K8 | ✓ | ✓ | ✓ | ✓ |
| | -4 | K9 | ✓ | ✓ | ✓ | ✓ |
| | -13 | K10 | ✓ | ✓ | ✓ | ✓ |
| | -21 | K11 | ✓ | ✓ | ✓ | ✓ |
| | -50 | K15 | ✓ | ✓ | ✓ | ✓ |
| | -95 | K16 | | ✓ | ✓ | ✓ |
| SGH 133 | 62 | K32 | ✓ | ✓ | ✓ | ✓ |
| | 57 | K31 | | | | |
| | 54 | K30 | | | | |
| | 50 | K29 | ✓ | ✓ | ✓ | ✓ |
| | 47 | K28 | | | | |
| | 43 | K27 | | | | |
| | 40 | K26 | | | | |
| | 37 | K25 | | | | |
| | 33 | K24 | | | | |
| | 29 | K23 | | | | |
| | 25 | K22 | ✓ | ✓ | ✓ | ✓ |
| | 17 | K21 | ✓ | ✓ | | |
| | 8 | K20 | ✓ | ✓ | ✓ | ✓ |
| | 3 | K19 | ✓ | ✓ | ✓ | ✓ |
| | 1 | K18 | | | | |
| | -6 | K17 | ✓ | ✓ | ✓ | ✓ |
| SGH 132 | 79 | K46 | | | | |
| | 67 | K45 | | | | |
| | 55 | K44 | | | | |
| | 42 | K43 | ✓ | ✓ | ✓ | ✓ |
| | 33 | K42 | | | | |
| | 22 | K41 | ✓ | ✓ | ✓ | ✓ |
| | 8 | K40 | ✓ | ✓ | | |
| | 1 | K39 | ✓ | | | |
| | -12 | K38 | ✓ | ✓ | ✓ | ✓ |
| | -32 | K37 | | | | |
| | -43 | K36 | | | | |
| | -55 | K35 | ✓ | ✓ | ✓ | ✓ |
| | -68 | K34 | ✓ | ✓ | ✓ | ✓ |
| | -80 | K33 | | | | |
| E-27 | 38 | K55 | | | | |
| | 31 | K54 | ✓ | ✓ | ✓ | ✓ |
| | 20 | K53 | ✓ | ✓ | ✓ | ✓ |
| | 7 | K52 | ✓ | ✓ | ✓ | ✓ |
| | -4 | K51 | ✓ | ✓ | ✓ | ✓ |
| | -16 | K50 | ✓ | ✓ | ✓ | ✓ |
| | -27 | K49 | ✓ | ✓ | ✓ | ✓ |
| | -36 | K48 | ✓ | ✓ | ✓ | ✓ |
| | -42 | K47 | | | | |
| SGH 103 | 31 | K61 | ✓ | ✓ | ✓ | ✓ |
| | 19 | K60 | ✓ | ✓ | ✓ | ✓ |
| | 7 | K59 | ✓ | ✓ | ✓ | ✓ |
| | -5 | K58 | ✓ | ✓ | ✓ | ✓ |
| | -16 | K57 | ✓ | ✓ | ✓ | ✓ |
| | -28 | K56 | ✓ | ✓ | ✓ | ✓ |

Table 3.2: List of Lubin mining district hand samples and thin sections.

| Location | Depth (cm) | Sample # | Geochemistry | Thin Section | Stain | |
|---|---|---|---|---|---|---|
| | | | | | Calcite | Ferrous Iron |
| Rudna 1 | 50 | K62 | | ✓ | | ✓ |
| | 40 | K63 | ✓ | ✓ | | ✓ |
| | 30 | K64 | | | | |
| | 20 | K65 | ✓ | ✓ | | ✓ |
| | 0 | K66 | ✓ | ✓ | | ✓ |
| | 10 | K67 | ✓ | | | |
| | -10 | K68 | ✓ | ✓ | | ✓ |
| | -25 | K69 | ✓ | ✓ | | ✓ |
| | -130 | K70 | ✓ | ✓ | | ✓ |
| Rudna 2 | 120 | K77 | | | | |
| | 70 | K78 | | | | |
| | 50 | K79 | | | | |
| | 40 | K80 | | | | |
| | 40 | K82 | | | | |
| | 35 | K71 | | ✓ | | ✓ |
| | 20 | K76 | ✓ | ✓ | | ✓ |
| | 20 | K81 | | | | |
| | 10 | K72 | | ✓ | | ✓ |
| | -10 | K73 | | ✓ | | ✓ |
| | -100 | K74 | | ✓ | | ✓ |
| Lubin 1 | 140 | K83 | | | | |
| | 110 | K84 | ✓ | ✓ | ✓ | ✓ |
| | 90 | K85 | | | | |
| | 70 | K86 | | | | |
| | 50 | K87 | | ✓ | | ✓ |
| | 40 | K88 | ✓ | ✓ | | ✓ |
| | 20 | K89 | ✓ | ✓ | | ✓ |
| | 0 | K90 | | | | |
| | x | K91 | ✓ | ✓ | | ✓ |
| | -10 | K92 | ✓ | ✓ | | ✓ |
| | -20 | K93 | ✓ | ✓ | | ✓ |
| | -120 | K94 | ✓ | ✓ | | ✓ |
| Lubin 2 | 120 | K105 | ✓ | ✓ | ✓ | ✓ |
| | 50 | K104 | ✓ | ✓ | ✓ | ✓ |
| | 30 | K103 | ✓ | ✓ | ✓ | ✓ |
| | 25 | K102 | ✓ | ✓ | | ✓ |
| | 20 | K101 | ✓ | | | |
| | 0 | K100 | ✓ | ✓ | | ✓ |
| | BD | K99 | ✓ | | ✓ | ✓ |
| | BD | K98 | ✓ | | ✓ | ✓ |
| | -5 | K97 | ✓ | ✓ | | ✓ |
| | -50 | K96 | ✓ | ✓ | | ✓ |
| | -120 | K95 | ✓ | ✓ | | ✓ |

# CHAPTER 4 - RESULTS

## 4.1 Hand Samples

Examination of Kupferschiefer and Weissliegend hand samples from the five different Sangerhausen locations and four Lubin mining district locations reveals mineralization that is visible with, and occasionally without, the aid of a hand-lens (10x). A few Sangerhausen samples exhibit mineralization coarse enough to view without the sample being wet and/or lightly polished. Samples from the Sangerhausen Basin include the entire thickness of the Kupferschiefer, and some samples higher in the column are from the base of the overlying Zechstein limestone. Sangerhausen Weissliegend samples were taken from depths ranging between immediately below the basal contact of the Kupferschiefer to 95 cm below the contact. Not all locations from the Lubin mining district include the entire thickness of the Kupferschiefer, but the locations that do also encompass the base of the overlying Zechstein limestone. Lubin and Rudna Weissliegend samples were taken from depths ranging between immediately below the basal contact of the Kupferschiefer to 130 cm below the contact.

Mineralization that can be viewed in hand sample, with or without the aid of a hand-lens, is described as "macro" mineralization. For example, macro-disseminated, macro-bleb, macro-framboidal, and macro-aggregate mineralization can be identified in the Sangerhausen samples (Figure 4.1). For the purposes of this thesis, aggregates are generally larger than blebs (compare Figure 4.1 A and B). Disseminated mineralization is in the form of small (less than a mm) spherules or pods. Macro-mineralization is also observed in the form of veins and bedding-parallel horizons.

The "matrix" of a hand sample is commonly one of three types: black, and seemingly featureless (Figure 4.2 A); alternating clay- and carbonate-rich lenses or pods (Figure 4.2 B and D); or an inter-tonguing of light and dark gray material (Figure 4.2 C and D). In the following descriptions, features such as veins or macro-blebs are described as being bedding-parallel or bedding-perpendicular depending on the orientation of the feature in relation to the matrix or bedding (Figure 4.3). For example, a bleb of

mineralization described as being bedding-parallel would have the longer axis parallel to the longer axes of the interlaminated clay- and carbonate-rich pods that make up the rock.

Hand samples are described from the top of the section to the bottom, in reverse order of deposition: Kupferschiefer samples (and possible Zechstein limestone samples) are described before the underlying Weissliegend samples. The sample number is given at the beginning of each description, which includes a unique identifier followed by the depth of the sample in relation to the basal contact of the Kupferschiefer. For example, K14+54 indicates the sample, in this case number 14, was taken 54 cm above the basal contact; K9-4 indicates the sample was taken 4 cm below the basal contact. The sample number is followed by a depth range; in the case of K14+54, which is 8.5 cm thick, the sample encompasses the shale 58.5 to 50 cm above the contact. Sample K9-4 is 7 cm thick, and includes the Weissliegend at the basal contact (0 cm) to 7 cm below the contact. Descriptions for Sangerhausen Basin samples include the hand sample color according to a Munsell® color chart (Geological Society of America). Colors were determined while the sample was dry, unless otherwise noted.

A: 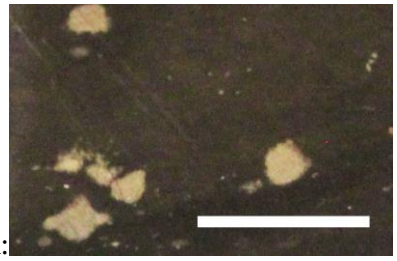 B: 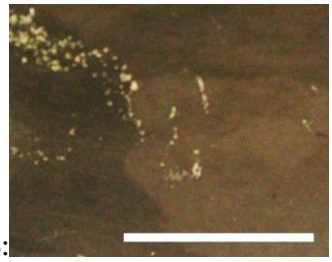 C: 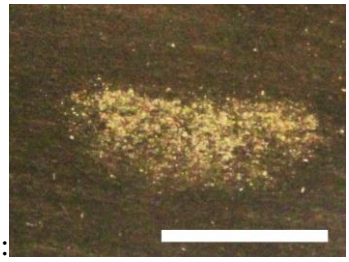

Figure 4.1: Examples of macro-mineralization seen in hand sample. A: macro-blebs and macro-disseminated mineralization; B: macro-framboidal-aggregates; C: macro-aggregate. The white bars measure 1 cm.

A:  B: 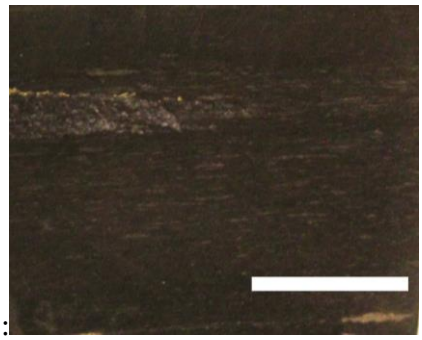

C: 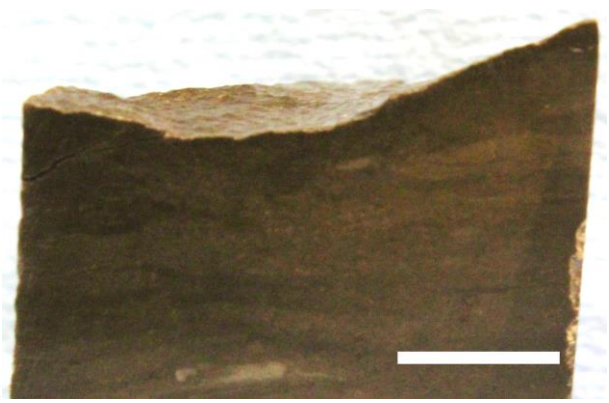 D: 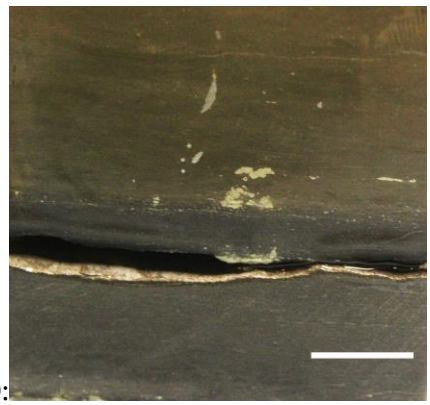

Figure 4.2: Types of hand sample matrix above the contact. A) black, apparently featureless matrix, B) matrix composed of alternating lenses, and C) inter-tonguing grays. D illustrates a shift from alternating lenses (bottom) to inter-tonguing grays (top). The white bars measure 1 cm.

A: 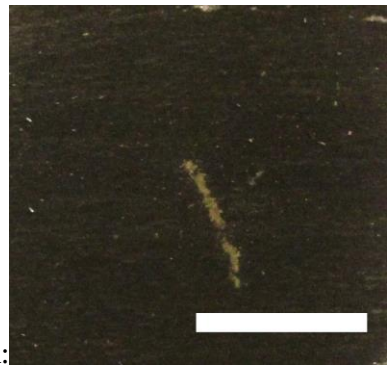 B: 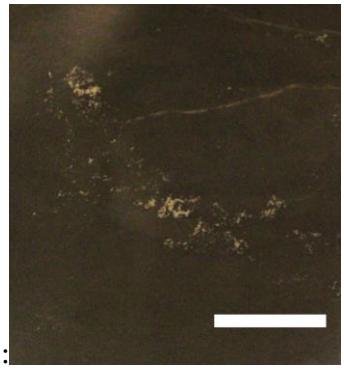 C: 

Figure 4.3: Examples of macro-mineralization A) at an angle to the bedding (bedding-perpendicular), B) mineralization that does not appear to be related to the bedding in any way, C) bedding-parallel mineralization, and a vein at an angle to the bedding. The white bars measure 1 cm.

### 4.1.1 Sangerhausen Basin

**Wettelrode Mine**

**K14+54** (58.5 to 50 cm above the contact) The sample is carbonate-rich; it contains a dolomitic vein with an average thickness of 3 mm, though in one location it is ≥1 cm in thickness. The sample is

medium gray (Munsell® color chart: N5) in color. There is no apparent mineralization, although small black spheres are present, about 0.2 mm in size, which may be sulfides.

**K13+35** (40 to 36 cm above the contact) The matrix is composed of inter-tonguing medium dark gray (N4) and dark gray (N3) material (Figure 4.4). The sample contains small (≤1 mm thick) quartz veins, that are approximately straight, but not bedding-parallel. Most of these veins are at an angle of ~25˚ to 30˚ from the bedding, though a few, which are approximately 0.1 mm in width, are bedding-perpendicular. Mineralization is present as macro-blebs or -aggregates, ranging from <0.5 mm to 4 mm in width. The mineralization color is that of pyrite, though it should be noted that this is simply a comment on the color and not the composition, as a definite identification was not made. Macro-disseminated mineralization is also present in this sample. The bedding is not affected by the presence of mineralization or veins.

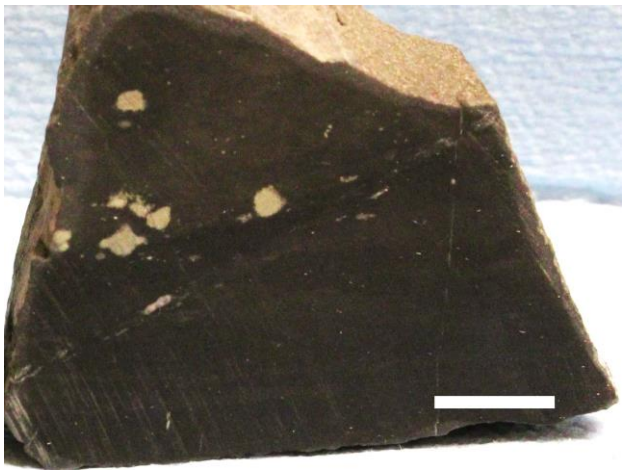

Figure 4.4: Sample K13+35; note the macro-bleb mineralization, the thin, bedding-perpendicular quartz vein on the right hand side, and inter-tonguing of lighter and darker grays on the bottom half. The white bar measures 1 cm.

**K12+31** (36 to 27 cm above the contact) The matrix is composed of fine alternating lenses, averaging dark gray in color (N3). Yellowish mineralization is present in the form of macro-aggregate, macro-blebs, and macro-dissemination. There is a quartz vein, approximately 1 mm thick, that is roughly

bedding-parallel and has smaller veins coming off it that fade out or leave the cut plane. One vein is bedding-perpendicular, and may be a filled fracture.

**K2+26** (27.5 to 25 cm above the contact) The matrix is composed of alternating lenses, dark gray (N3) in color. This sample contains a relatively large carbonate vein, 1 to 6 mm thick (Figure), at an angle of 75˚ to the bedding. Smaller carbonate veins are present as well, one of which is approximately bedding-parallel but wanders in and out of the cross section of the sample. This particular vein is made up of <1 mm-thick segments, present over a total thickness of ~2 mm. The other smaller carbonate vein is present at 80˚ to the bedding, with a thickness of ≤1 mm. This sample exhibits no visible macro-mineralization. The alternating lenses are slightly deformed around the larger, high angle vein.

**K3+24** (25 to 23.5 cm above the contact) No alternating lenses are visible; the sample is dark gray (N3) in color. Macro-disseminated mineralization is present in some areas of the black, carbon-rich matrix; there is no visible macro-mineralization in the gray, carbonate face along one side of the sample, which may be the remnants of a carbonate vein or horizon (Figure 4.5).

Figure 4.5: Left: Sample K2+26; note the thick carbonate vein and the thinner vein to the left. The white arrow points to the vein that appears to wander in and out of the cross section. Right: Sample K3+24; note the difference between the black, carbonaceous piece and the gray, carbonate face of the lower piece. The white bars measure 1 cm.

**K1+22** (23 to 21.5 cm above the contact) No visible alternating lenses or inter-tonguing grays are present; different pieces of this sample are medium dark gray (N4) or dark gray (N3) in color. The sample exhibits macro-disseminated mineralization and possible blebs of carbonate material.

**K4+20** (24 to 16 cm above the contact) This sample has a dark gray (N3) matrix with easily visible alternating lenses of clay- and carbonate-rich material. This sample also exhibits an approximately bedding-perpendicular <0.5 mm carbonate vein, and a bedding-parallel macro-aggregate of mineralization (~18 mm long by 1 to 3 mm thick).

**K5+14** (15.5 to 12 cm above the contact) Alternating lenses are visible in the dark gray (N3) sample. There is a horizon of mineralization (<0.5 mm thick), a discontinuous quartz vein approximately 1 mm thick, and a large carbonate bleb, all of which are bedding-parallel (Figure 4.6).

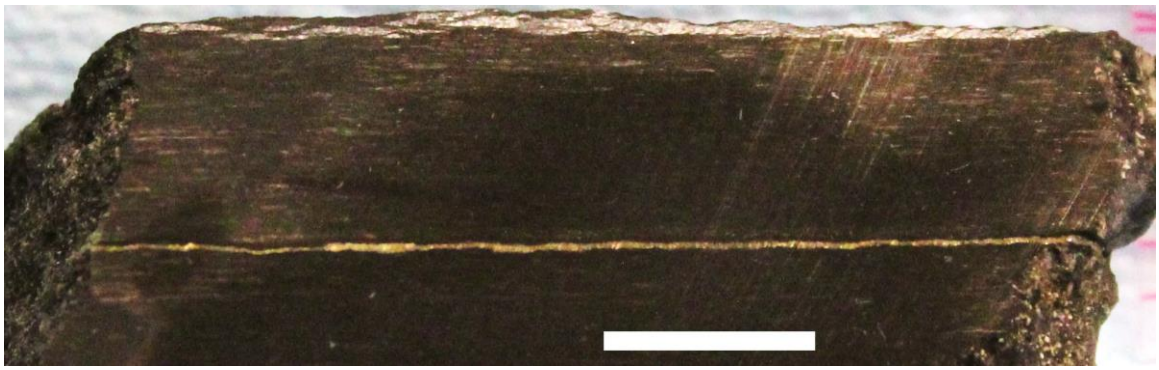

Figure 4.6: Sample K5+14, showing a bedding-parallel horizon of mineralization and, on the top, a "discontinuous" quartz vein. The white bar measures 1 cm.

**K6+10** (11.5 to 9 cm above the contact) The dark gray (N3) sample exhibits faint alternating lenses; in some areas they are difficult to discern. There is a discontinuous, bedding-parallel quartz vein on the top half, and little or no mineralization. In the bottom half of the sample, there is macro-disseminated mineralization as well as a bedding-parallel macro-bleb of mineralization.

**K7+8** (9 to 7.5 cm above the contact) This sample is relatively soft, possibly a result of high organic content, and dark gray (N3) in color. It exhibits macro-disseminated and macro-aggregate mineralization. Alternating lenses and inter-tonging grays are absent; the sample is black, and no minerals are visible to aid in the identification of bedding orientation.

**K8+0** (7.5 to 0 cm above the contact) The matrix is composed of alternating lenses and is dark gray (N3) in color. The base of this sample, close to the basal contact, began to rub off after being wetted

with water and held for observation; this section of the sample is likely very rich in organic matter. Two or three discontinuous, bedding-parallel quartz veins (~1 mm thick) are present. Smaller (≤0.1 mm) veins are observed bedding-perpendicular; some are composed of quartz and others of carbonate. Mineralization is in the form of bedding-parallel lenses or pods (3 mm long and <0.2 mm thick), and macro-disseminated mineralization. Mineralization horizons are also present, some of which are at low angles to the bedding (~10˚) and may be associated with fractures; the other horizons are bedding-parallel. Some mineralization is associated with a quartz vein, and one of the bedding-parallel mineralization horizons has additional mineralization below it in the form of macro-aggregate (Figure 4.7A).

**K9-4** (0 to 7 cm below the contact) The sample is fine grained, pale yellowish brown (10YR 6/2) in color, and exhibits interstitial macro-mineralization. Some of the mineralization is concentrated in what resembles laminations; the concentrations of the sulfides are irregular and discontinuous. The sulfide mineralization decreases in concentration further away from the contact with the Kupferschiefer; after about 3 cm the sulfides gradually peter out (Figure 4.7B).

**K10-13** (7 to 18 cm below the contact) This sample is a fine grained sandstone, pale yellowish brown (10YR 6/2) in color. Some grains of medium coarseness are also present, and appear to be associated with slightly whiter laminations within the sample. Sulfide mineralization in the sample is interstitial-disseminated and does not show any apparent association with the slightly coarser grains that are present.

**K11-21** (18 to 22.5 cm below the contact) The Weissliegend continues to be a fine grained sandstone, pale yellowish brown (10YR 6/2) in color, with a lamination of medium to coarse sand grains. Discontinuous fractures in the sample appear to be associated with slightly whiter sand grains (Figure 4.8). Interstitial "aggregates" of mineralization are present.

A:  B: 

Figure 4.7: A) Sample K8+0; note the discontinuous quartz veins roughly parallel with the matrix, and the horizons of mineralization parallel and at low angles to the bedding. The bedding-parallel horizon of mineralization with macro-aggregate immediately below it is located at the top right of the sample. B) Sample K9-4; note the "laminations" of mineralization near the top of the sample, and the decrease in concentration of the mineralization as depth increases. The white bars measure 1 cm.

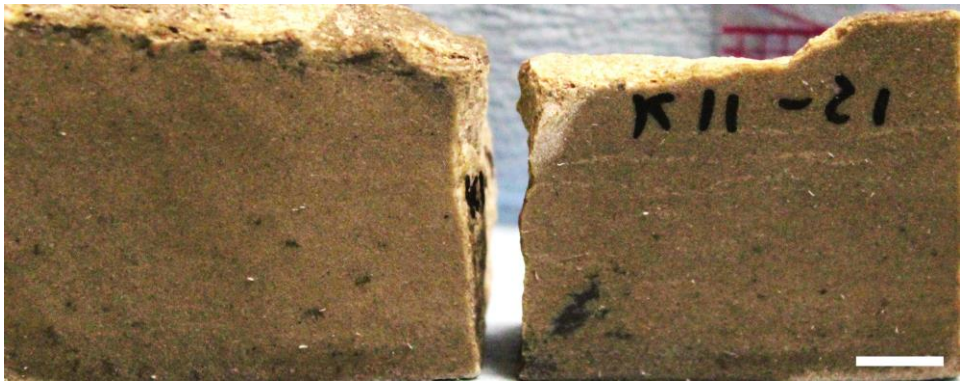


Figure 4.8: Sample K11-21; note the discontinuous fractures associated with whiter sand grains in the right half of the sample. The white bar measures 1 cm.

**K15-50** (48 to 53 cm below the contact) The sample is a moderately-sorted fine to medium grained sandstone, light olive gray (5Y 6/1) in color, that exhibits sulfide mineralization concentrated in three different bands (Figure 4.9). There is approximately 1 cm separating each mineralized band, and all three bands are associated with a lamination of coarser grains; all sulfides are either directly above or

directly below the coarse laminations (no orientation marking is present on the sample to be able to fully determine the relationship). The mineralized bands are not continuous across the width of the sample (~6.5 cm), though the mineralization reaches lengths of at least 3.5 to 6.5 cm before pinching out.

**K19-95** (92.5 to 97 cm below the contact) The sample is a moderately-sorted coarse grained sandstone, light olive gray (5Y 6/1) in color. It contains lenses composed of mud and/or very fine grained sand that measure approximately 4.5 cm long by 0.5 cm (or less) thick (Figure 4.9). These fine grained lenses have sulfides within them.

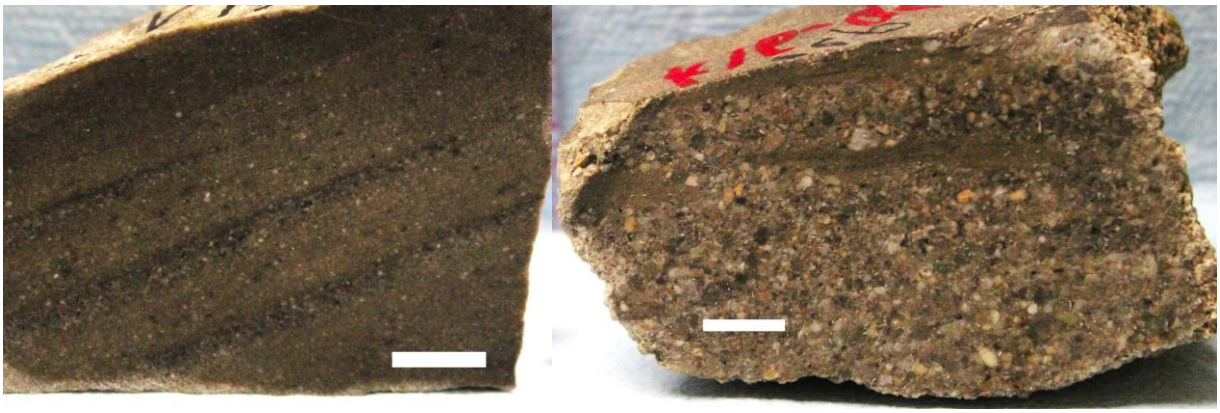

Figure 4.9: Left: Sample K15-50; note the mineralized bands (seen in this sample at an angle due to the cut of the sample). Right: Sample K16-95; note the chips of finer grains in the top half of the sample, and the black sulfide mineralization within. The white bars measure 1 cm.

**Core SGH-133**

**K32+62** (64 to 62 cm above the contact) Alternating lenses and mineralization are not visible in this sample, though there are possible lenses of carbonate or discontinuous fractures; the sample is dark gray (N3) in color. **K31+57** (62 to 56.5 cm above the contact) The medium dark gray (N4) sample shows no visible mineralization or alternating lenses, although inter-tonguing gray lenses are present. When wet, the alternating laminations are grayish black (N2) and dark gray (N3) in color. **K30+54** (56.5 to 52.5 cm above the contact) The medium dark gray (N4) sample has no visible alternating lenses; mineralization is present in the form of macro-dissemination and macro-aggregates. The macro-aggregate mineralization has a framboidal-like character.

**K29+50** (52.5 to 48.5 cm above the contact) The medium dark gray (N4) sample exhibits inter-tonguing grays, which are dark gray (N3) and medium dark gray (N4) when wet. Mineralization is present in the form of macro-dissemination and macro-aggregates. The larger macro-aggregate is ~1.4 cm by 0.5 cm (Figure 4.10).

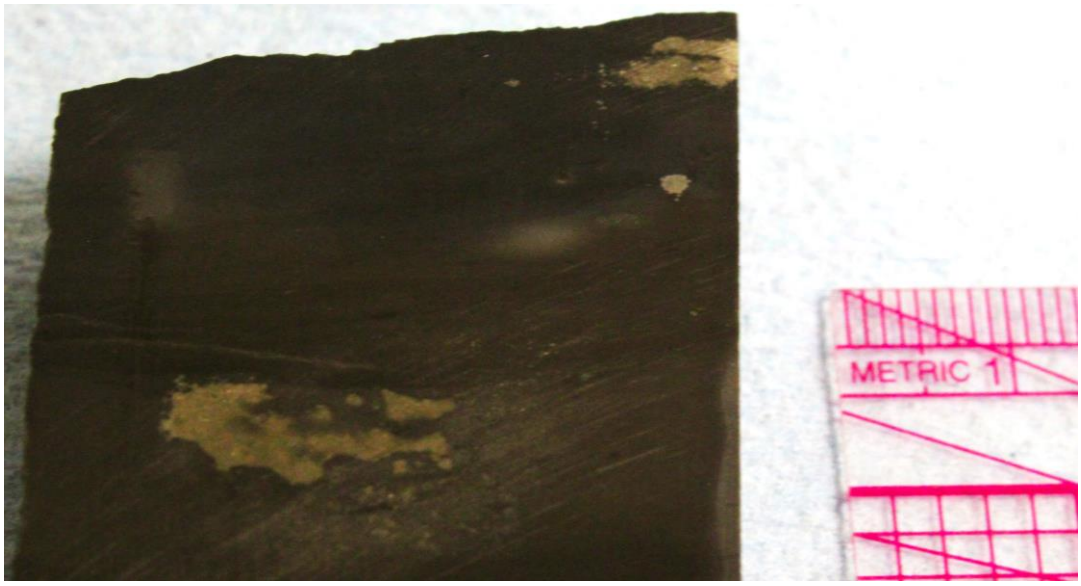

Figure 4.10: Sample K29+50; note the macro-aggregate and macro-bleb sulfide mineralization. The lighter color to the bottom right of the large macro-aggregate is a relic from the cutting of the sample.

**K28+47** (48.5 to 45 cm above the contact) The matrix is composed of inter-tonguing medium gray (N5) and medium dark gray (N4). The sample contains macro-aggregate and macro-disseminated mineralization. Small darker gray blebs (~1 mm long by < 0.5 mm tall) that may be carbonates are present.

**K27+43** (45 to 41 cm above the contact) The sample exhibits inter-tonguing medium gray (N5) and medium dark gray (N4), and mineralization in the form of macro-dissemination and macro-aggregates. Some of the smaller macro-aggregates/blebs have a more silvery center instead of the more common pyrite-yellow color. One macro-aggregate is rimmed by a black material.

**K26+40** (41 to 39 cm above the contact) The matrix of the dark gray (N3) sample is composed of inter-tonguing grays, which are dark gray (N3) and medium dark gray (N4) when wet. In some areas of

the sample, no pattern can be discerned at all within the matrix. Macro-aggregate, macro-bleb, and macro-disseminated mineralization is present.

**K25+37** (39 to 34.5 above the contact) The top of the medium dark gray (N4) sample is a darker, possibly more organic rich band composed of alternating lenses, and below this is a slightly lighter band composed of inter-tonguing grays that are grayish black (N2) and light olive gray (5Y 6/1) when wet. Macro-disseminated mineralization, and macro-aggregates are approximately bedding-parallel (Figure 4.11A). The strongest mineralization is in the darker top portion. Stratigraphically above the darker band is the lightest band found in this sample, possibly a result of a higher concentration of carbonate.

**K24+33** (34.5 to 32 cm above the contact) This dark gray (N3) sample has a top section composed of inter-tonguing grays, and a bottom section that exhibits faint alternating lenses. The inter-tonguing grays are grayish black (N2) and light olive gray (5Y 6/1) when wet. Mineralization is present in the form of macro-blebs and macro-dissemination.

**K23+29** (32 to 27 cm above the contact) The sample exhibits a matrix of alternating lenses and is dark gray (N3) in color. A disseminated quartz vein is present, cutting across the sample at an angle of 25˚ to the bedding (Figure 4.11B). Mineralization is present in the form of bedding-parallel macro-aggregates; macro-dissemination is also present in some areas of the sample.

**K22+25** (27 to 23.25 cm above the contact) The sample shows alternating lenses and is dark gray (N3) in color. A bedding-parallel macro-bleb of mineralization (5 mm by 1 mm) is present.

**K21+17** (20.75 to 13.5 cm above the contact) This sample is dark gray (N3) in color, exhibits a matrix of alternating lenses, and contains a macro-aggregate (4+ cm long by 7+ mm thick) sulfide mineralization.

A:  B: 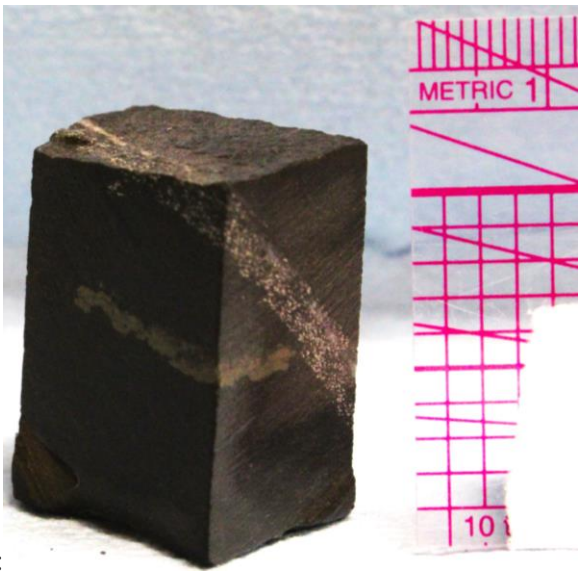


Figure 4.11: A) Sample K25+37; note the change in matrix color at the top and the presence of macro-aggregate mineralization. The white bar measures 1 cm. B) Sample K23+29; note the disseminated quartz vein and the macro-aggregate mineralization.

**K20+8** (12 to 4.5 cm above the contact) The dark gray (N3) sample exhibits alternating lenses, and multiple types of macro-mineralization. There are two bedding-parallel horizons of mineralization about 2.5 cm from each other, both approximately 0.1 mm thick, with macro-bleb/aggregates immediately adjacent to them (Figure 4.12A). Relatively dense macro-dissemination is also present at the bottom of the sample. One of the aggregates associated with the upper mineralization horizon has a small sulfide vein branching off at a 60˚ angle from the bedding.

**K19+3** (3.25 to 2.75 cm above the contact) This sample is dark gray (N3) in color and contains faint alternating lenses, which are occasionally difficult to make out. Mineralization is present in the form of framboidal-like macro-blebs in some areas of the sample.

**K18+1** (2 to 0 cm above the contact) The dark gray (N3) sample has no apparent alternating lamination, and exhibits macro-disseminated mineralization. Small, discontinuous, bedding-parallel fractures are present, and some are filled with sulfides (Figure 4.12B).

**K17-6** (0 to 11.75 cm below the contact) The sample is a poorly sorted conglomerate with sub-angular to sub-rounded grains (Figure 4.13), exhibiting a range of colors from medium (N5) to medium

dark (N4) to dark gray (N3). There is reverse grading 1 to 11 cm below the contact; a sudden decrease in grain size is present 1 cm below the contact, becoming mostly fine- to medium-sand grained, with a few coarse-sand sized grains. No sulfide mineralization is visible.

A: 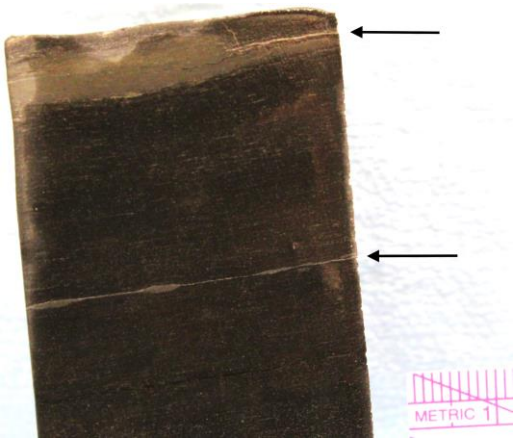 B: 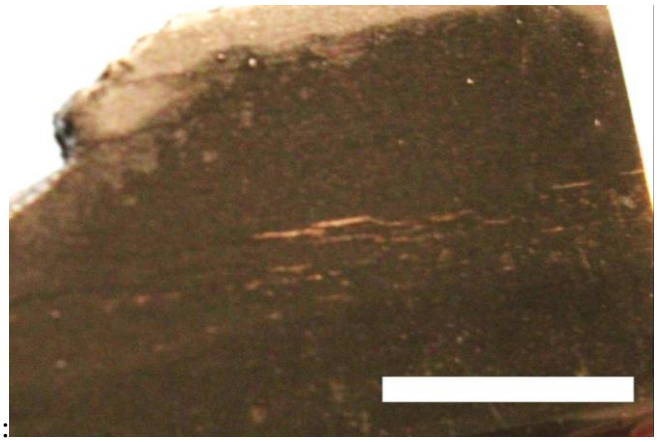

Figure 4.12: A) Sample K20+8; note the two bedding-parallel mineralization horizons indicated by the arrows, and the macro-blebs and macro-aggregates that are directly associated with the horizons. To the right of the macro-aggregate at the top of the sample, the small vein of mineralization at a high angle compared to the bedding can be seen. B) Sample K18+1; note the sulfide-filled fractures in the center of the sample. The white bar measures 1 cm.

Figure 4.13: Sample K17-6; the top of the sample includes the bottom of the Kupferschiefer. Note the gradual decrease in grain size as depth increases. The white bar measures 1 cm.

**Core SGH-132**

**K46+79** (85.5 to 73 cm above the contact) The medium dark gray (N4) sample exhibits a matrix of inter-tonguing grays that are dark gray (N3) and olive gray (5Y 4/1) when wet. Mineralization is present in the form of very fine macro-dissemination and very small macro-aggregates; the mineralization may be loosely associated with lighter gray-white streaks. Small discontinuous fractures are also present.

**K45+67** (73 to 61 cm above the contact) The medium dark gray (N4) sample exhibits inter-tonguing lighter and darker grays and very fine macro-disseminated mineralization. Lenses of more carbonate-rich material are present; these lenses are composed at least in part of calcite, since they effervesce lightly with 3% HCl, and the rest of the matrix effervesces less or not at all (Figure 4.14).

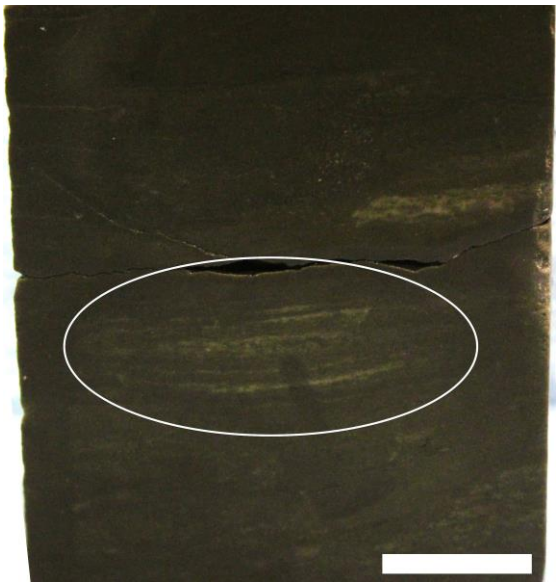

Figure 4.14: Sample K45+67. Note the lenses of lighter material (circled in white); these are not mineralization lenses The white bar measures 1 cm.

**K44+55** (61 to 46.5 cm above the contact) In this medium dark gray (N4) sample, the stratigraphically higher half exhibits numerous fractures, which may be a relic of coring, and no apparent mineralization. The lower half exhibits inter-tonguing grays, macro-aggregates, and possible soft sediment deformation or bioturbation (Figure 4.15). When wet, the inter-tonguing grays are grayish black (N2) and olive gray (5Y 4/1) in color.

A: 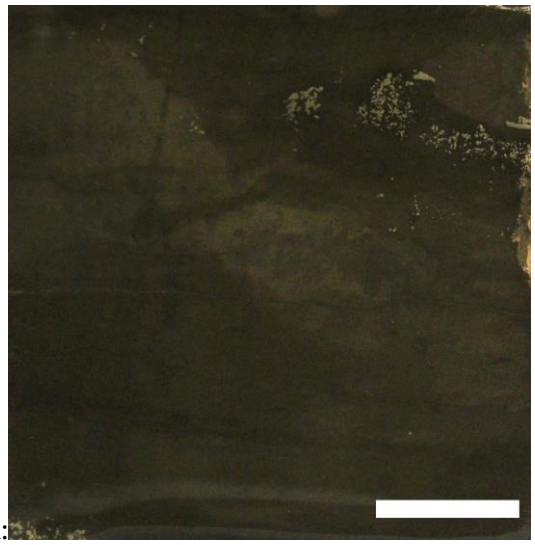 B: 

Figure 4.15: Sample K44+55, showing two sides from the same sample. Note the mineralization and the inter-tonguing gray matrix. The white bars measure 1 cm.

**K43+42** (46.5 to 35 cm above the contact) The medium dark gray (N4) sample shows a very faint inter-tonguing of grays, which are grayish black (N2) and olive gray (5Y 4/1) in color when wet. Mineralization is present in the form of macro-blebs, macro-aggregates, and very fine macro-dissemination.

**K42+33** (35 to 26 cm above the contact) In this sample, there is a color transition; the top third is medium gray (N5), while the bottom 2/3rds of the sample are dark gray (N3) (Figure 4.16) (when wet, the top is olive gray (5Y 4/1) and the bottom is grayish black (N2)). The bottom 2/3rds grade into a darker gray with decreasing stratigraphic depth, until the sudden shift to lighter gray. The two sub-sections also differ slightly in mineralization: macro-aggregates and macro-blebs are present in the lower 2/3rds, while macro-blebs (framboidal in character) are present in the upper third. The macro-aggregates and blebs are, for the most part, bedding-parallel, though some are at an angle of 25-30˚ to the bedding.

Figure 4.16: Sample K42+33; note the color change two thirds of the way up the sample. The white bar measures 1 cm.

**K41+22** (26 to 18 cm above the contact) The dark gray (N3) sample exhibits both inter-tonguing grays and alternating lenses. Discontinuous fractures are present, parallel to the matrix and possibly a relic of coring. Mineralization occurs in the form of macro-aggregates, macro-blebs, and very fine (i.e. small grain size) macro-dissemination.

**K40+8** (13.5 to 1 cm above the contact) The dark gray (N3) sample exhibits alternating lenses. Mineralization is mostly in the form of pods or lenses, parallel with the matrix. Some macro-blebs are also present, and one section approximately 3 mm thick is more mineralized, in the form of macroscopic pod-like lenses, than the rest. The sample also contains bedding-parallel horizons of mineralization, some of which are slightly disseminated (Figure 4.17). **K39+1** (1 to 0 cm above the contact) This sample has a grayish black (N2) matrix and no visible mineralization. The sample is in the form of a few small (<1.5

cm) rock chips, which suggests a fissile nature; the chips are soft and can be scratched with a fingernail, likely because the sample is carbonaceous.

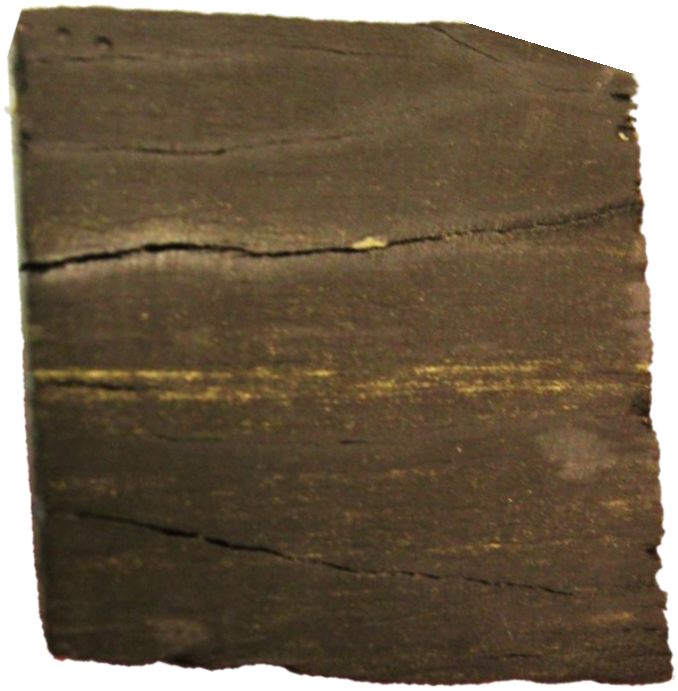

Figure 4.17: Sample K40+8; note the disseminated bedding-parallel mineralization horizons. The width of the sample is approximately 3.5 cm.

**K38-12** (0 to 24.25 cm below the contact) The yellowish gray (5Y 8/1) sample is slightly less well-sorted immediately below contact (about 0.5 cm) compared to the rest of the sample. It is mostly composed of medium sized grains, with coarser-grained "laminations" at 5.5, 22, and 24 cm below the contact. Each coarse lamination is less than 0.5 cm thick, and the lamination 24 cm below the contact has coarse-sand and granule sized grains associated with mud grains. The sample does not contain visible sulfide mineralization.

**K37-32** (25 to 37 cm below the contact) The sample is a fine to medium grained sandstone, light olive gray (5Y 6/1) and yellowish gray (5Y 8/1) in color. The bottom of the sample is darker in color than the rest of the sample, and may be the result of interstitial sulfide mineralization. The change in color shows no apparent association with a change in sediment type or grain size (Figure 4.18A).

Halfway down the sample there is a repeated alternation between fine and very fine grained sandstone; there are about seven laminations of the finer grains.

**K36-43** (37 to 49 cm below the contact) This light olive gray (5Y 6/1) and yellowish gray (5Y 8/1) sample exhibits the same laminations of finer sand grains as in the sample taken above it. At approximately 48 cm below the contact, there is a lamination that includes granule sized grains, and 1 to 2 cm above it there is an interstitial macro-aggregate of sulfides (Figure 4.18B).

**K35-55** (49 to 61.5 cm below the contact) The light olive gray (5Y 6/1) and yellowish gray (5Y 8/1) sample exhibits what appear to be black grains, which may be a form of sulfide mineralization (perhaps grains coated by sulfides). Going from top to bottom, the sample becomes an increasingly darker shade of gray, possibly signaling an increase in mineralization (Figure 4.18C). The darker gray coloring forms horizons or laminations within the sample. This sample also exhibits the laminations of finer sand grains as seen in samples K36-43 and K37-32. Slightly coarser grains are present 59.5 to 61.5 cm below the contact.

**K34-68** (61.5 to 76.5 cm below the contact) The light olive gray (5Y 6/1) and olive gray (5Y 4/1) sample is composed of poorly cemented coarse-grained sandstone for the top 3 cm, 61.5 to 64.5 cm below the contact. This section is also relatively dark in color, possibly an indication of sulfide mineralization, and exhibits a pale blue green color (5BG 7/2) of oxidized copper at the very top of the sample. The middle of the sample is mostly composed of moderately sorted fine and medium sand grains. The bottom 1.5 cm, 75 to 76.5 cm below the contact, is composed of slightly coarser sand grains, and immediately above this coarser layer there is a bedding-parallel horizon of darker gray material, possibly sulfides.

**K33-80** (76.5 to 84.5 cm below the contact) This light olive gray (5Y 6/1) sample is mostly a fine- to medium-grained sandstone. It contains multiple laminations of coarser grained sand, which are darker than the rest of the sample, possibly a result of sulfide mineralization.

A:  B:  C: 

Figure 4.18: A) Sample K37-32; note the dark bands, which may be sulfides. B) Sample K36-43; note the color banding throughout the sample, the granules near the bottom of the sample, and the sulfide mineralization above the granule lamination. C) Sample K35-55; note the banding throughout the sample, and the darker color of the bottom third. The white bars measure 1 cm.

**Core E-27**

**K55+38** (45 to 38 cm above the contact) The sample exhibits a dark gray (N3) matrix composed of alternating lenses (grayish black (N2) when wet), with mineralization in the form of macro-dissemination, macro-(framboidal-like) blebs, and bedding-parallel macro-aggregates. Discontinuous fractures are present along the same horizon as the macro-aggregates and macro-blebs. Immediately underneath the horizon with the macro-mineralization there is a bedding-parallel quartz vein (~1.5 cm thick), exhibiting relatively sharp upper and lower contacts, but with a disseminated nature within (Figure 4.19A). A few cm lower, the sample transitions to a medium gray (N5) matrix with inter-tonguing grays (Figure 4.19B), and then another horizon of mineralization in the form of bedding-parallel macro-aggregates, macro-blebs at angles that are nearly bedding-perpendicular, and macro-dissemination within a darker gray band. Further below this there is an abrupt transition to lighter gray, with inter-tonguing of

even lighter and slightly darker grays, and macro-bleb/aggregates of mineralization. Some mineralization, in the form of elongated macro-blebs perpendicular to the matrix, bridge this transition.

A:  B: 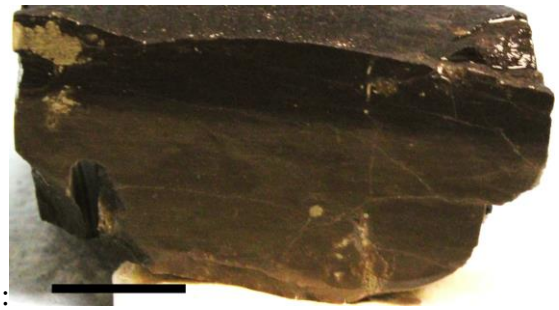

Figure 4.19: Sample K55+38. A) Note the disseminated quartz vein with sharp upper and lower contacts. B) Note the abrupt change in color, and that mineralization that is present in both shades of gray. The white and black bars measure 1 cm.

**K54+31** (37 to 30 cm above the contact) The medium dark gray (N4) sample is composed of alternating lenses. The sample exhibits no apparent mineralization, though fractures that are parallel and perpendicular to the bedding are present.

**K53+20** (30 to 16 cm above the contact) The dark gray (N3) sample exhibits a matrix of alternating lenses. Mineralization is present in the form of macro-dissemination along a horizon (<2 mm thick), and in a separate horizon (<1 mm thick) at the very base of the sample; there are macro-blebs of mineralization immediately above it. Carbonate is present along fractures where sets of bedding-parallel and bedding-perpendicular fractures connect, and a bedding-parallel disseminated quartz vein (~2 to 3 mm). Two or three horizons are present that contain more carbonate pods among the alternating lenses of carbonate and clay.

**K52+7** (16 to 0 cm above the contact) The dark gray (N3) sample exhibits alternating lenses, with mineralization present in the form of bedding-parallel macro-blebs and macro-aggregates, and macro-disseminated mineralization that is very fine grained and relatively dense. In one section of the sample there is mineralization associated with carbonates that crosses multiple "layers" of alternating lenses (Figure 4.20A and B). Mineralization also appears to be associated with dark gray or black blebs, which

are always found bedding-parallel, or with disseminated carbonate veins (Figure 4.20C), which are not always bedding-parallel. In these occurrences the mineralization is stratigraphically above the associated features. Finally, a *Palaeoniscus freieslebeni* fish fossil is present on a bedding plane of this sample (Figure 4.20D).

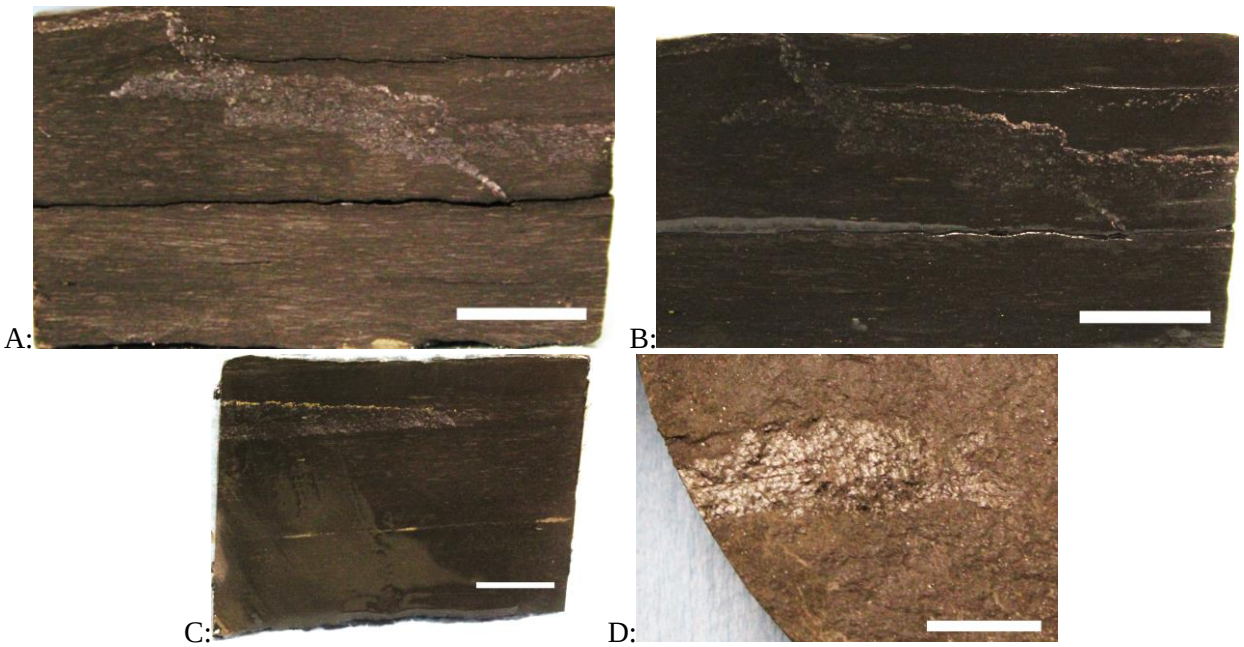


Figure 4.20: Sample K52+7. A) Note the mineralization associated with carbonates; the sample is dry, to make the identification of the carbonates easier. B) Note he mineralization associated with carbonates; the sample has been wet with water, to make the identification of the mineralization easier. C) Note the mineralization immediately above the disseminated carbonate vein, and the bedding-parallel macro-blebs associated with the mineralization horizon further down in the sample. D) Palaeoniscus freieslebeni fish fossil (the sample is dry). The white bars measure 1 cm.

**K51-4** (0 to 9 cm below the contact) Macro-disseminated mineralization is present within the sliver of Kupferschiefer at the top of the sample. Sulfide mineralization is present throughout the light olive gray (5Y 6/1) to yellowish gray (5Y 8/1) sandstone, but is most abundant immediately below the contact and at about 0.5-1.5 cm below the contact (Figure 4.21A). In the latter case, there are abundant bedding-parallel bleb-like spots of mineralization. The upper mineralization contact is comparatively sharper, while the lower contact is more gradational. There is no apparent change in lithology or grain size associated with the mineralization.

**K50-16** (9 to 25.5 cm below the contact) The yellowish gray (5Y 8/1) sample is a fine grained sandstone from 9 to 21 cm below the contact, and has laminations of sulfide mineralization or darker grains alternating approximately every mm or every few mm. There is an increase in sulfide mineralization in the bottom 5 cm of the sample, 20.5 to 25.5 cm below the contact; there is no apparent change in grain size. A few coarse sand grains are present in the sample, and mineralization is present in the form of macro-dissemination.

**K49-27** (25.5 to 32.5 cm below the contact) The medium light gray (N6) sample is a fine grained sandstone with occasional coarser grains (up to pebble size). Mud chips are present within the sandstone that have halos of sulfide mineralization as well as mineralization within (Figure 4.21B); the chips vary in orientation but are all within 20˚ of bedding-parallel. Macro-blebs of mineralization also present.

**K48-36** (32.5 to 48.5 cm below the contact) This medium light gray (N6) to medium gray (N5) sample is composed of alternating layers of conglomerate and fine sandstone (Figure 4.21C). Conglomerate layers range between 0.75 and 1.25 cm thick, with a sharp transition about 43 cm below the contact from dominantly sandstone higher in the column to dominantly conglomerate lower in the column. A few mm above the 1.25 cm thick conglomerate layer, there is a sulfide layer (~1 mm thick). The top contact of the sulfide mineralization is slightly sharper than bottom contact. Above the 0.75 cm thick conglomerate layer, there are a few mud chips that are roughly bedding-parallel and exhibit sulfide halos. There are some sulfides in the 3 cm above this conglomerate layer, mostly bedding-parallel in character, with a sharper upper contact between visibly mineralized sandstone and relatively barren sandstone.

**K47-42** (48.5 to 57 cm below the contact) The medium gray (N5) sample is a moderately sorted conglomerate; grain sizes range between fine sand and pebbles (up to 1.5 cm) and are sub-rounded. There is no visible sulfide mineralization.

A:  B:  C: 

Figure 4.21: A) Sample K51-4; note the sliver of Kupferschiefer at the top, the mineralization within the Weissliegend immediately below the contact, and 1.5 cm below. B) Sample K49-27; note the mud chips (marked by arrows). C) Sample K48-36; note the conglomerate layers and the horizon of sulfide mineralization above the conglomerate layer in the center of the photo. The white bars measure 1 cm.

**Core SGH-103**

**K61+31** (33 to 26 cm above the contact) The sample exhibits a matrix transition between inter-tonguing grays and alternating lenses. The inter-tonguing grays are medium (N5) and medium dark (N4) gray in color, while the matrix composed of alternating lenses is dark gray (N3) in color. Mineralization is present in both matrix types, although in different forms. Macro-dissemination is present in both, but the spherules are coarser in the inter-tonguing gray section compared to those found with the alternating lenses. Macro-aggregates are present near the boundary between the two matrices, and are mostly within 0.5 cm above or below the transition. The macro-aggregates are roughly bedding-parallel; macro-blebs are present and bedding-parallel among the inter-tonguing grays. Some macro mineralization within the upper, lighter section is almost bedding-perpendicular (Figure 4.22).

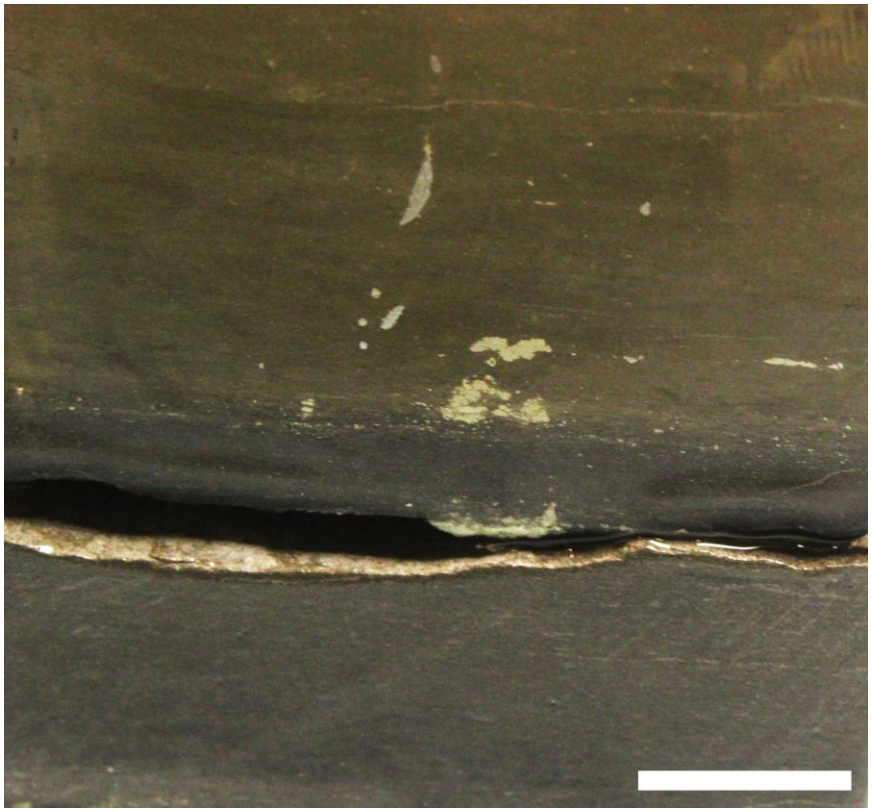

Figure 4.22: Sample K61+31; note the change from inter-tonguing grays at top to alternating lenses at the bottom. Macro-aggregates can be seen along the boundary, and some of the mineralization is bedding-perpendicular. The white bar measures 1 cm.

**K60+19** (26 to 12.5 cm above the contact) The medium dark gray (N4) sample exhibits a matrix of alternating lenses. Mineralization is present in the form of macro-aggregates and macro-blebs, with the longer axes bedding-parallel. Macro-disseminated mineralization is present as both spheres and pods; the pods are mostly found 16.5 to 12.5 cm above the contact.

**K59+7** (12.5 to 0 cm above the contact) This dark gray (N3) sample exhibits alternating lenses. Mineralization is present in the form of a bedding-parallel macro-bleb; the bleb is closer to a white-gray color (chalcocite?) than the usual pyrite-yellow color seen (chalcopyrite?). A bedding-parallel mineralization horizon is also present: 6.25 cm above the basal contact, there is a 1 mm thick green layer, possibly malachite.

**K58-5** (0 to 9.5 cm below the contact) The very top of the yellowish gray (5Y 8/1) and light medium gray (N6) sample includes a sliver of Kupferschiefer. Below the abrupt contact, the top 4.5 cm

includes granules (<5 mm) within fine sand. Near the bottom of the sample, 8.5 cm below the contact, there is a black lens of sulfides (<0.5 mm) (Figure 4.23A). The sample also contains a few laminations of coarse to medium sand, and occasional granules are scattered through the sample.

**K57-16** (9.5 to 21.5 cm below the contact) The sample exhibits an inter-tonguing mix of granules to very fine sand and sulfide lenses 9.5 to 17 cm below the contact (Figure 4.23B), and ranges from light (N7) to medium light (N6) to medium gray (N5) in color. From 17 to 21.5 cm below the contact, the sample is composed of fine sand with a gradually increasing concentration of sulfides as depth increases.

A: 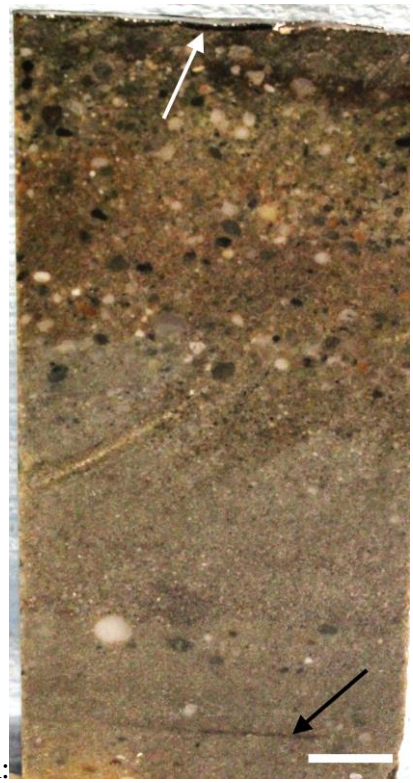 B: 

Figure 4.23: A) Sample K58-5; the white arrow identifies the contact with the Kupferschiefer at the top of the sample; the black arrow points to the sulfide mineralization near the bottom of the sample. B) Sample K57-16; note the granules and fine sand in the top of the sample, and the increasing concentration of dark material in the bottom of the sample. The white bars measure 1 cm.

**K56-28** (21.5 to 32.5 cm below the contact) The sample is a very fine grained sandstone for the uppermost centimeter, stained dark with sulfides. At 23 to 22.5 cm below the contact, there is black layer that appears to be associated with meandering fractures (Figure 4.24), some of which appear to be filled

with carbonates. The black material is finer grained and has a different appearance than the average sulfide mineralization within the Weissliegend. Immediately below the layer with the fractures and the black material, there is a sprinkling of granules. The sample then returns to an inter-tonguing of light and darker gray fine sandstone, with the occasional granule. Some of the lighter gray material is stained a red-pink color. The colors range from light (N7) to medium light (N6) to medium (N5) to medium dark gray (N4) in color; the "black" areas previously mentioned are dark gray (N3) in the Munsell® color chart.

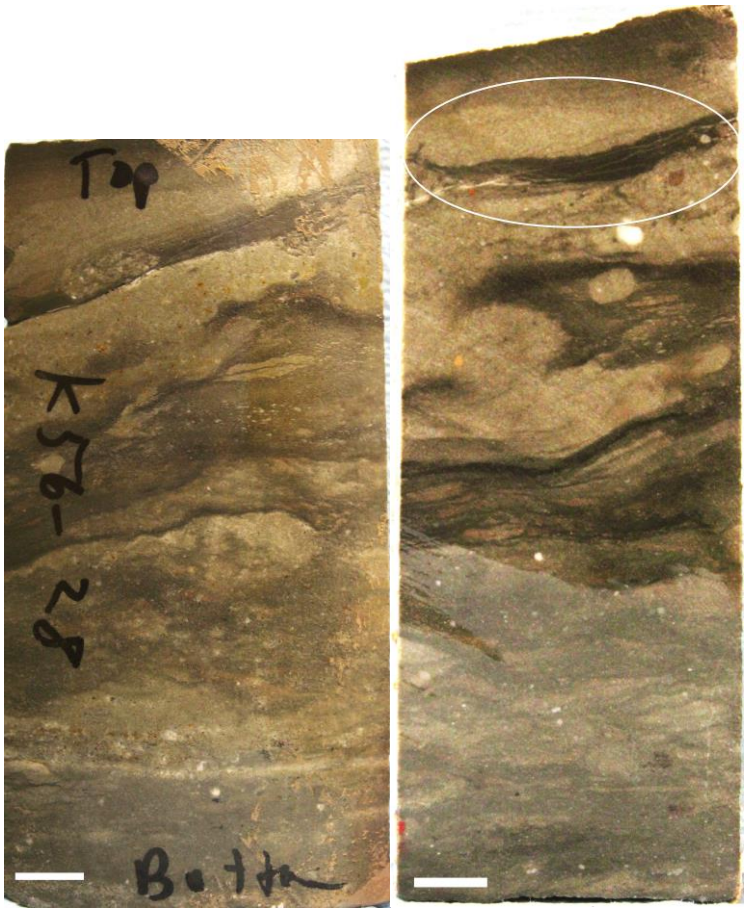


Figure 4.24: Sample K56-28; the picture on the left shows part of the circumference of the core sample; the picture on the right is the continuation of the right hand side of the circumference, into the core sample. Note the fine grained sandstone and the inter-tonguing of the colors. The white oval marks the location of the black material and fractures mentioned in the text. The white bars measure 1 cm.

The data described above are illustrated in Figure 4.25 and Table 4.1.

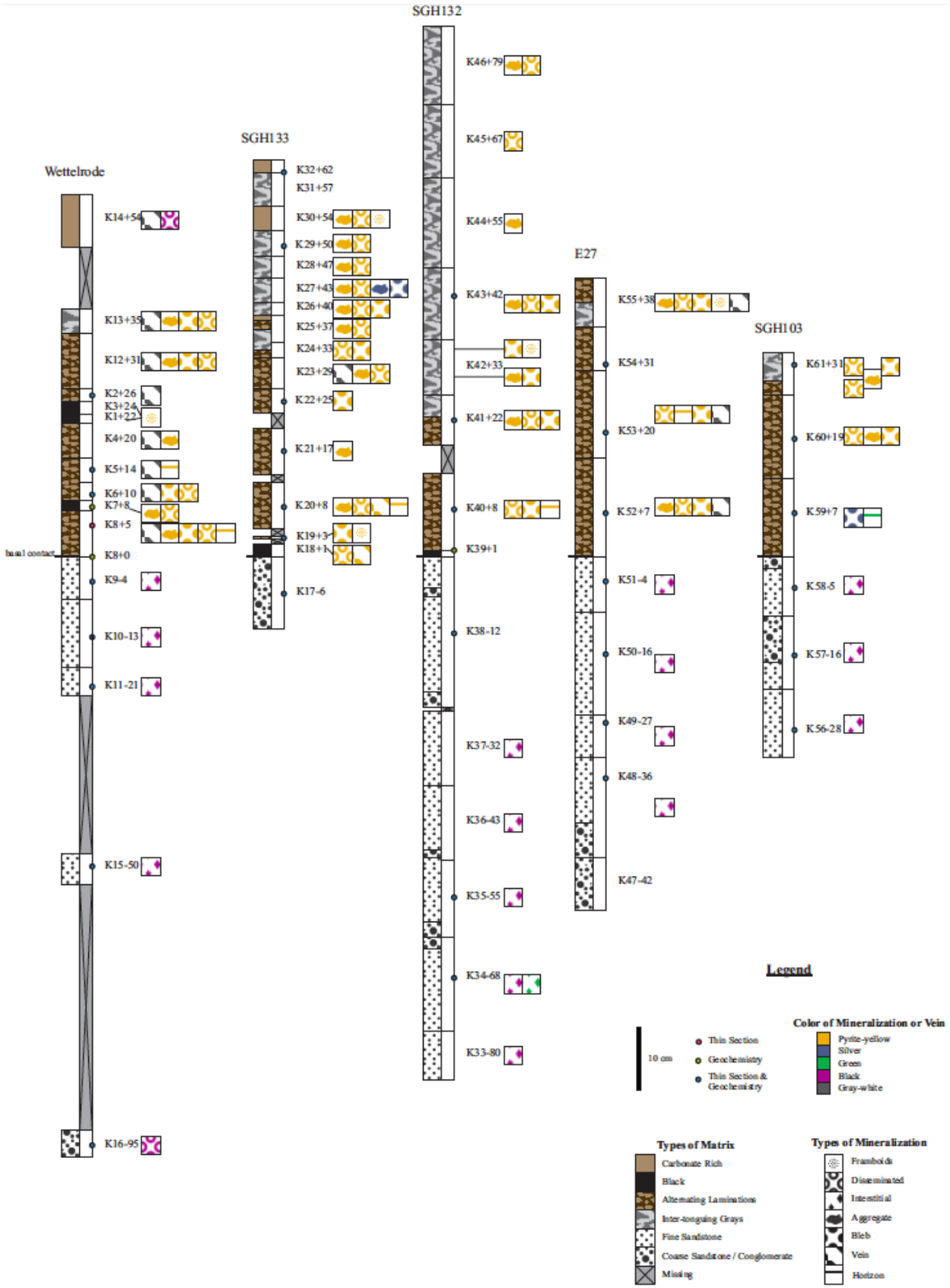


Figure 4.25: Sangerhausen hand sample matrix and mineralization, stratigraphically by core.

Table 4.1: Illustration of matrix, macro-mineralization, and veins present within Sangerhausen hand samples.

| Hand Samples | | Matrix | | | | Macro-Mineralization | | | Veins | |
|---|---|---|---|---|---|---|---|---|---|---|
| Location | Depth* (cm) | None | Alternating Laminations | Inter-tonguing Grays | Sandstone or Larger | Disseminated | Bleb | Aggregate | ~Parallel to Matrix | At Angle to Matrix |
| Wettelrode | 54 | carbonate-rich? | | | | possible | | | | ~85° |
| | 35 | | | ✓ | | ✓ | ✓ | ✓ | | ~20-30°, 90° |
| | 31 | | ✓ | | | ✓ | ✓ | ✓ | ✓ | 90° |
| | 26 | | ✓ | | | | | | ✓ | 75°, 80° |
| | 24 | ✓ | | | | possible | | | | |
| | 22 | ✓ | | | | ✓ | | | | |
| | 20 | | ✓ | | | | | ✓ | | 90° |
| | 14 | | ✓ | | | | | "horizon" | ✓ | |
| | 10 | | ✓ | | | ✓ | ✓ | | ✓ | |
| | 8 | ✓ | | | | ✓ | | ✓ | | |
| | 0 | | ✓ | | | ✓ | ✓ | "horizons" | ✓ | 90° |
| | -4 | | | | ✓ | interstitial | | interstitial | | |
| | -13 | | | | ✓ | interstitial | | | | |
| | -21 | | | | ✓ | | | interstitial | | |
| | -50 | | | | ✓ | interstital, bands | | | | |
| | -95 | | | | ✓ | | | in chips | | |
| SGH133 | 62 | carbonate-rich | | | | | | | | |
| | 57 | carbonate-rich | | ✓ | | | | | | |
| | 54 | carbonate-rich | | | | ✓ | | framboidal-like | | |
| | 50 | carbonate-rich | | ✓ | | ✓ | | ✓ | | |
| | 47 | | | ✓ | | ✓ | | ✓ | | |
| | 43 | | | ✓ | | ✓ | ✓ | ✓ | | |
| | 40 | | | possible | | ✓ | ✓ | ✓ | | |
| | 37 | | ✓ | ✓ | | ✓ | | ✓ | | |
| | 33 | | ✓ | possible | | ✓ | ✓ | | | |
| | 29 | | ✓ | | | possible | | ✓ | | 25° |
| | 25 | | ✓ | | | | ✓ | | | |
| | 17 | | ✓ | | | | | ✓ | | |
| | 8 | | ✓ | | | ✓ | ✓, vein | ✓, horizons | | |
| | 3 | | possible, faint | | | | framboidal-like | | | |
| | 1 | | not apparent | | | ✓ | infilling fractures | | | |
| | -6 | | | | ✓ | | | | | |
| SGH132 | 79 | | | ✓ | | ✓ | | ✓ | | |
| | 67 | | | ✓ | | ✓ | | | | |
| | 55 | | | ✓ | | | | ✓ | | |
| | 42 | | | ✓ (faint) | | ✓ | ✓ | ✓ | | |
| | 33 | | | ✓ | | | ✓ | ✓, some framboidal | | |
| | 22 | | ✓ | ✓ | | ✓ | ✓ | ✓ | | |
| | 8 | | ✓ | | | ✓ | ✓ | pods | | |
| | 1 | no information | - | - | - | - | - | - | - | - |
| | -12 | | | | ✓ | | | | | |
| | -32 | | | | ✓ | | | interstitial banding? | | |
| | -43 | | | | ✓ | possible interstitial | | ✓ | | |
| | -55 | | | | ✓ | | | | | |
| | -68 | | | | ✓ | possible interstitial | | | | |
| | -80 | | | | ✓ | possible interstitial | | | | |
| E-27 | 38 | | ✓ | ✓ | | ✓ | ✓ | ✓, framboidal-like | disseminated | |
| | 31 | | ✓ | | | | | | | |
| | 20 | | ✓ | | | ✓ | ✓ | vein-like | disseminated | |
| | 7 | | ✓ | | | fine grained, dense | ✓ | ✓ | | |
| | -4 | | | | ✓ | interstitial | interstitial | | | |
| | -16 | | | | ✓ | interstitial | | possible interstital laminations | | |
| | -27 | | | | ✓ | within mud chips | interstitial | interstitial halos around mud chips | | |
| | -36 | | | | ✓ | | | interstitial layer | | |
| | -42 | | | | ✓ | | | | | |
| SGH103 | 31 | | ✓ | ✓ | | ✓ | ✓ | ✓ | | |
| | 19 | | ✓ | | | ✓ | ✓ | ✓ | | |
| | 7 | | ✓ | | | | ✓ | horizon | | |
| | -5 | | | | ✓ | | interstital | | | |
| | -16 | | | | ✓ | interstital | | | | |
| | -28 | | | | ✓ | interstital | | | | |

### 4.1.6 Lubin Mining District

**Rudna 1**

**K62+50**: The grayish black (N2) sample exhibits faint alternating lenses, carbonate pods (up to 2 cm x 1 cm) (Figure 4.26), lenses of quartz grains, and individual grains of detrital quartz. Veins of quartz are present; some are bedding-parallel and some are at a low angle (~10 to 20˚) to the bedding. No macro-mineralization is observed.

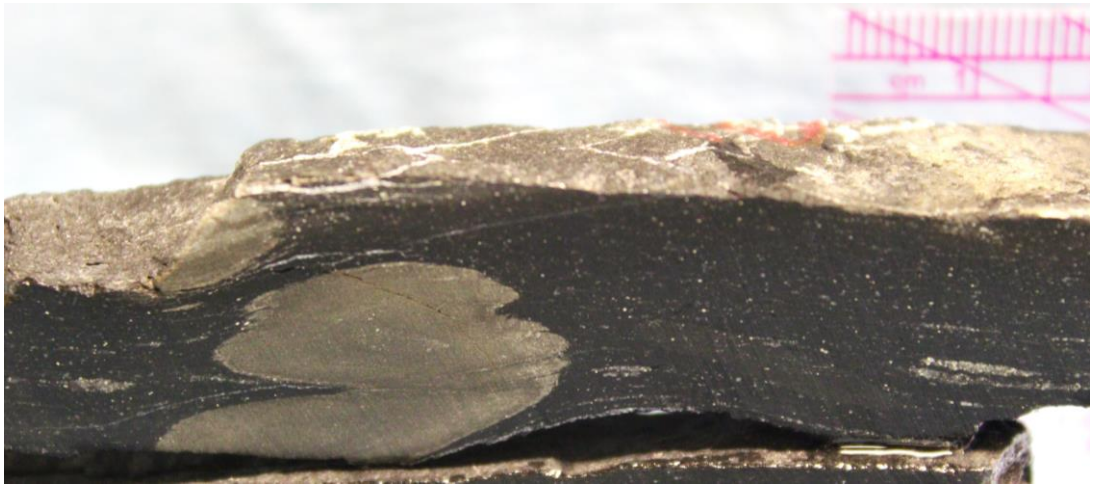

Figure 4.26: Sample K62+50; note the alternating lenses and the carbonate pods.

**K63+40**:The dark gray (N3) sample exhibits a matrix composed of alternating lenses. Detrital quartz grains and bedding-parallel quartz veins are present. No macro-mineralization is observed.

**K64+30**: The sample is grayish black (N2) in color, composed of alternating lenses, and exhibits detrital quartz grains and bedding-parallel quartz veins. Macro-mineralization is present in the form of disseminated silver-colored spherules and a bedding-parallel "lens" of silver macro-mineralization (~5mm long, ~0.2 mm thick).

**K65+20**: This sample is grayish black (N2) in color and composed of alternating lenses. Macro-mineralization is present in the form of bedding-parallel silver- and golden-colored blebs, disseminated silver spherules, and a 1- to 2-mm-thick vein (~65˚ from bedding orientation). The vein has blue-pink-golden colored zoning from inside to outside (Figure 4.27). Mineralization between the size of

disseminated and macro-bleb categories is also present, in the form of golden-colored sphere-blebs (~0.3 mm).

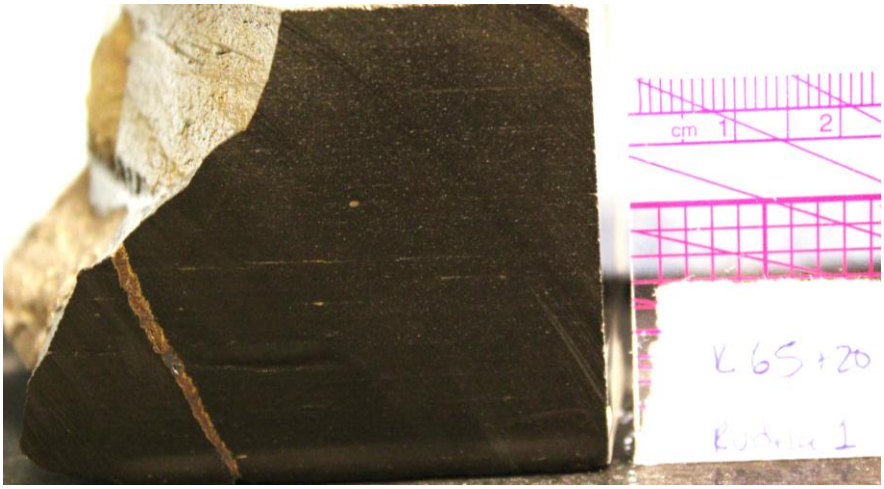

Figure 4.27: Sample K65+20; note the bornite-chalcopyrite vein in the lower left of the sample.

**K67+10**: This soft, grayish black (N2), carbonaceous sample contains blebs of medium light gray (N6) to medium gray (N5) colored material. Chunks of carbonate material (up to 1.5 cm x 1 cm) are also present; both matrix types exhibit golden-colored mineralization. Mineralization is also present in the form of bedding-parallel disseminated golden mineralization and "aggregates" of macro-disseminated golden mineralization.

**K66+0**: This sample contains the transition from the Kupferschiefer, dark gray(N3) in color, to Boundary Dolomite, light olive gray (5Y 6/1) in color. Disseminated silver mineralization is present above the contact. Bedding-parallel and -perpendicular calcite veins are present in the Boundary Dolomite; some of the bedding-perpendicular veins widen parallel to the contact when they reach the Kupferschiefer (Figure 4.28). Bedding-parallel blebs of golden-colored mineralization are observed in the lower 2 to 3 mm of the Kupferschiefer. In this location, the Boundary Dolomite is only 3.0 to 3.2 cm thick, and laminations of shale are present below the dolomite. Bornite- or chalcopyrite-colored mineralization associated with a calcite vein within the Boundary Dolomite.

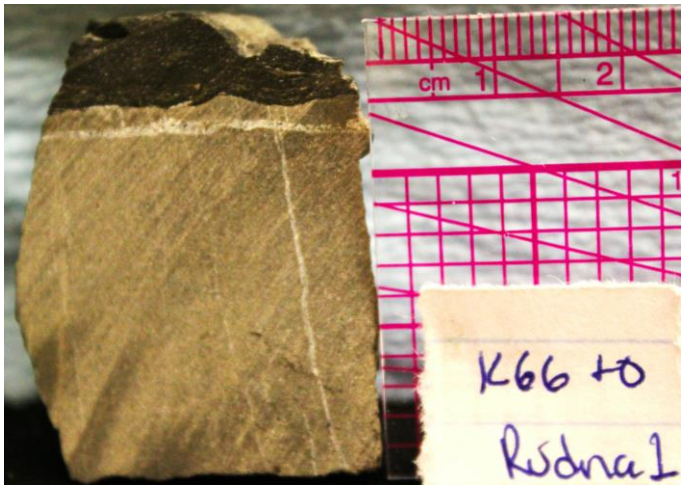

Figure 4.28: Sample K66+0; note the bedding-parallel and -perpendicular veins within the Boundary Dolomite. (Note: the photo was taken while the sample was dry.)

**K68-10**: This very fine, very well sorted (rounded) sandstone is medium gray (N5) in color, with dark gray (N3) areas that may be composed of organic carbon. Golden-yellow colored mineralization is present that appears to be associated with some of the dark gray spots.

**K69-25**: The sample is yellowish gray (57 8/1) in color, composed of very fine, very well sorted (sub-rounded to sub-angular) sandstone. It is poorly cemented and exhibits interstitial golden-yellow mineralization. Black areas within sample are sometimes associated with the mineralization.

**K70-130**: The sample is composed of fine, well sorted sandstone, yellowish gray (57 8/1) in color, and exhibits black interstitial material (possibly sulfides). The sample is poorly cemented and comparatively porous.

**Rudna 2**

**K77+120**: A bleb of quartz or carbonate material (~2 mm x 3 mm) is present within the medium dark gray (N4) sample. Macro-blebs of golden-yellow and silver colored mineralization are observed.

**K78+70**: The sample is composed of a matrix of inter-tonguing medium grays (N5) with medium dark gray (N4) bleb-like areas. Carbonate veins and stringers are oriented at angles to the bedding. Mineralization is present in the form of disseminated silver spherules and golden-yellow blebs and small aggregates.

**K79+50**: In at least some areas of the dark gray (N3) sample, alternating lenses can be observed. Blebs of carbonate material(?) present at all angles to the bedding. No macro-mineralization is observed.

**K80+40**: The dark gray (N3) sample is slightly fissile; disseminated small blebs of silver mineralization are present but rare.

**K82+40**: The matrix of the dark gray (N3) sample is composed of alternating lenses. Black sulfide mineralization is present within a quartz vein that is oriented at an angle to the bedding. A silver-colored vein is mostly bedding-parallel, though in some spots it "steps" vertically up or down; the vein is surrounded ~0.5 cm above and below by disseminated silver-colored spherules. Mineralization is also present in the form of thin, bedding-parallel elongated silver-colored blebs.

**K71+35**: The dark gray (N3) to grayish black (N2) matrix is composed of alternating lenses; without the aid of a hand lens it can be observed that the bedding is disrupted on a millimeter to centimeter scale (Figure 4.29). Some macro-aggregates of golden-yellow mineralization are disrupted by fractures, and carbonate material seems to be along the edges of the broken bedding and within the undisturbed sections.

**K76+20**: The dark gray (N3) matrix is composed of alternating lenses, with grains of detrital quartz. A bedding-parallel horizon rich in detrital quartz also contains mineralization (purple/brownish in colors). The top or bottom of the sample exhibits yellow-golden, red-brown, and purple colored mineralization (no orientation is recorded on the sample).

**K81+20**: The dark gray (N3) sample is fissile and the matrix is composed of alternating lenses. Mineralization is present in the form of disseminated silver spherules, golden-yellow colored blebs, and a bedding-parallel horizon of silver-colored mineralization. Short carbonate veins are oriented at high angles to the bedding.

Figure 4.29: Sample K71+35; note the disrupted bedding and the abundant carbonate veins.

**K72+10**: The grayish black (N2) sample is composed of fissile chips, likely composed of carbonaceous material. No alternating lenses are observed. Mineralization is present in the form of disseminated silver spherules.

**K82+10**: The sample dark gray (N3) exhibits disseminated silver spherules and red-brown colored mineralization that is associated with a carbonate(?) vein perpendicular to the bedding.

**K73-10**: The light gray (N7) sample is a very fine grained, well sorted sandstone with sub-angular to rounded grains. The top of the sample contains a lamination of the overlying Kupferschiefer, or a bedding-parallel horizon very rich in sulfides. The sample is 9 cm tall; 5 mm below the upper contact is black sulfide mineralization that grades into relatively barren sandstone with increasing depth (the upper contact is sharp, the lower contact is graded). Blebs of dark material, possibly sulfides, are present within the sample. Disseminated interstitial golden-yellow mineralization is also observed.

**K74-100**: The light gray (N7) sample is composed of fine, well sorted, relatively porous sandstone. Mineralization is present in the form of interstitial black (sulfide) blebs and interstitial golden-yellow aggregates.

**Lubin 1**

**K83+140**: The light olive gray (5Y 6/1) sample is carbonate rich, with dark gray (N3) mm-sized spherical or elongated areas that may be composed of micrite. Blebs of carbonate are also present; no

macro-mineralization is observed. A thin (~1 mm) vein of carbonate is present; its orientation relative to bedding is unknown because there is no indication of sample orientation.

**K84+110**: The sample is composed of inter-tonguing medium light (N6) and medium (N5) grays; the matrix is carbonate rich, with spherical carbonate blebs (0.1-mm scale), and exhibits disseminated silver mineralization as well as silver mineralization within darker gray areas.

**K85+90**: The sample is carbonate-rich, with inter-tonguing very light (N8) and light (N7) grays; small fossils may be present. Mineralization is in the form of blebs and disseminated spherules; some of the blebs are elongated at varying angles, though the orientation relative to bedding cannot be determined because there is no orientation to the sample.

**K86+70**: The light olive gray (5Y 6/1) sample is carbonate rich, with bedding-parallel elongated medium dark gray (N4) blebs (probably sulfide mineralization). The sample also exhibits disseminated silver mineralization and millimeter scale carbonate blebs.

**K87+50**: The sample is composed of a light olive gray (5Y 6/1) carbonate-rich section and a grayish black (N2) carbonaceous section. The carbonate-rich section exhibits cavities with calcite crystals. In one of the sample pieces, the transition from carbonate-rich to carbonaceous is composed of alternating lenses; this area is rich in small carbonate spherules and exhibits multiple bedding-parallel carbonate veins (≤2 mm thick), and a few thin veins at an angle (~30˚) to matrix (Figure 4.30). This sample also contains a bedding-perpendicular silver-colored vein (~1 mm thick); when rotated 90˚, the vein exhibits both bedding-parallel and -perpendicular orientation.

**K88+40**: The dark gray (N3) sample has a matrix composed of alternating lenses. The sample contains bedding-parallel carbonate veins, some of which are at a low angle (~20˚) to matrix. Mineralization is present in bedding-perpendicular silver veins, disseminated silver spherules, and very small, almost bedding-perpendicular veins.

**K89+20**: The dark gray (N3) sample has a matrix composed of alternating lenses. Mineralization is present as disseminated silver spherules and silvery veins (possibly galena?). Carbonate veins are observed bedding-parallel and at a 30˚ angle to the bedding.

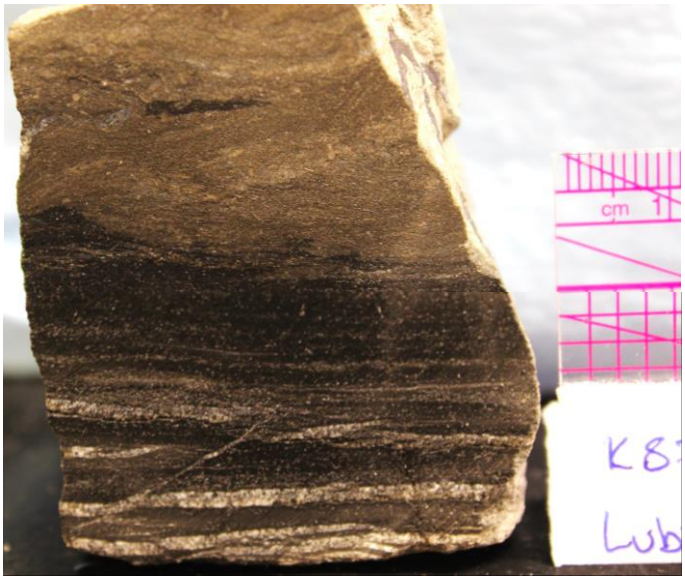


Figure 4.30: Sample K87+50; note the change in matrix from carbonate rich to clay rich, and the presence of bedding-parallel carbonate veins.

**K90(+0?)**: There is a sharp transition between the grayish black (N2) shale cap and the light olive gray (5Y 6/1) carbonate rich section. Golden-brown mineralization is present in the lower few millimeters of the shale cap; the lower few centimeters of carbonate rich section has bedding-parallel stringers of black material, which may be composed of sulfides or carbonaceous or clay material. The top few centimeters of the carbonate rich section also exhibits silver and gray/blue blebs of mineralization.

**K91**: The grayish black (N2) matrix is fissile, soft (carbonaceous), and composed of alternating lenses with bedding-parallel lenses and/or veins of carbonate or mineralization. Some of the veins are at a low angle (10˚) to the bedding. Mineralization is present in the form of disseminated silver spherules.

**K92-10**: The very fine grained, well sorted sandstone with sub-angular to sub-rounded grains is very light gray (NN8) to light gray (N7) in color. Mineralization is present in the form of blebs of interstitial black sulfides.

**K93-20**: The very fine grained, well sorted sandstone is light gray (N7) in color. Grains are sub-angular to sub-rounded; mineralization is present in the form of blebs of interstitial black sulfides.

**K94-120**: The very fine grained, well sorted sandstone is light gray (N7) in color; grains are sub-angular to sub-rounded. Sulfide mineralization is present in the form of bands of interstitial sulfides, each exhibiting one sharp contact and one graded contact (no sample orientation) (Figure 4.31).

Figure 4.31: Sample K94-120; note the bands of sulfide mineralization, and the two types of contact: sharp and gradational.

**Lubin 2**

**K105+120**: The light olive gray (5Y 6/1) sample is carbonate rich, with spherical blebs of carbonate, and elongated, thin, approximately bedding-parallel blebs of mineralization. Disseminated spherules of silver mineralization are also present.

**K104+50**: The medium gray (N5) and light olive gray (5Y 6/1) colored sample is carbonate rich. Spherical blebs of carbonate are present, one of which seems to be associated with silver mineralization. A very high angle carbonate vein is almost bedding-perpendicular, and changes directions so that it "zigzags" through the sample. Blebs of black material are present, and at least one silver bleb that runs bedding-parallel for about 1.7 cm.

**K103+30**: The grayish black (N2) shale pieces have veins very similar to those found 50 cm above contact in Lubin 1, i.e. multiple bedding-parallel carbonate veins (≤1.5 mm thick). The medium light gray (N6) carbonate-rich piece has a carbonate vein with disseminated silver mineralization

associated with it. The disseminated silver mineralization is mostly aligned bedding-parallel; there is also a lamination of black shale within the carbonate rich piece.

**K102+25**: This grayish black (N2) sample has faint alternating lenses and bedding-parallel carbonate veins. Mineralization is present in the form of disseminated spherules and small bedding-parallel lenses silver in color, and golden-brown colored disseminated aggregates. Some of the mineralization is associated with carbonate veins (Figure 4.32). Veins at a low angle (~5˚) to the bedding are also present; a light bluish gray (5B 7/1) tint to sides of samples hint at oxidized copper mineralization.

**K101+20**: This grayish black (N2) sample contains alternating lenses; the bedding seems folded or disrupted. Carbonate is present in fractures that are bedding-parallel to an angle of ~55˚. Mineralization is present in the form of elongated silver-colored blebs and disseminated silver spherules.

**K100+0**: The grayish black (N2) sample exhibits light green (5G 7/4) tint of oxidized copper mineralization along uncut sides. Boudinage-shaped silver-colored mineralization is associated with a carbonate vein. Mineralization in the form of silver-colored bedding-parallel disseminated spherules is concentrated along horizons; the sample also exhibits small elongated bedding-parallel lenses. Carbonate veins are mostly bedding-parallel, with a few small millimeter-scale bedding-perpendicular veins.

**K99_LBD**: This medium gray (N5) sample is from the Boundary Dolomite between the Kupferschiefer and the Weissliegend. Blebs of silver-colored mineralization are present within the sample, which are elongated bedding-parallel or at a high angle to the bedding; some of the mineralization is associated with blebs of coarser grained dolomite. The sample exhibits a lamination or "cap" of dark gray (N3) Kupferschiefer, which contains a bedding-parallel carbonate vein. Some laminations of black material (shale?) are present within the dolomitic section.

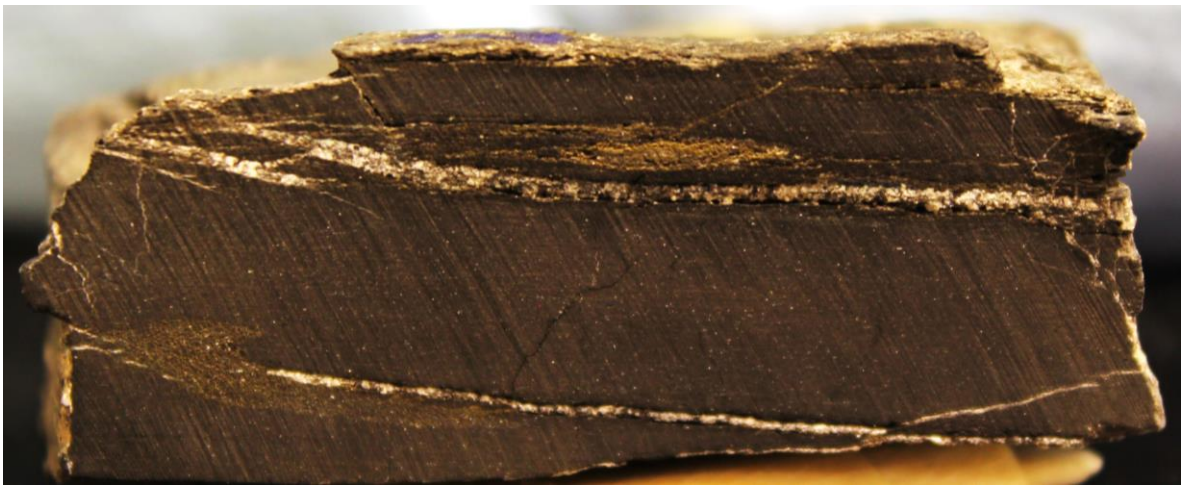

Figure 4.32: Sample K102+25; note the mineralization associated with the carbonate veins. The sample is 5.3 cm by 2 cm

**K98_UBD**: The medium (N5) to medium dark (N4) gray dolomite sample contains fossils, possibly pieces of shells (Figure 4.33). Some disseminated silver-colored spherules are associated with blebs of coarser grained dolomite. The dolomite is bounded by grayish black (N2) carbonaceous material; the Boundary Dolomite in this sample is ~4.5 cm thick.

**K97-5**: The sandstone is well sorted, with sub-angular to sub-rounded grains, and very fine light (N7) to medium light (N6) gray in color. A lamination of grayish black (N2) carbonaceous material is on the top or bottom of the sample (no clear sample orientation) and exhibits some very pale green (10G 8/2) coloration that likely results from oxidized copper mineralization. Interstitial blebs of silver mineralization are present. This particular sandstone is not as "clean" as the other Weissliegend samples from the Lubin mining district, possibly because of lithic grains.

**K96-50**: The light gray (N7) sample is a well sorted, very fine sandstone, with sub-angular grains and interstitial blebs of black sulfides.

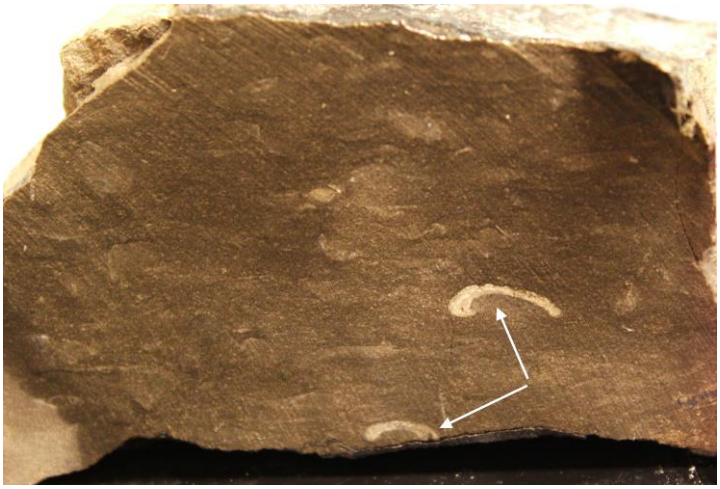

Figure 4.33: Sample K98_UBD; note the fossils (arrows) present in the sample. The sample is 6.7 cm wide by 4 cm tall.

**K95-120**: The sample is a very fine grained very light (N8) to light gray (N7) sandstone with interstitial blebs of sulfides. The grains are well sorted, sub-rounded, and not well cemented. The sulfides approximately align along a bedding-parallel horizon, similar to sulfide bands, with blebs sprouting up or down from them (Figure 4.34). A bleb of pale green (10G 6/2) is present along one of the uncut sides, likely an indication of oxidized copper mineralization.


Figure 4.34: Sample K95-120; note the banded sulfide mineralization, with blebs branching off from the bands.

## 4.2 Thin Sections

Of the 61 Sangerhausen samples, 35 thin sections were made: 19 from above the Kupferschiefer-Weissliegend contact, and 16 from below the contact. Of the 40 Lubin mining district samples, 30 thin sections were made: 14 from above the contact, and 16 from below the contact.. None of the thin sections have a cover slip.

Thin sections taken from above the contact exhibit two main types of matrix: one composed of alternating lenses of carbonate and carbonaceous/clay material (Figures 4.35 and 4.36), and a carbonate-rich matrix (Figure 4.37). Most of the Kupferschiefer samples, from both the Sangerhausen Basin and the Lubin mining district, exhibit alternating carbon- and carbonate-rich lenses to different degrees. Angular to sub-rounded detrital quartz grains are also present above the contact in varying amounts. Matrix and mineralization data for Sangerhausen Basin thin sections is summarized in Figure 4.38.

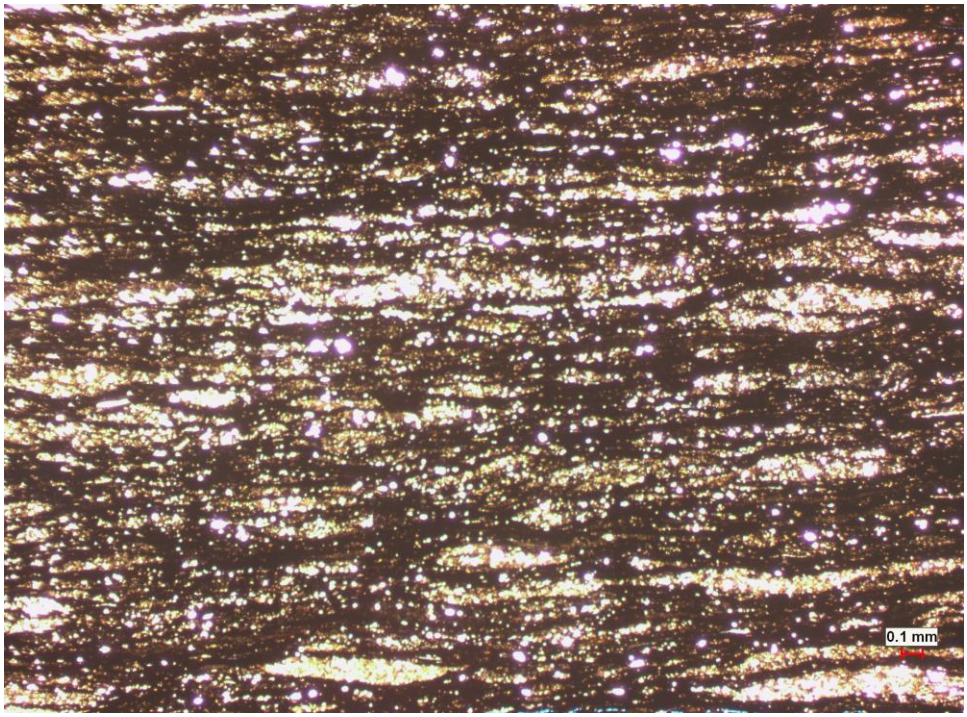


Figure 4.35: Sample K8+5 from Wettelrode mine, Sangerhausen Basin. Example of alternating lenses of carbon-rich (black) and carbonate-rich (translucent) material under crossed polarized light.

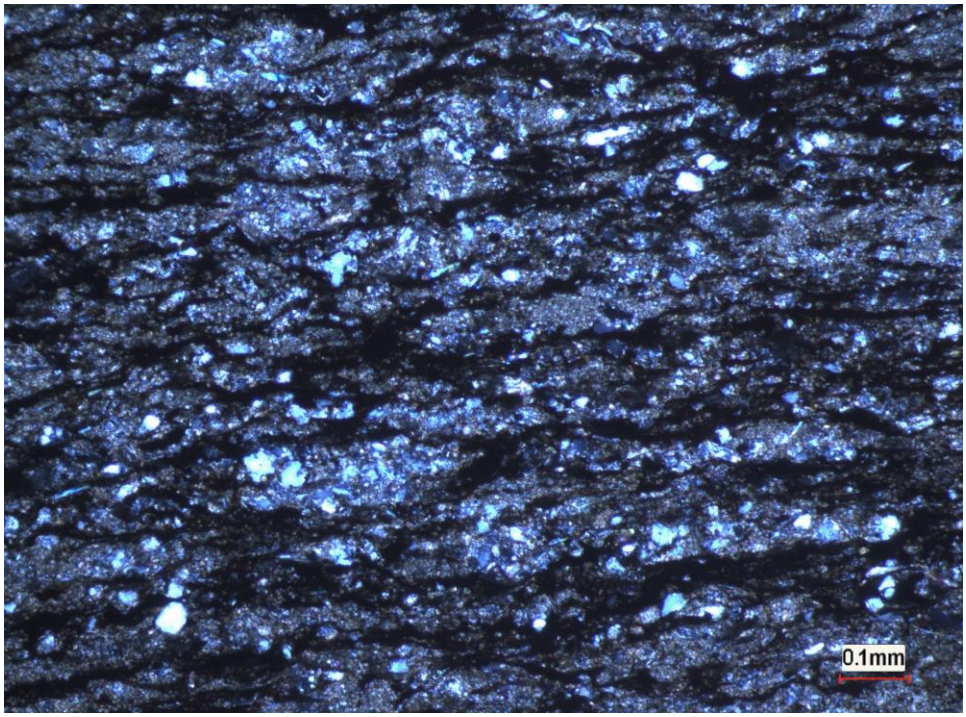


Figure 4.36: Sample K54+31 from core E-27, Sangerhausen Basin. Example of alternating lenses of carbon-rich (black) and carbonate-rich (translucent) material under plain polarized light. Note the greater abundance of carbonate material compared to the amount of carbon-rich material (compare to Figure- previous).

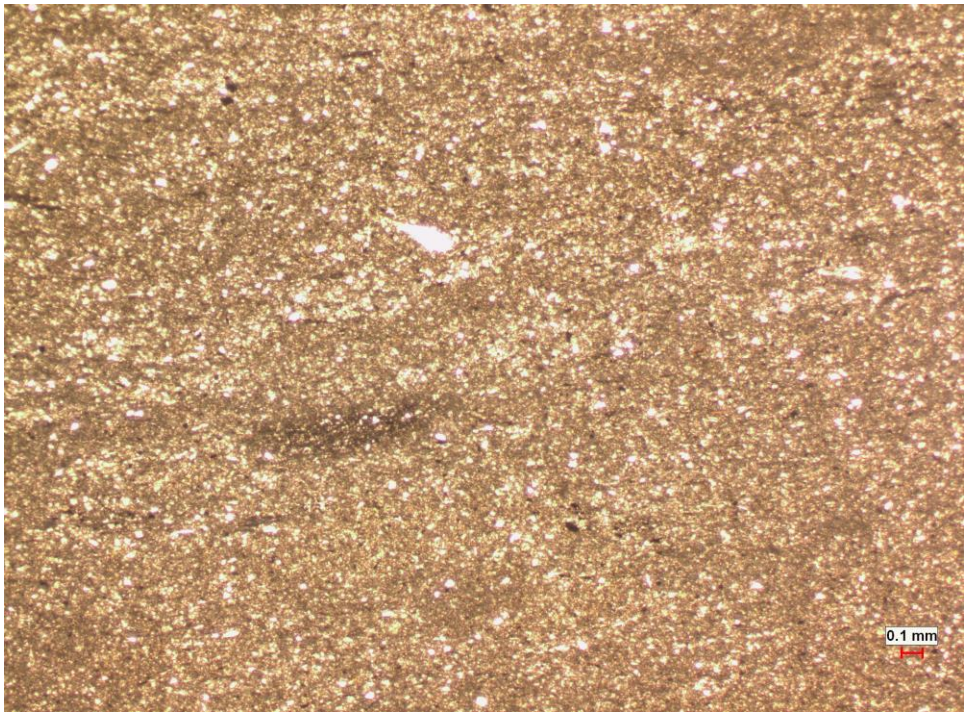


Figure 4.37: Sample K29+50 from core SGH133, Sangerhausen Basin. Example of carbonate-rich material under plain polarized light.

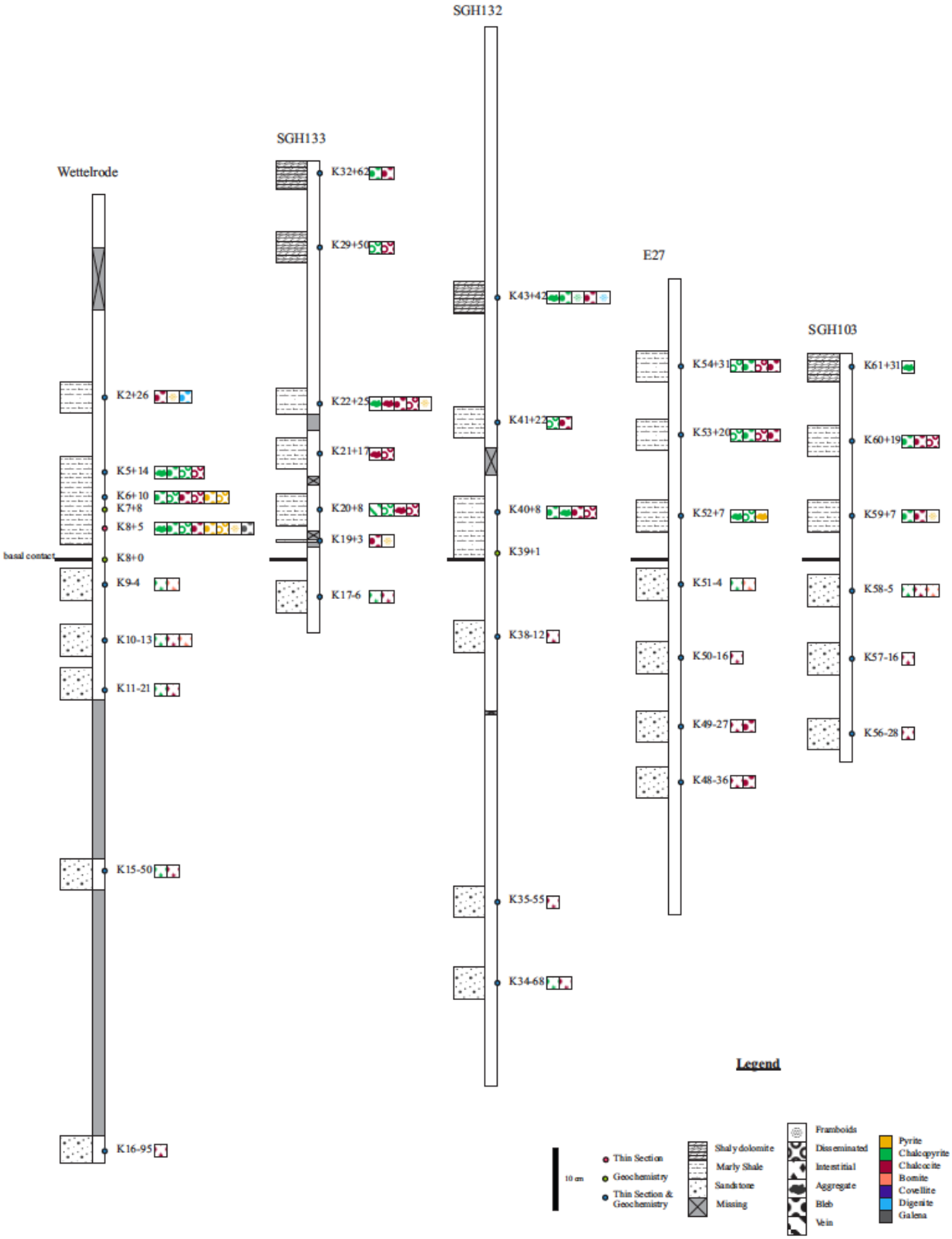


Figure 4.38: Sangerhausen thin section matrix and mineralization data. Note: the alternating lenses referred to in the text fall under the label of "marly shale" in this figure.

### 4.2.1 Sangerhausen Basin: Matrix

**Wettelrode:** Samples 26 and 14 cm above the contact exhibit alternating carbon-rich and carbonate lenses; the former contains a slightly higher concentration of carbonate material relative to carbonaceous material compared to the latter. The sample from 10 cm above the contact is composed mostly of carbonaceous and clay material, with very little carbonate material. The sample taken 5 cm above the contact exhibits alternating lenses similar to the sample from 14 cm above the contact.

**SGH133:** Samples from 62 and 50 cm above the contact are carbonate-rich; the sample from 25 cm above the contact contains alternating lenses of carbonaceous/clay and carbonate, but carbonate lenses are more abundant than those composed of carbonaceous/clay material. The samples from 17 and 5 cm above the contact are mostly composed of carbonaceous and clay material. The sample from 8 cm above the contact contains alternating lenses of carbonate and carbonaceous material.

**SGH132:** The sample from 42 cm above the contact is carbonate rich. The samples from 22 and 8 cm above the contact have alternating lenses of carbonaceous material and carbonate; the sample from 22 cm has a slightly higher abundance of the carbonate material compared to the carbonaceous/clay material, while the sample from 8 cm has a greater concentration of carbonaceous/clay material.

**E-27:** All three thin sections from above the contact exhibit alternating lenses of carbonaceous/clay and carbonate material. The sample from 31 cm has the greatest concentration of carbonate compared to clay, followed by the sample from 20 cm; the sample from 7 cm above the contact has slightly more carbonaceous/clay material compared to carbonate.

**SGH103:** The sample from 31 cm above the contact is carbonate-rich. The samples from 19 and 7 cm above the contact exhibit alternating lenses of carbonaceous/clay material and carbonate; the sample from 19 cm has a lower concentration of carbonate material compared to the sample from 7 cm.

### 4.2.2 Lubin Mining District: Matrix

**Rudna 1:** The sample taken 50 cm above the contact exhibits either large (≥1 cm) carbonate chips or aggregates within a carbon/clay rich matrix with detrital quartz, or inter-tonguing of carbonate-rich matrix with carbon- and clay-rich matrix (Figure 4.39). Samples from 40 and 20 cm above the

contact exhibit alternating lenses of carbonaceous/clay and carbonate material; the sample at 40 cm contains larger grains of detrital quartz compared to the sample at 20 cm, and has a slightly greater concentration of carbonate material relative to carbonaceous/clay material (up to ~85% carbonate). The sample taken at the basal contact is composed mostly of carbon and clay within the Kupferschiefer, in addition to detrital quartz grains. This marly shale is underlain by carbonate-rich material, most likely a lens of Boundary Dolomite (Figure 4.40).

**Rudna 2:** The sample from 35 cm above the contact has a matrix composed of alternating pods of carbonate and carbonaceous/clay material; it also exhibits a lot of disturbance, in the form of many small fractures at different angles. The detrital quartz in this thin section shows evidence of strain, such as sub-grains and bulging recrystallization (i.e., boundary migration) (Figure 4.41). Samples from 20 and 10 cm above the contact exhibit a matrix of alternating lenses of carbonate and carbonaceous/clay material. The sample at 20 cm is relatively rich in detrital quartz, making up approximately 15% of the sample. At 10 cm above the contact, the thin section contains more carbonate material than carbonaceous/clay material.

**Lubin 1:** The sample taken 110 cm above the basal contact is carbonate rich, composed at least in part by calcite, as indicated by the red staining of alizarin red. At 50 cm above the contact, the thin section is half carbonate rich and half carbonate and clay rich. The carbonate rich section contains ~15% detrital quartz, and some of the carbonate is slightly darker than the rest of the thin section (Figure 4.42). The sample from 40 cm above the contact is composed of alternating lenses of carbonate and carbonaceous/clay material, and also exhibits horizons relatively rich in detrital quartz (sometimes reaching 50% or greater). The thin sections taken at the contact and 20 cm above the contact have carbon/clay rich matrixes; the pods of carbonate material are relatively small, generally less than 0.1 mm when they are present at all.

**Lubin 2:** Thin sections from 120, 50, and 30 cm above the contact exhibit a carbonate-rich matrix; all three samples also contain detrital quartz grains. At 25 cm above the contact, the matrix is composed of alternating lenses of carbonate and carbonaceous/clay material, as well as detrital quartz

grains. The thin section made at the contact shows an inter-tonguing of carbonate-rich material with a matrix composed of alternating lenses of carbonate and carbonaceous/clay material. Detrital quartz is present among the matrix of alternating lenses.

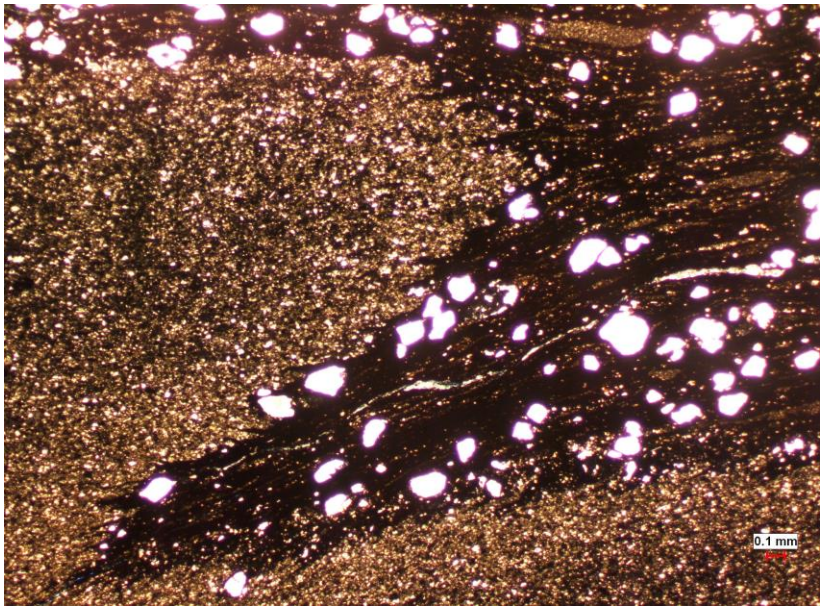


Figure 4.39: Sample K62+50 from Rudna 1, Lubin mining district. Note the carbonate material inter-tonguing with the matrix of alternating lenses of carbonaceous clay, and the detrital quartz present among the alternating lenses. Transmitted plain polarized light.

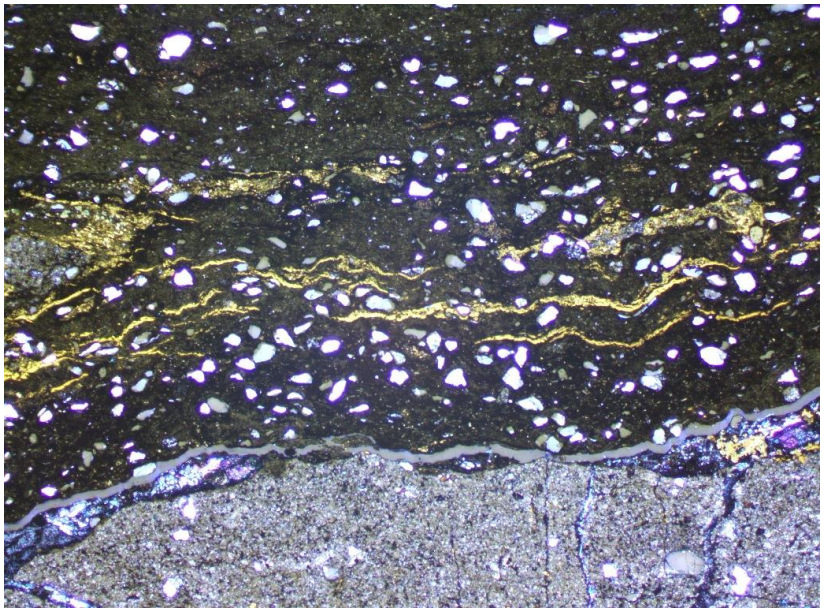

Figure 4.40: Sample K66+0 from Rudna 1, Lubin mining district. Photo taken with a combination of transmitted (plain polars) and reflected light. Note the marly shale, underlain by carbonate. Detrital quartz is present in both compositions, but is more abundant within the shale. Sulfide mineralization is chalcopyrite. Photo is 1.5 mm wide.

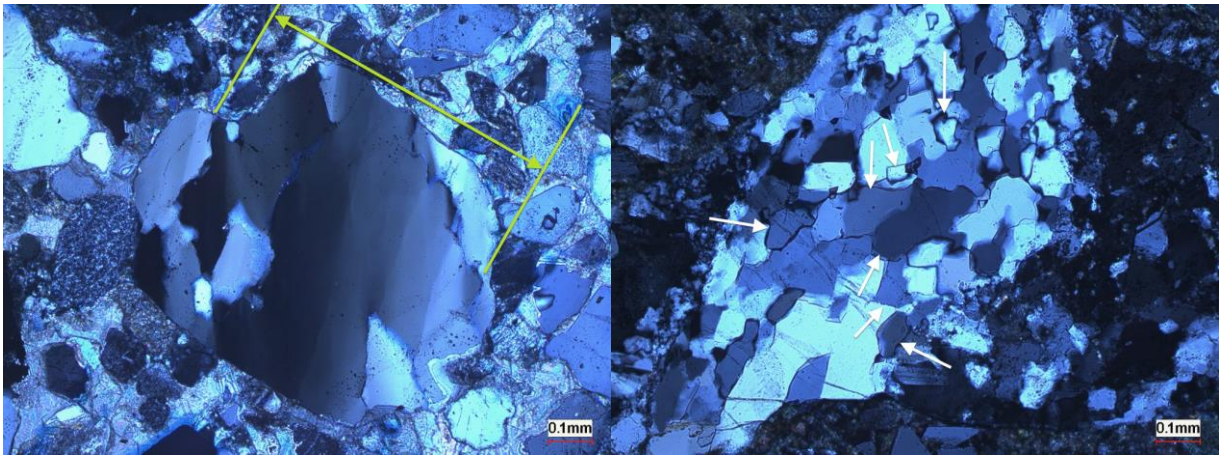

Figure 4.41: Sample K58-5 from core SGH103, Sangerhausen Basin. Examples of quartz grains within the Weissliegend that exhibit indicators of strain: the picture on the left shows a quartz grain with undulose extinction; the picture on the right exhibits sub-grain rotation (white arrows point to examples of sub grains).

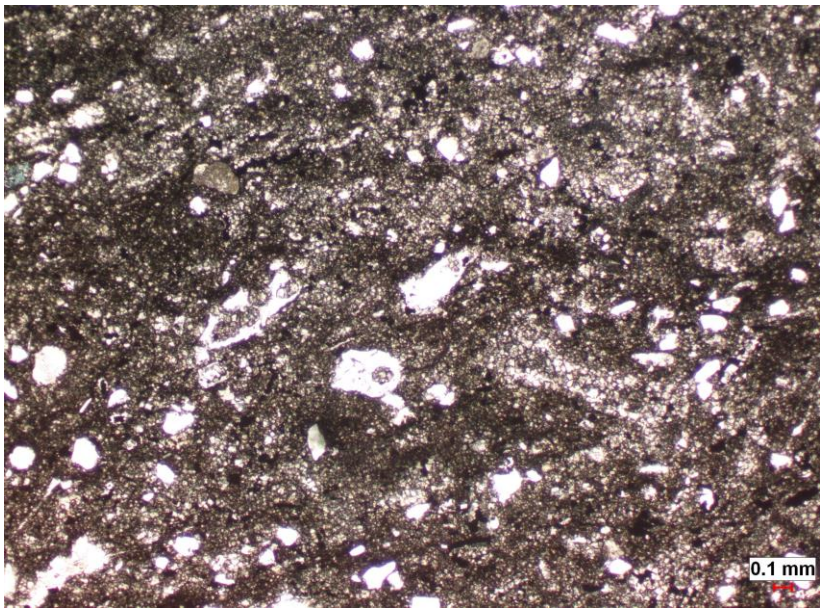

Figure 4.42: Sample K87+50 from Lubin 1, Lubin mining district; note the lighter and darker components of the carbonate-rich matrix.

### 4.2.3 General Petrographic Observations

Lenses of carbonate above the basal contact range in thickness from ~0.01 mm to 0.4 mm. Their lateral length is most commonly on the order of tenths of millimeters, rarely reaching 1 to 2 mm. The most common thickness for a carbonate lens is between 0.025 and 0.2 mm; samples from the Sangerhausen Basin exhibit lenses as thick as 0.3 to 0.4 mm, while samples from the Lubin mining

district have an approximate maximum thickness of 0.3 mm. The thinnest carbonate lenses measured are 0.01 to 0.02 mm.

The only samples above the basal contact that do not contain detrital quartz are those composed of carbonate within the Sangerhausen Basin: 50 and 60 cm above the contact in core SGH133, 42 cm above the contact in SGH132, and 31 cm above the contact in SGH103. Carbonate-rich samples above the Kupferschiefer in the Lubin district (50 and 110 cm above the contact in Lubin 1, and 50 and 120 cm above the contact in Lubin 2) do contain detrital quartz, though it is more likely to be sub-angular, compared to the sub-rounded grains found deeper in the section.

Transitions from clay- and carbon-rich marly shale to carbonate-rich shale/limestone are present between the samples taken 25 and 50 cm above the basal contact in SGH133, samples 22 and 42 cm above the contact in SGH132, and samples from 19 and 31 cm above the contact in SGH103. It should be noted that 22 cm above the contact in core SGH132, and 20 cm above the contact in core E-27, the thin sections show thick, relatively abundant carbonate lenses. The sample taken 31 cm above the contact in E-27 is composed of mostly carbonate aggregates or lenses; it contains only 5 to 10% clay. Thin sections produced from Wettelrode mine only sampled to 26 cm above the basal contact, and all thin sections from this location exhibit a matrix composed of alternating lenses; thin sections from this site therefore cannot be used to aid in the determination of the approximate depth where the transition from clay-rich to carbonate-rich shale takes place.

The thin section from 30 cm above the contact in Lubin 2 shows abundant carbonate, with a calcite vein appearing to separate a more carbonate-rich section with abundant detrital quartz from and a second section with interlaminated clay and carbonate lenses. The only observed occurrence of calcite within the matrix (i.e. not part of a vein), indicated by red staining from the alizarin red, was found in a sample from Lubin 1, at 110 cm above the basal contact of the Kupferschiefer. This sample is from the carbonate-rich upper half of the Kupferschiefer, and the calcite is dispersed among the other carbonate, likely dolomite, and detrital quartz.

Below the contact, the Sangerhausen Weissliegend sandstone samples vary in grain size, degree of compaction, and the presence or absence of laminations composed of coarser or finer material. The Weissliegend samples are composed mostly of quartz, feldspar (especially anorthite ($CaAl_2Si_2O_8$)) and volcanic clasts (Table 4.2). As observed previously at hand-sample scale, samples from the Lubin mining district do not vary in grain size as greatly as the samples from the Sangerhausen Basin. The grains that make up the Sangerhausen Weissliegend are most commonly sub-rounded to sub-angular, though in some samples, grains are angular or, more rarely, rounded. Grains that make up the Weissliegend in the Lubin mining district are most likely to be sub-rounded; rounded or sub-angular grains are also observed. Sorting in the Sangerhausen Weissliegend ranges from well sorted to very poorly sorted, with most of the samples being moderately to poorly sorted; in the Lubin mining district, almost all samples are moderately sorted, with some samples moderately well to very well sorted. In samples from both locations, calcite cement is the most common, with some samples exhibiting anhydrite, silica, or clay cement.

Using the visibility of blue epoxy as an approximate gauge for intergranular porosity (Figure 4.43), it can be determined that the samples taken 4 and 95 cm below the contact in the Wettelrode mine show a greater degree of porosity compared to the samples from 13, 21, and 50 cm below the contact. In core SGH133 only one thin section was made from a Weissliegend sample, at 6 cm below the contact; this sample does not show much, if any, porosity. Thin sections were made at 12, 55, and 68 cm below the contact from core SGH132; porosity is present at 12 cm, but absent at 55 and 68 cm. In the 2 cm immediately below the contact in core E-27, porosity is present, as well as 16 cm below the contact; occasional porosity at 27 cm, and no evident porosity at 36 cm below the contact. In the three Weissliegend samples from core SGH103, porosity is present at 5 cm below the contact; no porosity is recorded at 16 and 28 cm below the contact. In the Lubin mining district, Rudna 1 exhibits porosity at 25 and 130 cm below the contact, but not at 10 cm below the contact. In Rudna 2, porosity is present 10 cm below the contact, with horizons of greater and lesser amounts. Porosity is relatively abundant at 100 cm below the contact. In Lubin 1, samples from 10, 20, and 120 cm below the contact exhibit porosity, with

the greatest abundance present at 10 cm, followed by 20 and 120 cm. In Lubin 2, porosity is greatest in the sample from 50 cm below the contact, followed by the sample from 120 cm below the contact; porosity is present but not abundant at 5 cm below the contact. In samples that exhibit porosity, the porosity generally makes up less than 5% of the sample, although porosity of up to 20% is recorded in the thin section from 130 cm below the contact in Rudna 1. In the absence of porosity, interstitial spaces are filled with carbonate cement or sulfide mineralization, and in some samples, what is either silica cement or very fine grains of quartz.

The Boundary Dolomite, a thin carbonate unit occasionally present between the Kupferschiefer and Weissliegend units, is only found within samples from the Lubin mining district. The sample taken from the basal contact at Rudna 1 shows carbonate below the marly shale, as opposed to a sandstone. In this section, the Boundary Dolomite is less than 10 cm thick (a sample taken from 10 cm below the contact is composed of sandstone). A sample from the contact was not taken at Rudna 2, and at Lubin 1 the sample at the contact shows only the Kupferschiefer, and not what lies immediately beneath it. Two samples from Lubin 2, taken approximately 2 and 4 cm below the contact, have been identified as the Boundary Dolomite; here the unit is less than 5 cm thick, since a sample from 5 cm below the contact is composed of sandstone.

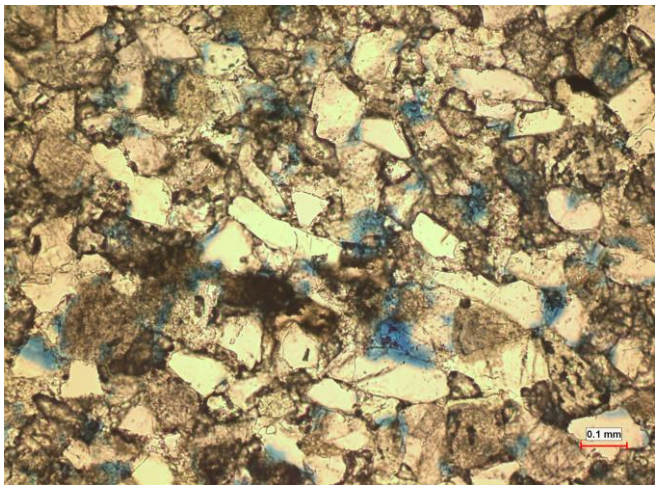


Figure 4.43: Sample K50-16 from core E-27, Sangerhausen Basin. An example of interstitial porosity, as illustrated by the presence of blue epoxy. Photomicrograph taken under plain polarized light.

Table 4.2: Summary of Weissliegend sorting, grain roundness, cement type, and main mineral composition. "xx" denotes relative abundance, especially compared to other components ("x").

| Sample # | Location Depth | Sorting | | | | | Grains | | | | Cement | | | Minerals | | | |
|---|---|---|---|---|---|---|---|---|---|---|---|---|---|---|---|---|---|
| | | very well | well | moderate | poor | very poor | round | sub round | sub angular | angular | calcite/anhydrite | silica | clay | quartz | feldspar | calcic feldspar (anorthite) | volcanic clasts |
| **K** | **Wettelrode** | | | | | | | | | | | | | | | | |
| 9 | -4 | | | | x | | x | x | | | | x? | x? | x | x | | x |
| 10 | -13 | | | x | | | | | | x | x | | | x | x | | x |
| 11 | -21 | | x | | | | | x | x | | x | | | | | x | |
| 15 | -50 | | | | x | | | x | | | x | | x? | xx | x | | x |
| 16 | -95 | | | | | x | x | x | | | | xx | | x | x | | xx |
| **K** | **SGH133** | | | | | | | | | | | | | | | | |
| 17 | -6 | | | | | x | x | x | | | x | | | | | | xx |
| **K** | **SGH132** | | | | | | | | | | | | | | | | |
| 38 | -12 | | | | x | | | x | x | | x | | | x | x | | x |
| 35 | -55 | | | | | x | | x | x | | x | | | x | x | | x |
| 34 | -68 | | | | x | | | | x | x | | | x? | x | x | | x |
| **K** | **E-27** | | | | | | | | | | | | | | | | |
| 51 | -4 | | x | | | | | | x | x | | | x | xx | | x | x |
| 50 | -16 | | | | x | | | | x | x | x | | | xx | | xx | |
| 49 | -27 | | x | | | | | x | x | | x | | | xx | | | |
| 48 | -36 | x | | | | | | | x | | x | | | x | x | | x |
| **K** | **SGH103** | | | | | | | | | | | | | | | | |
| 58 | -5 | | | | | x | | x | x | | | | | x | | x | xx |
| 57 | -16 | | | | | x | | x | x | x | xx | | | x | x | x | xx |
| 56 | -28 | | | x | | | | | x | x | x | | x | x | | xx | |
| | | | | | | | | | | | | | | | | | |
| **K** | **Rudna 1** | | | | | | | | | | | | | | | | |
| 68 | -10 | | | x | | | | x | x | | x | | | x | | x | |
| 69 | -25 | | | x | | | x | x | | | x? | | | xx | | x | |
| 70 | -130 | | | x | | | x | x | | | | | | xx | | xx | |
| **K** | **Rudna 2** | | | | | | | | | | | | | | | | |
| 73 | -10 | x | | | | | x | x | | | x | | | xx | x | x | |
| 74 | -100 | | | x | | | x | x | | | x | x? | | xx | | xx | |
| **K** | **Lubin 1** | | | | | | | | | | | | | | | | |
| 92 | -10 | | | x | | | | x | | | x | | | xx | x | xx | x |
| 93 | -20 | | x | | | | | x | | | xx | | | xx | | xx | x |
| 94 | -120 | | | x | | | | x | | | x | | | xx | | xx | |
| **K** | **Lubin 2** | | | | | | | | | | | | | | | | |
| 97 | -5 | | | x | | | | x | x | | | | | x | x | | x? |
| 96 | -50 | x | | | | | | x | | | x | | | x | | xx | |
| 95 | -120 | xx | | | | | | x | | | x | | | xx | | xx | |

### 4.2.4 Veins

At the Wettelrode location in the Sangerhausen Basin, a sample from 26 cm above the Kupferschiefer basal contact contains two carbonate veins. The thicker of the two (≤6 mm) is nearly perpendicular to the alternating lenses of carbonaceous/clay material and carbonate that make up the matrix, while the thinner of the two (≤0.2 mm) is at a high angle to the laminations, but not quite perpendicular. The laminations appear to exhibit slight offset on either side of the thinner vein, but it is difficult to definitively say due to the discontinuous nature of the lenses of clay and carbonate. Anastomosing horizontal veins are present in the thin sections from 14, 10, and 5 cm above the basal contact in the Wettelrode mine (Figure 4.44), 8 cm above the contact in core SGH133, and 7 cm above the contact in E-27. No veins are observed in SGH132 and SGH103.

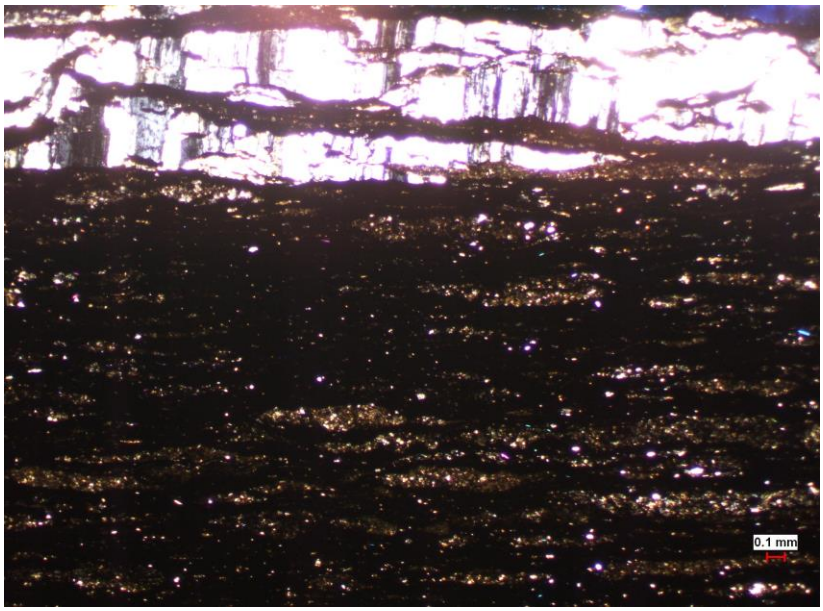


Figure 4.44: Sample K5+14 from Wettelrode mine, Sangerhausen Basin. An example of a quartz vein within the Kupferschiefer. Photomicrograph taken under cross polarized light.

In thin sections from Rudna 1, two veins are observed at a low angle to the horizontal: one at 50 cm above the contact, and one within the Boundary Dolomite immediately below contact. The latter is a quartz vein, with smaller veins appearing to branch off from the main vein at high angles to the horizontal. In Rudna 2, calcite is present in vein-like features at 35 cm above the contact. Due to the

fractured nature of the matrix it is difficult to say if the feature was originally a vein and was disrupted with the matrix, or if the calcite formed after the disruption (Figure 4.45). At 10 cm above the contact, calcite veins are partially intersected by the thin section; they are oriented parallel, perpendicular, and at ~45˚ to the alternating lenses. At 10 cm below the contact in Rudna 2, the sample exhibits what appear to be compacted carbonate veins that have been partially intersected by the thin section. Thin sections from Lubin 1 exhibit horizontal veins in samples taken from 50, 40, 20, and 0 cm above the contact. At 40 cm above the contact, some smaller calcite veins are nearly perpendicular to horizontal, and at 20 cm what appear to be offshoots of a roughly horizontal vein travel across the matrix at low angles. In Lubin 2, horizontal calcite veins are present at 30 and 25 cm above the contact, and a carbonate vein is observed within the Boundary Dolomite a few cm below the contact.

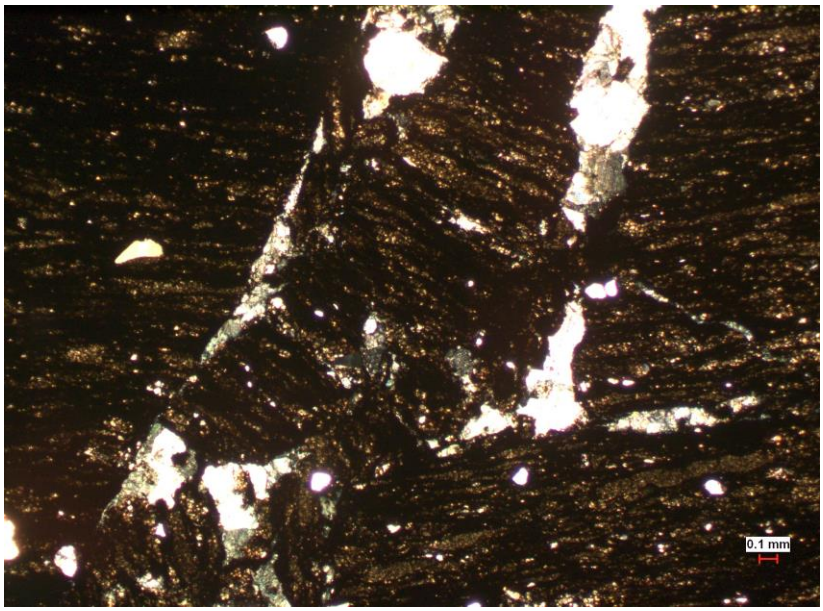


Figure 4.45: Sample K71+35 from Rudna 2, Lubin mining district. Note the carbonate in between sections of disrupted matrix.

### 4.2.5 Sangerhausen Basin: Mineralization

Mineralization that can be viewed under the microscope is described using terms similar to those used by Sawłowicz (1990). Descriptors of mineralization visible under microscope are used without a

prefix, unlike the mineralization described in the hand samples, and is simply described as disseminated, bleb, aggregate, and so on.

Sulfides are present to some degree in all Sangerhausen samples. Most of the mineralization observed in the Sangerhausen Kupferschiefer and Weissliegend samples is chalcocite; the second most abundant sulfide mineral is chalcopyrite. Other mineralization present in samples from the Sangerhausen Basin includes pyrite, digenite, galena, and bornite. Pyrite framboids are present above the contact.

**Wettelrode:** The thin section from 26 cm above the contact exhibits small blebs of chalcocite and chalcopyrite, abundant pyrite framboids, small blebs of digenite, and possible rutile or titanite. Some (chalco)pyrite framboids exhibit a chalcocite rim. At 14 cm above the contact, the thin section contains disseminated chalcocite, and aggregates, blebs, and disseminated spherules of chalcopyrite. Chalcocite, chalcopyrite, and pyrite are present as blebs and disseminated spherules 10 cm above the contact (Figure 4.46). At and immediately above the contact, chalcopyrite is present in the form of aggregates, blebs, and disseminated mineralization; the sample also exhibits chalcocite blebs and blebs, spherules, and framboids of pyrite. Digenite and covellite may also be present (or it may be tarnish). The only recorded presence of galena is found in this sample: a 0.2 mm bleb of galena is surrounded by chalcopyrite, and a ~0.06 mm bleb of galena is present, independent of chalcopyrite (Figure 4.47). At 4 and 13 cm below the contact, interstitial chalcopyrite, chalcocite, and bornite are present; very small amounts of digenite and covellite are also present. Thin sections taken 21 and 50 cm below the contact exhibit interstitial chalcopyrite and chalcocite. Fifty cm below the contact, at least one occurrence of digenite and covellite is recorded. Interstitial chalcocite is rare in the thin section from 95 cm below the contact.

**SGH133:** Mineralization in the thin section 62 cm above the contact is scarce, but chalcopyrite and chalcocite are present in the form of blebs. Framboidal-like chalcopyrite is observed at 50 cm above the contact (Figure 4.48), as well as disseminated chalcocite. The framboidal-like chalcopyrite exhibits tarnished edges. The sample from 25 cm above the contact contains chalcopyrite aggregates, pyrite framboids, and chalcocite aggregates, blebs, and disseminated spheres. No chalcopyrite is observed in the thin section from 17 cm above the contact, but chalcocite is present in the form of aggregates and

disseminated spheres. At 8 cm above the contact, chalcocite is observed in the form of aggregates and disseminated spherules; chalcopyrite is present as disseminated spherules and within an irregular vein that is oriented parallel and nearly perpendicular to the matrix (Figure 4.48). The sample from 3 cm above the contact contains what appear to be pyrite framboids and chalcocite blebs, but it is difficult to be certain as the thin section was carbon coated for scanning electron microscopy before the mineralization characterization was performed. The sample from 6 cm below the contact exhibits interstitial chalcocite and scarce interstitial chalcopyrite.

**SGH132:** The thin section from 42 cm above the contact exhibits framboidal-like chalcopyrite blebs and aggregates of these blebs; chalcocite blebs are scarce. Edges of aggregates may be composed of bornite or digenite, or simply tarnished. At 22 cm above the contact, small spherules of chalcopyrite and blebs of chalcocite are present. The sample from 8 cm above the contact contains chalcopyrite blebs and aggregates, and blebs and disseminated spheres of chalcocite. The edges of the aggregates may be composed of bornite, or simply tarnished. The thin section samples from 12 and 55 cm below the contact contain interstitial chalcocite. The sample from 68 cm below the contact contains interstitial chalcopyrite and chalcocite; some of the chalcopyrite blebs appear to have a bornite rim (or it may be tarnish).

**E-27:** The thin sections from 31 and 20 cm above the contact exhibit spherules and blebs of chalcopyrite and chalcocite. At 7 cm above the contact, the thin section contains aggregate and spherules of chalcopyrite, and aggregates of pyrite. The thin section from 4 cm below the contact contains interstitial chalcopyrite and bornite, and rare occurrences of digenite and covellite; the samples from 16, 27, and 36 cm below the contact contain interstitial blebs of chalcocite.

**SGH103:** The thin section from 31 cm above the contact exhibits chalcopyrite aggregates. At 19 cm above the contact, blebs and disseminated spherules of chalcocite are present; blebs of chalcopyrite are scarce. The sample from 7 cm above the contact contains blebs of chalcocite, pyrite framboids, and scarce blebs of chalcopyrite. At 5 cm below the contact, interstitial chalcocite is present; interstitial chalcopyrite is scarce. The thin section from 16 cm below the contact contains interstitial chalcocite. In the sample from 28 cm below the contact, interstitial chalcocite is present in very small amounts.

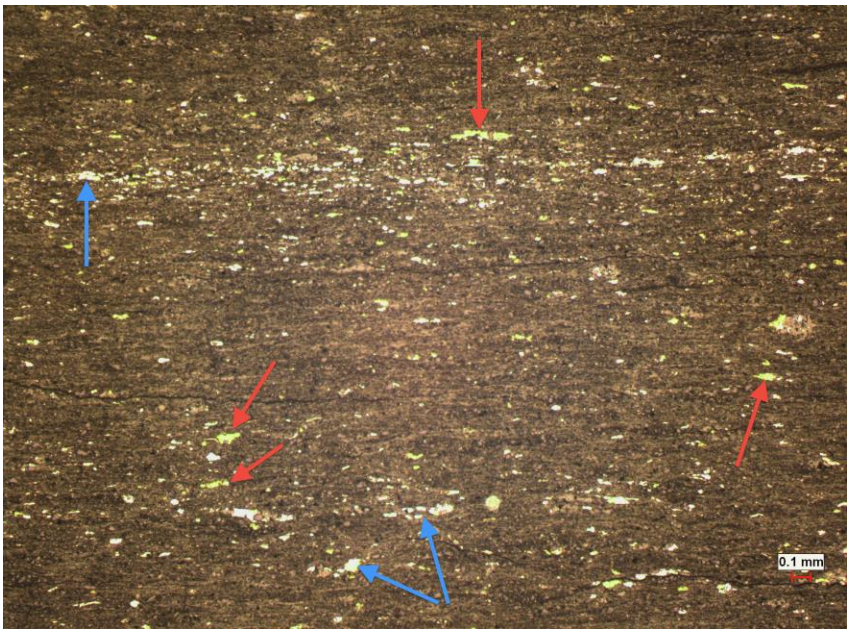

Figure 4.46: Sample K6+10 from Wettelrode mine, Sangerhausen Basin. Note the yellow (chalcopyrite, red arrows) and white-yellow (chalcocite, blue arrows) blebs of mineralization.

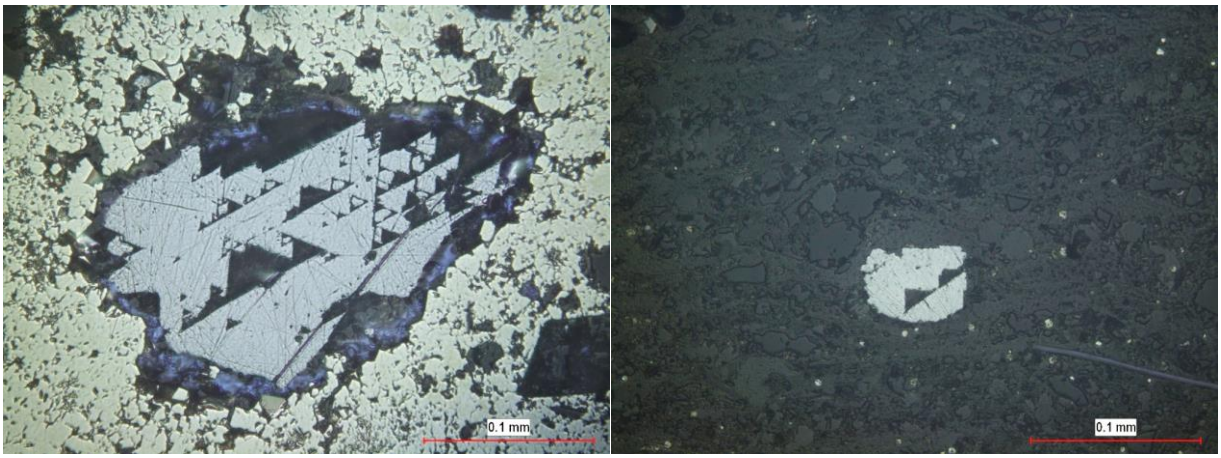

Figure 4.47: Sample K8+5 from Wettelrode mine, Sangerhausen Basin. Galena, exhibiting characteristic triangular pits, surrounded by chalcopyrite (left) and as an independent bleb (right).

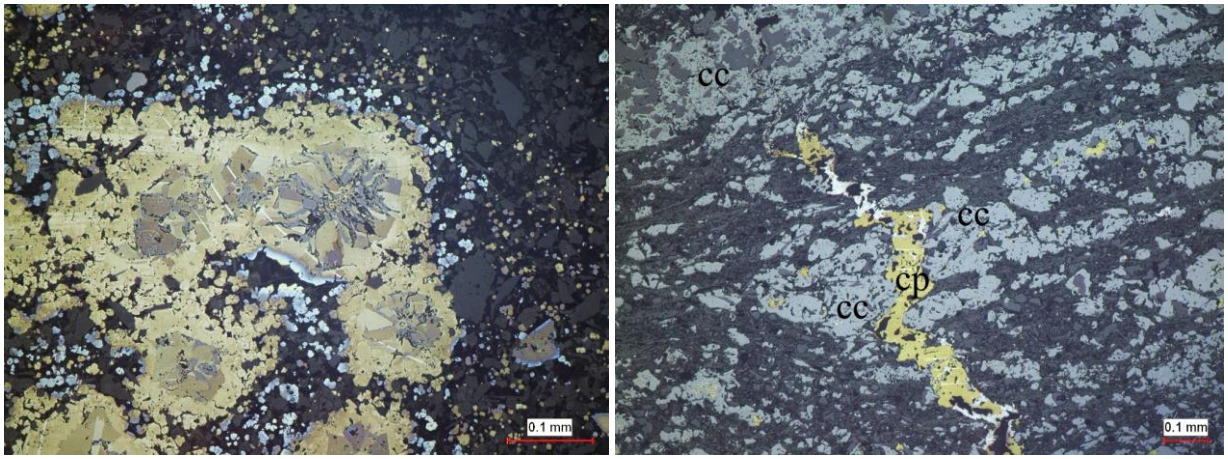

Figure 4.48: Samples K29+50 (left) and K20+8 (right) from core SGH133; note the framboidal-like chalcopyrite mineralization rimmed with bornite 50 cm above the contact, and the high angle vein of chalcopyrite (cp) and the aggregate chalcocite (cc) mineralization 8 cm above the contact.

### 4.2.6 Lubin Mining District: Mineralization

Sulfide mineralization in Lubin mining district samples includes chalcopyrite, chalcocite, bornite, pyrite, sphalerite, digenite, and covellite. Most of the mineralization observed in the Lubin mining district samples is chalcocite, with the exception of the sample from 20 cm above the contact in Rudna 2, where bornite is the most abundant sulfide. Pyrite framboids are present above the contact and in the Boundary Dolomite.

**Rudna 1:** The thin section from 50 cm above the contact contains chalcopyrite aggregates and framboids, chalcocite aggregates, blebs, and framboids, and pyrite framboids. Sphalerite is also present, associated with chalcocite. The mineralization at this depth is more common proximal to larger detrital quartz grains, and is generally more abundant within the carbonate matrix than in the shale matrix. Mineralization is more likely to be blebs and disseminated spheres in the shale, and more likely to be aggregate-like in the carbonate. At 40 cm above the contact, the thin section exhibits aggregates and blebs of chalcopyrite, blebs and disseminated spherules of chalcocite, and what appears to be an aggregate of pyrite. Sphalerite is present as "blebs" surrounded by dolomite crystals (Figure 4.49). The thin section from 20 cm above the contact contains blebs and disseminated spherules of chalcocite, and what is either tarnish or bornite associated with the chalcocite. Chalcopyrite and pyrite may also be

present, but cannot be differentiated from tarnish. The thin section made at the contact exhibits mineralization within the Boundary Dolomite that immediately underlies the Kupferschiefer. Chalcopyrite is present within fractures found in the Boundary Dolomite; chalcocite is present as small spherules throughout the thin section, and interstitially among the dolomite grains. Bornite is present interstitially and as disseminated spherules within the dolomite, and occasionally rimmed with chalcopyrite; pyrite is present in the form of spherules above and below the contact. Sphalerite is present in the thin section taken at the contact, adjacent to a carbonate vein that contains fluorescent hydrocarbons (Figure 4.50). At 10, 25, and 130 cm below the contact, interstitial chalcopyrite, chalcocite, and bornite are present. The bornite at 25 cm below the contact is found within the interstitial chalcopyrite.

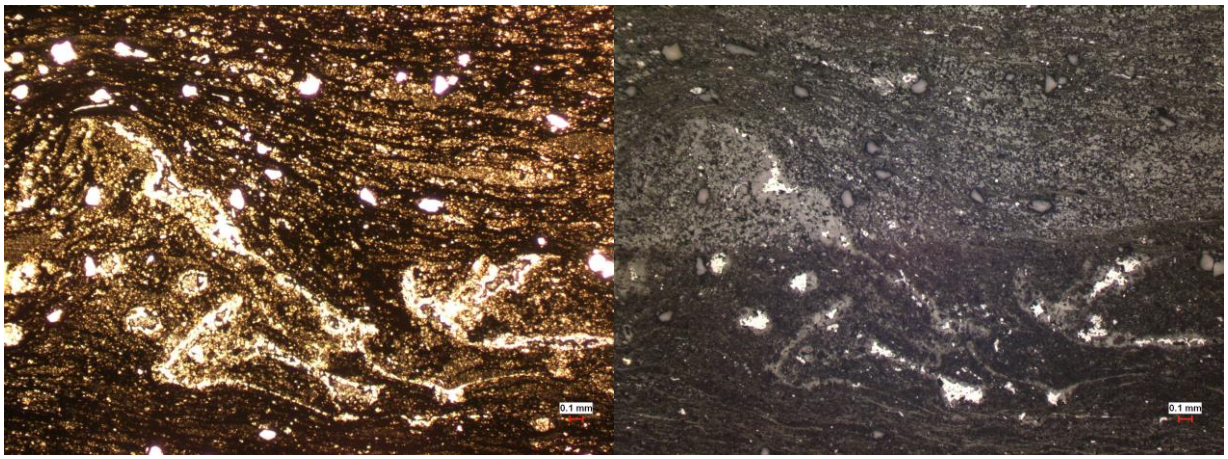

Figure 4.49: Sample K63+40 from Rudna 1. Top left: plane-polarized transmitted light. Top right: same area of the thin section, under reflected light; the lighter color of the top half is the result of ferrous iron staining. Sulfide mineralization surrounded by dolomite crystals and light gray with a brown tint under reflected light is sphalerite.

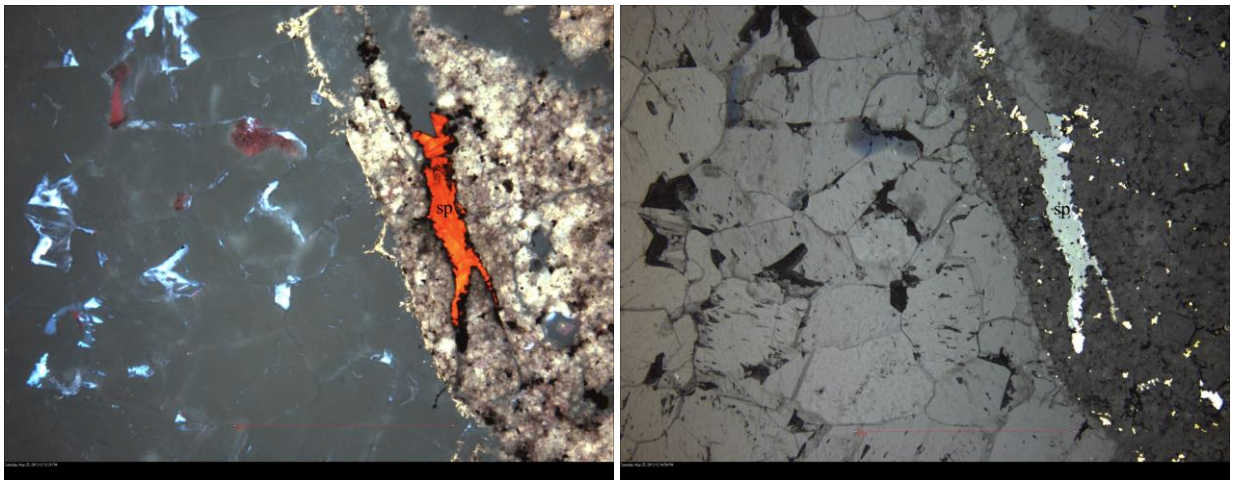

Figure 4.50: Sample K66+0 from Rudna 1, Lubin mining district. The photomicrograph on the left was taken under fluorescent light; the one on the right was taken under reflected light. Note the presence of sphalerite (sp) (fluorescing red, reflecting gray), and the presence of hydrocarbons within the carbonate vein.

**Rudna 2:** The thin section from 35 cm above the contact exhibits spherules and what appear to be replaced framboids composed of chalcocite; blebs and disseminated spherules of chalcocite in addition to chalcocite are present within calcite veins; bornite may be present, or it might simply be tarnish; pyrite is present as spherules and framboids. At 20 cm above the contact mineralization is found proximal to concentrations of quartz grains and preferentially along laminations. Chalcopyrite is observed in the form of aggregates parallel to alternating lenses of carbonaceous/clay material and carbonate, and as a vein with bornite inside. Bornite is also observed as blebs, aggregates, veins, and framboids. Chalcocite is present as blebs and aggregates, and pyrite is observed as framboids and spherules. The thin section from 10 cm above the contact blebs and disseminated spherules of chalcocite; blebs, spherules, and replaced framboids composed of bornite (possibly just tarnish); framboids and spherules of pyrite; and possible framboids and spherules of chalcopyrite. Some framboids of (chalco)pyrite have a bornite rim. At 10 cm below the contact, the thin section exhibits interstitial chalcopyrite, chalcocite, and bornite. Bornite is most commonly seen with chalcopyrite rims. The thin section from 100 cm below the contact contains interstitial chalcocite and chalcopyrite; interstitial bornite is also observed, with blebs of chalcopyrite within.

**Lubin 1:** The thin section from 110 cm above the contact contains aggregates of chalcocite and chalcopyrite; framboids of pyrite, some of which have been replaced by chalcopyrite and/or have a bornite rim; bornite is also present in the form of small blebs. At 50 cm above the contact, chalcocite blebs, disseminated spherules, and framboidal-like features are present. Pyrite is observed as framboids, and bornite is present as disseminated spherules, a vein (Figure 4.51), and associated with chalcocite. Chalcopyrite is present as rims to bornite blebs. The thin section from 40 cm above the contact exhibits blebs, veins parallel to the matrix, and disseminated spherules of chalcocite; bornite as disseminated spherules and veins rimmed with chalcopyrite within carbonate veins; pyrite framboids occasionally with chalcocite rims. The thin section from 20 cm above the contact contains chalcopyrite as blebs and as rims to bornite within a calcite vein (Figure 4.52); chalcocite blebs, disseminated spherules, and veins associated with and independent of calcite veins (Figure 4.53); "interstitial" bornite within a calcite vein; and pyrite framboids with rims of bornite or chalcopyrite. Digenite and covellite are present within blebs composed of other sulfides; digenite is also present as blebs. In the thin section taken at the contact, chalcocite is present as disseminated spherules, blebs, sections of veins, and aggregates. Pyrite framboids and digenite within chalcocite blebs are also present. Thin sections from 10, 20, and 120 cm below the contact exhibit interstitial chalcocite; chalcopyrite is also present in very small amounts at 120 cm below the contact.

**Lubin 2:** The thin section from 120 cm above the contact contains chalcocite blebs; pyrite framboids that are rimmed by bornite, covellite, and possibly chalcopyrite; and blebs of digenite and covellite. The thin section taken 50 cm above the contact only exhibits large blebs of chalcocite. At 30 cm above the contact, the thin section exhibits blebs and disseminated spherules of chalcocite, as well as "interstitial" chalcocite within calcite veins. Bornite blebs are present, occasionally rimmed by chalcopyrite and associated with calcite veins (Figure 4.54); digenite and covellite are observed within the blebs composed of other sulfides, digenite is also present in the form of blebs. Blebs are the most common form of mineralization 25 cm above the contact, composed of chalcopyrite, chalcocite, bornite, and digenite. Chalcopyrite is also observed as rims to bornite blebs; bornite veins are present; as well as

pyrite framboids with rims of digenite and/or bornite. The thin section taken at the contact contains blebs and aggregates of chalcocite, pyrite framboids, blebs of covellite, and veins of bornite. Mineralization is more abundant within the Kupferschiefer than the underlying Boundary Dolomite, and follows laminations within the Kupferschiefer. Two thin sections were made from the Boundary Dolomite; both exhibit interstitial chalcocite, pyrite framboids, and digenite rims (or simply tarnish) on chalcocite mineralization. The deeper of these two thin sections, closer to the Weissliegend, also exhibits rare covellite blebs, and bornite on digenite blebs. The thin section from 5 cm below the contact contains interstitial chalcocite and covellite; bornite (or tarnish) is rims some of the chalcocite. The thin section from 50 cm below the contact exhibits interstitial chalcocite, bornite, digenite, and covellite. What appears to be chalcopyrite is also present in the form of small cubes. The thin section from 120 cm below the contact contains interstitial chalcocite, chalcopyrite, and bornite in sulfide bands. Some instances of chalcopyrite appear to have been partially replaced by sphalerite.

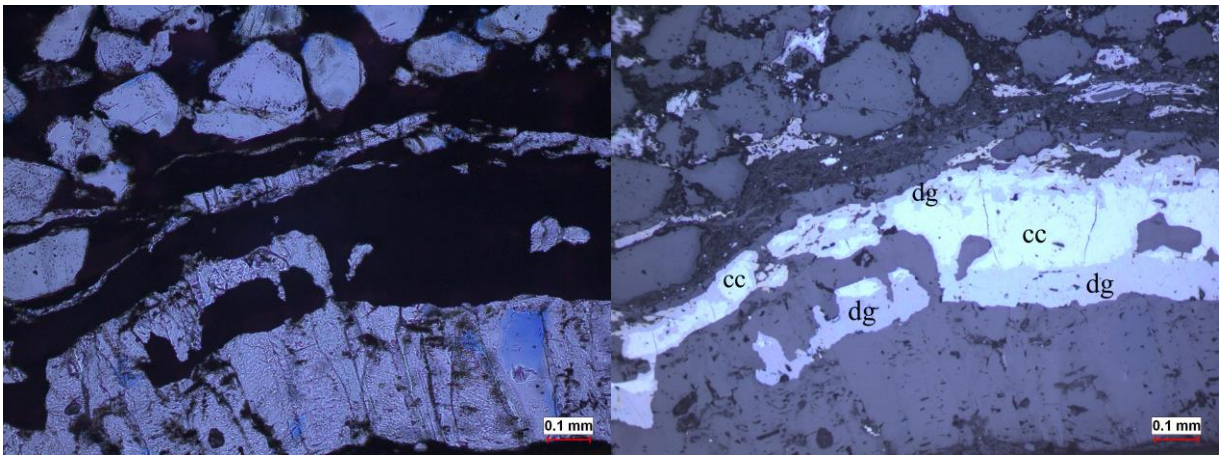

Figure 4.51: Sample K87+50 from Lubin 1, Lubin mining district. Sulfide mineralization associated with a vein: an image taken with transmitted light (left, plain polarized) and reflected light (right) of the same thin section location. The mineralization is chalcocite (cc, white-blue) surrounded by digenite (dg, dusky blue). Note the detrital quartz in the upper left corner. The blue color in the lower left corner of the transmitted light photo is epoxy.

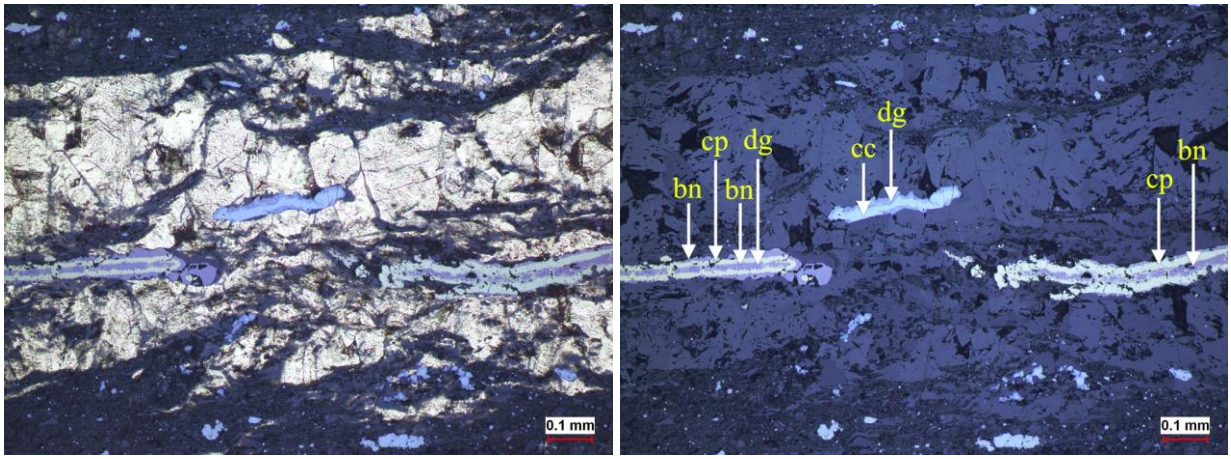

Figure 4.52: Sample K89+20 from Lubin 1, Lubin mining district. Sulfide mineralization associated with a vein: an image taken with a combination of transmitted and reflected light (left, plain polarized) and only reflected light (right) of the same thin section location. The mineralization from center to rim is: chalcocite (cc, white-blue), digenite (dg, dusky blue), bornite (bn, pale purple), and chalcopyrite (cp, yellow). The vein is composed of calcite.

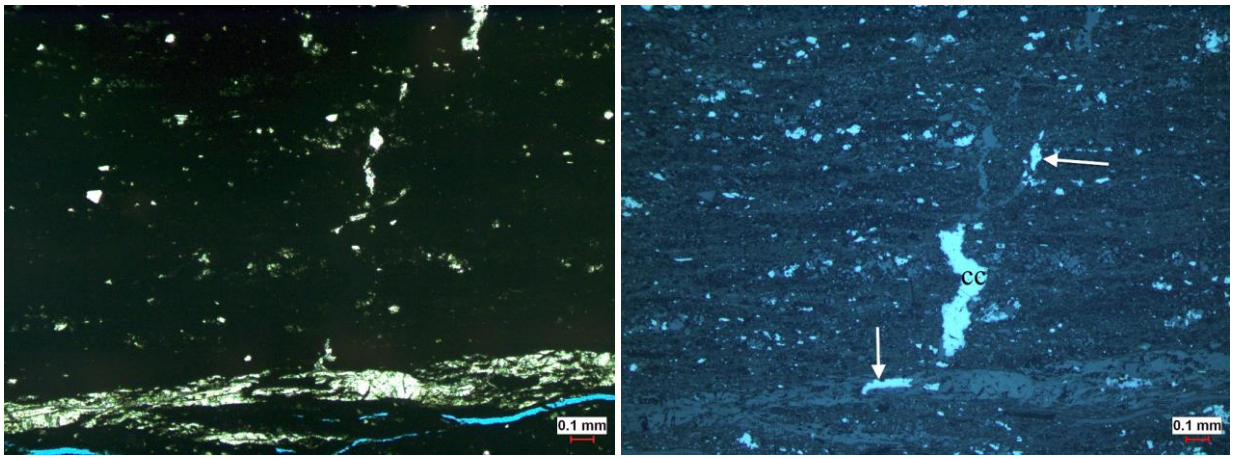

Figure 4.53: Sample K89+20 from Lubin 1, Lubin mining district. Sulfide mineralization associated with a vein: an image taken with transmitted light (left, plain polarized) and reflected light (right) of the same thin section location. The mineralization is chalcocite (cc). Note the mineralization within the bedding-parallel vein, surrounded by carbonate, and the mineralization that takes up the entire width of the bedding-perpendicular vein in some sections (see arrows).

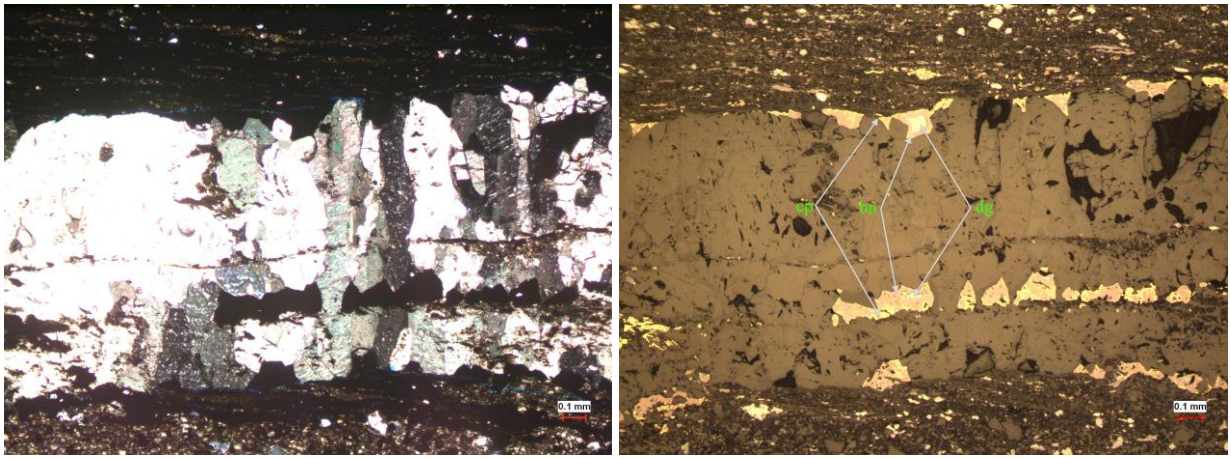

Figure 4.54: Sample K103+30 from Lubin 2, Lubin mining district. Sulfide mineralization associated with a vein: an image taken with transmitted light (left, cross polarized light) and reflected light (right) of the same thin section location. The mineralization is digenite (dg, dusky blue), bornite (bn, pale purple), and chalcopyrite (cp, yellow) (bottom). The vein is composed of calcite.

### 4.2.7 Other Features

The sample from 5 cm above the contact in the Wettelrode mine contains a mud lens with what appears to be insect remains in it. There are up to a dozen pieces of remains that are a yellow-brown color in transmitted light and dimly glow blue under fluorescent light. Sulfide mineralization in the form of chalcocite and chalcopyrite is associated with some of the remains; a few pieces have been fractured, and mineralization has filled in these fractures. Other pieces appear to have been replaced by the sulfide mineralization (Figure 4.55). Mud lenses, or chips, observed 3 cm above the contact in core SGH133 and 7 cm above the contact in core E-27 also appear to contain insect remains.

A few of the thin sections that have matrices composed of alternating lenses of carbonaceous clay and carbonate material exhibit features that may be interpreted as ripples (Figure 4.56). As seen in the photomicrograph examples, alternating lenses appear to be curved, as if in a mound, or cross a lamination horizon. These features are similar to what might be observed in hand sample- or outcrop-scale ripples. Samples that exhibit this feature include (but are not necessarily limited to): 14 cm above the contact in Wettelrode, 8 and 17 cm above the contact in SGH133, 7 cm above the contact in SGH103, 20 cm above the contact in Rudna 1, 10 and 20 cm above the contact in Rudna 2, and 25 cm above the contact in Lubin 2.

The sample taken 35 cm above the contact in Rudna 2 contains multiple mud chips, or lenses, that are oriented at different angles within the thin section, some of which also exhibit small fractures. In the thin section from 40 cm above the contact in Lubin 1, an approximately horizontal aggregate exhibits offset of approximately 0.1 mm, suggesting a micro-fault.

Other features within the Weissliegend include quartz grains at 5 and 16 cm below the contact in SGH103 that show signs of recovery from micro-tectonic strain, such as undulose extinction and subgrain rotation (Passchier and Trouw, 2005) (ex: Figure 4.41). A 1 mm wide patch (~square?) of carbonate cement is present 10 cm below the contact in Rudna 1; the poikilotopic cement (defined as pre-compaction cementation where the cement is composed of one crystal that encompasses multiple smaller sedimentary grains, in this case quartz) goes extinct at the same time under crossed polars (Figure 4.57). Mud chips are present within the sample taken 27 cm below the contact in E-27.

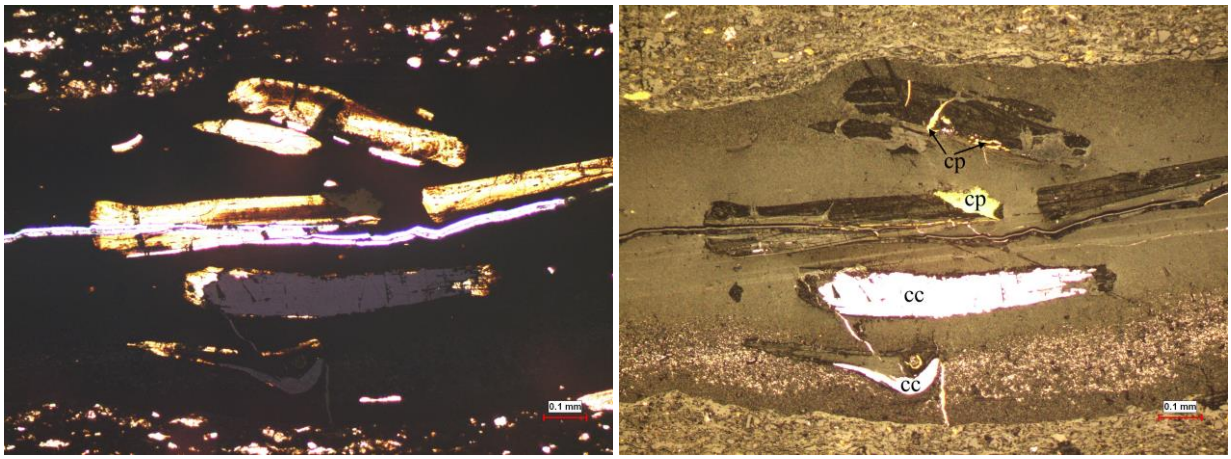

Figure 4.55: Sample K8+5 from Wettelrode mine, Sangerhausen Basin. A mud chip with what appear to be insect remains in plain-polarized light (left) and reflected light (right); note the translucent brown color of the insect remains in transmitted light, and how some of the remains have been mineralized with chalcocite (cc) and chalcopyrite (cp).

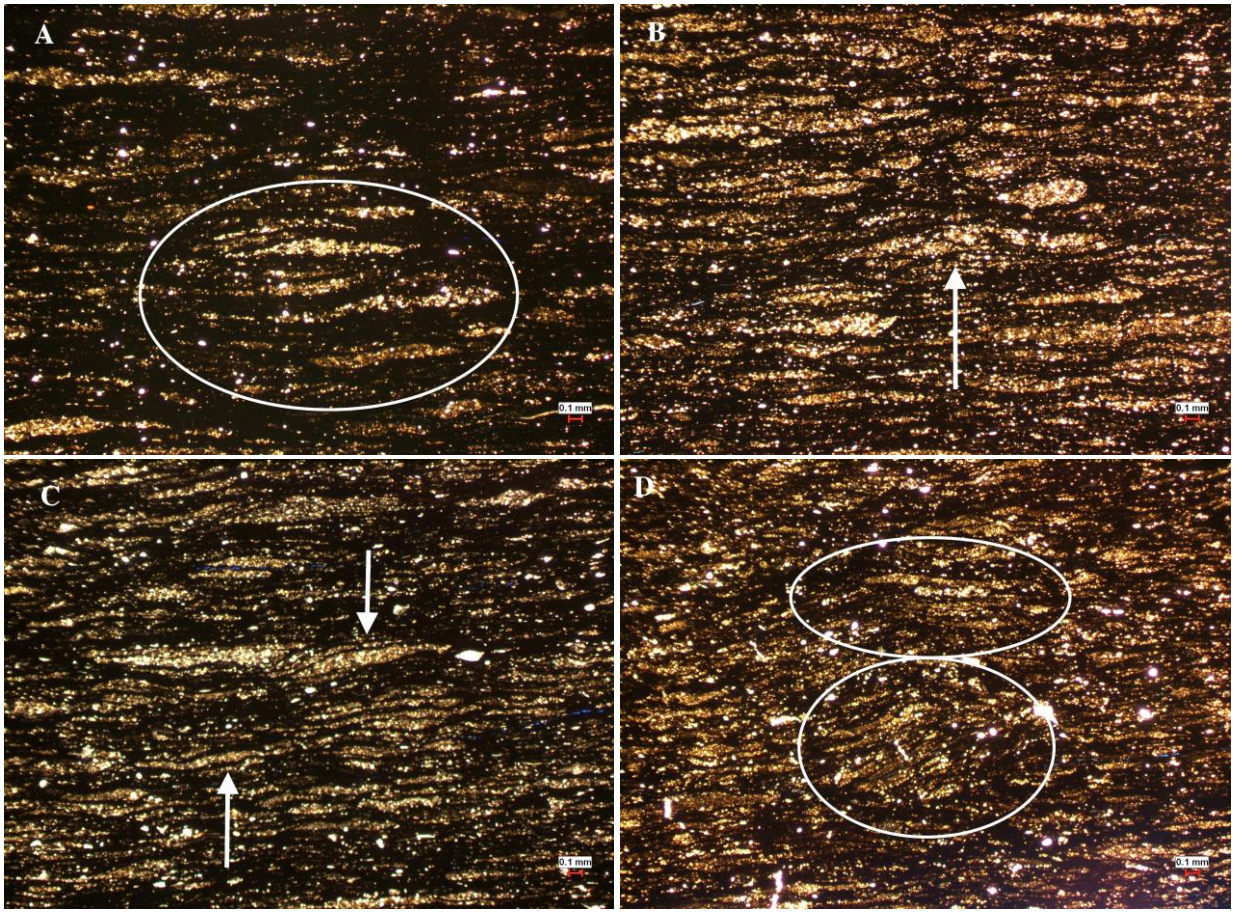

Figure 4.56: Examples of features that might be interpreted as ripples, highlighted by white arrows and circles: A) K5+14, Wettelrode; B)K20+8, SGH133; C) K59+7, SGH103; D) K72+10, Rudna 2.

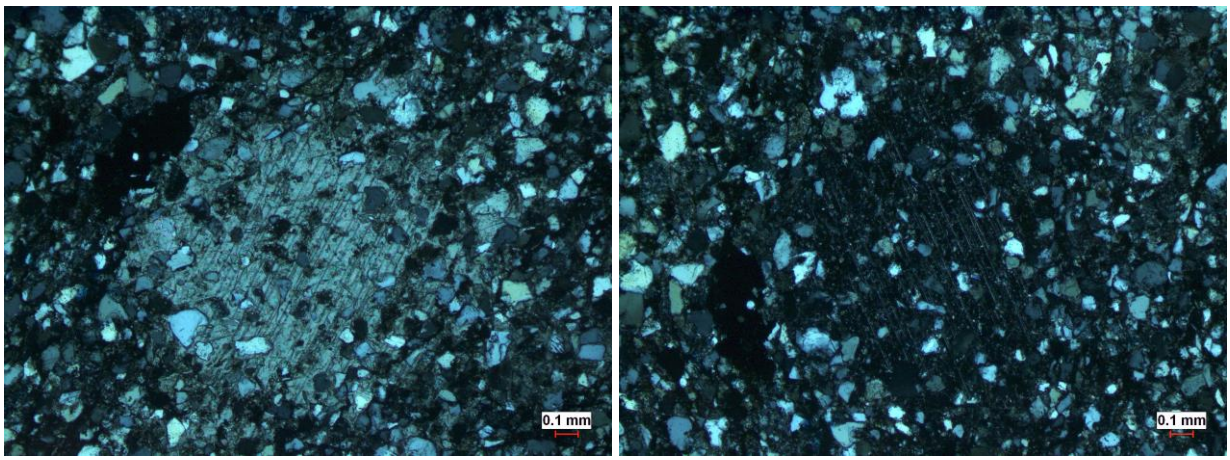

Figure 4.57: Sample K68-10 from Rudna 1, Lubin mining district. Taken in transmitted light with crossed polars; the stage is rotated ~35˚ counterclockwise from the left photo to the right photo. Note the uniform extinction of the calcite cement, and the increased compaction of sand grains outside of the calcite cement.

### 4.2.8 Fluorescence

Fluorescence in Kupferschiefer and Weissliegend thin sections is mostly blue to yellow in color, though occasionally red or green fluorescence is present as well. Sources of fluorescence within the Kupferschiefer include organic matter such as bitumen, oil, and insect remains (Figures 4.58, 4.59, 4.60, 4.61), and carbonate grains such as dolomite (Figure 4.62, 4.63, 4.64). Some fluorescence is associated with sulfide mineralization, illustrated by close proximity to the mineralization (Figure 4.65). Samples from 17 cm above the contact in SGH133 and 40 cm above the contact in Rudna 1 exhibit sulfide mineralization, most likely sphalerite, that fluoresces a red-orange color (Figure 4.66). Fluorescence in the Weissliegend occurs due to the presence of organic matter in the form of oil droplets that have solidified (bitumen) (Figure 4.67) and interstitial oil (Figure 4.68), and as fluorescent accessory minerals within the sand grains (Figure 4.69). In at least 5 of the 31 Weissliegend samples [*K15, 17, 34, 35, 73, 74, 93*], inclusions within individual grains fluoresce (Figure 4.70).

The most abundant fluorescence, in both the Sangerhausen Basin and Lubin mining district samples, is found in carbonate and quartz veins above the basal contact of the Kupferschiefer (Figures 4.58, 4.71, 4.72). The sample taken from 26 cm above the contact in the Wettelrode mine, Sangerhausen Basin, exhibits the greatest amount oil of all the samples studied in this thesis. The bitumen, which is occasionally accompanied by small bubbles of methane gas, is present within fractures of carbonate minerals that make up the larger of two veins that are at a high angle to the matrix. The fluorescence is mostly blue in color, although yellow fluorescence is also observed in both the carbonate vein (Figure 4.58) and within the matrix. The matrix in closer proximity to the large carbonate vein exhibits a higher concentration of fluorescence compared to more distal matrix. The smaller vein exhibits some blue and yellow fluorescence, though it is not nearly as common as in the larger vein.

The thin section from 14 cm above the contact in Wettelrode contains relatively abundant blue fluorescence among the alternating lenses of carbonate and carbonaceous/clay material, in the form of ~1 μm sized spheres (Figure 4.59). Occasional yellow fluorescence is also observed. Zoned dolomite grains are present within some of the carbonate lenses. In at least one location, fluorescence appears to be

intimately associated with sulfide mineralization: a small bleb of chalcopyrite, visible under reflected light, is observed to be rimmed with blue fluorescence under fluorescent light. It is also possible that this fluorescence is the result of reflections, however. Yellow fluorescence is present in the thin section taken 10 cm above the contact in Wettelrode, within inclusion trails in a quartz vein and in the matrix adjacent to the vein.

The most clearly zoned carbonate grains are found in the matrix, 50 and 62 cm above the contact in core SGH133, 42 cm above the contact in SGH132, 20 cm above the contact in Rudna 2, and 50 cm above the contact in Lubin 1. Most of the zoned carbonate grains are 10 μm, plus or minus a few μm, and exhibit three to four zones. The zonation starts with a dark nucleus, and is followed by a light band, a dark band, and sometimes another light band. Thin sections almost exclusively composed of zoned carbonate (dolomite) grains can be identified as micrite due to the dolomitic composition and the average size of the grains (~10 μm) (Flügel, 2004). Zoned dolomite grains are also observed within carbonate lenses in some samples, for example 8 cm above the contact in SGH132 (Figure 4.64).

In some thin sections from samples taken above the contact, yellow fluorescence appears as a long and sinuous band among the alternating pods of carbonaceous clay and carbonate (Figure 4.61). This fluorescence is most likely the result of bitumen smears. Samples that are rich in carbonate rarely show fluorescence resulting from inclusions, though some samples exhibit clear dolomite zonation under the fluorescent microscope. The only observed instance of an oil droplet present within a carbonate-rich sample is from the Boundary Dolomite present in Lubin 2, from 4 cm below the contact. Some fluorescence is a direct result of the presence of sulfide mineralization; sphalerite glows red under fluorescent light in the sample taken 40 cm above the contact in Rudna 1. In the sample from 5 cm above the contact in the Wettelrode mine, features that appear to be insect remains lightly fluoresce green in the mud chip (Figure 4.60). The thin section made from the sample immediately below the contact in core E-27 (K51-4) contains relatively abundant interstitial oil within the Weissliegend. This thin section includes a sliver of the overlying Kupferschiefer; the interstitial oil fluoresces the brightest near the contact, and

shows a clear decrease in brightness approximately 1.5 to 2 cm below the contact. When the thin section is observed in plain light without the aid of a microscope, interstitial brown-colored material (oil) is observed, with the darkest coloring occurring closest to the Kupferschiefer contact and gradually decreasing in concentration as the distance increases

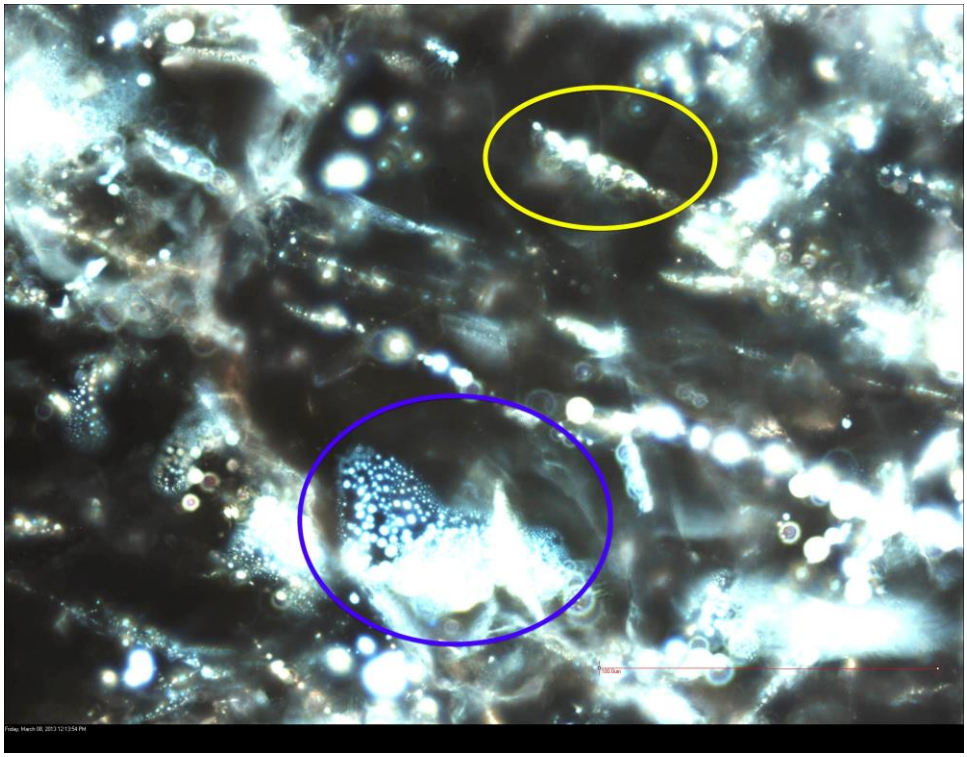

Figure 4.58: Sample K2+26 from the Wettelrode mine, Sangerhausen Basin; blue and yellow fluorescence within carbonate vein indicating inclusions of oil with two different maturities. Examples are circled in the corresponding color. Scale measures 100.0 μm.

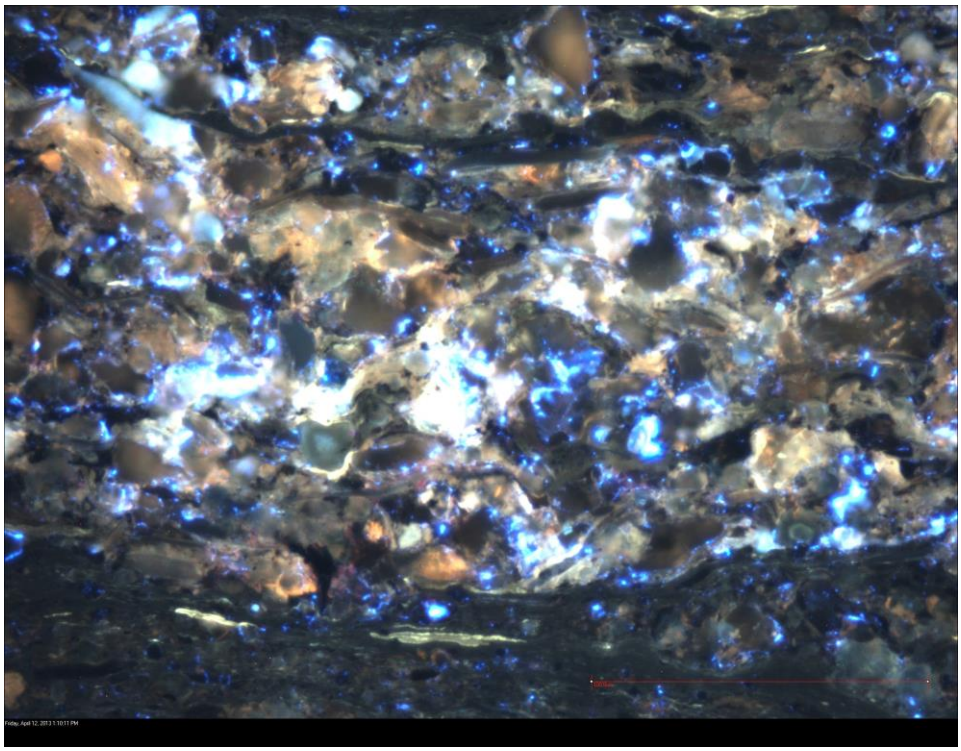

Figure 4.59: Sample K2+26 from the Wettelrode mine, Sangerhausen Basin; blue fluorescence within carbonate and carbon/clay lenses. Scale measures 100.0 μm.

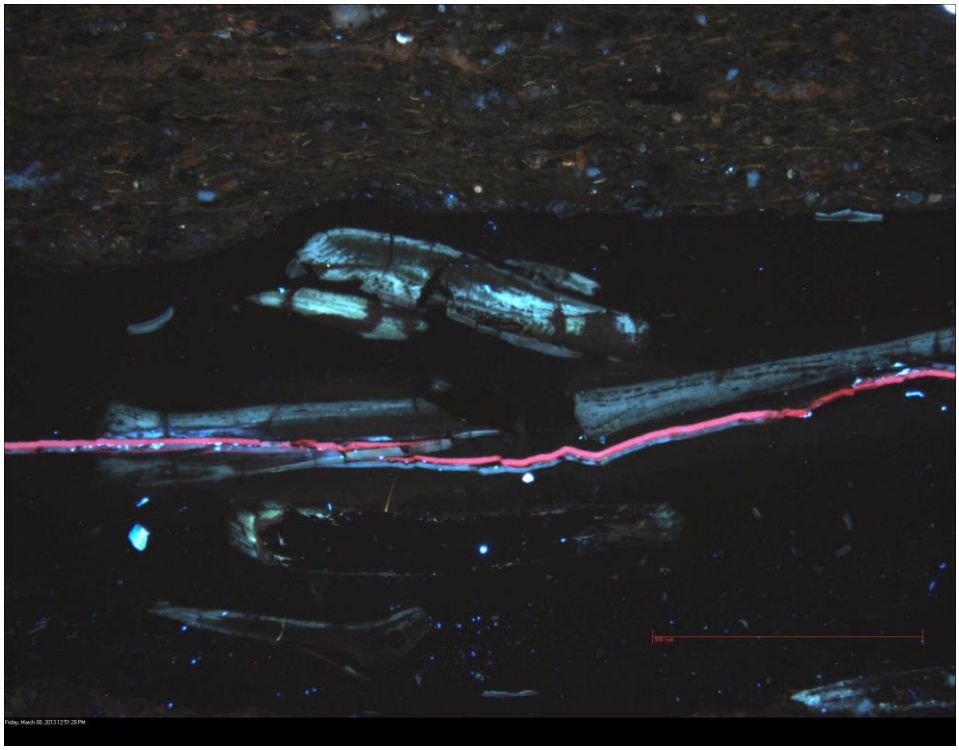

Figure 4.60: Sample K8+5 from the Wettelrode mine, Sangerhausen Basin; blue-green fluorescence of organic matter (most likely insect parts) within a mud chip. Scale measures 500.1 μm.

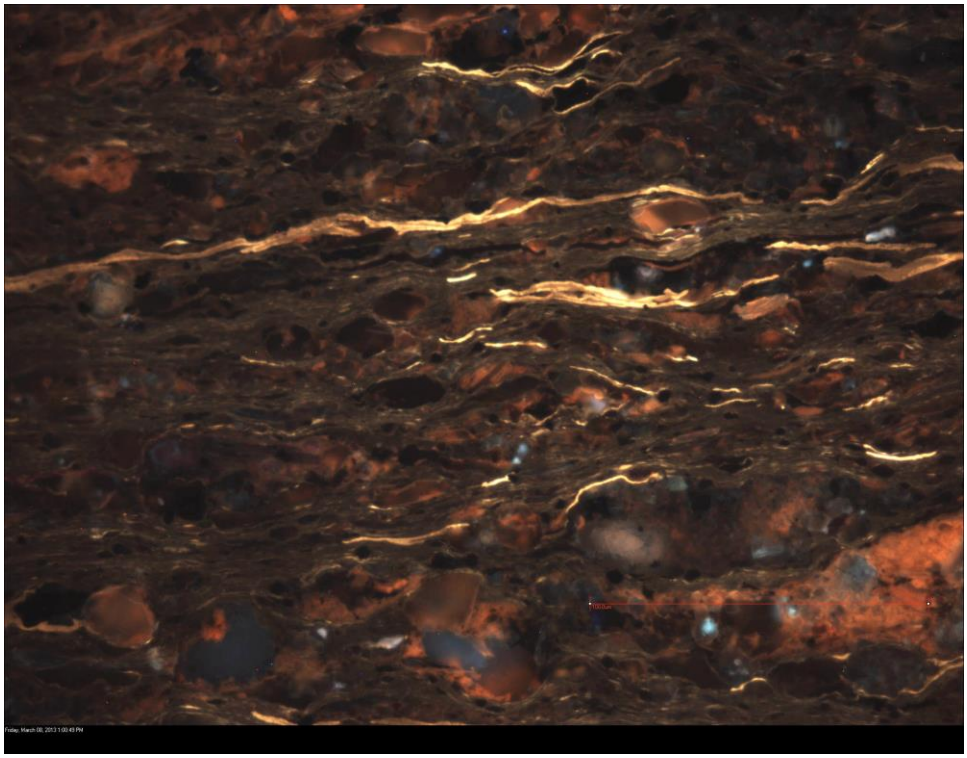

Figure 4.61: Sample K8+5 from the Wettelrode mine, Sangerhausen Basin; note the yellow fluorescence resulting from bitumen smears. Scale measures 100.0 μm.

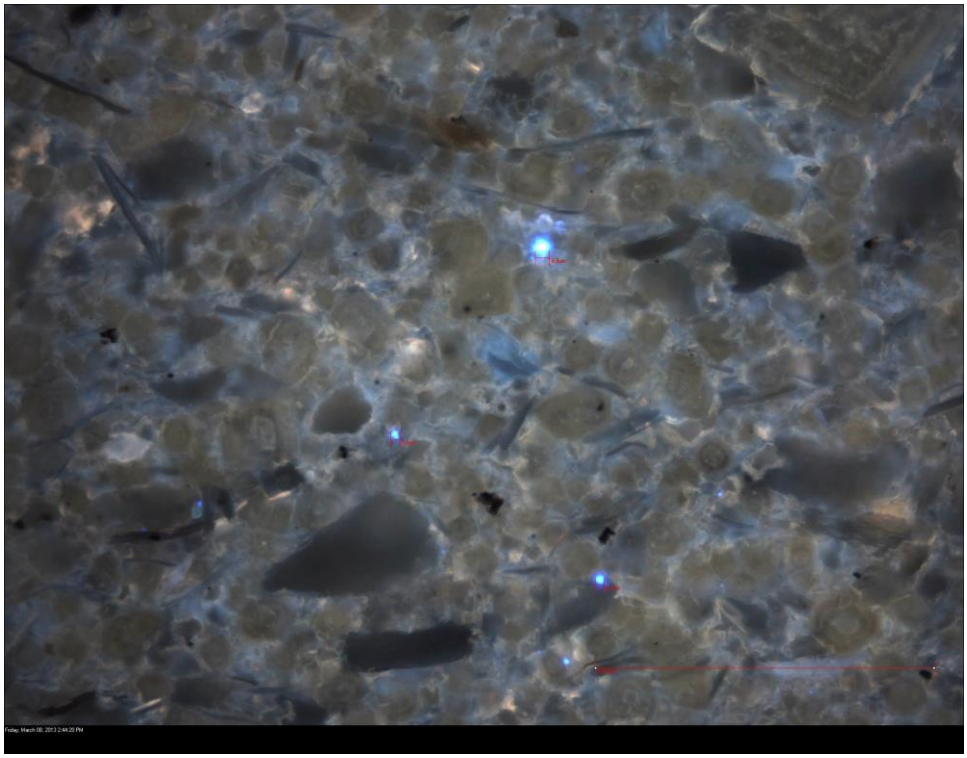

Figure 4.62: Sample K29+50 from core SGH133, Sangerhausen Basin; note the blue fluorescence among the carbonate grains, and the zoned character of the carbonate grains. Scale measures 100.0 μm.

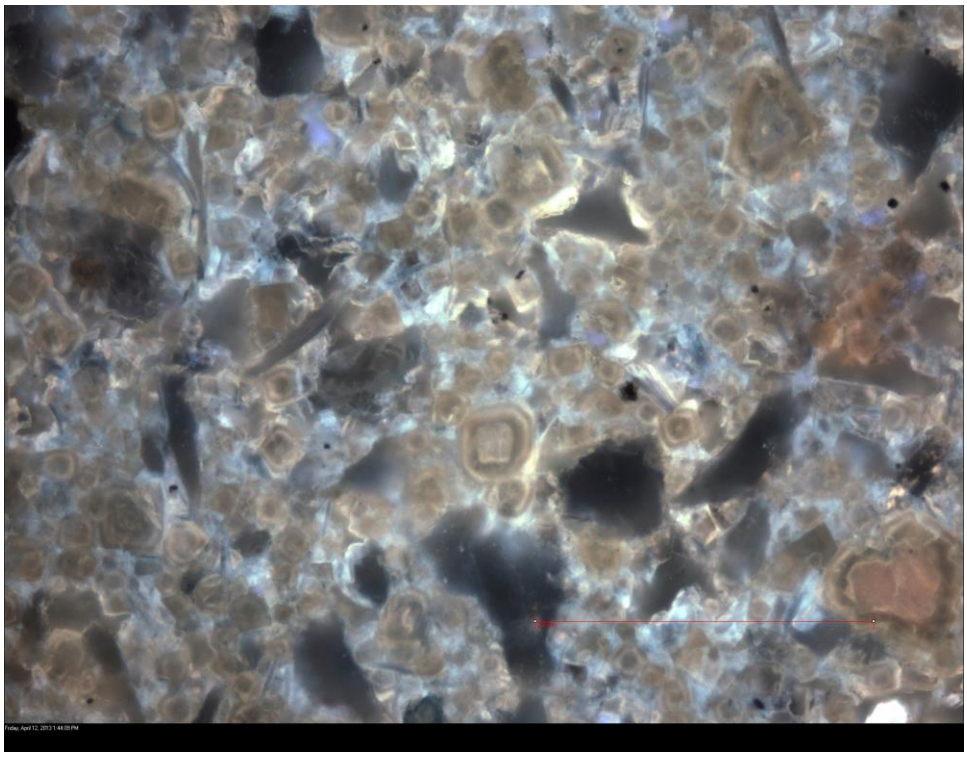

Figure 4.63: Sample K43+42 from SGH132, Sangerhausen Basin; note the zoned dolomite grains. Scale measures 100.0 μm.

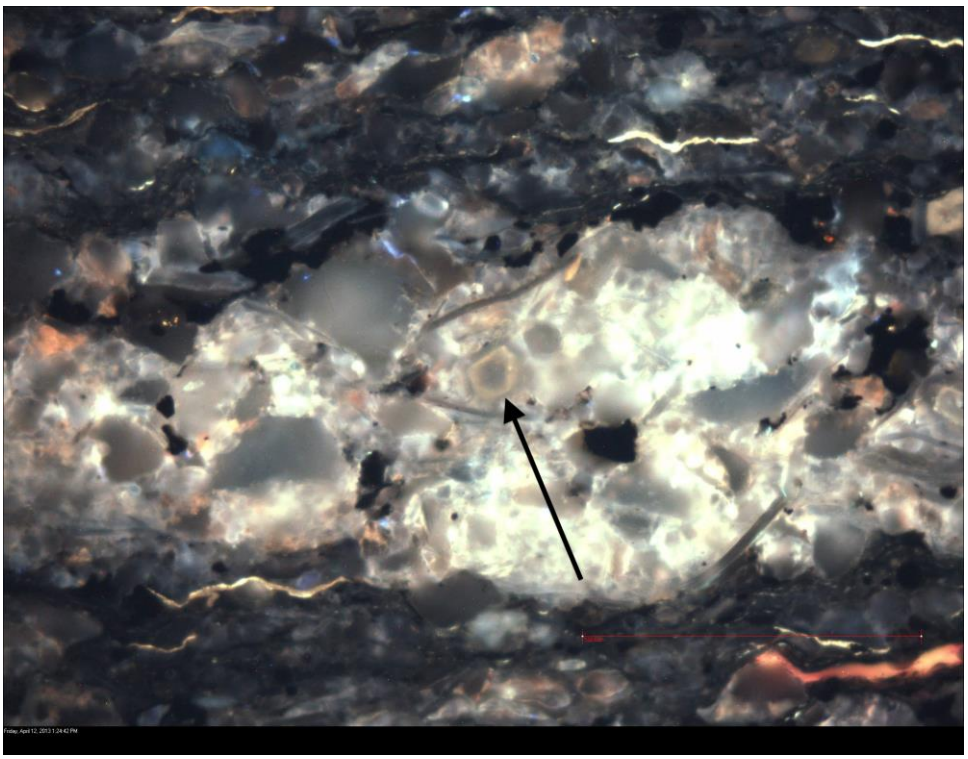

Figure 4.64: Sample K40+8 from core SGH132, Sangerhausen Basin; note the zoned dolomite crystals within the carbonate pod. Scale measures 100.0 μm.

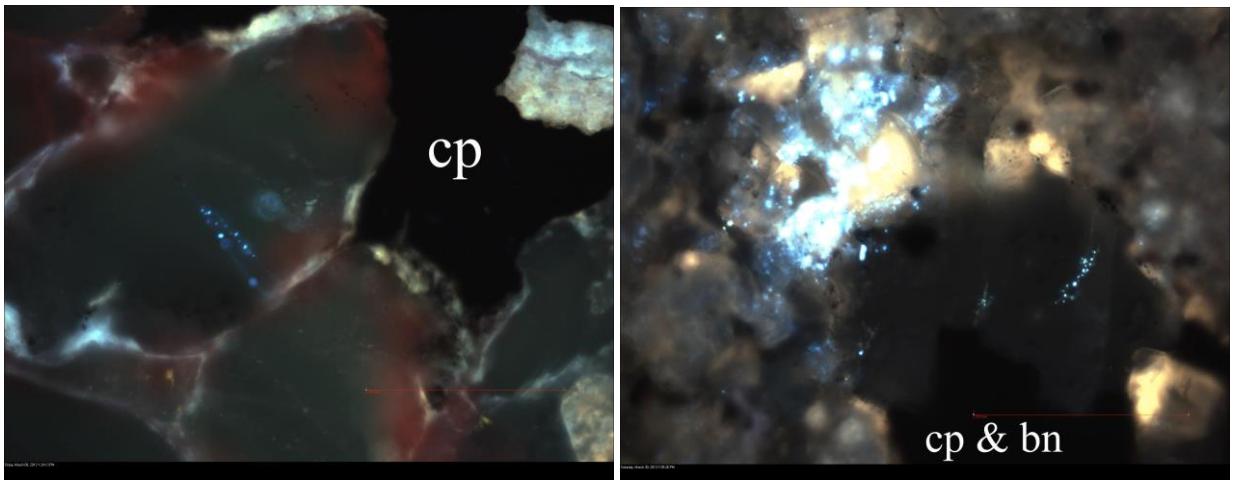

Figure 4.65: Left: Sample K9-4, from the Wettelrode mine, Sangerhausen Basin; note the blue fluorescence of the inclusions; the opaque black material is chalcopyrite (cp). Right: Sample K87+50 from Lubin 1, Lubin mining district; blue fluorescence identifies inclusions among carbonate grains adjacent to black opaque mineralization composed of chalcopyrite (cp) and bornite (bn). Scales measure 100.0 μm.

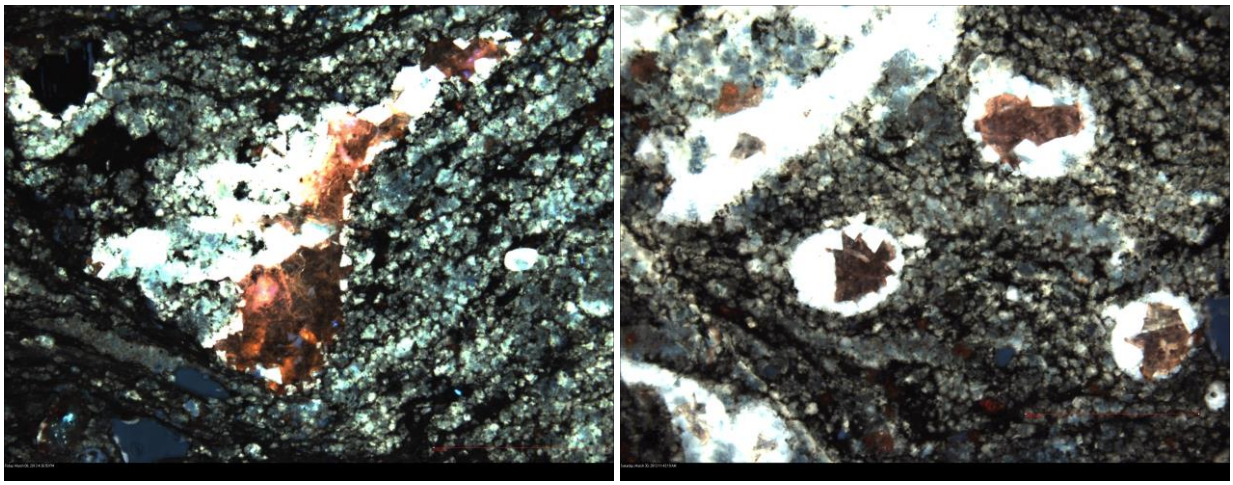
Figure 4.66: Sample K63+40 from Rudna 1, Lubin mining district; the slightly translucent red-orange fluorescence is sphalerite. Both scales measure 500 μm.

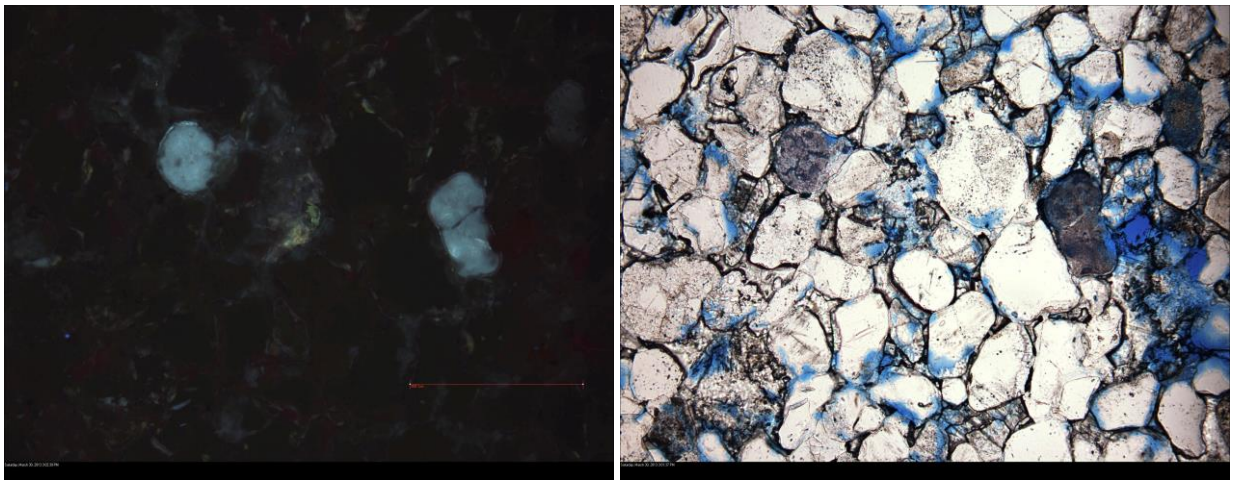

Figure 4.67: Sample K92-10 from Lubin 1, Lubin mining district; two pictures of a single thin section location, illustrating the pale blue fluorescence of two oil drops (left) that are a light brown color in plain light (right). Scale measures 500.1 μm.

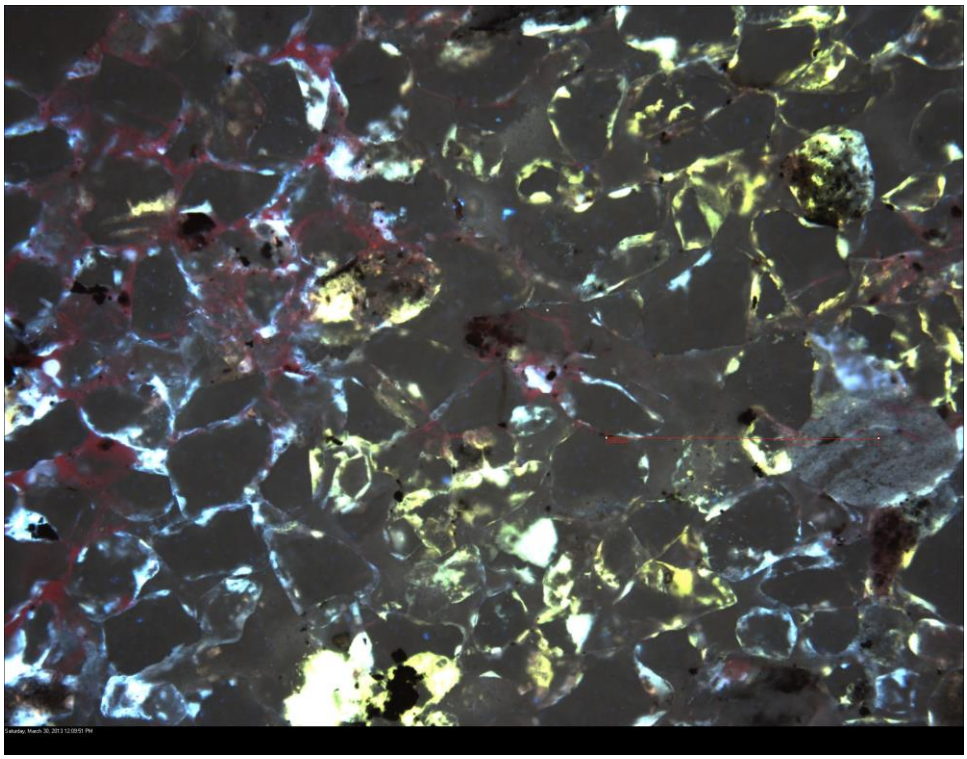

Figure 4.68: Sample K69-25 from Rudna 1, Lubin mining district; interstitial oil exhibiting yellow and blue fluorescence. Scale measures 500.1 μm.

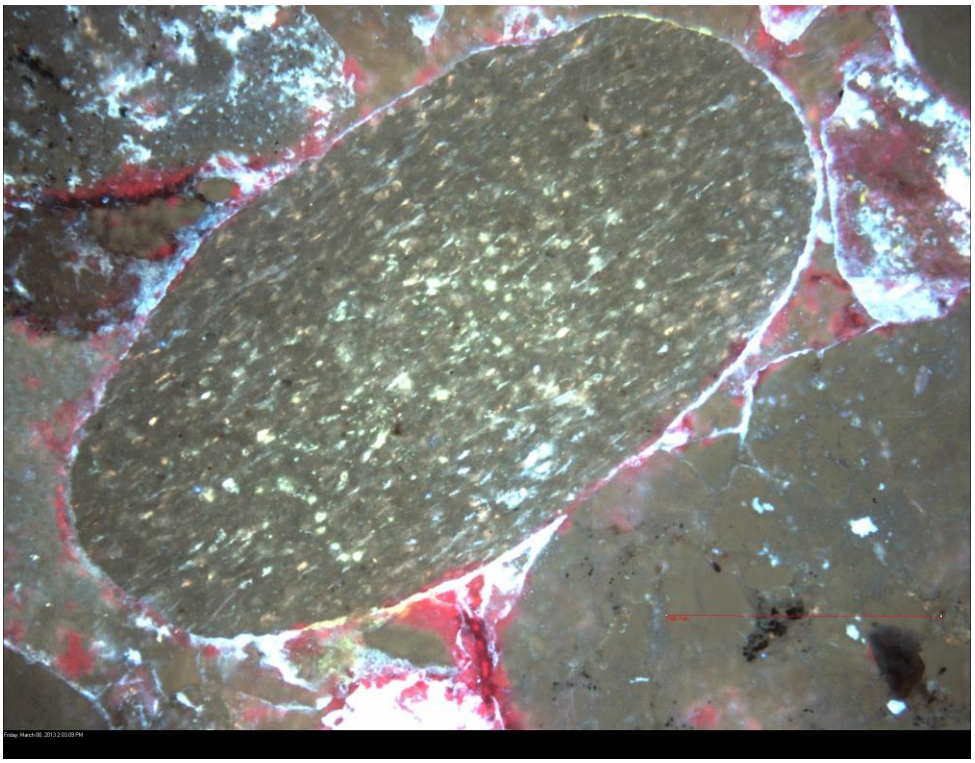

Figure 4.69: Sample K16-95 from the Wettelrode mine, Sangerhausen Basin; yellow accessory minerals in clast. Scale measures 500.1 μm.

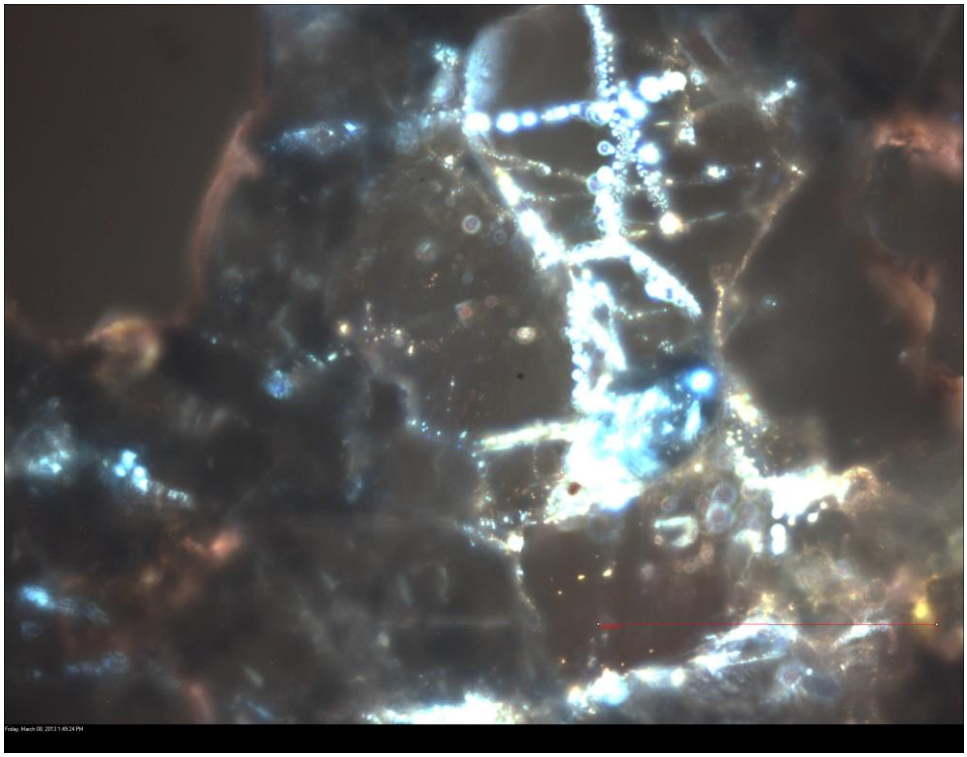

Figure 4.70: Sample K15-50 from the Wettelrode mine, Sangerhausen Basin; blue inclusions within quartz grains. Scale measures 100.0 μm.

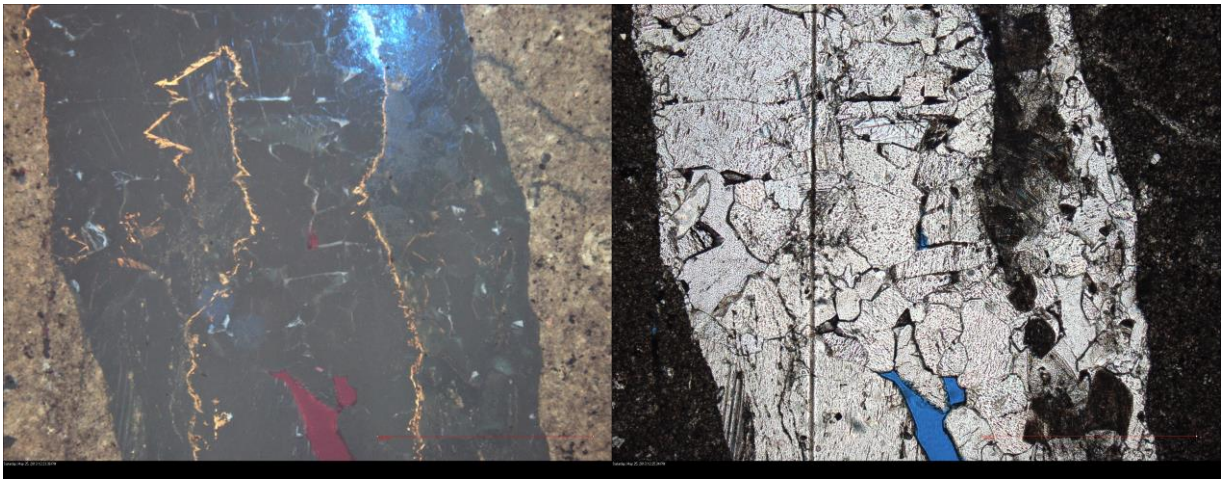

Figure 4.71: Sample K66+0 from Rudna 1, Lubin mining district; inclusion "seam" in a calcite vein. The photomicrograph on the left was taken under fluorescent light; the one on the right under plain polarized light. Scales measure 100 μm.

Figure 4.72: Sample K66+0 from Rudna 1, Lubin mining district; inclusion "seam" in quartz vein. Scale measures 500.1 μm.

## 4.3 Geochemistry

Geochemical data have been separated into five different sections: major elements, ore elements, historically mined ore elements, trace elements, and rare earth elements. Samples from the Lubin mining district are discussed alongside the samples from the Sangerhausen Basin. It should be noted that the Boundary Dolomite is present between the Kupferschiefer and Weissliegend in Lubin 2 of the Lubin mining district samples; this unit is represented by samples 2 and 4 cm below the contact in this location.

### 4.3.1 Major Elements

For the purposes of this thesis, the major elements are as follows: silicon ($SiO_2$), aluminum ($Al_2O_3$), iron ($Fe_2O_3$), manganese (MnO), magnesium (MgO), calcium (CaO), sodium ($Na_2O$), potassium ($K_2O$), titanium ($TiO_2$), and phosphorous ($P_2O_5$). With the exception of manganese and titanium, which have detection limits of 0.001 wt.%, the major elements have a detection limit of 0.01 wt.%. Sulfur (S) has been included due to the relatively high concentrations present in the samples. Data are listed in Table 4.3 and Table 4.4.

**Silicon** ($SiO_2$) increases in abundance below the basal contact of the Kupferschiefer in both Sangerhausen Basin and Lubin mining district samples. Concentrations nearly double from 30 to 40% in the Kupferschiefer to 60 to 70% in the Weissliegend in the Sangerhausen samples. There is a slight increase in concentration compared to other samples taken above the contact at approximately 20 cm above the contact, in cores SGH133, SGH103, and E-27, from roughly 30 wt.% to 45 wt.% $SiO_2$ (Figure 4.73). In the Lubin mining district samples, the concentration increases from 20 to 40 wt.% above the contact, to ~60 to 85 wt.% below the contact. The samples from 2 and 4 cm below the contact in Lubin 2 are an exception to the increase in Si below the contact, as these Boundary Dolomite samples have Si concentrations even lower than the samples above the contact, with <10 wt.% (Figure 4.74).

**Aluminum** ($Al_2O_3$) does not show any distinct trends in the Sangerhausen Basin samples (Figure 4.75), although there is an increase in concentration in core SGH132 at the basal contact of the shale and in core SGH133 about 20 cm above the contact. In the Lubin mining district samples, Al increases in

concentration within the Kupferschiefer (>8%) compared to the Weissliegend (4% and less), with a peak from 0 to 25 cm above the contact (up to 17%) (Figure 4.76).

**Magnesium** (MgO) shows gradual increased concentrations above the contact in Sangerhausen samples as distance from the basal contact increases (Figure 4.77), from 0.5 to 1.5 wt.% near the basal contact, up to 7-8.5 wt.% at 60 cm above the contact. Samples from the Lubin mining district exhibit higher concentrations of Mg above the contact than below the contact, with the exception of the two Boundary Dolomite samples, which have higher Mg concentrations than any of the other samples (Figure 4.78).

**Calcium** (CaO) concentrations in samples from the Sangerhausen Basin show a gradual increase above the contact as distance from the basal contact increases (Figure 4.79), from 5 to 10 wt.% near the basal contact, to 22 wt.% at 50 cm above the contact. In Lubin mining district samples, Ca shows a gradual, almost linear increase in concentration from 1% to 27% as depth decreases (Figure 4.80), with the exception of a sharp decrease in concentration back down to ~2% approximately 10 cm below to 20 cm above the contact. In Lubin 2, there is a large spike in both Ca and Mg in the samples from 2 and 4 cm below the contact marking the presence of the Boundary Dolomite; these samples are indicated in their respective figures by a black circle instead of the usual purple "*x*."

**Iron** ($Fe_2O_3$) is more abundant above the contact than below the contact in both Sangerhausen and Lubin mining district samples. Concentrations peak at 5.5 to 6 wt.% from the basal contact to 30 cm above the contact in the Sangerhausen (Figure 4.81). In the Lubin mining district samples, Fe concentrations rise to 3 to 6% at 0 to 20 cm above the contact in Rudna 1, with the rest of the samples showing concentrations of 3% or less (Figure 4.82); Lubin 1 and Lubin 2 also show a relative increase in Fe from samples taken between the contact and approximately 25 cm above the contact.

**Manganese** (MnO) does not show any strong trends in any of the Sangerhausen sites (Figure 4.83). Cores SGH133 and SGH132 show an increase in Mn upward from the basal contact. In the Lubin mining district, Mn concentrations are at or below 0.45 wt.%. The highest concentrations within the Boundary Dolomite 2 and 4 cm below the contact, and 30 cm above the contact in Lubin 2 (Figure 4.84).

The lowest Mn concentrations are observed between the contact and 25 cm above it, and 120 to 130 cm below the contact.

**Phosphorous** ($P_2O_5$) shows relatively stable concentrations (<0.2 wt.%) above and below the contact, with a strong peak (0.28 to 1.27 wt.%) 0 to 20 cm above the contact in samples from the Sangerhausen Basin (Figure 4.85). Samples from the Lubin mining district exhibit similar P concentrations above and below the contact (0.1 wt.% and 0.5 wt.%, respectively) (Figure 4.86), with a peak in concentration from the basal contact to 20 cm above the contact. **Potassium** ($K_2O$) appears to show an increase in concentration above the contact compared to below the contact in both Sangerhausen and Lubin mining district samples (Figures 4.87 and 4.88). **Sodium** ($Na_2O$) concentrations in Sangerhausen samples are lower above the contact (1% and lower) compared to below the contact (1.5 to 2%) (Figure 4.89); in Lubin mining district samples, Na increases slightly in concentration above the contact compared to below the contact (Figure 4.90).

**Titanium** ($TiO_2$) shows an increased concentration above the contact (≥0.4 wt.%) compared to below the contact (~0.2 wt.%) in Sangerhausen and Lubin mining district samples (~0.2 wt.% and ~ 0.1 wt.% respectively) (Figure 4.91). Lubin mining district samples show a peak occurring 0 to 20 cm above the contact (up to 0.75%) (Figure 4.92).

**Sulfur** concentrations in the samples from the Sangerhausen Basin exhibit a relative increase in samples taken from 30 cm above the contact down to the contact; in the case of the Wettelrode mine and cores SGH133 and E-27, this increase extends up to 6 cm below the contact (Figure 4.93). Samples taken from below the contact (with the exception of those previously mentioned) and more than 30 cm above the contact contain S concentrations below 1 wt.%. The highest sulfur concentration is present in the sample from 3 cm above the contact in SGH133, with 5% sulfur. Lubin mining district samples taken at the contact through 20 cm above the contact show the greatest relative increase within the Lubin and Rudna samples (Figure 4.94). The highest concentrations are found in samples taken from Rudna 1, at the contact (6.44%) and 10 cm above the contact (5.66%).

Table 4.3: Geochemical data for Sangerhausen Basin samples, major elements.

| Sangerhausen Basin | Analyte Symbol | S | SiO2 | Al2O3 | Fe2O3(T) | MnO | MgO | CaO | Na2O | K2O | TiO2 | P2O5 | LOI | Total |
|---|---|---|---|---|---|---|---|---|---|---|---|---|---|---|
| | Unit Symbol | % | % | % | % | % | % | % | % | % | % | % | % | % |
| | Detection Limit | 0.001 | 0.01 | 0.01 | 0.01 | 0.001 | 0.01 | 0.01 | 0.01 | 0.01 | 0.001 | 0.01 | | 0.01 |
| | Analysis Method | TD-ICP | FUS-ICP | FUS-ICP | FUS-ICP | FUS-ICP | FUS-ICP | FUS-ICP | FUS-ICP | FUS-ICP | FUS-ICP | FUS-ICP | FUS-ICP | FUS-ICP |
| | Sample Number | | | | | | | | | | | | | |
| Wettelrode | K2+26 | 1.62 | 33.76 | 9.69 | 2.97 | 0.288 | 6.65 | 12.58 | 0.67 | 2.01 | 0.527 | 0.11 | 25.66 | 94.92 |
| | K05+14 | 3.04 | 35.31 | 10.66 | 4.46 | 0.156 | 3.55 | 7.25 | 0.65 | 2.54 | 0.558 | 0.34 | 28.75 | 94.23 |
| | K6+10 | 4.05 | 30.19 | 8.89 | 4.5 | 0.236 | 3.05 | 6.88 | 0.87 | 2.28 | 0.496 | 1.27 | 32.91 | 91.57 |
| | K7+8 | 4.72 | 32.09 | 10.61 | 5.75 | 0.24 | 2.15 | 3.46 | 0.9 | 2.66 | 0.576 | 0.31 | 32.46 | 91.22 |
| | K8-0 | 4.68 | 31.39 | 9.98 | 5.78 | 0.233 | 2.5 | 4.62 | 0.68 | 2.47 | 0.546 | 0.35 | 32.3 | 90.85 |
| | K9-4 | 1.31 | 62.16 | 8.03 | 3.06 | 0.272 | 2.93 | 6.32 | 1.05 | 1 | 0.21 | 0.12 | 11.27 | 96.43 |
| | K10-13 | 0.485 | 64.3 | 8.9 | 1.85 | 0.225 | 2.74 | 6.41 | 1.14 | 0.57 | 0.2 | 0.1 | 11.08 | 97.5 |
| | K11-21 | 0.152 | 68.08 | 9.67 | 1.62 | 0.205 | 2.63 | 5.36 | 1.44 | 0.72 | 0.211 | 0.12 | 10.04 | 100.1 |
| | K15-50 | 0.126 | 65.33 | 8.46 | 2.23 | 0.212 | 2.82 | 6.6 | 1.14 | 0.51 | 0.167 | 0.09 | 11.07 | 98.63 |
| SGH133 | K32+62 | 0.068 | 35.71 | 9.95 | 2.95 | 0.244 | 7.42 | 16.68 | 0.91 | 2.55 | 0.546 | 0.14 | 21.66 | 98.76 |
| | K29+50 | 0.522 | 29.13 | 8.03 | 2.52 | 0.332 | 8.15 | 22.28 | 0.72 | 2.04 | 0.451 | 0.13 | 25.25 | 99.04 |
| | K22+25 | 1.52 | 45.93 | 12.82 | 3.88 | 0.143 | 5.16 | 7.31 | 1.12 | 3.4 | 0.7 | 0.14 | 16.03 | 96.63 |
| | K21+17 | 1.9 | 44.78 | 13.6 | 3.58 | 0.124 | 4.28 | 6.91 | 1.05 | 3.67 | 0.722 | 0.14 | 18.2 | 97.05 |
| | K20+8 | 4.49 | 25.88 | 7.99 | 2.46 | 0.164 | 1.63 | 12.26 | 0.71 | 2.04 | 0.426 | 0.42 | 31.5 | 85.49 |
| | K19+3 | 5 | 31.49 | 10.46 | 4.17 | 0.08 | 1.58 | 4.87 | 0.72 | 2.9 | 0.525 | 0.29 | 29.98 | 87.05 |
| | K17-6 | 1.56 | 71.07 | 5.55 | 1.47 | 0.147 | 0.46 | 8.09 | 1.14 | 1.73 | 0.232 | 0.1 | 7.73 | 97.72 |
| SGH132 | K43+42 | 0.534 | 29.19 | 8.01 | 2.08 | 0.634 | 7.06 | 22.73 | 0.6 | 2.06 | 0.46 | 0.11 | 25.81 | 98.72 |
| | K41+22 | 3.14 | 40.93 | 11.25 | 5.51 | 0.422 | 4.85 | 11.71 | 0.92 | 2.77 | 0.631 | 0.12 | 18.69 | 97.81 |
| | K40+8 | 1.96 | 44.62 | 13.13 | 3.99 | 0.244 | 3.39 | 9.04 | 0.87 | 3.3 | 0.726 | 0.16 | 18.99 | 98.44 |
| | K39+1 | 0.685 | 52.87 | 17.1 | 3.22 | 0.052 | 2.07 | 1.86 | 0.91 | 4.44 | 0.965 | 0.16 | 14.45 | 98.1 |
| | K38-12 | 0.048 | 67.32 | 7.85 | 0.93 | 0.215 | 0.52 | 10.16 | 1.84 | 1.33 | 0.265 | 0.12 | 9.17 | 99.72 |
| | K35-55 | 0.131 | 69.75 | 8.69 | 1 | 0.175 | 0.5 | 7.51 | 1.86 | 1.51 | 0.244 | 0.11 | 7.43 | 98.78 |
| | K34-68 | 0.993 | 72.73 | 9.46 | 1.96 | 0.075 | 0.51 | 2.94 | 1.73 | 3.12 | 0.302 | 0.1 | 4.58 | 97.5 |
| E-27 | K54+31 | 2.27 | 46.45 | 12.4 | 4.35 | 0.231 | 5.58 | 8.11 | 0.97 | 3.02 | 0.696 | 0.14 | 17.38 | 99.31 |
| | K53+20 | 1.66 | 31.48 | 8.84 | 3.01 | 0.381 | 8.7 | 14.44 | 0.65 | 2.23 | 0.493 | 0.13 | 26.51 | 96.85 |
| | K52+7 | 4.56 | 30.01 | 8.58 | 5.15 | 0.523 | 3.51 | 11.61 | 0.62 | 1.98 | 0.522 | 0.39 | 31.47 | 94.35 |
| | K51-4 | 1.24 | 67.21 | 9.25 | 1.28 | 0.195 | 0.72 | 6.56 | 1.94 | 1.11 | 0.277 | 0.12 | 7.22 | 95.88 |
| | K50-16 | 0.069 | 65.13 | 8.68 | 0.53 | 0.287 | 0.39 | 11.18 | 2.04 | 0.8 | 0.15 | 0.11 | 10.23 | 99.52 |
| | K49-27 | 0.023 | 63.68 | 9.53 | 0.77 | 0.299 | 0.46 | 10.87 | 1.62 | 1.15 | 0.248 | 0.11 | 10.31 | 99.04 |
| | K48-36 | 0.03 | 65.12 | 9.56 | 0.74 | 0.295 | 0.47 | 10.5 | 1.43 | 1.25 | 0.188 | 0.1 | 10.15 | 99.8 |
| SGH103 | K61+31 | 1.37 | 41.88 | 11.26 | 3.81 | 0.239 | 5.07 | 13.79 | 1.13 | 2.73 | 0.619 | 0.13 | 17.5 | 98.16 |
| | K60+19 | 2.31 | 40.84 | 11.5 | 2.84 | 0.183 | 2.21 | 11.77 | 1.04 | 2.91 | 0.625 | 0.12 | 20.1 | 94.13 |
| | K59+7 | 4.54 | 28.86 | 9.26 | 4 | 0.126 | 1.46 | 8.59 | 0.71 | 2.53 | 0.494 | 0.28 | 24.13 | 80.44 |
| | K58-5 | 0.088 | 62.7 | 7.04 | 1.26 | 0.492 | 0.69 | 12.72 | 1.57 | 2.06 | 0.313 | 0.12 | 10.71 | 99.68 |
| | K57-16 | 0.023 | 66.36 | 10.06 | 1.74 | 0.179 | 1.11 | 6.66 | 1.86 | 2.78 | 0.532 | 0.16 | 6.86 | 98.29 |
| | K56-28 | 0.023 | 65.29 | 11 | 2.2 | 0.193 | 1.37 | 6.46 | 1.93 | 2.9 | 0.606 | 0.17 | 6.93 | 99.05 |

Table 4.4: Geochemical data for Lubin mining district samples, major elements.

| Lubin Mining District | Analyte Symbol | S | SiO2 | Al2O3 | Fe2O3(T) | MnO | MgO | CaO | Na2O | K2O | TiO2 | P2O5 | LOI | Total |
|---|---|---|---|---|---|---|---|---|---|---|---|---|---|---|
| | Unit Symbol | % | % | % | % | % | % | % | % | % | % | % | % | % |
| | Detection Limit | 0.001 | 0.01 | 0.01 | 0.01 | 0.001 | 0.01 | 0.01 | 0.01 | 0.01 | 0.001 | 0.01 | | 0.01 |
| | Analysis Method | TD-ICP | FUS-ICP | FUS-ICP | FUS-ICP | FUS-ICP | FUS-ICP | FUS-ICP | FUS-ICP | FUS-ICP | FUS-ICP | FUS-ICP | FUS-ICP | FUS-ICP |
| | Sample Number | | | | | | | | | | | | | |
| Rudna 1 | K63+40 | 1.47 | 30.46 | 9.08 | 1.64 | 0.199 | 7.59 | 14.03 | 0.53 | 2.48 | 0.405 | 0.1 | 26.01 | 92.51 |
| | K65+20 | 4.1 | 26.35 | 9.65 | 3.16 | 0.169 | 4.02 | 5.38 | 0.34 | 2.91 | 0.422 | 0.09 | 24.22 | 76.7 |
| | K67+10 | 5.66 | 35.26 | 12.57 | 6.27 | 0.068 | 1.72 | 3.13 | 0.46 | 3.75 | 0.579 | 0.16 | 25.21 | 89.17 |
| | K66-0 | 6.44 | 37.88 | 11.16 | 6.41 | 0.058 | 1.85 | 2.2 | 0.37 | 3.36 | 0.555 | 0.15 | 20.88 | 84.88 |
| | K68-10 | 0.995 | 73.47 | 6.86 | 1.67 | 0.09 | 2.04 | 4.17 | 0.4 | 2.05 | 0.312 | 0.1 | 7.64 | 98.79 |
| | K69-25 | 0.476 | 75.53 | 3.76 | 1.1 | 0.136 | 0.29 | 8.36 | 0.32 | 1.44 | 0.099 | 0.05 | 8.15 | 99.23 |
| | K70-130 | 0.591 | 87.17 | 4.31 | 0.85 | 0.027 | 0.34 | 1.18 | 0.32 | 1.63 | 0.117 | 0.06 | 2.69 | 98.71 |
| Rudna 2 | K76+20 | 2.31 | 43.23 | 13.34 | 2.86 | 0.086 | 3.21 | 4.61 | 0.63 | 4.05 | 0.592 | 0.13 | 20.75 | 93.49 |
| Lubin 1 | K84+110 | 1.06 | 30.34 | 9.16 | 1.74 | 0.163 | 1.63 | 27.1 | 0.39 | 2.15 | 0.428 | 0.09 | 22.52 | 95.72 |
| | K88+40 | 1.65 | 35.89 | 12.1 | 1.53 | 0.17 | 3.22 | 14.14 | 0.23 | 3.2 | 0.489 | 0.15 | 22.2 | 93.31 |
| | K89+20 | 2.64 | 29.94 | 11.32 | 1.73 | 0.193 | 4.77 | 12.47 | 0.32 | 3.06 | 0.491 | 0.12 | 23.96 | 88.36 |
| | K91+0 | 3.02 | 32.03 | 12.54 | 1.65 | 0.16 | 4.04 | 9.08 | 0.17 | 3.45 | 0.538 | 0.14 | 22.9 | 86.69 |
| | K92-10 | 0.253 | 71.29 | 3.37 | 0.44 | 0.218 | 0.39 | 12.05 | 0.06 | 0.86 | 0.079 | 0.05 | 10.4 | 99.2 |
| | K93-20 | 0.143 | 73.63 | 4.5 | 0.29 | 0.19 | 0.63 | 10.11 | 0.06 | 1.07 | 0.1 | 0.06 | 9.22 | 99.86 |
| | K94-120 | 1.36 | 84.43 | 3.47 | 0.71 | 0.04 | 0.19 | 2.71 | 0.06 | 1.04 | 0.119 | 0.05 | 3.75 | 96.57 |
| Lubin 2 | K105+120 | 0.48 | 25.39 | 8.72 | 1.35 | 0.218 | 11.18 | 19.45 | 0.13 | 2.55 | 0.405 | 0.11 | 28.25 | 97.76 |
| | K104+50 | 0.728 | 26.94 | 8.5 | 1.13 | 0.245 | 10.95 | 18.81 | 0.12 | 2.53 | 0.437 | 0.11 | 26.75 | 96.51 |
| | K103+30 | 2.26 | 23.4 | 7.38 | 1.3 | 0.387 | 6.96 | 19.06 | 0.29 | 1.78 | 0.346 | 0.1 | 23.15 | 84.17 |
| | K102+25 | 3.74 | 37.15 | 15.08 | 2.59 | 0.052 | 1.67 | 2.74 | 0.14 | 4.28 | 0.659 | 0.11 | 17.77 | 82.24 |
| | K101+20 | 3.33 | 40.84 | 17.52 | 1.73 | 0.031 | 1.74 | 1.11 | 0.15 | 4.49 | 0.746 | 0.13 | 16.65 | 85.13 |
| | K100+0 | 3.65 | 36.45 | 14.29 | 1.66 | 0.098 | 2.27 | 3.74 | 0.15 | 4.02 | 0.717 | 0.26 | 19.07 | 82.72 |
| | K99-UBD | 0.685 | 9.31 | 3.32 | 0.78 | 0.453 | 16.17 | 26.25 | 0.16 | 0.38 | 0.133 | 0.12 | 36.24 | 93.31 |
| | K98-LBD | 0.676 | 7.28 | 2.29 | 0.82 | 0.416 | 17.48 | 27.27 | 0.11 | 0.22 | 0.078 | 0.09 | 38.15 | 94.19 |
| | K97-5 | 1.16 | 58.81 | 3.49 | 0.77 | 0.203 | 4.19 | 11.49 | 0.14 | 0.83 | 0.143 | 0.08 | 14.24 | 94.38 |
| | K96-50 | 0.502 | 74.88 | 3.35 | 0.55 | 0.176 | 0.28 | 9.56 | 0.06 | 0.81 | 0.083 | 0.06 | 8.49 | 98.3 |
| | K95-120 | 1.69 | 80.51 | 3.67 | 0.68 | 0.049 | 0.23 | 2.7 | 0.1 | 1.04 | 0.103 | 0.03 | 3.21 | 92.32 |

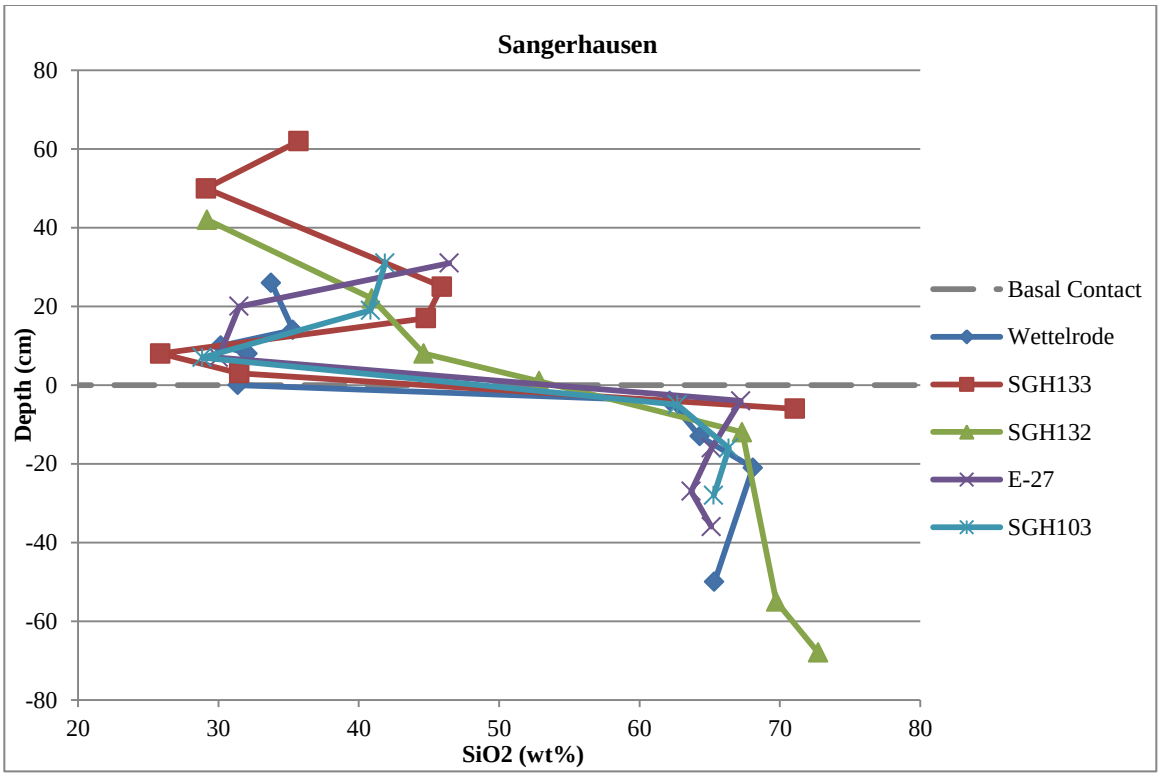


Figure 4.73: Silicon ($SiO_2$) wt.% by depth, Sangerhausen Basin.

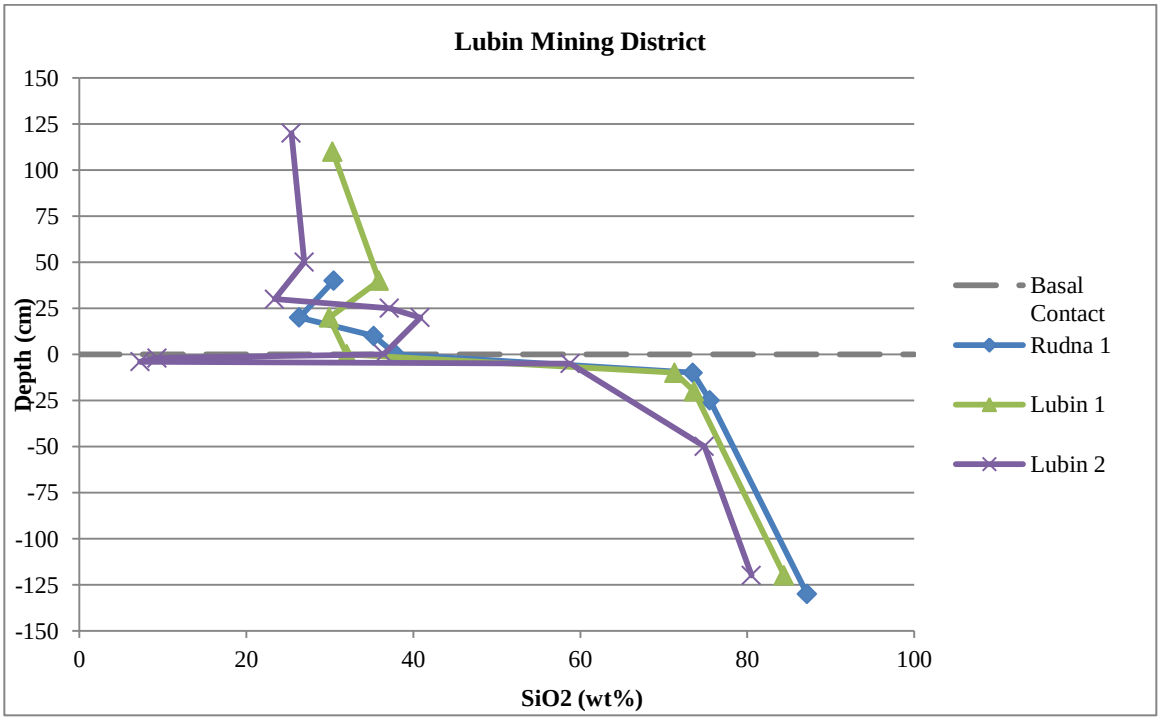


Figure 4.74: Silicon ($SiO_2$) wt.% by depth, Lubin mining district.

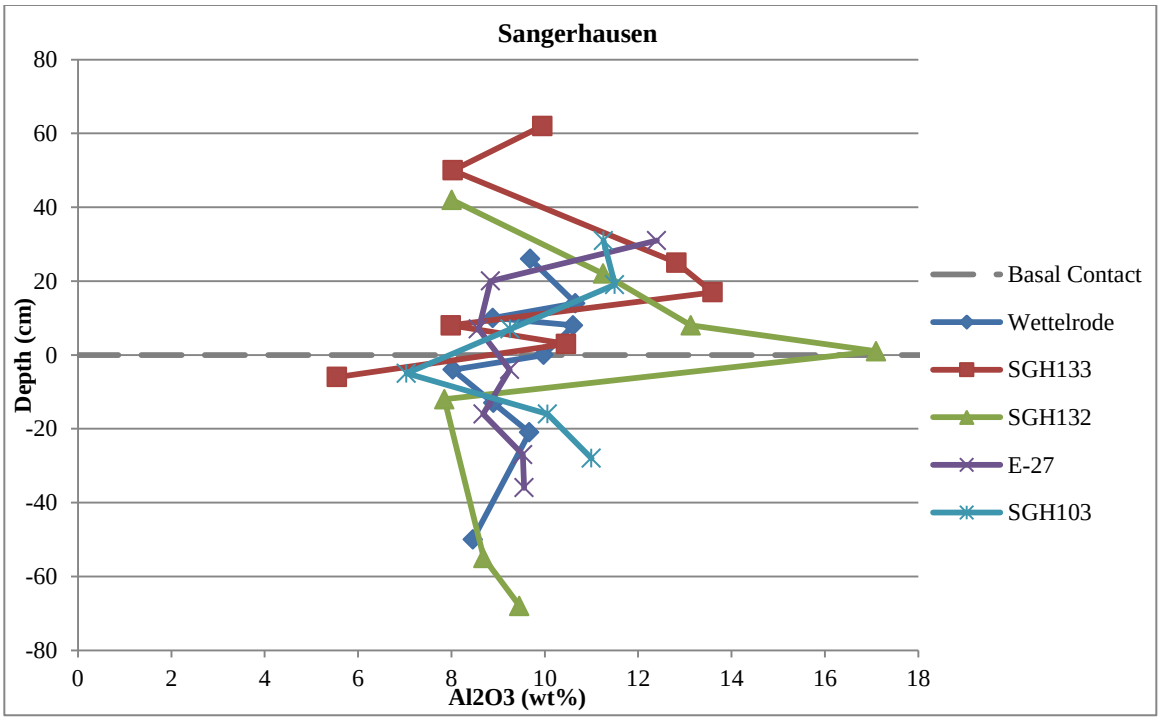


Figure 4.75: Aluminum ($Al_2O_3$) wt.% by depth, Sangerhausen Basin.

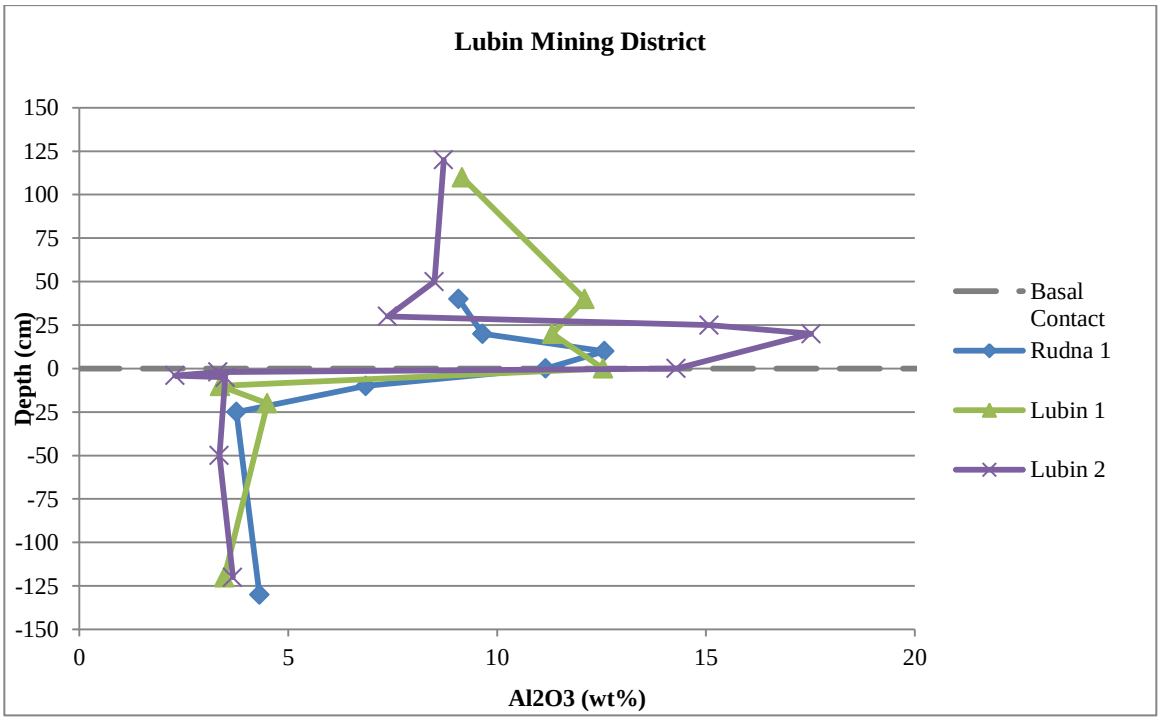


Figure 4.76: Aluminum ($Al_2O_3$) wt.% by depth, Lubin mining district.

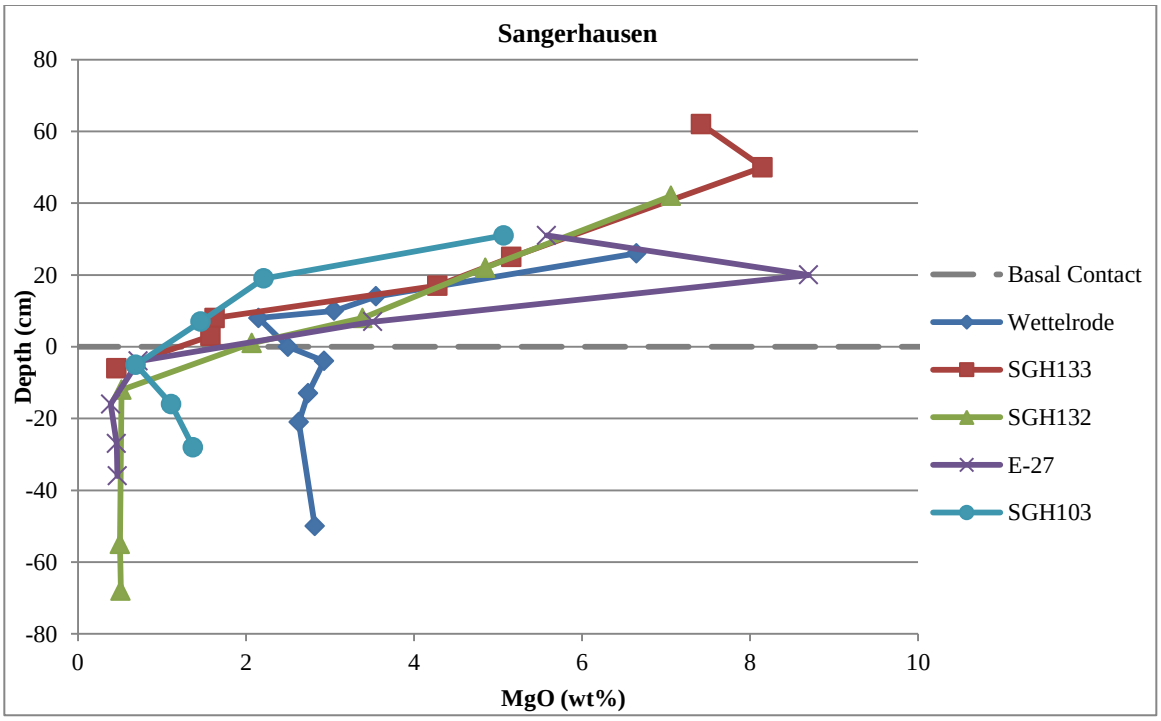


Figure 4.77: Magnesium (MgO) wt.% by depth, Sangerhausen Basin.

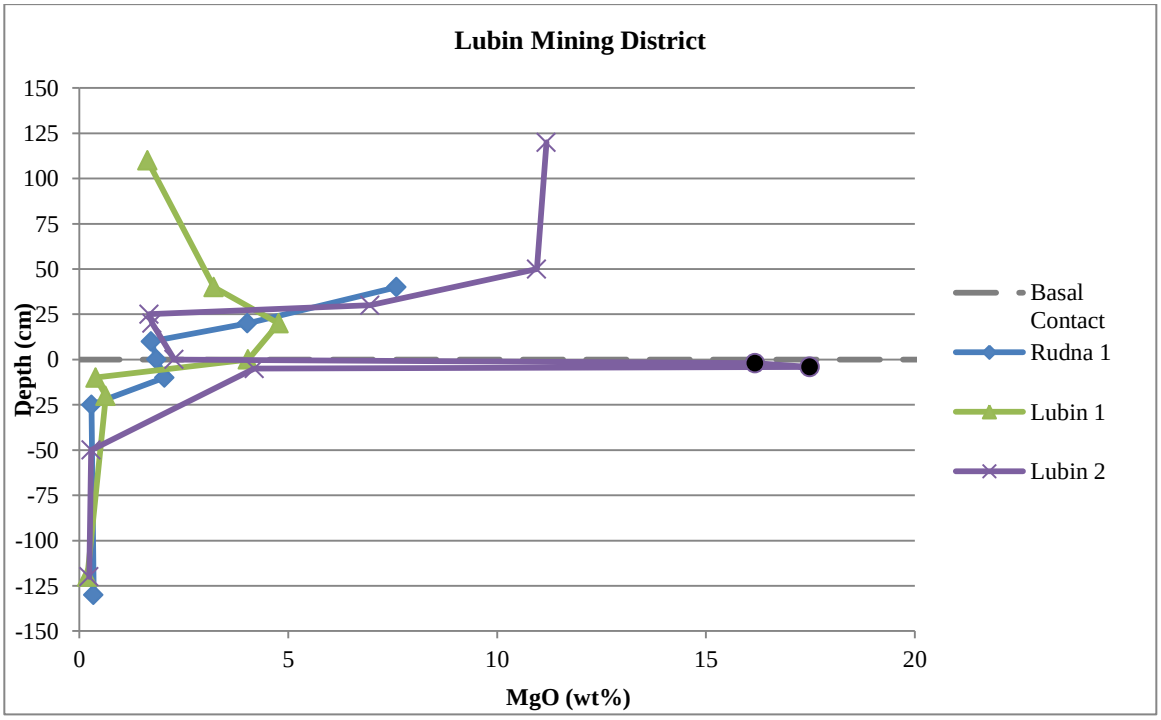


Figure 4.78: Magnesium (MgO) wt.% by depth, Lubin mining district. Note the Boundary Dolomite samples in Lubin 2, indicated by a black circle instead of the usual purple "*x*."

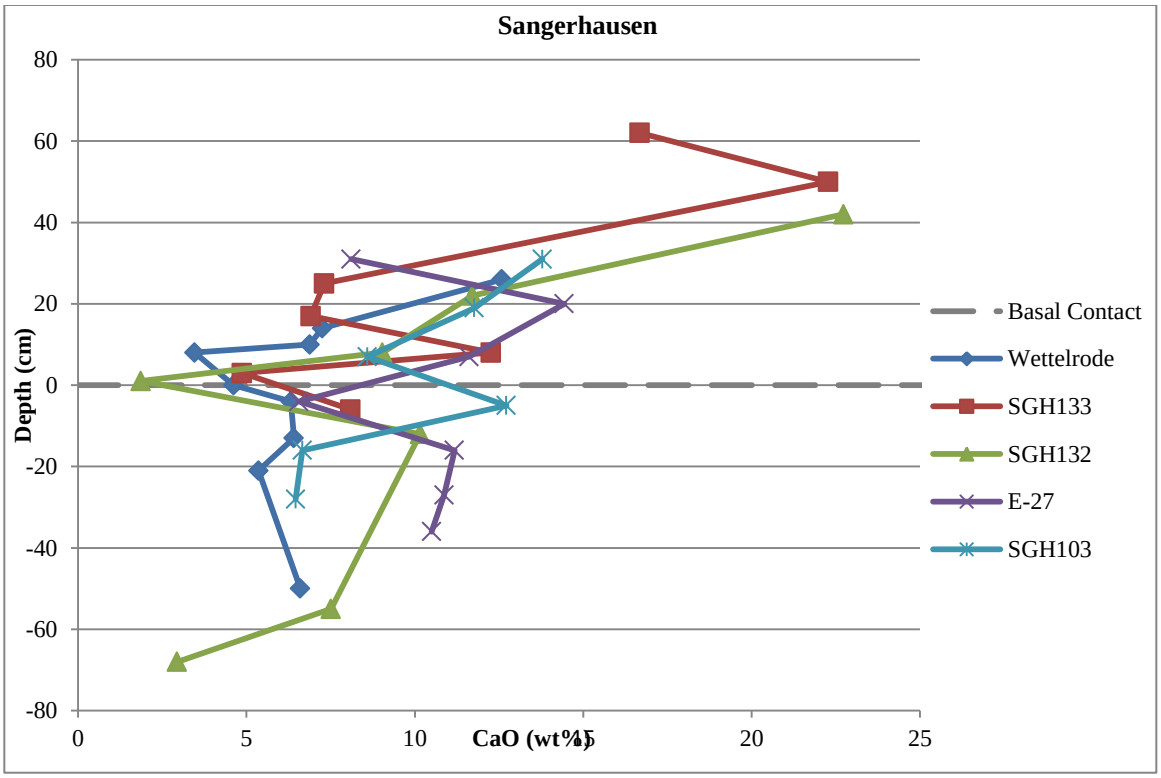


Figure 4.79: Calcium (CaO) wt.% by depth, Sangerhausen Basin.

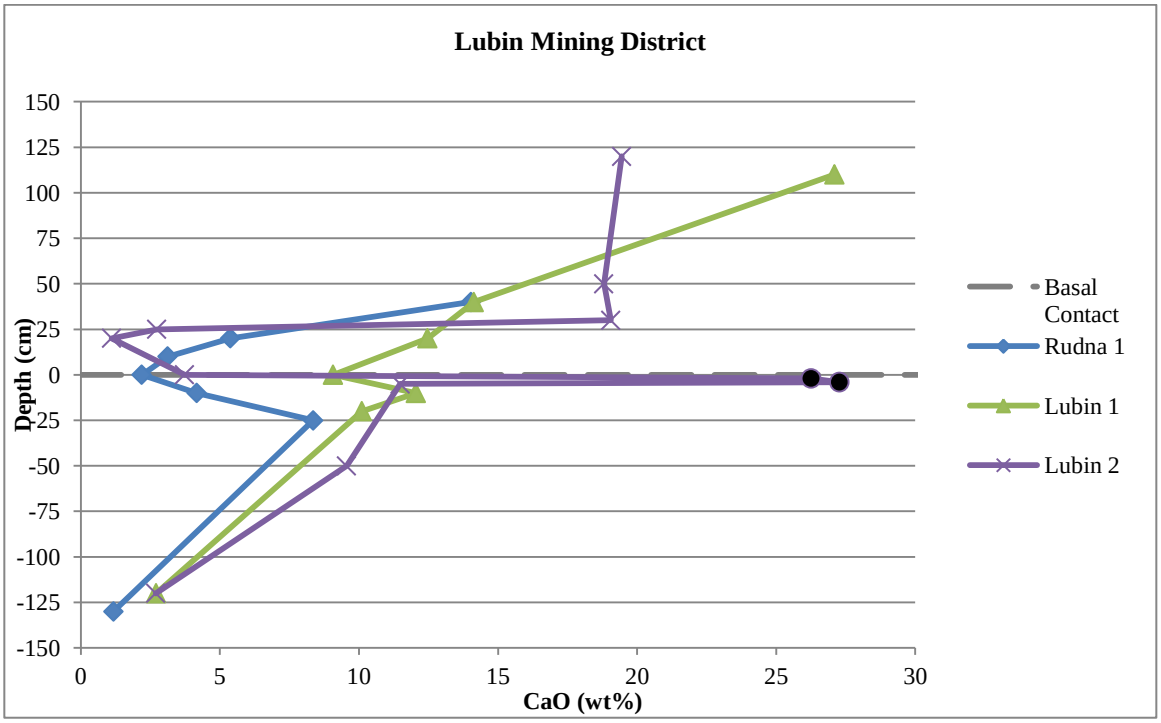


Figure 4.80: Calcium (CaO) wt.% by depth, Lubin mining district. Note the Boundary Dolomite samples in Lubin 2, indicated by a black circle instead of the usual purple "*x*."

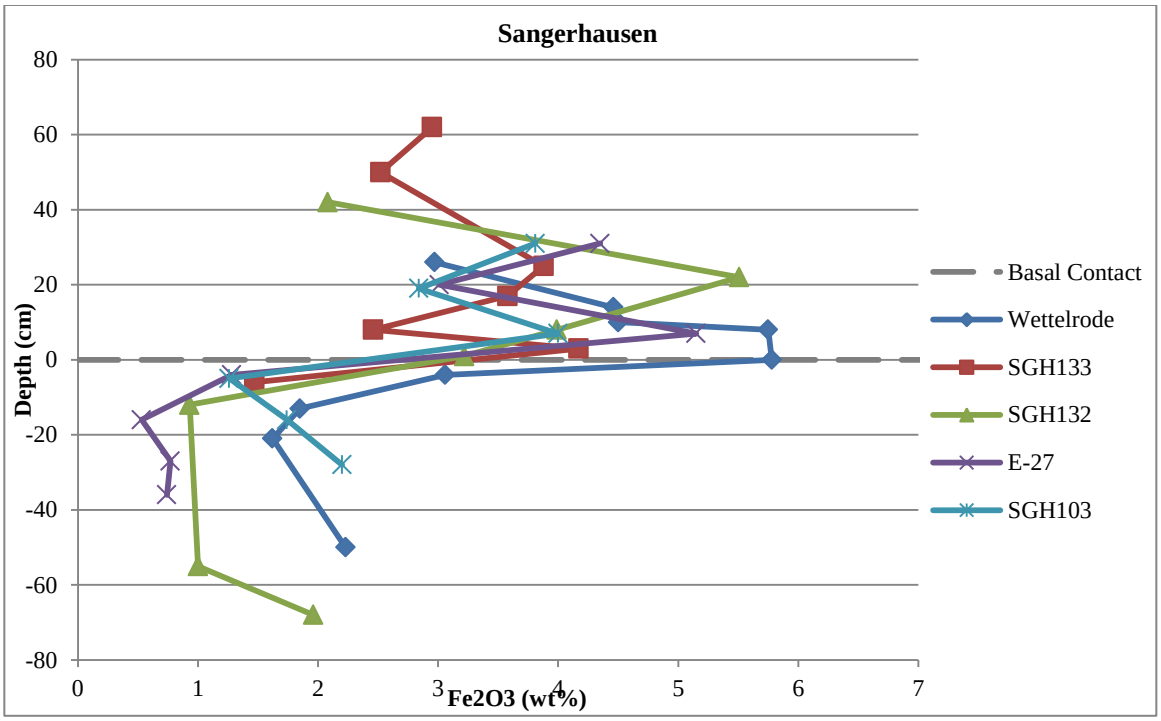


Figure 4.81: Iron ($Fe_2O_3$) wt.% by depth, Sangerhausen Basin.

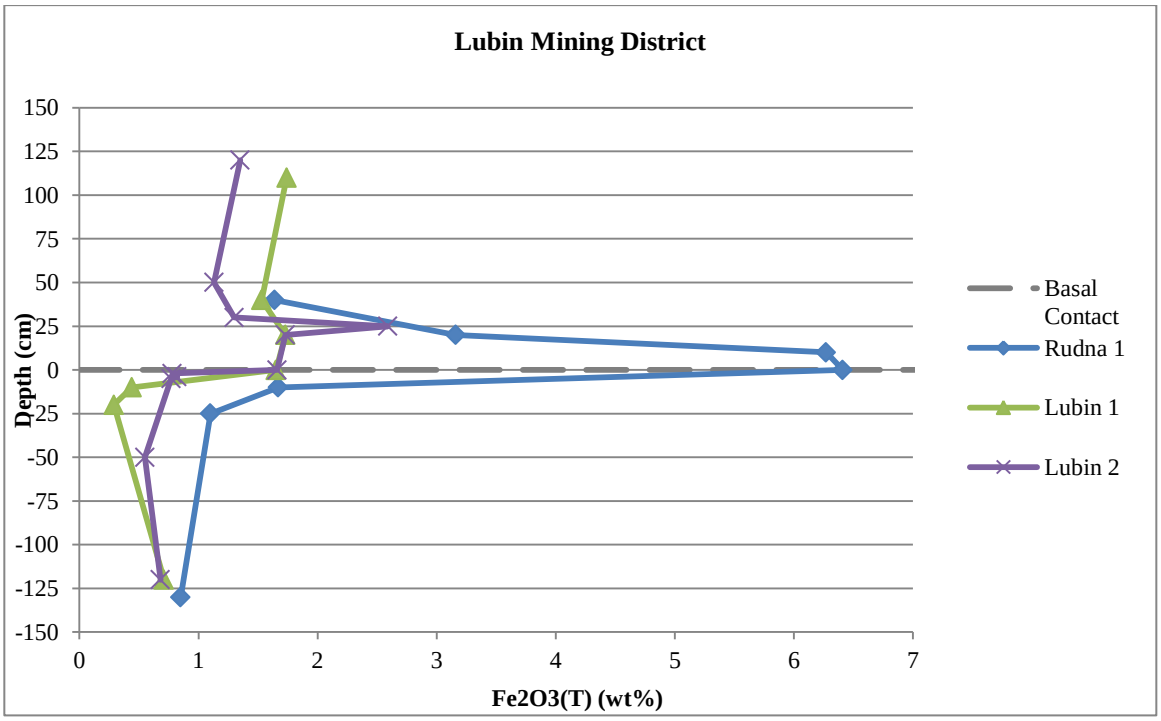


Figure 4.82: Iron ($Fe_2O_3$) wt.% by depth, Lubin mining district.

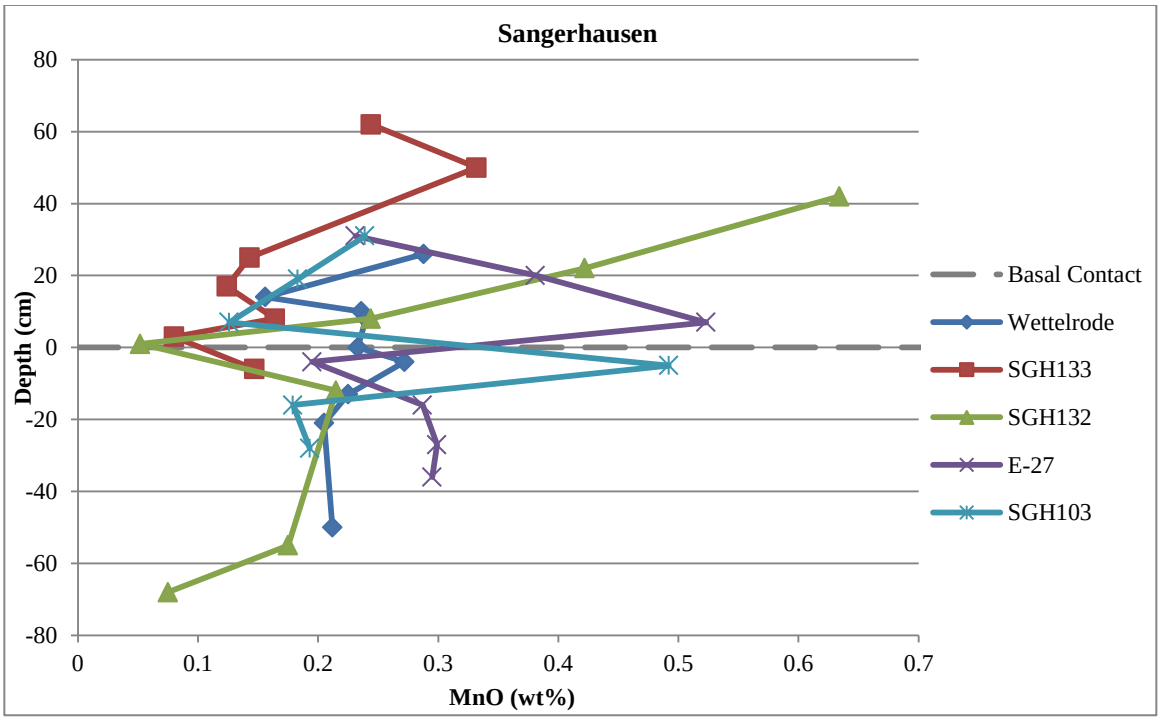


Figure 4.83: Manganese (MnO) wt.% by depth, Sangerhausen Basin.

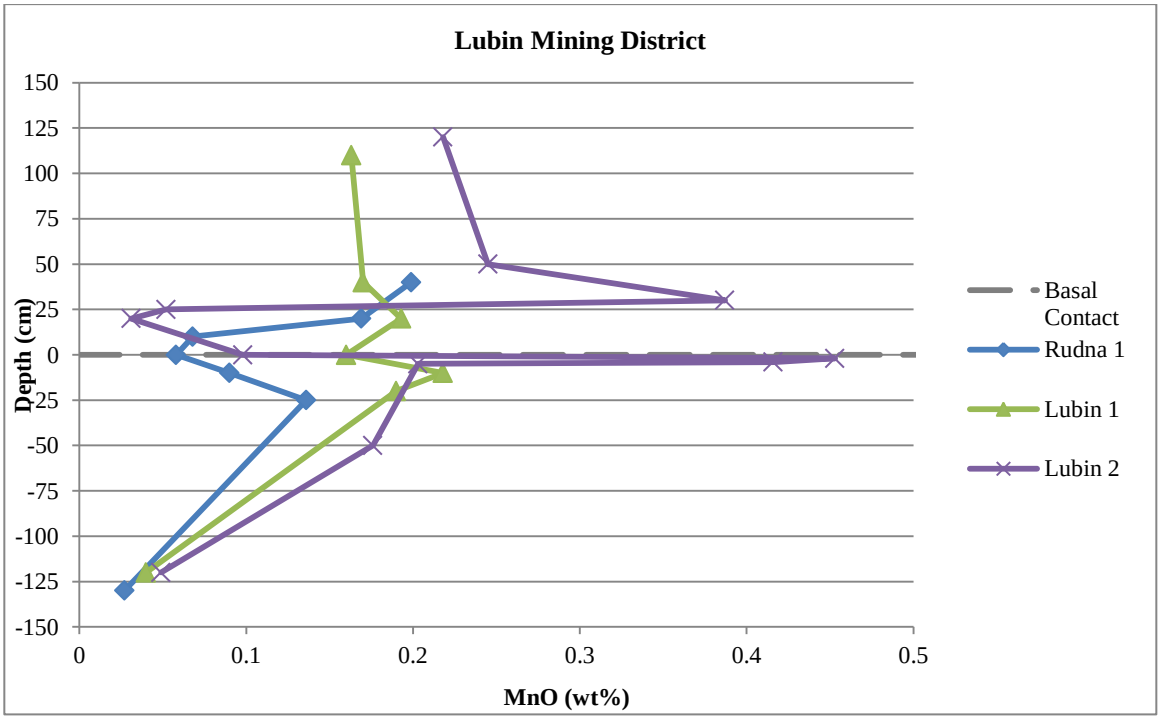


Figure 4.84: Manganese (MnO) wt.% by depth, Lubin mining district.

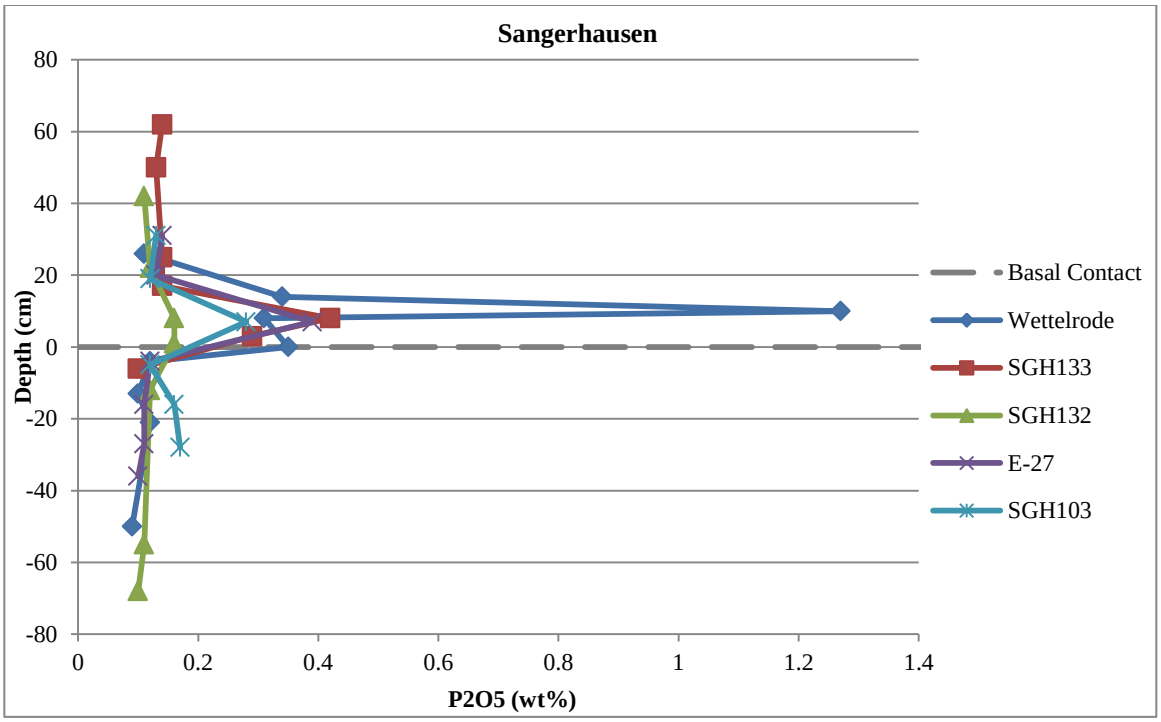


Figure 4.85: Phosphorous ($P_2O_5$) wt.% by depth, Sangerhausen Basin.

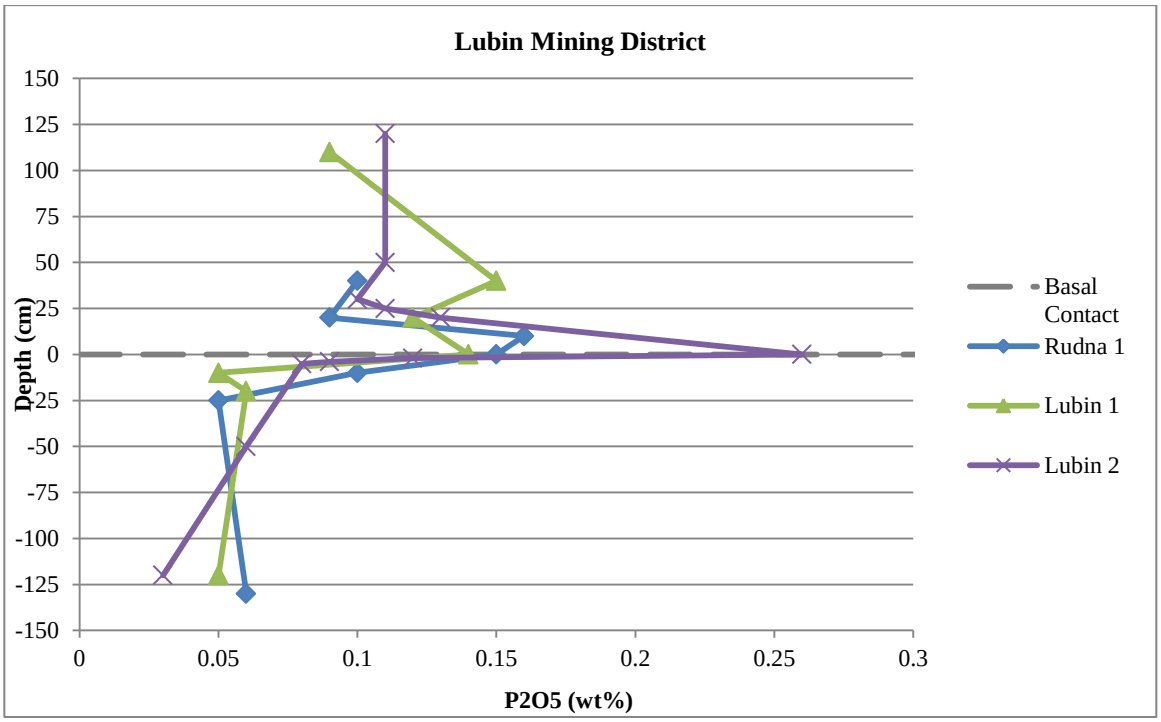


Figure 4.86: Phosphorous ($P_2O_5$) wt.% by depth, Lubin mining district.

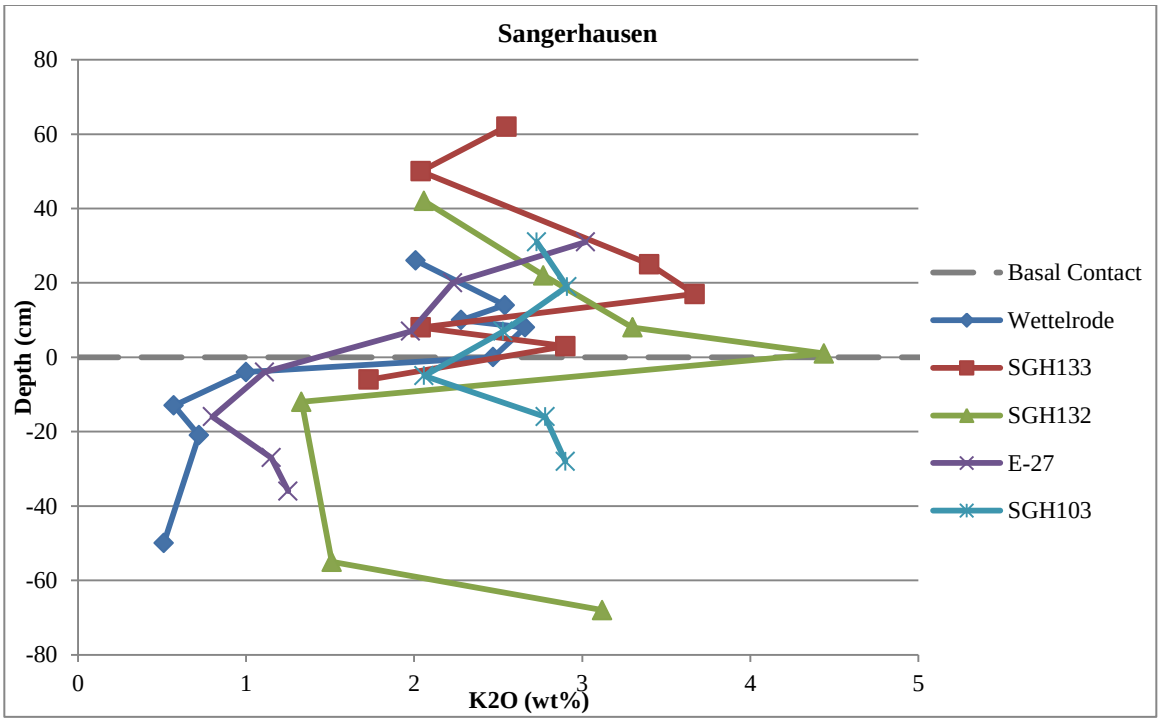


Figure 4.87: Potassium ($K_2O$) wt.% by depth, Sangerhausen Basin.

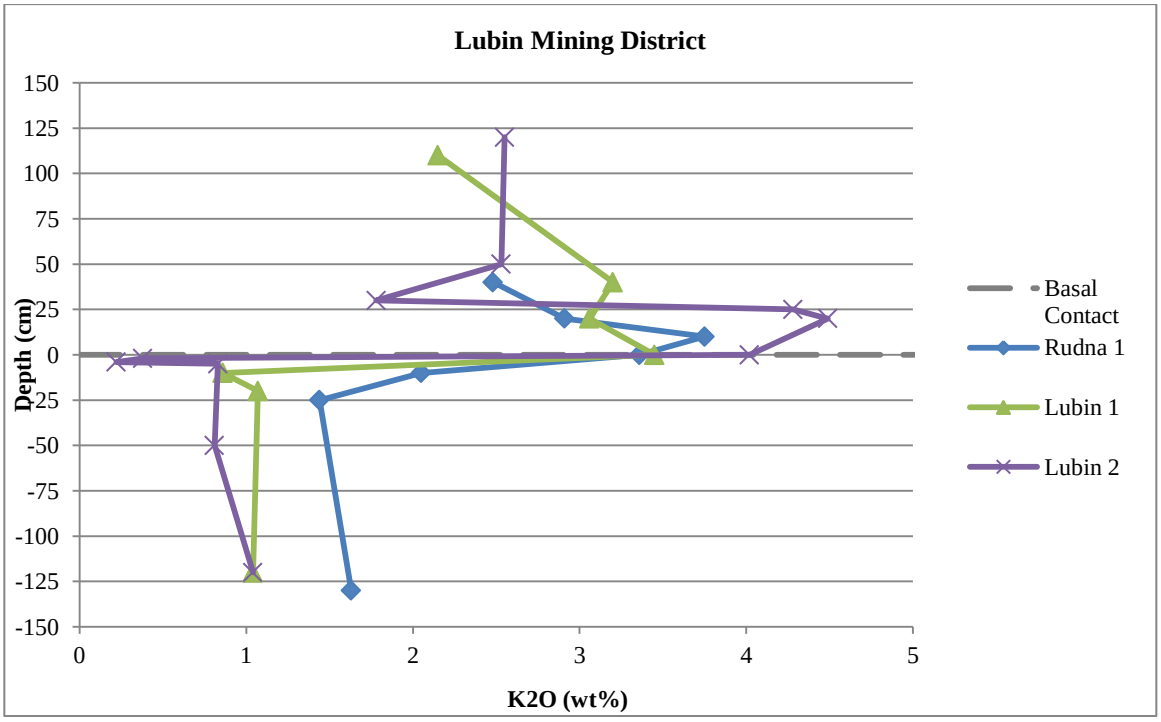


Figure 4.88: Potassium ($K_2O$) wt.% by depth, Lubin mining district.

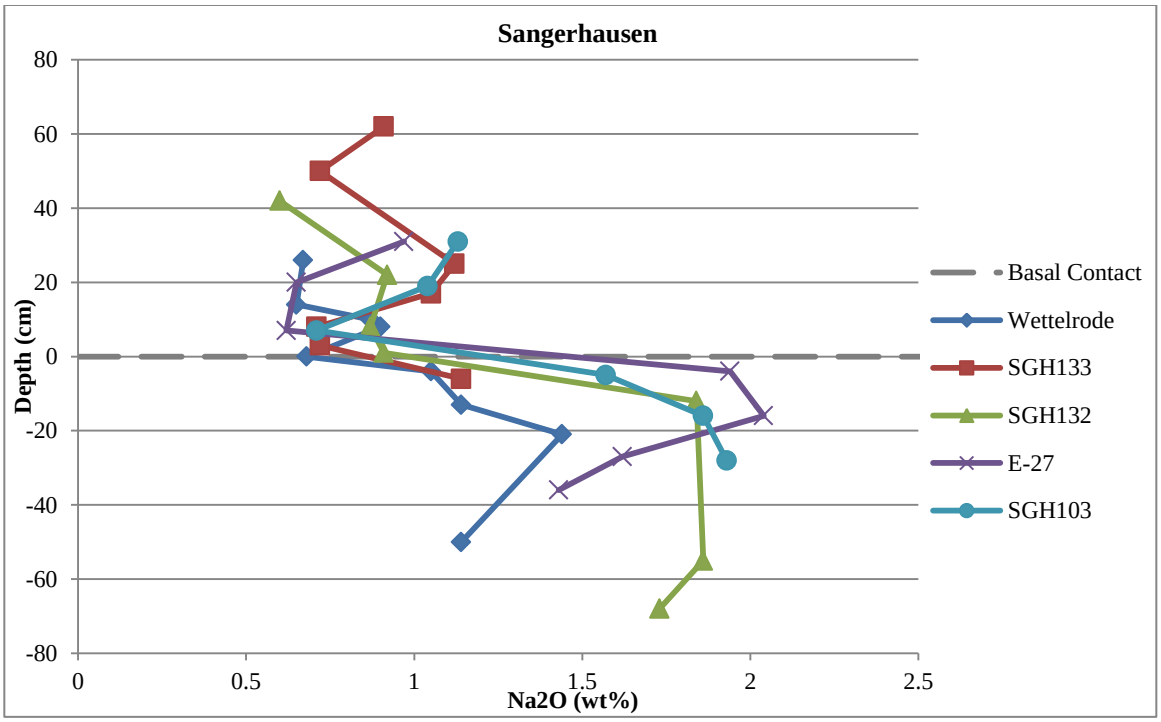


Figure 4.89: Sodium ($Na_2O$) wt.% by depth, Sangerhausen Basin.

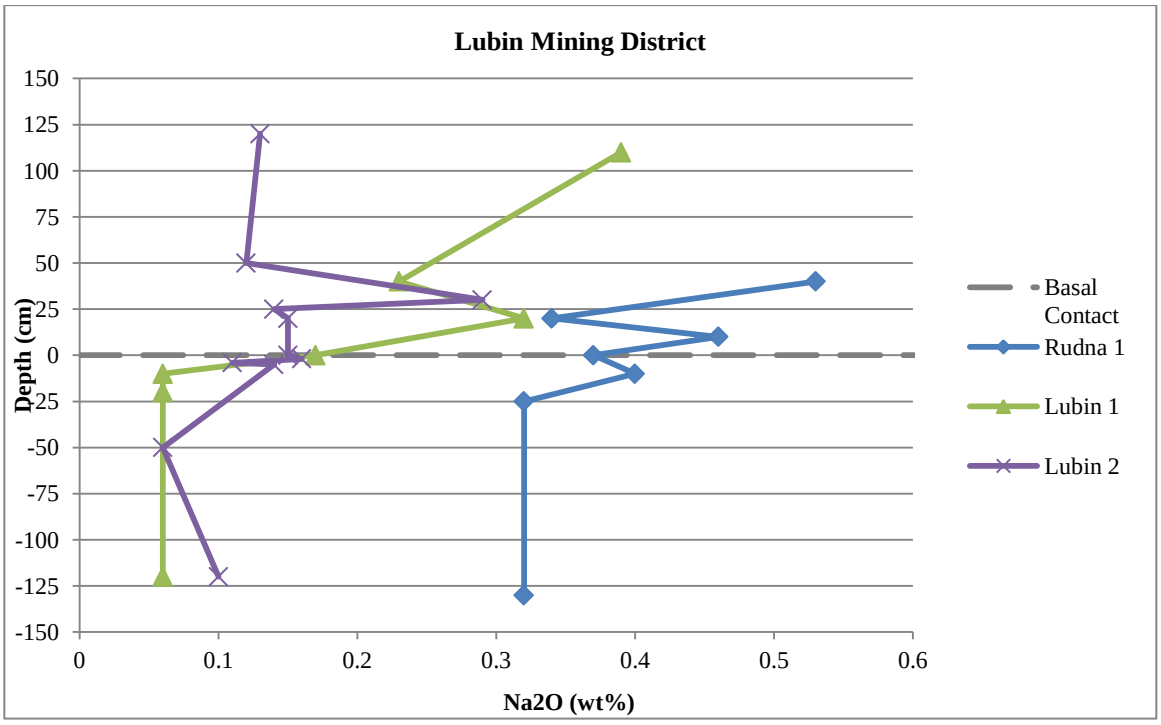


Figure 4.90: Sodium ($Na_2O$) wt.% by depth, Lubin mining district.

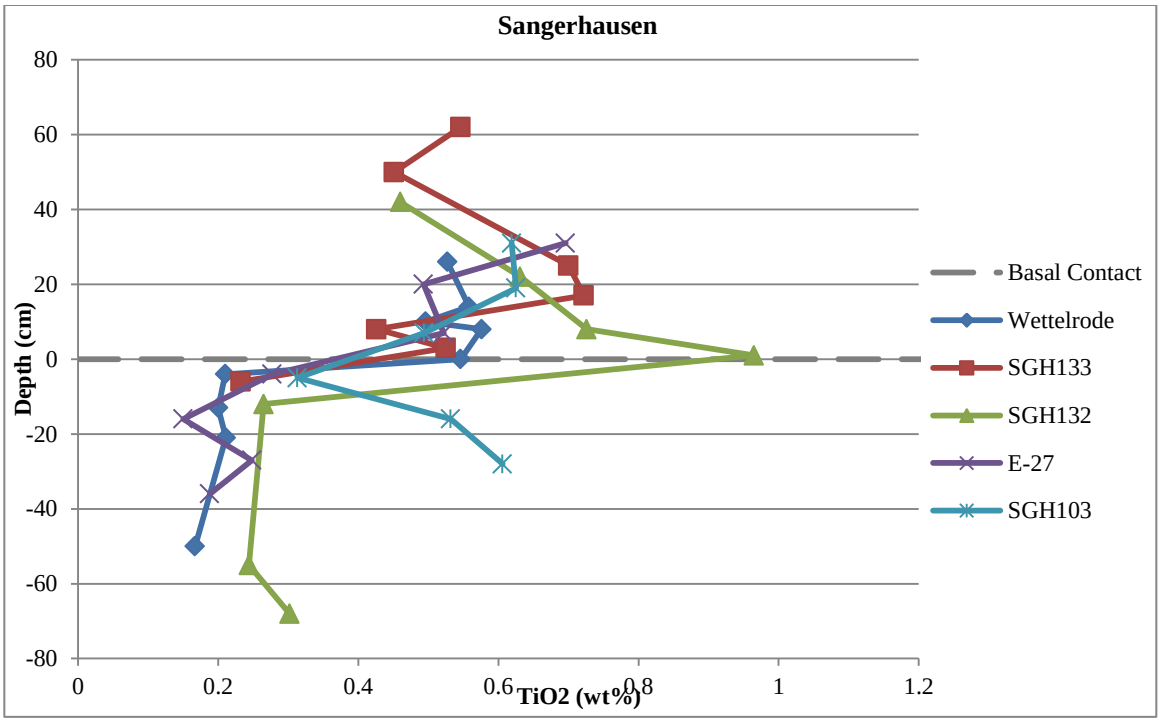


Figure 4.91: Titanium ($TiO_2$) wt.% by depth, Sangerhausen Basin.

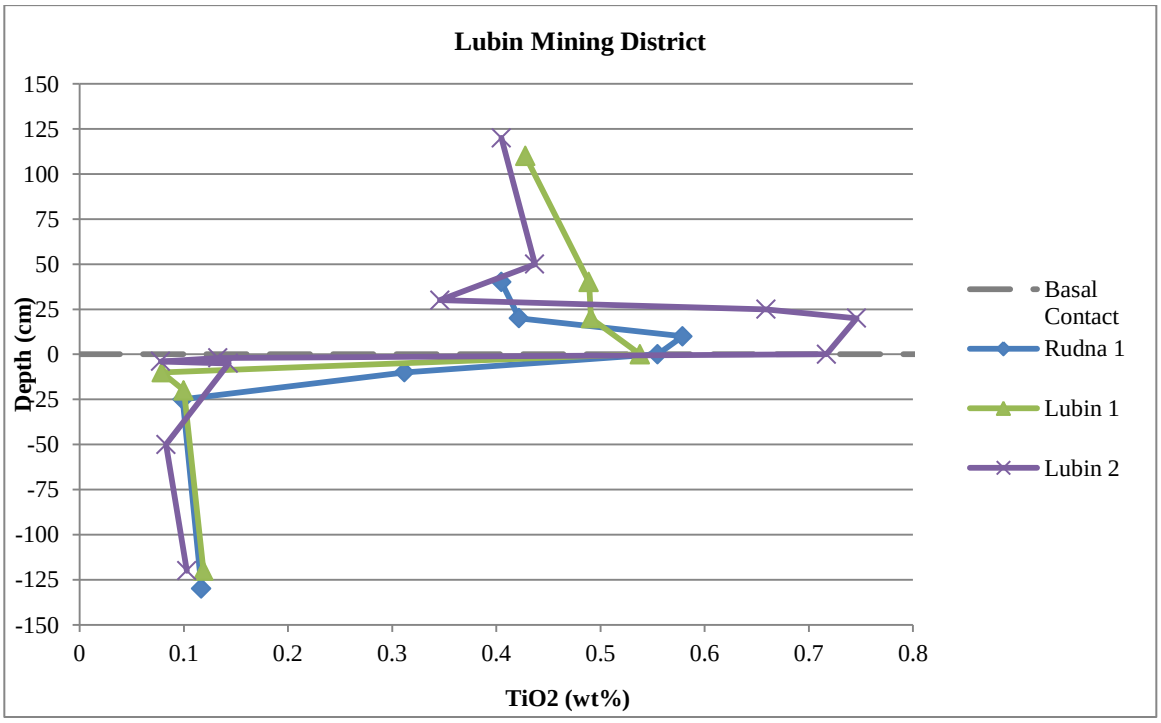


Figure 4.92: Titanium ($TiO_2$) wt.% by depth, Lubin mining district.

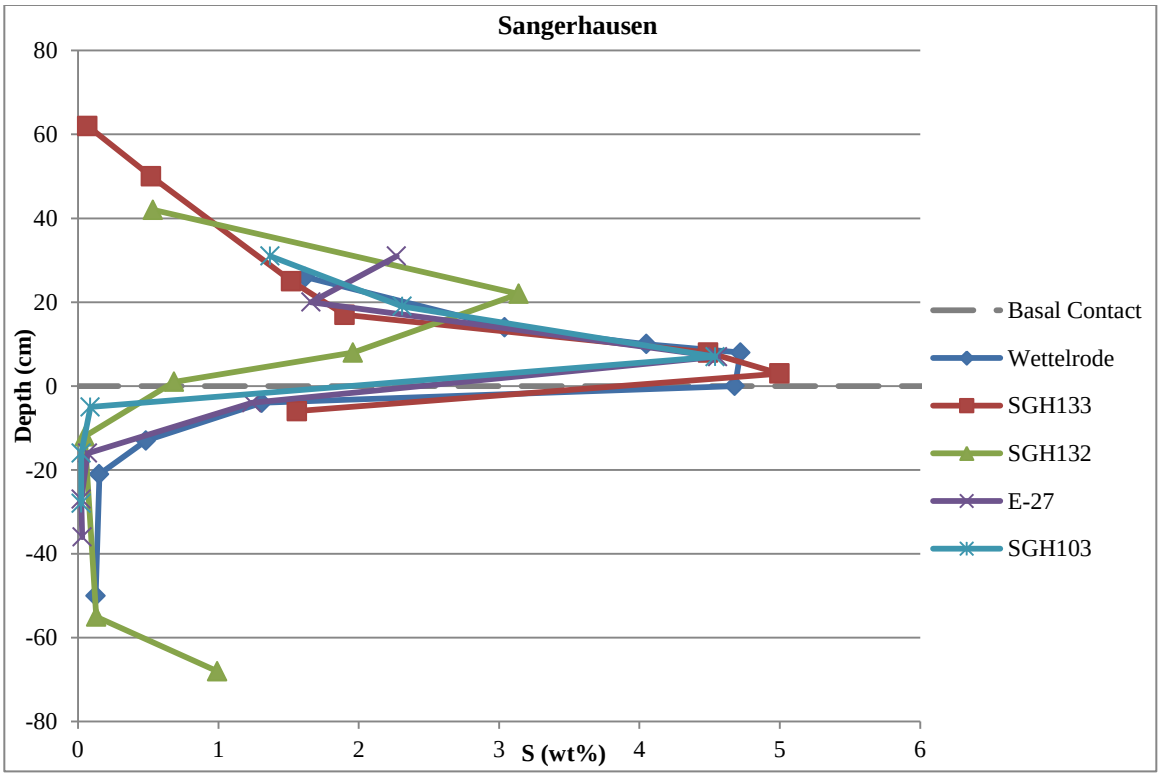


Figure 4.93: Sulfur (S) wt.% by depth, Sangerhausen Basin.

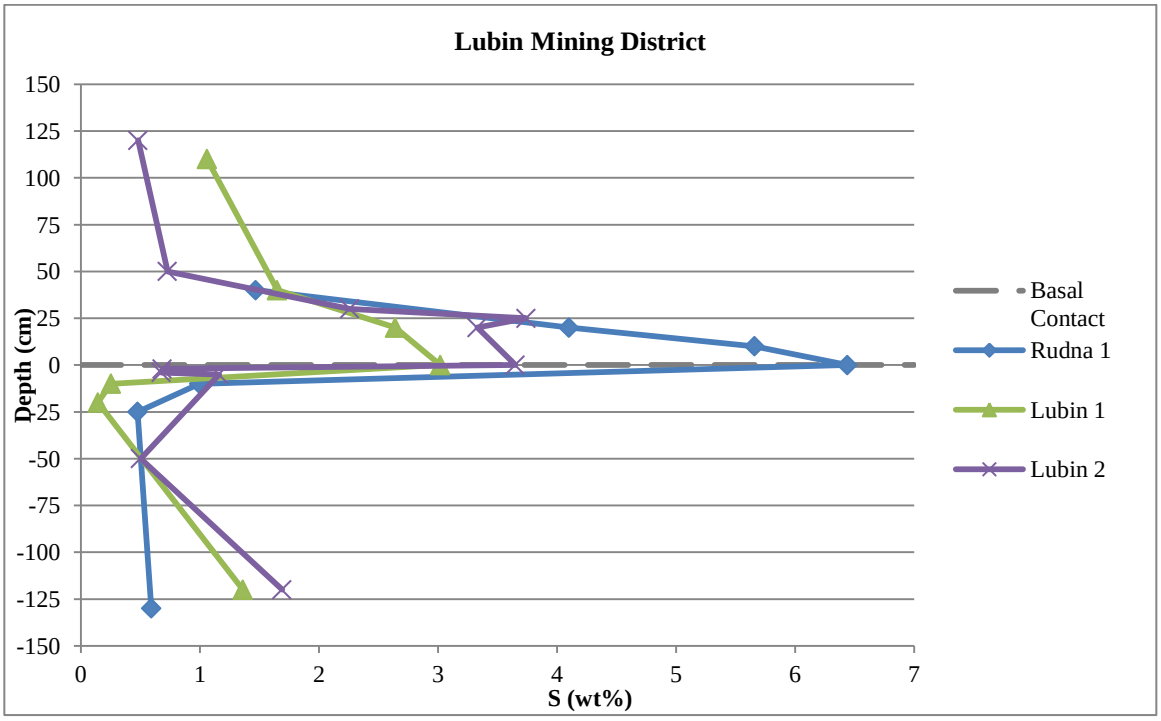


Figure 4.94: Sulfur (S) wt.% by depth, Lubin mining district.

### 4.3.2 Ore Elements

Data are listed in Table 4.5 and Table 4.6.

**Copper:** All of the Sangerhausen Basin and Lubin district geochemical samples have Cu concentrations greater than the average crustal composition, 55 ppm, except for two samples in core SGH133 (50 and 62 cm above the contact) and three samples in core E-27 (at 16, 27, and 36 cm below the contact). Ore grade levels of Cu (1%) are present in 7 of 36 Sangerhausen samples, and in 20 of 26 Lubin mining district samples (Figures 4.95 and 4.96). The Sangerhausen samples with ore grade copper are located 5 cm below the contact up to 10 cm above the contact. The Lubin and Rudna samples that contain ore grade copper are found 120 cm below the contact to 110 cm above the contact, although not all of the samples within this range exhibit ore grade Cu mineralization. In the Lubin and Rudna samples, the highest Cu concentrations are generally found at the Kupferschiefer/Weissliegend contact to 20 cm above the contact (Figure 4.96).

**Silver:** Ag present in samples from the Sangerhausen Basin is below ore grade (100 ppm) with the exception of 5 samples. The samples taken at the contact and 8 cm above the contact in Wettelrode, samples from 4 cm below and 7 cm above the contact in core E-27, and the sample taken 7 cm above the contact in core SGH103 all have concentrations of silver above 100 ppm (Figure 4.97). In the samples that do not reach ore grade, there is still a relative increase in concentration for all of the 5 Sangerhausen locations from 20 cm below the contact to 20 cm above the contact. In the samples taken from the Lubin mining district, there are 13 samples with ore grade silver concentrations. The samples are mostly from the contact to 30 to 40 cm above the contact; there are two Weissliegend samples from Lubin 2 that contain ore grade silver, at 5 and 120 cm below the contact (Figure 4.98).

**Lead:** None of the Sangerhausen samples contain ore grade concentrations of Pb (using 10 wt.% as ore grade; average crustal composition is 13 ppm). The Sangerhausen samples exhibit relative increases in Pb from 5 cm below the contact to 20 or 30 cm above the contact (Figure 4.99). A sample from Rudna 1, taken 20 cm above the contact, shows ore-level Pb concentrations (11.6 wt.%) (Figure 4.100). All other samples from the Lubin mining district have Pb values of less than 1 wt.%, though it

should be noted that relative increases in concentration are present 25 cm below the contact to 25 cm above the contact.

**Zinc:** Zn concentrations of 10 wt.% and greater are considered ore grade; average soil concentrations are approximately 70 ppm. None of the samples analyzed for this thesis reach ore grade for zinc. The highest zinc concentration present is exhibited by the sample taken 8 cm above the contact from core SGH133, with a concentration of 5.13 wt.% (Figure 4.101). Core SGH133 shows a peak in Zn between 3 and 8 cm above the contact; the other locations show an increase from just below the contact (approximately 4 cm) to 10 cm or so into the Kupferschiefer. Core SGH103 shows the strongest Zn peak 19 cm above the contact. Samples from the Lubin and Rudna mines contain less zinc, with the highest concentration in the sample from 40 cm above the contact from Rudna 1, with 1.55 wt.% (Figure 4.102). Samples from both Lubin 1 and Lubin 2 exhibit very slight increases in zinc from the contact to approximately 40 cm above the contact.

**Uranium:** In core SGH103, the sample from 7 cm above the contact shows anomalously high levels of U (968 ppm), just below ore grade (0.10%, or 1000 ppm) (Figure 4.103). Most other samples from the Sangerhausen Basin have U concentrations below 100 ppm; samples with more than 100 ppm U are observed in samples from the contact to 10 cm above the contact (Figure 4.104). The enrichment is stronger in the samples from the Sangerhausen Basin; Lubin district samples do not show U levels higher than 22.4 ppm, while the Sangerhausen samples have 5 samples with U concentrations greater than 200 ppm.

Table 4.5: Geochemical data for Sangerhausen Basin samples, ore elements.

| **Sangerhausen Basin** | Analyte Symbol | Cu | Ag | Pb | Zn | U |
|---|---|---|---|---|---|---|
| | Unit Symbol | wt. % | ppm | wt. % | wt.% | ppm |
| | Detection Limit | ** | ** | ** | ** | 0.1 |
| | Analysis Method | combined* | combined* | combined* | combined* | FUS-MS |
| | Sample Number | | | | | |
| Wettelrode | K2+26 | 0.0094 | 15.3 | 0.494 | 0.519 | 11.1 |
| | K05+14 | 0.455 | 1.7 | 0.0129 | 0.0218 | 57.8 |
| | K6+10 | 2.02 | 64.2 | 4.86 | 0.0085 | 218 |
| | K7+8 | 6.09 | 152 | 1.46 | 0.0089 | 313 |
| | K8-0 | 4.67 | 106 | 3.21 | 0.0378 | 188 |
| | K9-4 | 1.97 | 30.1 | 0.414 | 0.129 | 8.4 |
| | K10-13 | 0.256 | 4.9 | 0.159 | 0.0072 | 3.4 |
| | K11-21 | 0.156 | 2.1 | 0.0069 | 0.0056 | 5.1 |
| | K15-50 | 0.0741 | 1.6 | 0.0444 | 0.0024 | 1.4 |
| SGH133 | K32+62 | 0.0034 | 0.8 | 0.0036 | 0.0075 | 2.3 |
| | K29+50 | 0.0037 | 2.1 | 0.0769 | 0.0694 | 5 |
| | K22+25 | 0.0093 | 25.3 | 0.478 | 1.07 | 10.2 |
| | K21+17 | 0.0117 | 4 | 0.0158 | 0.0037 | 13.3 |
| | K20+8 | 0.17 | 73.7 | 1.72 | 5.13 | 258 |
| | K19+3 | 0.464 | 79.2 | 2.18 | 4.48 | 384 |
| | K17-6 | 0.779 | 29.2 | 0.456 | 0.0564 | 16.5 |
| SGH132 | K43+42 | 0.0201 | 1.4 | 0.0049 | 0.0038 | 6.8 |
| | K41+22 | 0.102 | 21.2 | 0.057 | 0.016 | 38 |
| | K40+8 | 0.388 | 70.5 | 0.0653 | 0.0267 | 144 |
| | K39+1 | 0.102 | 13 | 0.0689 | 0.0539 | 78.9 |
| | K38-12 | 0.0508 | 1.9 | 0.003 | 0.0168 | 7.5 |
| | K35-55 | 0.0202 | 0.7 | 0.0013 | 0.007 | 1.7 |
| | K34-68 | 0.374 | 22.2 | 0.168 | 0.022 | 9.2 |
| E-27 | K54+31 | 0.0494 | 15.8 | 0.0235 | 0.0055 | 12.2 |
| | K53+20 | 0.0947 | 15.8 | 0.0307 | 0.0054 | 21.6 |
| | K52+7 | 5.42 | 124 | 0.0149 | 0.0069 | 125 |
| | K51-4 | 3.65 | 146 | 0.0176 | 0.179 | 8.7 |
| | K50-16 | 0.0043 | 0.4 | 0.0008 | 0.0016 | 1.9 |
| | K49-27 | 0.0035 | 0.9 | 0.0009 | 0.0017 | 7.2 |
| | K48-36 | 0.0026 | 0.4 | 0.0009 | 0.0021 | 5.2 |
| SGH103 | K61+31 | 0.0249 | 18.1 | 0.493 | 0.352 | 6.5 |
| | K60+19 | 0.0331 | 42 | 1.54 | 2.83 | 15.6 |
| | K59+7 | 10 | 1150 | 0.201 | 0.401 | 968 |
| | K58-5 | 0.109 | 11.6 | 0.0136 | 0.0157 | 12.3 |
| | K57-16 | 0.0068 | 0.9 | 0.0026 | 0.0056 | 8.1 |
| | K56-28 | 0.0059 | 0.8 | 0.0024 | 0.007 | 6.3 |

Table 4.6: Geochemical data for Lubin mining district samples, ore elements.

| **Lubin Mining District** | Analyte Symbol | Cu | Ag | Pb | Zn | U |
|---|---|---|---|---|---|---|
| | Unit Symbol | wt. % | ppm | wt. % | wt.% | ppm |
| | Detection Limit | ** | ** | ** | ** | 0.1 |
| | Analysis Method | combined* | combined* | combined* | combined* | FUS-MS |
| | Sample Number | | | | | |
| Rudna 1 | K63+40 | 0.013 | 32.2 | 0.863 | 1.55 | 10.3 |
| | K65+20 | 2.02 | 131 | 11.6 | 0.0256 | 15.4 |
| | K67+10 | 7.52 | 812 | 0.698 | 0.0188 | 20.2 |
| | K66-0 | 11 | 1120 | 0.0687 | 0.0367 | 13.5 |
| | K68-10 | 1.34 | 80.9 | 0.0154 | 0.0048 | 11.9 |
| | K69-25 | 0.339 | 38.3 | 0.0073 | 0.0029 | 1.1 |
| | K70-130 | 0.82 | 28.7 | 0.003 | 0.004 | 1.1 |
| Rudna 2 | K76+20 | 4.63 | 230 | 0.159 | 0.171 | 19.2 |
| Lubin 1 | K84+110 | 1.4 | 62.3 | 0.0024 | 0.0015 | 4.6 |
| | K88+40 | 5.56 | 156 | 0.0027 | 0.0039 | 15.2 |
| | K89+20 | 9.41 | 290 | 0.0046 | 0.0025 | 16.7 |
| | K91+0 | 11.1 | 305 | 0.0064 | 0.0047 | 18.8 |
| | K92-10 | 0.822 | 20.4 | 0.0009 | 0.0017 | 7.8 |
| | K93-20 | 0.476 | 10.6 | 0.0009 | 0.0009 | 7.9 |
| | K94-120 | 3.55 | 71.1 | 0.0015 | 0.001 | 3.9 |
| Lubin 2 | K105+120 | 0.965 | 43.3 | 0.0012 | 0.0017 | 4.7 |
| | K104+50 | 3.12 | 95.1 | 0.0008 | 0.0015 | 6.5 |
| | K103+30 | 7.86 | 252 | 0.0024 | 0.002 | 11.4 |
| | K102+25 | 13.9 | 466 | 0.0058 | 0.0034 | 14 |
| | K101+20 | 12.6 | 459 | 0.0069 | 0.006 | 22.1 |
| | K100+0 | 14.2 | 351 | 0.0031 | 0.0062 | 22.4 |
| | K99-UBD | 2.65 | 71.2 | 0.0007 | 0.0018 | 10.3 |
| | K98-LBD | 2.6 | 73.6 | 0.0012 | 0.0023 | 10.4 |
| | K97-5 | 4.54 | 130 | 0.0034 | 0.0016 | 10.1 |
| | K96-50 | 1.84 | 48.1 | 0.0011 | 0.0014 | 1.7 |
| | K95-120 | 5.79 | 113 | 0.0021 | 0.0009 | 1.7 |

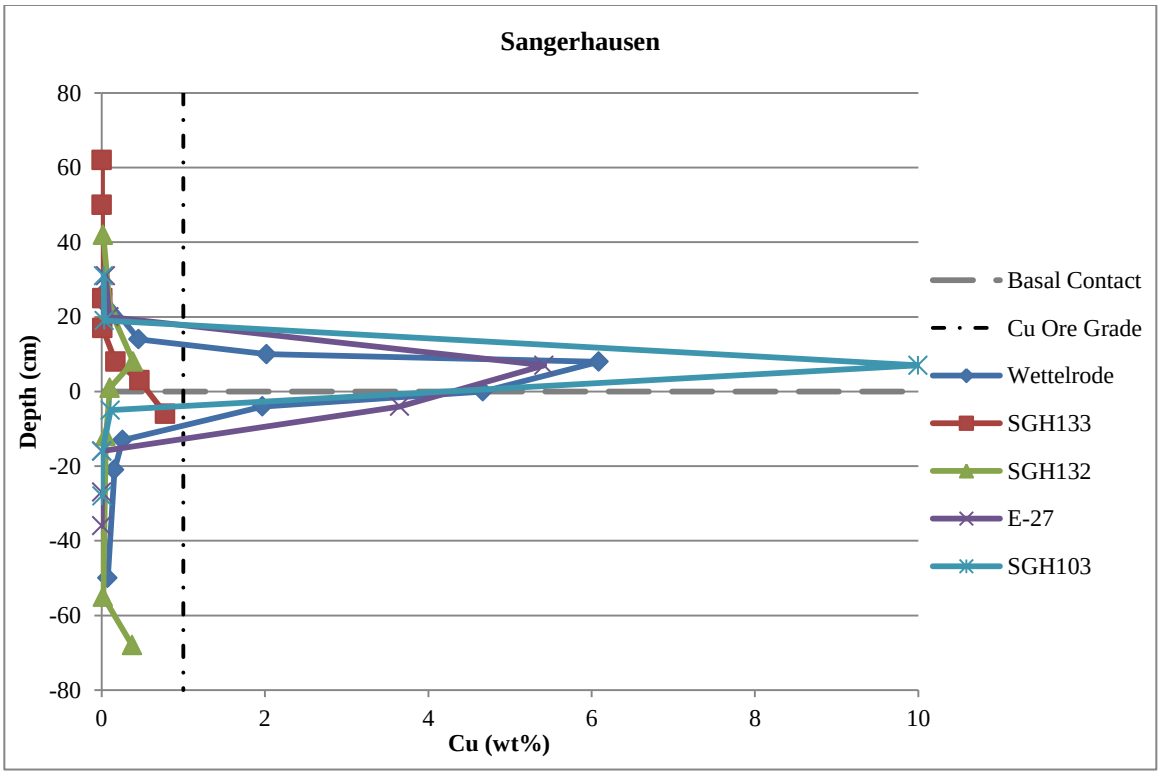


Figure 4.95: Copper by wt.% in Sangerhausen samples by depth, with the ore grade of copper (1%) indicated.

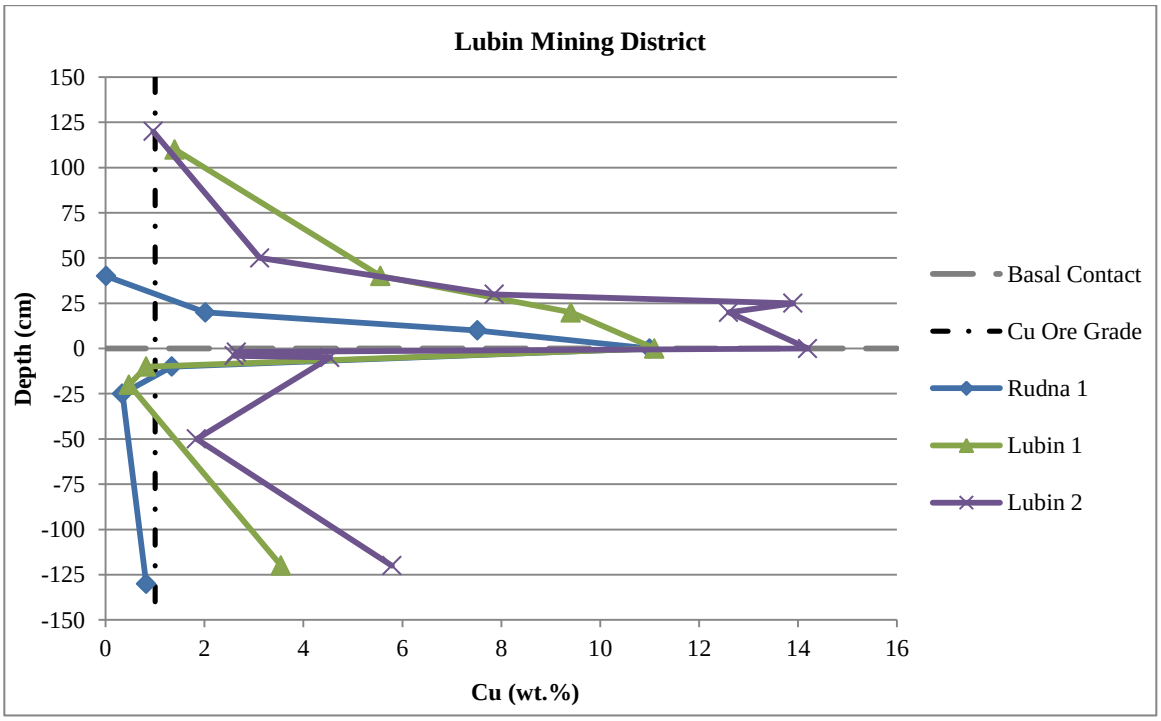


Figure 4.96: Copper by wt.% in Lubin and Rudna samples by depth, with the ore grade of copper (1%) indicated.

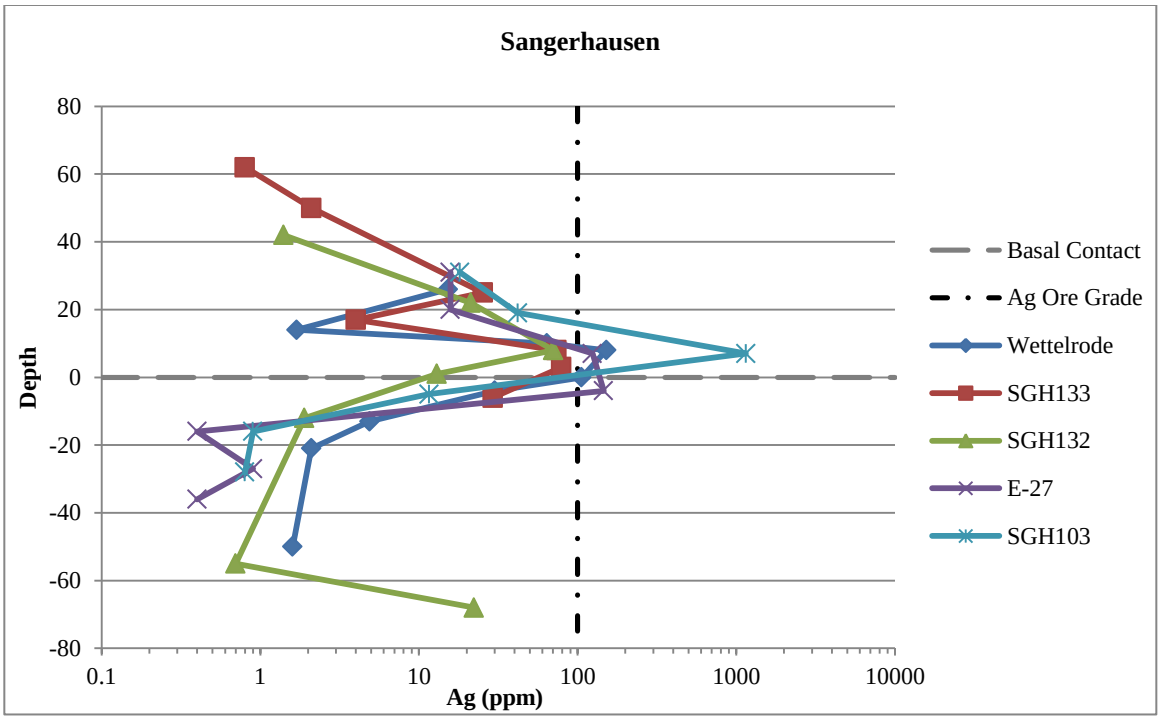


Figure 4.97: Silver concentrations in Sangerhausen Basin samples, with the ore grade of Ag (100 ppm) indicated. Note the log scale.

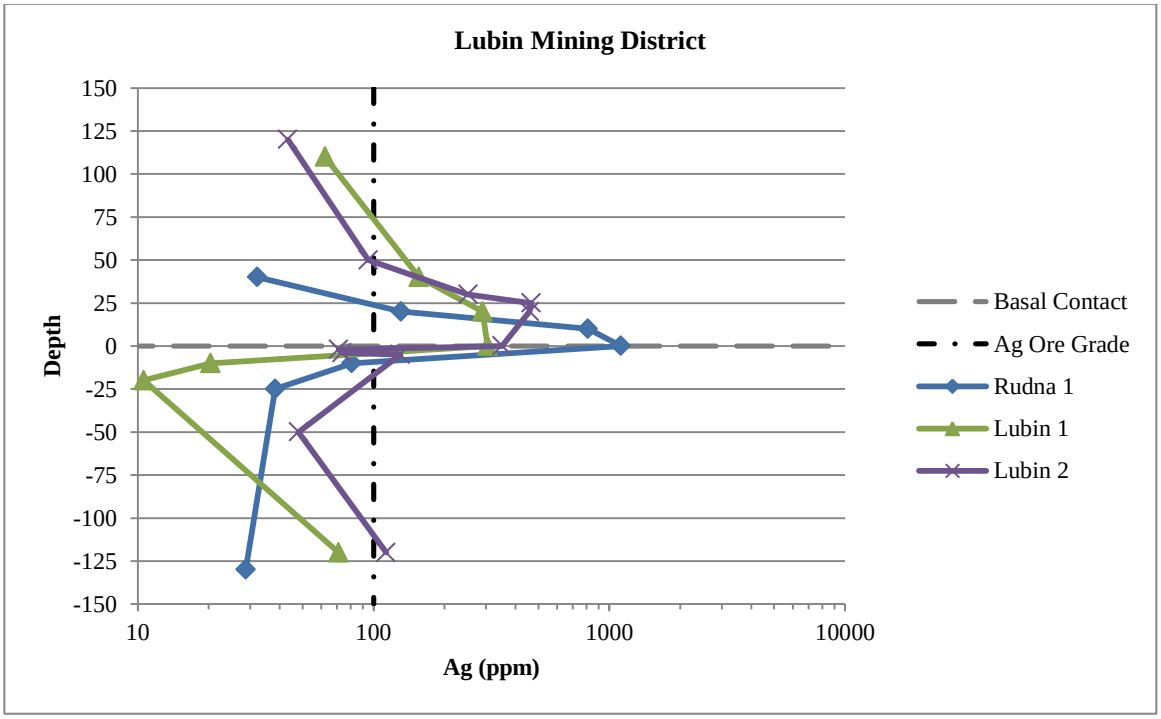


Figure 4.98: Silver concentrations in Lubin mining district samples, with the ore grade of Ag (100 ppm) indicated. Note the log scale.

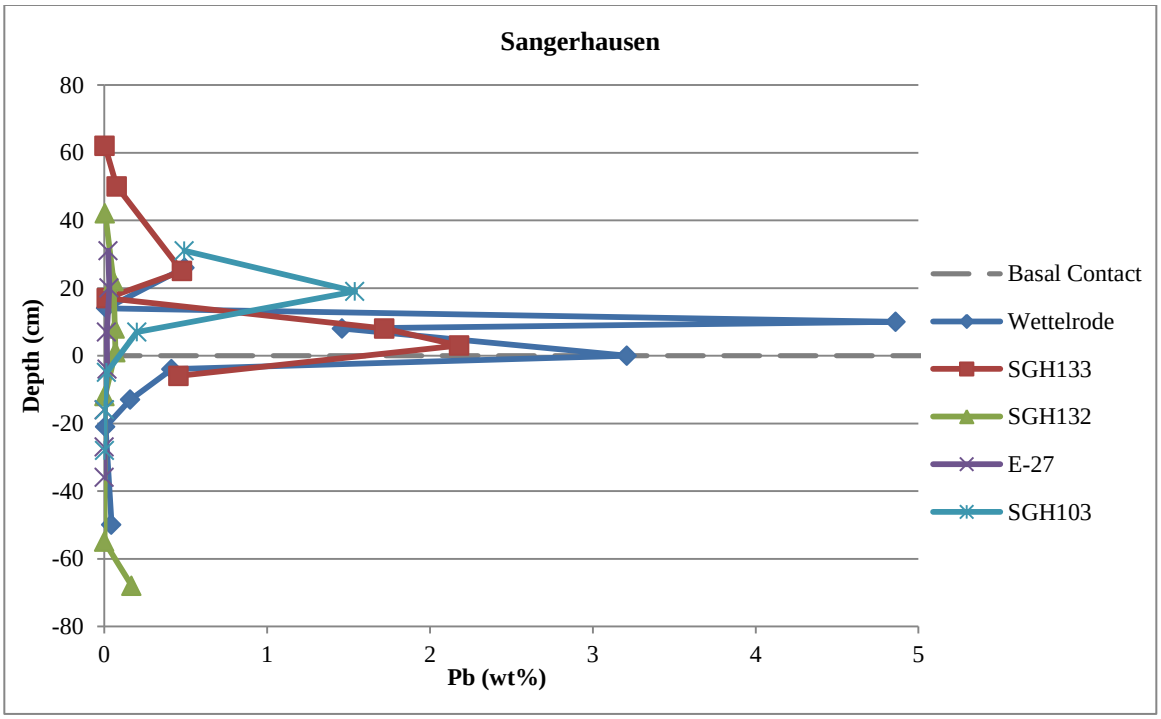


Figure 4.99: Lead (wt.%) concentrations in the Sangerhausen Basin samples.

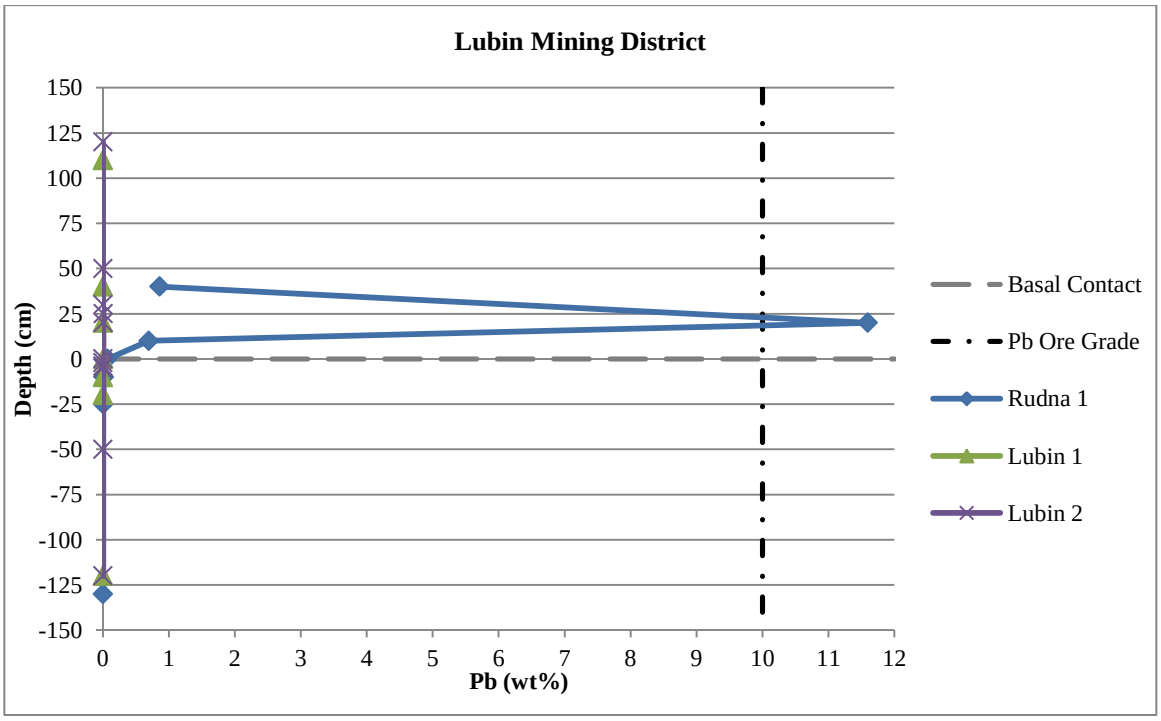


Figure 4.100: Lead (wt.%) concentrations in Lubin mining district samples, with the ore grade value of Pb (10%) marked.

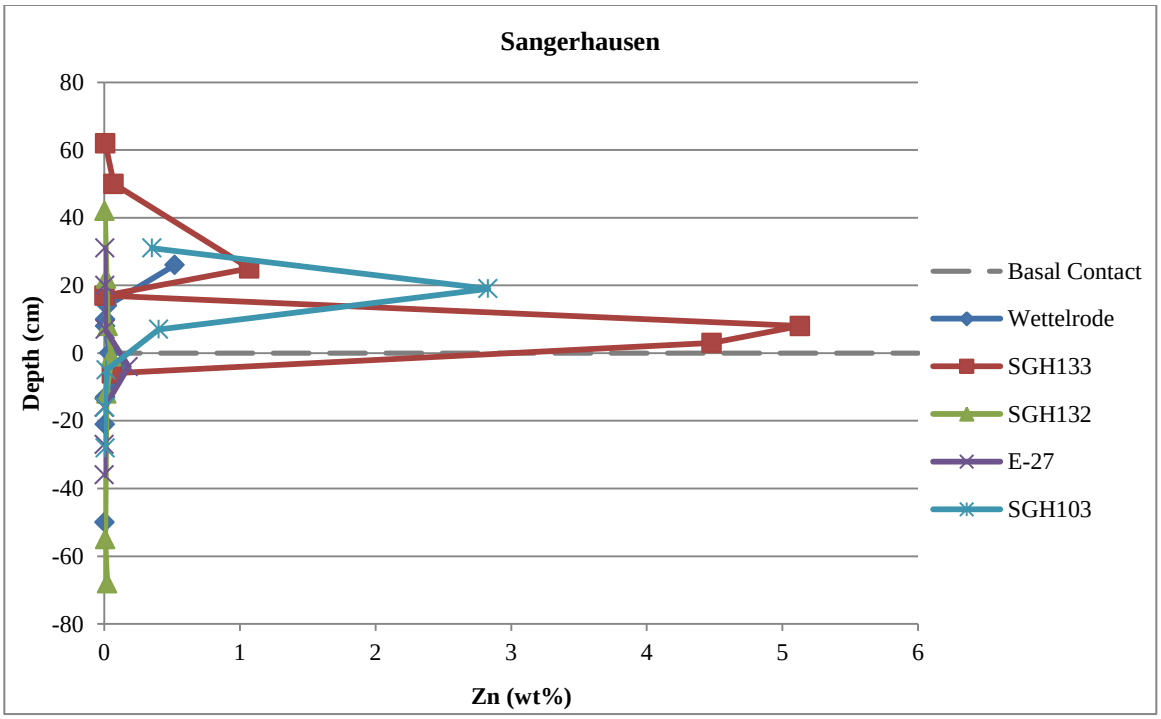


Figure 4.101: Zinc (wt.%) concentrations of Sangerhausen Basin samples.

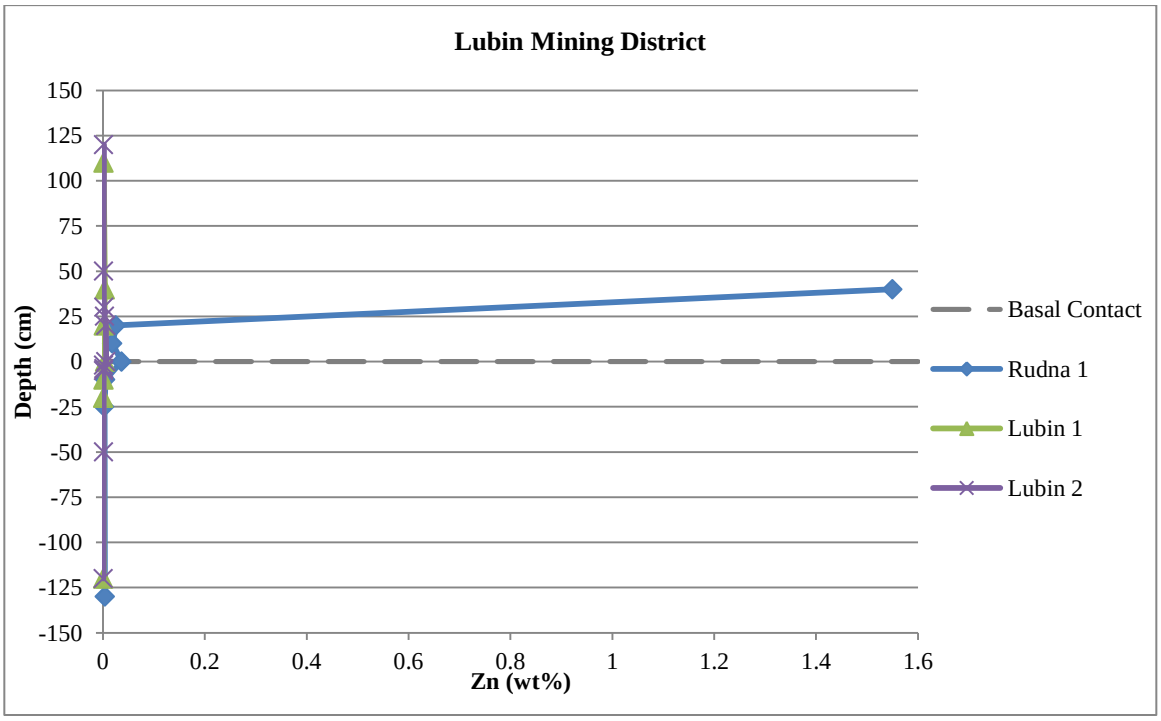


Figure 4.102: Zinc (wt.%) concentrations of the Lubin mining district samples.

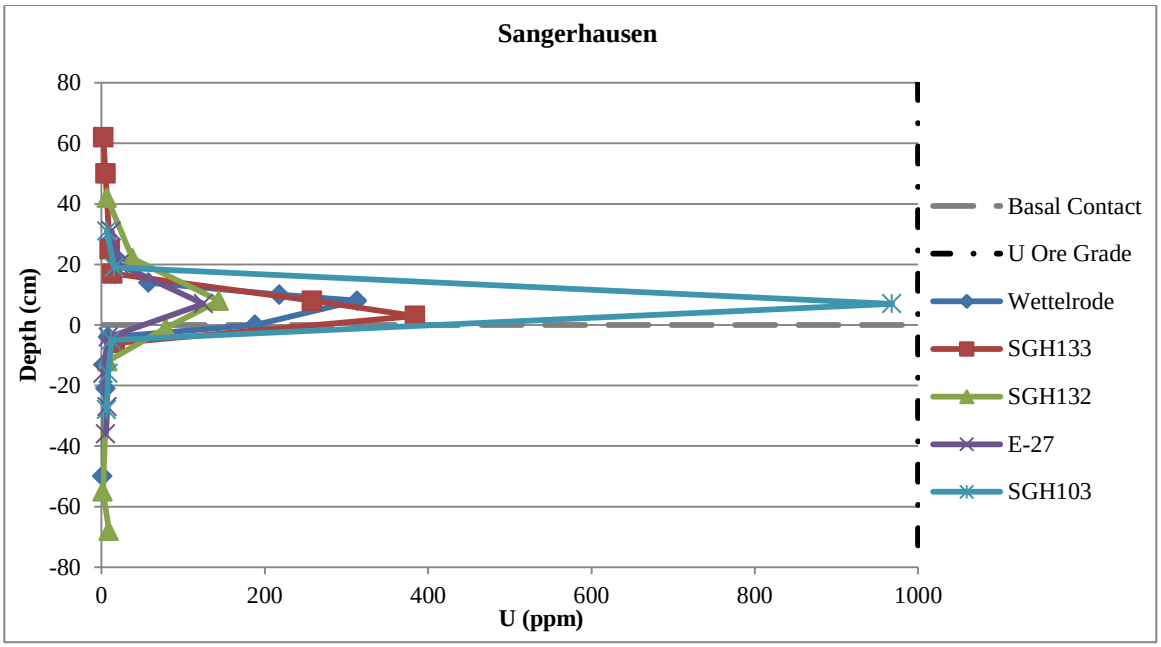


Figure 1.03: Uranium concentrations of Sangerhausen Basin samples, with the U ore grade (1000 ppm) marked.

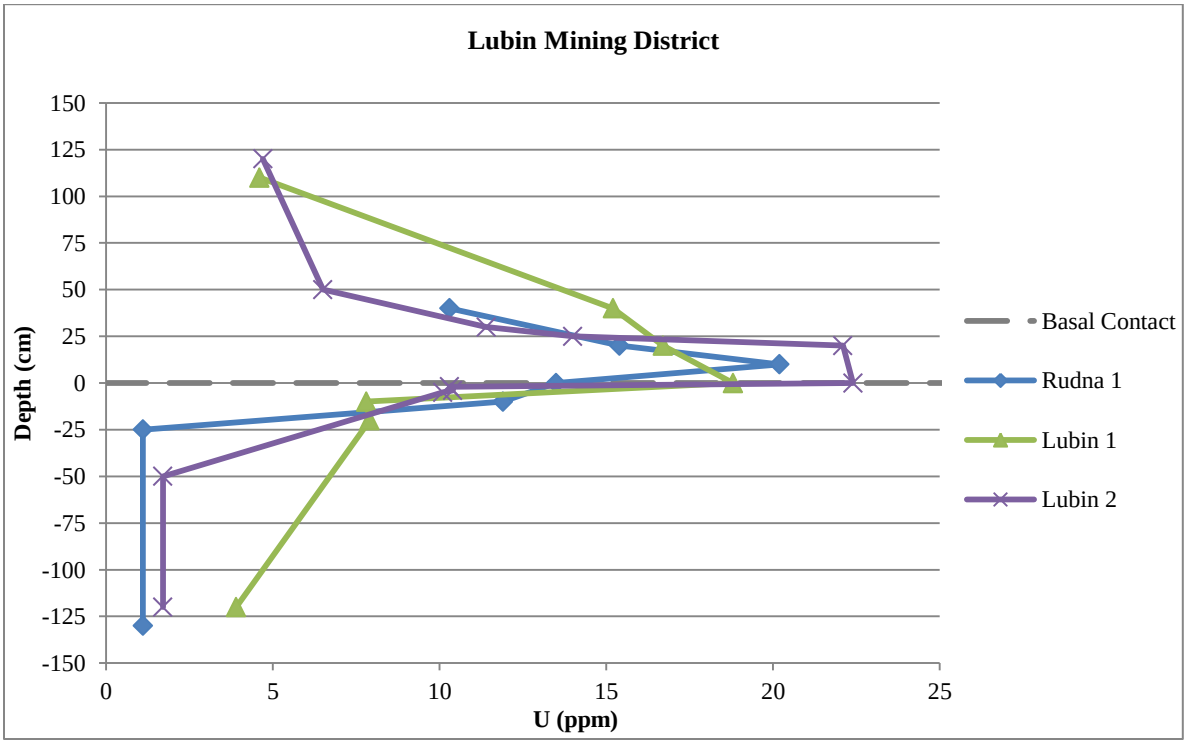


Figure 4.104: Uranium concentrations of Lubin mining district samples.

#### 4.2.2.1 Historical Ore Elements

Data listed in Table 4.7 and Table 4.8.

Other elements historically mined from the Kupferschiefer deposits include vanadium (V), platinum (Pt), selenium (Se), gold (Au), molybdenum (Mo), nickel (Ni), rhenium (Re), germanium (Ge), and cadmium (Cd). Of these elements, only the following were analyzed in our samples: Cd, Ni, V, Ge, Mo. Of these five elements, only Cd, Ni, V, and Mo produce graphs of any interest. The values for Ge concentration are very low (ranging from 1 to 4 ppm), and are very close to the detection limit (1 ppm) in both the Sangerhausen Basin and Lubin mining district samples. The graphs of Cd, Ni, V, and Mo by depth all exhibit an increase in concentration from approximately 5 cm below the contact to 20 cm above the contact.

**Cadmium:** Concentrations of Cd are highest in the Sangerhausen Basin samples from the contact to 20 cm above the contact in cores SGH133 and SGH103 (Figure 4.105). Localized maxima vary in depth and value: 28 ppm at 26 cm above the contact in the Wettelrode mine, 97.2 ppm at 19 cm above the contact in SGH103, and 61.6 ppm at 17 cm above the contact in SGH133. In the samples from the Lubin mining district, the samples taken from both Lubin mine stops exhibit Cd levels below the detection limit (0.5 ppm) (Figure 4.106). In the samples from Rudna 1, higher Cd values are seen at the contact and 40 cm above the contact; the Weissliegend samples show the lowest Cd values. Only one sample from Rudna 2 was analyzed, so no trend can be determined but this sample does happen to fall along the line between the stratigraphically overlying and underlying Rudna 1 samples.

**Nickel:** Ni concentrations above that of average crustal concentrations (75 ppm) are exhibited in Kupferschiefer samples taken at the basal contact to approximately 30 cm above the contact in the Sangerhausen samples, and 40 cm above the contact in the samples from the Lubin mining district (Figures 4.107 and 4.108). None of the samples reach ore grade (1%).

**Vanadium:** V shows an increase in concentration approximately at the basal contact to 30 cm above the contact in the Sangerhausen, and 40 cm above the contact in the Lubin mining district (Figures 4.109 and 4.110). The average crustal value of V is 97 ppm (Rudnick and Gao, 2003); samples more than

31 cm above the contact in Sangerhausen and more than 40 cm above the contact in the Lubin mining district have V concentrations below this level. All Weissliegend samples are also below the V crustal average, with the exception of 4 cm below the contact in Wettelrode, 12 cm below in SGH132, and 4 cm below in E-27.

**Molybdenum:** The detection limit for Mo (2 ppm) is higher than that of the average crustal value (1.5 ppm), and none of the samples reach ore grade for Mo (0.3%). All five Sangerhausen Basin locations exhibit an increase in Mo concentration, from the basal contact to approximately 30 cm above the contact (Figure 4.111). A similar increase in Mo values is present in the samples from the Lubin mining district (Figure 4.112); in these samples, the concentration increase is present from approximately 10 cm below the contact to 40 cm above the contact.

Table 4.7: Geochemical data for Sangerhausen Basin samples, historical ore elements. "b.d.l." = below detection limit. (Note: K40+8 was in a second batch of samples sent for analysis, and for some reason was not given a value for Mo in the data returned from the lab.)

| **Sangerhausen Basin** | Analyte Symbol | Cd | Ni | V | Mo |
|---|---|---|---|---|---|
| | Unit Symbol | ppm | ppm | ppm | ppm |
| | Detection Limit | 0.5 | 1 | 5 | 2 |
| | Analysis Method | TD-ICP | TD-ICP | FUS-ICP | FUS-MS |
| | Sample Number | | | | |
| Wettelrode | K2+26 | 28 | 377 | 644 | 116 |
| | K05+14 | 3.3 | 418 | 1211 | 136 |
| | K6+10 | 1.1 | 453 | 1648 | 570 |
| | K7+8 | 1.4 | 520 | 2719 | 1440 |
| | K8-0 | 1.9 | 495 | 2315 | 897 |
| | K9-4 | 3.5 | 20 | 116 | 23 |
| | K10-13 | b.d.l. | 9 | 35 | b.d.l. |
| | K11-21 | b.d.l. | 7 | 29 | b.d.l. |
| | K15-50 | b.d.l. | 8 | 20 | b.d.l. |
| SGH133 | K32+62 | b.d.l. | 26 | 66 | b.d.l. |
| | K29+50 | 3.5 | 24 | 78 | 5 |
| | K22+25 | 48.9 | 162 | 405 | 52 |
| | K21+17 | 61.6 | 298 | 734 | 81 |
| | K20+8 | 220 | 340 | 1309 | 787 |
| | K19+3 | 142 | 423 | 2031 | 1200 |
| | K17-6 | 2.2 | 9 | 86 | 14 |
| SGH132 | K43+42 | b.d.l. | 20 | 64 | 5 |
| | K41+22 | 1 | 131 | 199 | 91 |
| | K40+8 | < 0.5 | 364 | 863 | |
| | K39+1 | 1.9 | 228 | 1585 | 59 |
| | K38-12 | 0.7 | 16 | 109 | 28 |
| | K35-55 | b.d.l. | 10 | 31 | 12 |
| | K34-68 | 0.8 | 21 | 33 | 21 |
| E-27 | K54+31 | 0.7 | 154 | 269 | 106 |
| | K53+20 | b.d.l. | 306 | 556 | 147 |
| | K52+7 | 0.9 | 311 | 1328 | 280 |
| | K51-4 | 7.3 | 36 | 131 | 21 |
| | K50-16 | b.d.l. | 4 | 19 | 2 |
| | K49-27 | b.d.l. | 10 | 33 | 22 |
| | K48-36 | b.d.l. | 9 | 21 | 7 |
| SGH103 | K61+31 | 12.2 | 52 | 157 | 8 |
| | K60+19 | 97.2 | 296 | 697 | 169 |
| | K59+7 | 16.4 | 356 | 1616 | 529 |
| | K58-5 | 1 | 18 | 85 | 75 |
| | K57-16 | b.d.l. | 22 | 84 | 5 |
| | K56-28 | 0.5 | 26 | 77 | 4 |

Table 4.8: Geochemical data for Lubin mining district samples, historical ore elements. "b.d.l." = below detection limit.

| **Lubin Mining District** | Analyte Symbol | Cd | Ni | V | Mo |
|---|---|---|---|---|---|
| | Unit Symbol | ppm | ppm | ppm | ppm |
| | Detection Limit | 0.5 | 1 | 5 | 2 |
| | Analysis Method | TD-ICP | TD-ICP | FUS-ICP | FUS-MS |
| | Sample Number | | | | |
| Rudna 1 | K63+40 | 79 | 244 | 946 | 122 |
| | K65+20 | 1.8 | 331 | 1105 | 285 |
| | K67+10 | 2.6 | 525 | 2182 | 581 |
| | K66-0 | 4.2 | 469 | 1508 | 414 |
| | K68-10 | 0.5 | 48 | 42 | 175 |
| | K69-25 | 0.8 | 8 | 9 | 21 |
| | K70-130 | b.d.l. | 8 | 13 | b.d.l. |
| Rudna 2 | K76+20 | 5.7 | 466 | 1436 | 242 |
| Lubin 1 | K84+110 | b.d.l. | 20 | 80 | 4 |
| | K88+40 | b.d.l. | 198 | 830 | 119 |
| | K89+20 | b.d.l. | 278 | 1203 | 256 |
| | K91+0 | b.d.l. | 329 | 1466 | 353 |
| | K92-10 | b.d.l. | 22 | 13 | 49 |
| | K93-20 | b.d.l. | 17 | 15 | 61 |
| | K94-120 | b.d.l. | 6 | 17 | 3 |
| Lubin 2 | K105+120 | b.d.l. | 15 | 65 | b.d.l. |
| | K104+50 | b.d.l. | 14 | 82 | 3 |
| | K103+30 | b.d.l. | 87 | 330 | 95 |
| | K102+25 | b.d.l. | 446 | 1458 | 338 |
| | K101+20 | b.d.l. | 407 | 1577 | 504 |
| | K100+0 | b.d.l. | 379 | 839 | 120 |
| | K99-UBD | b.d.l. | 25 | 78 | 46 |
| | K98-LBD | b.d.l. | 9 | 49 | 78 |
| | K97-5 | b.d.l. | 18 | 38 | 60 |
| | K96-50 | b.d.l. | 5 | 10 | 7 |
| | K95-120 | b.d.l. | 3 | 16 | 5 |

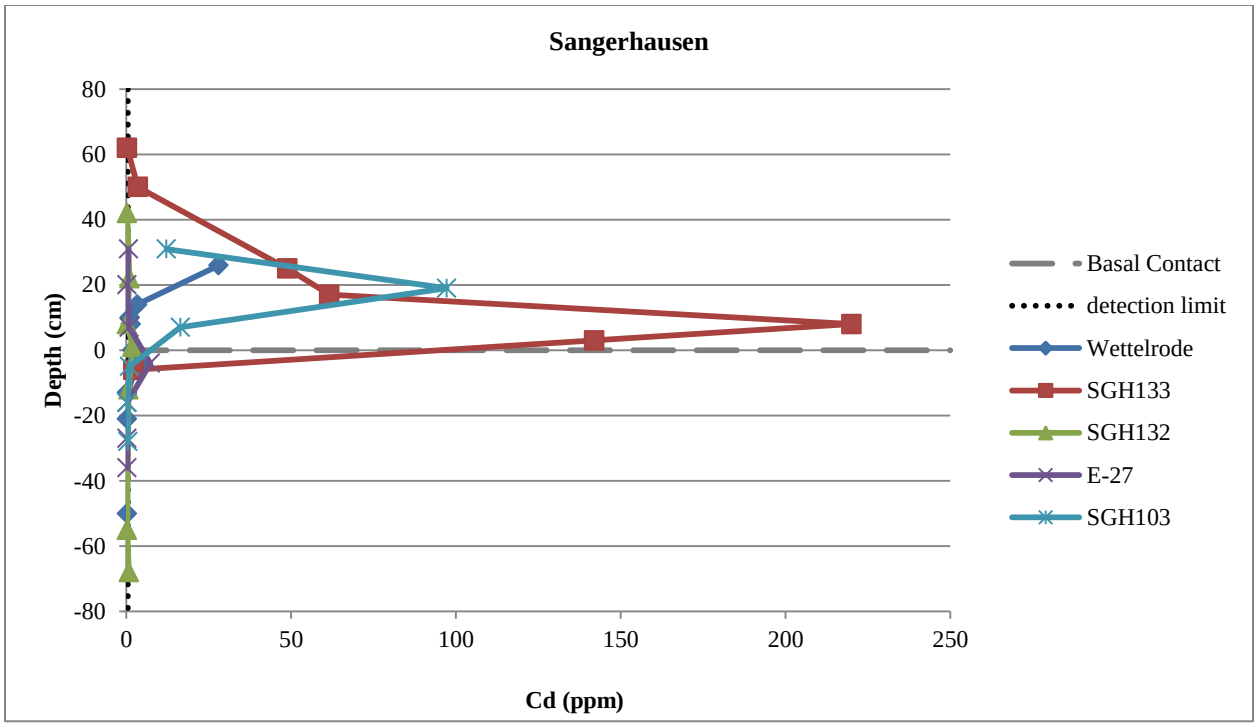


Figure 4.105: Cadmium (ppm) concentrations of Sangerhausen Basin samples.

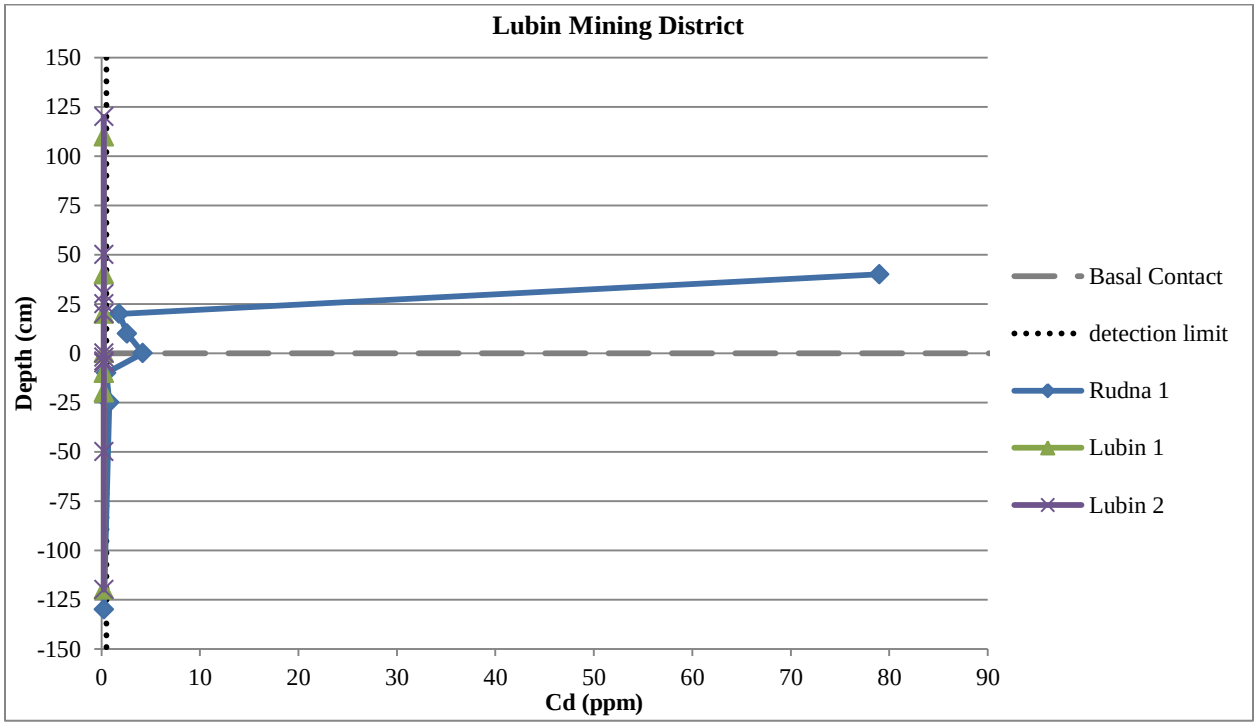


Figure 4.106: Cadmium (ppm) concentrations of Lubin mining district samples.

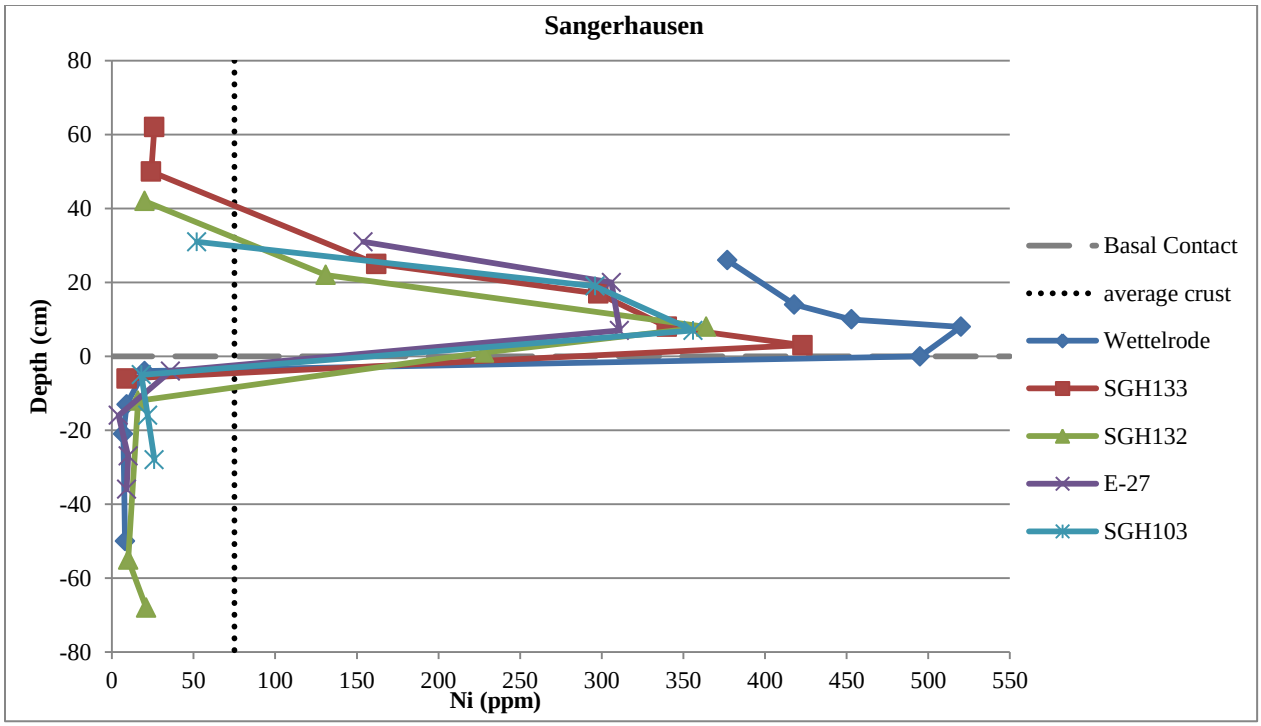


Figure 4.107: Nickel (ppm) concentrations of Sangerhausen Basin samples, with the average crustal value (75 ppm) indicated.

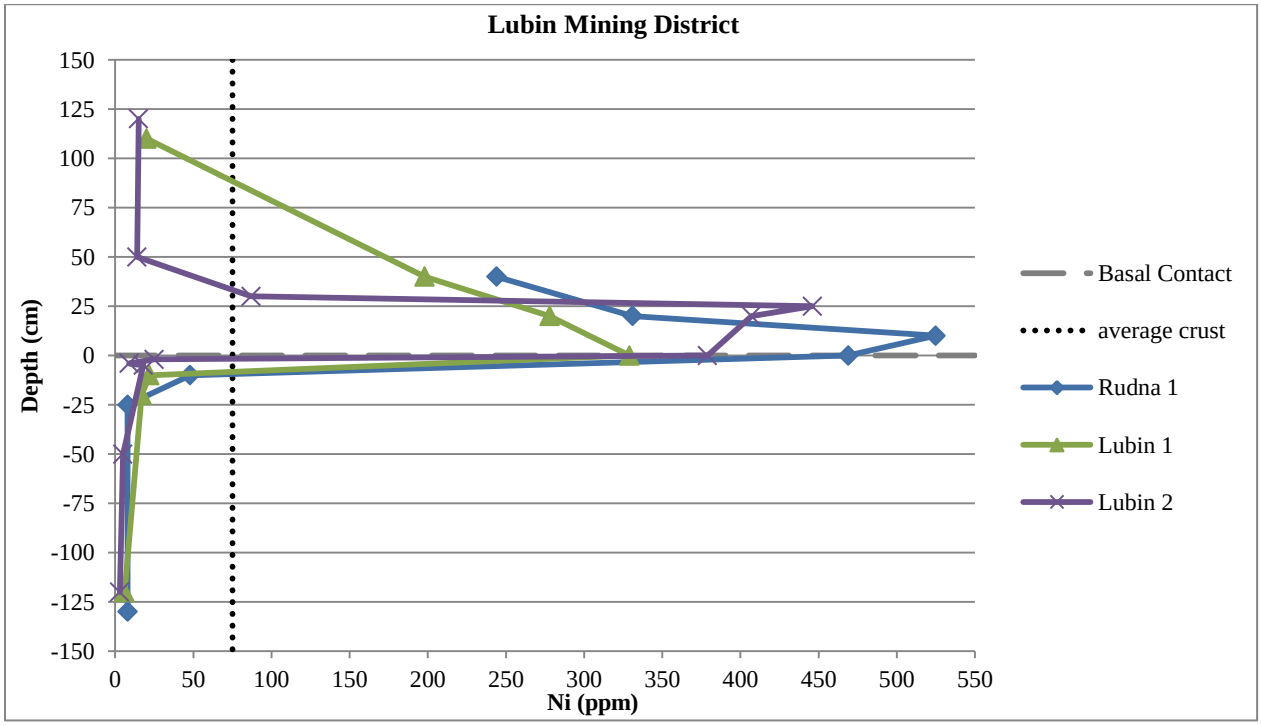


Figure 4.108: Nickel (ppm) concentrations of Lubin mining district, with the average crustal value (75 ppm) indicated.

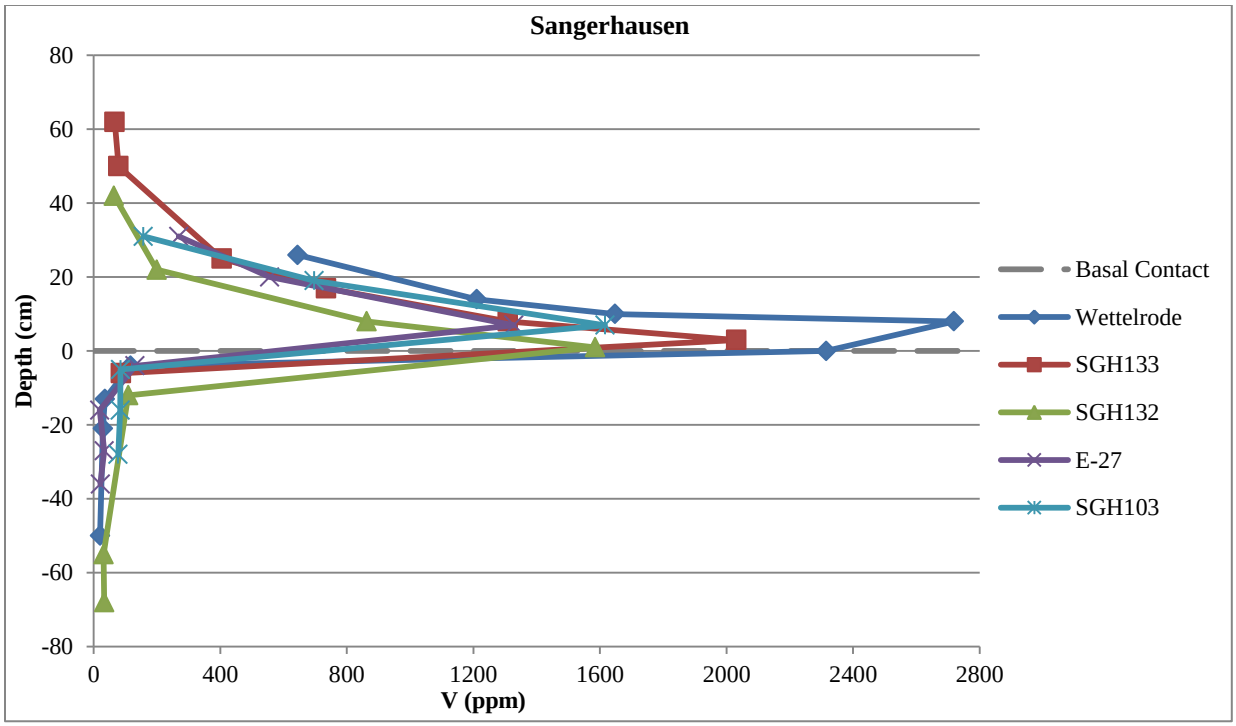


Figure 4.109: Vanadium (ppm) concentrations of Sangerhausen Basin samples.

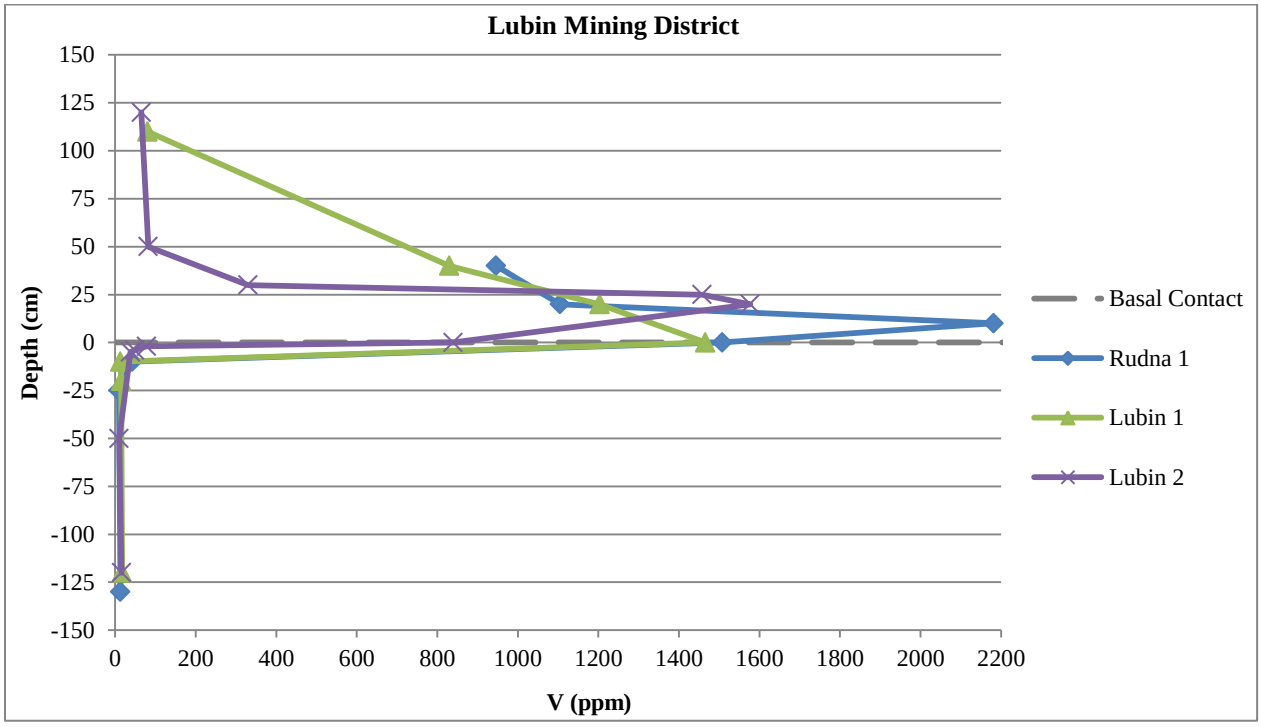


Figure 4.110: Vanadium (ppm) concentrations of Lubin mining district samples.

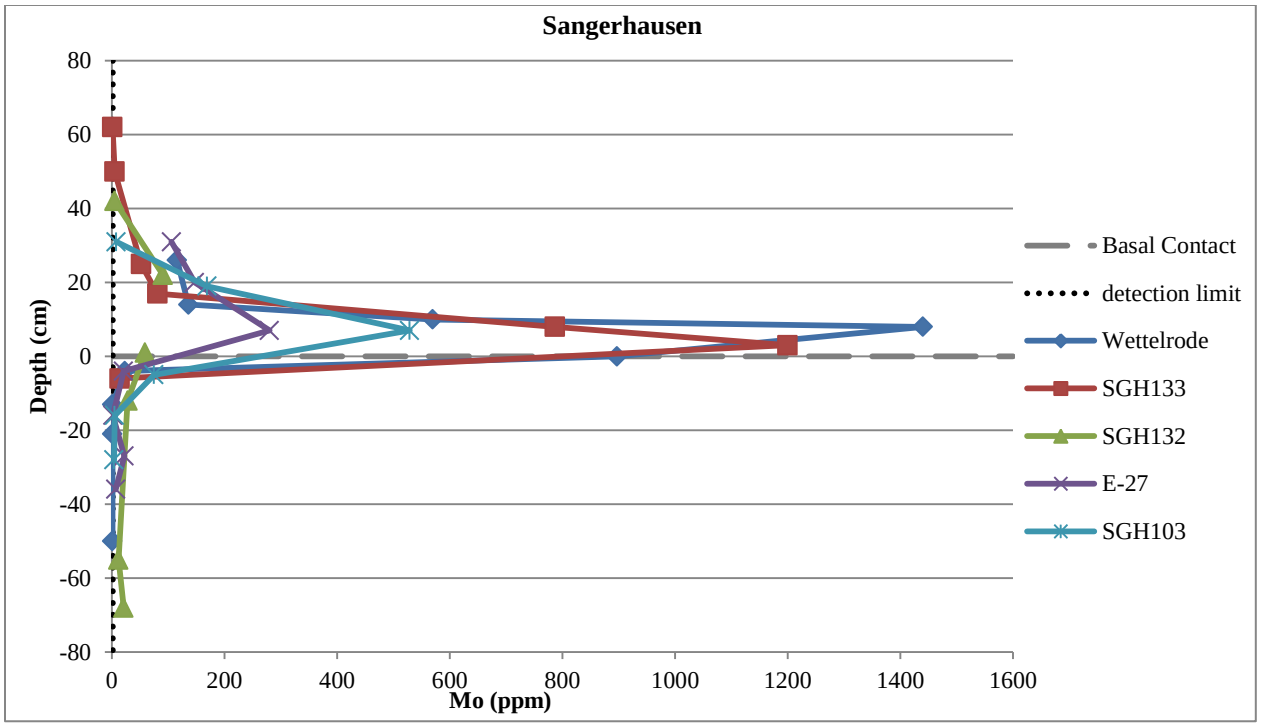


Figure 4.111: Molybdenum (ppm) concentrations for Sangerhausen Basin samples.

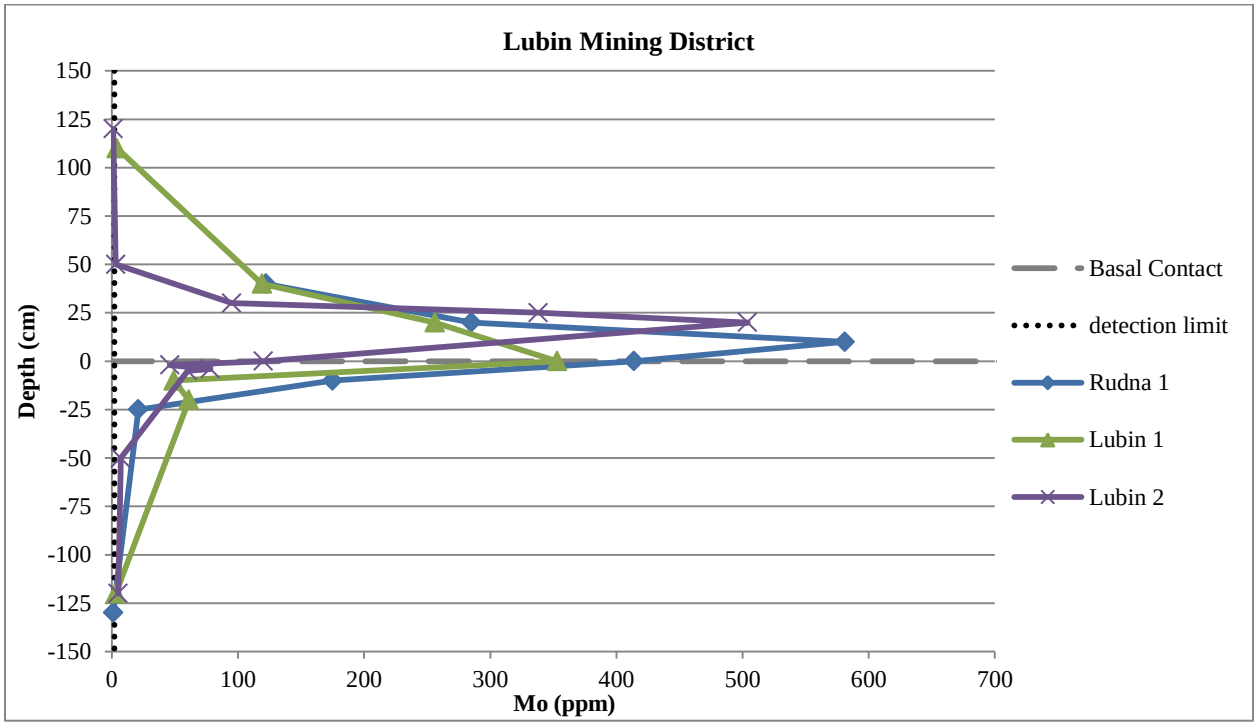


Figure 4.112: Molybdenum (ppm) concentrations of Lubin mining district samples.

### 4.3.3 Trace Elements

Data listed in Table 4.9 and Table 4.10.

Additional trace elements analyzed include scandium (Sc), chromium (Cr), cobalt (Co), arsenic (As), rubidium (Rb), strontium (Sr), zirconium (Zr), antimony (Sb), cesium (Cs), barium (Ba), hafnium (Hf), tantalum (Ta), and thorium (Th). The samples are plotted in comparison to the North American Shale Composite (NASC) in order to determine the enrichment or depletion of the Kupferschiefer compared to other shales. In the case of these elements, NASC values differ little from Post Archaean Average Shale (PAAS) values, and because PAAS values could not be found for all the trace elements examined, NASC is being used. It should be noted that this method will affect the plotting of the Weissliegend samples below the contact, as the sandstone samples are not directly comparable to shale samples. Most of the samples plotted for each element range from the concentrations found within the NASC ("1") to an order of magnitude less than the NASC ("0.1").

**Scandium:** Samples from the Sangerhausen Basin and the Lubin mining district exhibit an increase in Sc within the shale compared to the concentration in the sandstone (Figures 4.113 and 4.114). Scandium values are highest within the lower 25 cm of the Kupferschiefer samples from the Lubin mining district; a similar pattern is not clearly seen in the Sangerhausen samples. All Sc values are below that of the NASC, with the exception of two samples from Lubin 1 (20 and 25 cm above the contact); these are approximately equal to the Sc values determined for average shales.

**Chromium:** For the geochemical analysis of chromium, most of the Weissliegend samples register Cr values below the detection limit of 20 ppm (Figures 4.115 and 116). Within the Sangerhausen samples, the sample 3 cm below the contact in SGH133 is an exception, as are all the Weissliegend samples from SGH103, and the sample from 4 cm below the contact in E-27. In the Lubin mining district, the sample from 10 cm below the contact in Rudna 1, 120 cm below the contact in Lubin 1, and all Weissliegend samples except the one from 50 cm below the contact in Lubin 2 are above the detection limit. The highest Cr concentration in Sangerhausen Basin samples is 2 times that of the NASC; in the

Lubin mining district, the highest concentration is 1.7 times that of the NASC. Chromium concentrations are highest from the contact through the bottom 30 to 40 cm of the shale.

**Cobalt:** The concentration of cobalt shows a clear peak located approximately in the bottom portion of the Kupferschiefer, from the contact to 25 to 30 cm above the contact in the Sangerhausen Basin, and to 20 to 40 cm above the contact in the Lubin mining district (Figures 4.117 and 4.118). The highest Co concentration in the Sangerhausen samples is 38.6 times that of the NASC; in the Lubin mining district the highest concentration is 24.3 times that of the NASC.

**Arsenic:** Concentrations of arsenic vary from less than that of the NASC up to 37.7 times the NASC in the Sangerhausen samples (E-27, 4 cm below the contact) and 42.6 times the NASC in the Lubin mining district (Lubin 2, at the contact) (Figures 4.119 and 4.120). Local maxima in both the Sangerhausen Basin and the Lubin mining district are observed at or very near the contact. Arsenic levels peak from the contact to 25 cm above the contact in Wettelrode, SGH133, E-27, and SGH103. In SGH132, the highest concentration is found 1 cm above the contact to 8 cm above the contact. In samples from the Lubin mining district, the highest As levels are found from the contact to 25 cm above the contact; in the case of Rudna 1 and Lubin 2, this enrichment continues up to 10 cm below the contact. None of the Lubin mining district samples are below the detection limit, but eight of the Sangerhausen samples register below 5 ppm.

**Rubidium:** Most of the samples contain concentrations of rubidium at or below levels found in the NASC (Figures 4.121 and 4.122). The samples that contain at least the amount of Rb found in average shales are located 62, 25, 17, and 3 cm above the contact in SGH133; 22, 8, and 1 cm above the contact in SGH132; 31 cm above the contact in E-27; and 31 and 19 cm above and -28 cm below the contact in SGH103. In the Lubin mining district, the samples with at least NASC levels of Rb are found 20 and 10 cm above the contact in Rudna 1; 20 cm above the contact in Rudna 2; 40, 20, and 0 cm above the contact in Lubin 1; and 25, 20, and 0 cm above the contact in Lubin 2.

**Strontium:** In both the Sangerhausen Basin and Lubin mining district samples, strontium values range from below NASC levels to 8 times that found in average shales (Figures 4.123 and 4.124).

Samples from the Sangerhausen Basin mostly contain 0.5 to ~1.5 times the Sr compared to the NASC. Values above this range are found 26 cm (6.4x), 14 cm (8.3x), and 10 cm (2.8x) above the contact in Wettelrode, and 31 cm (2.3x) and 20 cm (2x) above the contact in E-27. Samples taken 10 cm (5.6x) and 0 cm (3.8x) above the contact in Rudna 1, and 20 cm (3.6x), 0 cm (3x) above the contact, and 2 cm below the contact (1.9x) in Lubin 2 exceed this range as well.

**Zirconium:** Concentrations of zirconium vary from 0.4 to 2 times that of the NASC in Sangerhausen Basin samples, and from ~0.2 to 0.96 times the NASC in Lubin mining district samples (Figures 4.125 and 4.126). The sample that contains 2.05 times the Zr found in average shales was taken 16 cm below the contact in core SGH103.

**Antimony:** Sb concentrations range from below the detection limit to 50 times the NASC concentration in the Sangerhausen samples, and from below the detection limit to 3.5 times the NASC in the Lubin mining district samples (Figures 4.127 and 4.128). The highest Sb values are 10 cm above the contact to 4 cm below the contact in Wettelrode, 8 cm above the contact to 6 cm below the contact in SGH133, 22 cm above to 12 cm below the contact in SGH132, 7 cm above to 4 cm below the contact in E-27, and 19 cm above to 5 cm below the contact in SGH103. Most of the Lubin and Rudna samples are below the detection limit; the highest value is found 10 cm above the contact in Rudna 1.

**Cesium:** Kupferschiefer samples exhibit an increase in cesium concentration compared to the Weissliegend samples; this increase is present in both the Sangerhausen Basin and Lubin mining district samples (Figures 4.129 and 4.130). The Sangerhausen Weissliegend samples have Cs concentrations below that of the NASC, with the exception of 16 and 28 cm below the contact in SGH103 (both approximately 2 times the NASC) and 1 cm above the contact in SGH132 (5.25 times NASC). This is repeated in the Lubin mining district samples, with the exception of 10 cm below the contact in Rudna 1 (1.4x). The samples taken 2 and 4 cm below the contact in Lubin 2 are the only two samples to have Cs concentrations below the detection limit.

**Barium:** Ba concentrations in samples from the Sangerhausen Basin range from 0.25 to 44.6 times that of the NASC, while the Ba in samples from the Lubin mining district range from .005 to 3 times the NASC (Figures 4.131 and 4.132). There is no clear pattern in the Ba data.

**Hafnium:** Hf values in the Kupferschiefer and Weissliegend samples from the Sangerhausen Basin are mostly below the NASC concentrations, with the exception of a few samples that reach up to 1.8 times the NASC (Figure 4.133). All of the samples from the Lubin mining district have Hf values below that of the NASC (Figure 4.134). There is no clear pattern in the Hf data.

**Tantalum and Thorium:** There is a slight increase in tantalum concentrations within the Kupferschiefer compared to the Weissliegend (Figures 4.135 and 4.136); this signal is more clear in the Lubin and Rudna samples than the Sangerhausen samples. Most of the sample concentrations are below the NASC Ta levels, with the exception of a few that reach up to 1.5 times the NASC in the Sangerhausen samples, and up to 1.2 times the average in the Lubin mining district samples. Similarly, thorium concentrations in the samples are mostly below NASC levels. There is no clear pattern within the Sangerhausen samples, but the Lubin mining district samples appear to have higher Th levels within the Kupferschiefer compared to the Weissliegend. The highest Th concentration in the Sangerhausen samples is 1.4 times the NASC; in the Lubin and Rudna samples, the highest Th concentration reaches approximately the same value as the NASC.

Table 4.9: Geochemical data for Sangerhausen Basin samples, trace elements. "b.d.l." = below detection limit. Data in the following graphs are normalized to the North American Shale Composite data listed.

| Sangerhausen Basin | Analyte Symbol | Sc | Cr | Co | As | Rb | Sr | Zr | Sb | Cs | Ba | Hf | Ta | Th |
|---|---|---|---|---|---|---|---|---|---|---|---|---|---|---|
| | Unit Symbol | ppm | ppm | ppm | ppm | ppm | ppm | ppm | ppm | ppm | ppm | ppm | ppm | ppm |
| | Detection Limit | 1 | 20 | 1 | 5 | 2 | 2 | 4 | 0.5 | 0.5 | 3 | 0.2 | 0.1 | 0.1 |
| | Analysis Method | FUS-ICP | FUS-MS | FUS-MS | FUS-MS | FUS-MS | FUS-ICP | FUS-ICP | FUS-MS | FUS-MS | FUS-ICP | FUS-MS | FUS-MS | FUS-MS |
| | NASC | 14.9 | 124.5 | 25.7 | 28.4 | 125 | 142 | 200 | 2.09 | 5.16 | 636 | 6.3 | 1.12 | 12.3 |
| | Sample Number | | | | | | | | | | | | | |
| Wettelrode | K2+26 | 10 | 120 | 166 | 28 | 99 | 914 | 154 | 3.9 | 13.6 | 11190 | 4.3 | 1 | 12.3 |
| | K05+14 | 10 | 110 | 218 | 71 | 122 | 1181 | 157 | 0.9 | 18.3 | 28390 | 4.3 | 1.2 | 10.5 |
| | K6+10 | 10 | 140 | 991 | 964 | 116 | 401 | 80 | 45.9 | 15.7 | 10270 | 3.2 | 0.8 | 11.4 |
| | K7+8 | 12 | 140 | 1150 | 395 | 123 | 122 | 154 | 95.1 | 19.9 | 335 | 3.6 | 0.9 | 13.3 |
| | K8-0 | 11 | 140 | 1020 | 330 | 114 | 228 | 146 | 80.1 | 18.1 | 5054 | 3.5 | 0.9 | 10.5 |
| | K9-4 | 5 | 30 | 161 | 22 | 44 | 97 | 114 | 47.7 | 2.9 | 961 | 3.2 | 0.4 | 8 |
| | K10-13 | 3 | b.d.l. | 16 | 9 | 26 | 175 | 132 | 3.8 | 2.3 | 5165 | 3.6 | 0.4 | 5.1 |
| | K11-21 | 4 | b.d.l. | 8 | b.d.l. | 32 | 157 | 123 | 0.9 | 2.9 | 5152 | 3.3 | 0.4 | 7.5 |
| | K15-50 | 2 | b.d.l. | 10 | 6 | 22 | 145 | 102 | 3 | 2.1 | 3494 | 2.9 | 0.4 | 7.2 |
| SGH133 | K32+62 | 10 | 50 | 2 | b.d.l. | 129 | 188 | 142 | b.d.l. | 19.8 | 214 | 4.6 | 1 | 16.5 |
| | K29+50 | 8 | 50 | 3 | 35 | 107 | 206 | 132 | b.d.l. | 15.7 | 159 | 3.4 | 0.7 | 11.7 |
| | K22+25 | 12 | 100 | 31 | 20 | 168 | 155 | 190 | 1.8 | 25.7 | 321 | 5.9 | 1.2 | 17.7 |
| | K21+17 | 12 | 140 | 37 | 28 | 184 | 174 | 187 | 1.6 | 24.9 | 307 | 4.9 | 1.3 | 11.9 |
| | K20+8 | 8 | 140 | 84 | 98 | 114 | 209 | 119 | 12 | 16.6 | 180 | 3.9 | 0.9 | 12.8 |
| | K19+3 | 11 | 200 | 260 | 313 | 163 | 150 | 138 | 37.1 | 24.8 | 220 | 4.5 | 1.1 | 15.5 |
| | K17-6 | 3 | b.d.l. | 13 | 31 | 71 | 199 | 205 | 19.1 | 4.6 | 395 | 5.7 | 0.5 | 11.8 |
| SGH132 | K43+42 | 7 | 50 | 12 | 57 | 98 | 193 | 120 | b.d.l. | 13.7 | 191 | 3.5 | 0.7 | 9.4 |
| | K41+22 | 10 | 70 | 172 | 88 | 126 | 181 | 191 | 10.7 | 18.8 | 198 | 5.8 | 1 | 11.2 |
| | K40+8 | 12 | 120 | 267 | 126 | 151 | 195 | 192 | 17.4 | 22.2 | 242 | 5.3 | 1.2 | 12 |
| | K39+1 | 14 | 260 | 490 | 788 | 191 | 151 | 241 | 7.9 | 27.1 | 443 | 6.7 | 1.7 | 17.6 |
| | K38-12 | 4 | b.d.l. | 38 | 39 | 49 | 82 | 185 | 11.1 | 3.9 | 251 | 5.4 | 0.4 | 6.4 |
| | K35-55 | 3 | b.d.l. | 4 | b.d.l. | 53 | 178 | 159 | b.d.l. | 3.9 | 2640 | 4.7 | 0.4 | 6.3 |
| | K34-68 | 3 | b.d.l. | 49 | 42 | 115 | 115 | 208 | 3.8 | 5 | 562 | 5.7 | 0.5 | 6.6 |
| E-27 | K54+31 | 11 | 90 | 83 | 32 | 137 | 322 | 207 | 4.9 | 19 | 1593 | 6.6 | 1.3 | 13 |
| | K53+20 | 9 | 90 | 155 | 112 | 116 | 291 | 126 | 5.2 | 16.1 | 501 | 3.6 | 0.8 | 11.1 |
| | K52+7 | 9 | 130 | 671 | 693 | 106 | 170 | 370 | 19.6 | 15.2 | 212 | 3.9 | 0.8 | 9.4 |
| | K51-4 | 4 | 30 | 167 | 1070 | 50 | 214 | 245 | 106 | 4.7 | 2743 | 7 | 0.4 | 6.7 |
| | K50-16 | 2 | b.d.l. | b.d.l. | b.d.l. | 32 | 180 | 123 | b.d.l. | 3 | 2368 | 3.6 | 0.3 | 5 |
| | K49-27 | 3 | b.d.l. | 1 | b.d.l. | 46 | 91 | 316 | b.d.l. | 4.8 | 341 | 8.7 | 0.5 | 8.3 |
| | K48-36 | 3 | b.d.l. | 2 | b.d.l. | 47 | 96 | 162 | b.d.l. | 4.6 | 298 | 4.8 | 0.5 | 8.4 |
| SGH103 | K61+31 | 11 | 70 | 35 | 241 | 164 | 194 | 178 | 2.2 | 18.2 | 231 | 5.2 | 1 | 10.7 |
| | K60+19 | 11 | 130 | 94 | 225 | 160 | 191 | 170 | 6.2 | 26.3 | 244 | 5.1 | 1.1 | 12.2 |
| | K59+7 | 11 | 120 | 544 | 589 | 116 | 155 | 146 | 9.8 | 17.9 | 168 | 3.6 | 0.8 | 8.7 |
| | K58-5 | 4 | 20 | 13 | 20 | 80 | 129 | 207 | 10.2 | 4.7 | 362 | 5.9 | 0.5 | 7 |
| | K57-16 | 6 | 50 | 4 | b.d.l. | 124 | 128 | 410 | b.d.l. | 10.7 | 366 | 11.6 | 0.9 | 13.8 |
| | K56-28 | 7 | 50 | 5 | b.d.l. | 127 | 113 | 358 | b.d.l. | 11.9 | 394 | 10.7 | 1 | 14.8 |

Table 4.10: Geochemical data for Lubin mining district samples, trace elements. "b.d.l." = below detection limit. Data in the following graphs are normalized to the North American Shale Composite data listed.

| Lubin Mining District | Analyte Symbol | Sc | Cr | Co | As | Rb | Sr | Zr | Sb | Cs | Ba | Hf | Ta | Th |
|---|---|---|---|---|---|---|---|---|---|---|---|---|---|---|
| | Unit Symbol | ppm | ppm | ppm | ppm | ppm | ppm | ppm | ppm | ppm | ppm | ppm | ppm | ppm |
| | Detection Limit | 1 | 20 | 1 | 5 | 2 | 2 | 4 | 0.5 | 0.5 | 3 | 0.2 | 0.1 | 0.1 |
| | Analysis Method | FUS-ICP | FUS-MS | FUS-MS | FUS-MS | FUS-MS | FUS-ICP | FUS-ICP | FUS-MS | FUS-MS | FUS-ICP | FUS-MS | FUS-MS | FUS-MS |
| | NASC | 14.9 | 124.5 | 25.7 | 28.4 | 125 | 142 | 200 | 2.09 | 5.16 | 636 | 6.3 | 1.12 | 12.3 |
| | Sample Number | | | | | | | | | | | | | |
| Rudna 1 | K63+40 | 9 | 200 | 19 | 8 | 114 | 122 | 95 | 0.5 | 25.5 | 169 | 2.7 | 0.7 | 7 |
| | K65+20 | 9 | 130 | 239 | 300 | 131 | 62 | 81 | 2.1 | 40.1 | 166 | 2.3 | 0.8 | 6.6 |
| | K67+10 | 14 | 210 | 625 | 383 | 150 | 795 | 125 | 7.3 | 43.7 | 507 | 2.9 | 1 | 7.9 |
| | K66-0 | 11 | 200 | 1190 | 1100 | 122 | 534 | 162 | 4.7 | 31.4 | 372 | 3.5 | 0.8 | 8.1 |
| | K68-10 | 4 | 40 | 159 | 1040 | 76 | 60 | 192 | 1.4 | 7.1 | 198 | 5.1 | 0.5 | 5.5 |
| | K69-25 | 2 | b.d.l. | 10 | 15 | 47 | 66 | 76 | b.d.l. | 3.4 | 268 | 2 | 0.2 | 1.8 |
| | K70-130 | 2 | b.d.l. | 7 | 6 | 52 | 60 | 87 | b.d.l. | 3.7 | 270 | 2.3 | 0.2 | 2.1 |
| Rudna 2 | K76+20 | 12 | 290 | 129 | 84 | 194 | 88 | 143 | 1.8 | 51.8 | 236 | 4.3 | 1.3 | 10.6 |
| Lubin 1 | K84+110 | 9 | 70 | 24 | 35 | 95 | 169 | 128 | 0.8 | 15.2 | 612 | 3.9 | 0.8 | 7.9 |
| | K88+40 | 12 | 160 | 90 | 177 | 164 | 178 | 93 | b.d.l. | 38 | 237 | 2.7 | 0.9 | 8.7 |
| | K89+20 | 12 | 160 | 172 | 43 | 153 | 167 | 94 | b.d.l. | 31.9 | 253 | 2.8 | 1 | 8.7 |
| | K91+0 | 14 | 170 | 251 | 1190 | 162 | 149 | 94 | 0.6 | 40.4 | 182 | 2.6 | 0.9 | 8.2 |
| | K92-10 | 2 | b.d.l. | 23 | 69 | 26 | 69 | 67 | b.d.l. | 2 | 316 | 1.9 | 0.1 | 1.8 |
| | K93-20 | 3 | b.d.l. | 13 | 38 | 34 | 73 | 61 | b.d.l. | 2.8 | 353 | 1.7 | 0.2 | 2.2 |
| | K94-120 | 2 | 30 | 3 | 19 | 33 | 190 | 128 | b.d.l. | 2.2 | 2407 | 3.6 | 0.2 | 2.4 |
| Lubin 2 | K105+120 | 8 | 50 | 10 | 11 | 108 | 229 | 89 | b.d.l. | 19.2 | 386 | 2.6 | 0.7 | 6.9 |
| | K104+50 | 8 | 40 | 3 | 8 | 101 | 216 | 107 | b.d.l. | 18.5 | 421 | 3.3 | 0.6 | 7.4 |
| | K103+30 | 9 | 90 | 46 | 46 | 83 | 248 | 111 | b.d.l. | 11.7 | 261 | 2.9 | 0.6 | 7 |
| | K102+25 | 15 | 160 | 211 | 178 | 171 | 209 | 135 | b.d.l. | 41.4 | 201 | 3.2 | 1.1 | 9.4 |
| | K101+20 | 16 | 200 | 243 | 260 | 205 | 518 | 149 | 0.9 | 49.6 | 353 | 2.7 | 1.2 | 10.8 |
| | K100+0 | 14 | 230 | 541 | 1210 | 174 | 429 | 134 | 0.6 | 34.3 | 244 | 3.6 | 1.1 | 12 |
| | K99-UBD | 6 | 70 | 36 | 120 | 12 | 274 | 55 | b.d.l. | b.d.l. | 57 | 1.3 | 0.2 | 2.7 |
| | K98-LBD | 4 | 20 | 6 | 76 | 7 | 218 | 39 | 2.8 | b.d.l. | 45 | 0.9 | 0.1 | 2.1 |
| | K97-5 | 4 | 30 | 23 | 332 | 31 | 131 | 77 | b.d.l. | 2.9 | 170 | 2 | 0.2 | 3.1 |
| | K96-50 | 2 | b.d.l. | 1 | 8 | 26 | 145 | 58 | b.d.l. | 1.8 | 967 | 1.5 | 0.2 | 3.3 |
| | K95-120 | 2 | 20 | 2 | 11 | 35 | 167 | 90 | b.d.l. | 2.4 | 1946 | 2.3 | 0.2 | 2.6 |

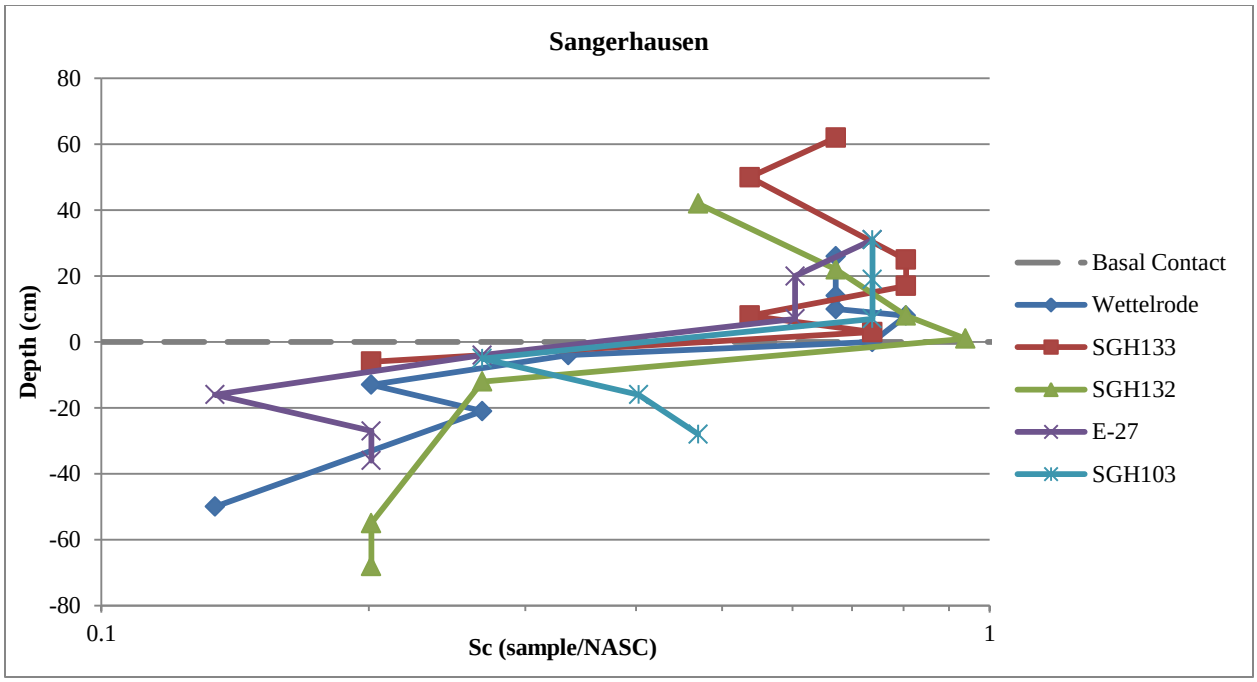


Figure 4.113: Scandium concentrations for Sangerhausen Basin samples.

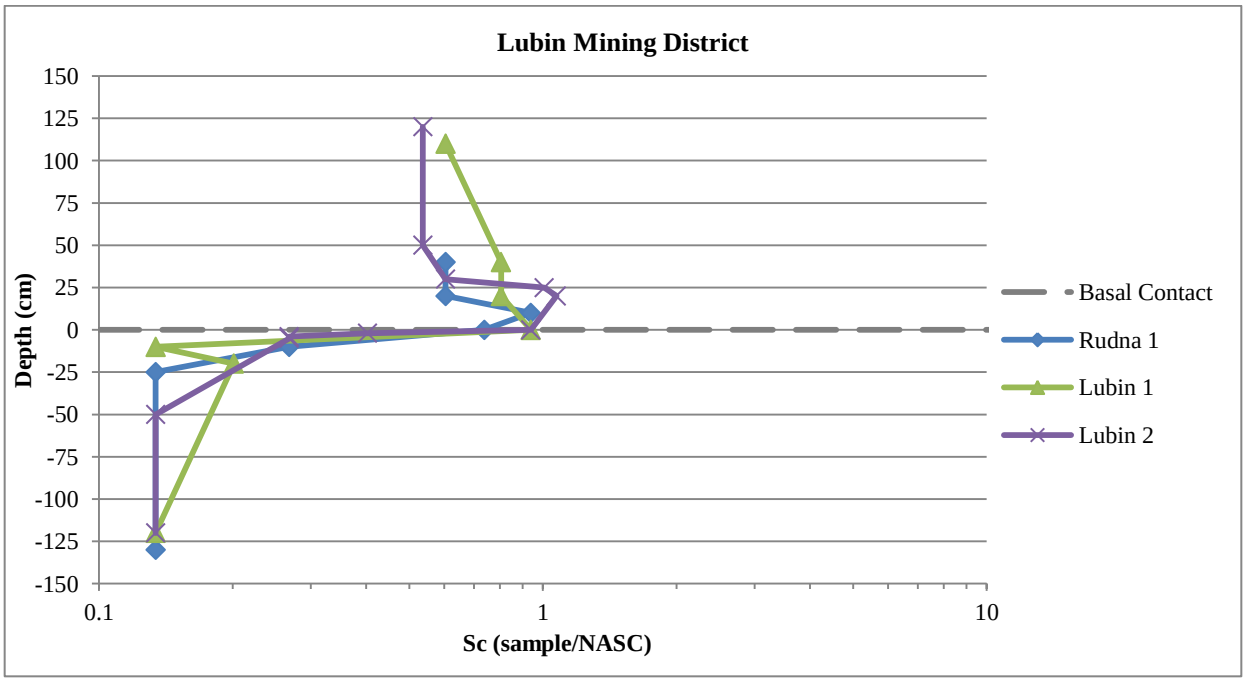


Figure 4.114: Scandium concentrations for Lubin mining district samples.

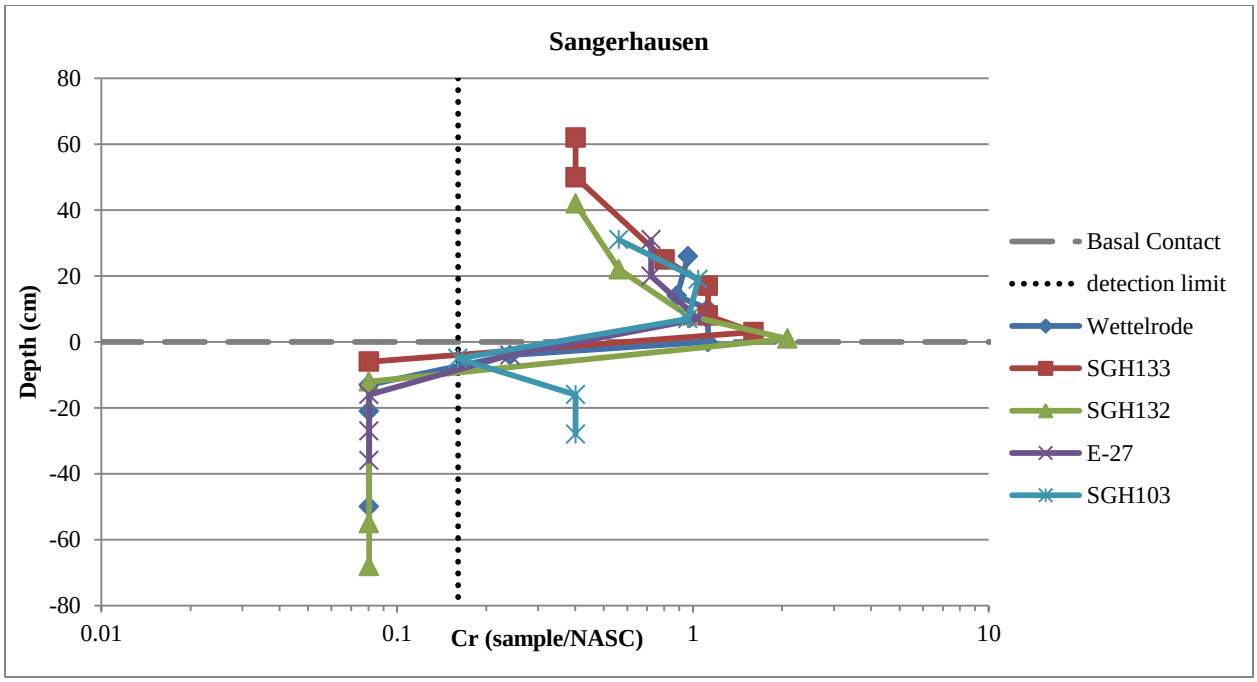


Figure 4.115: Chromium concentrations for Sangerhausen Basin samples.

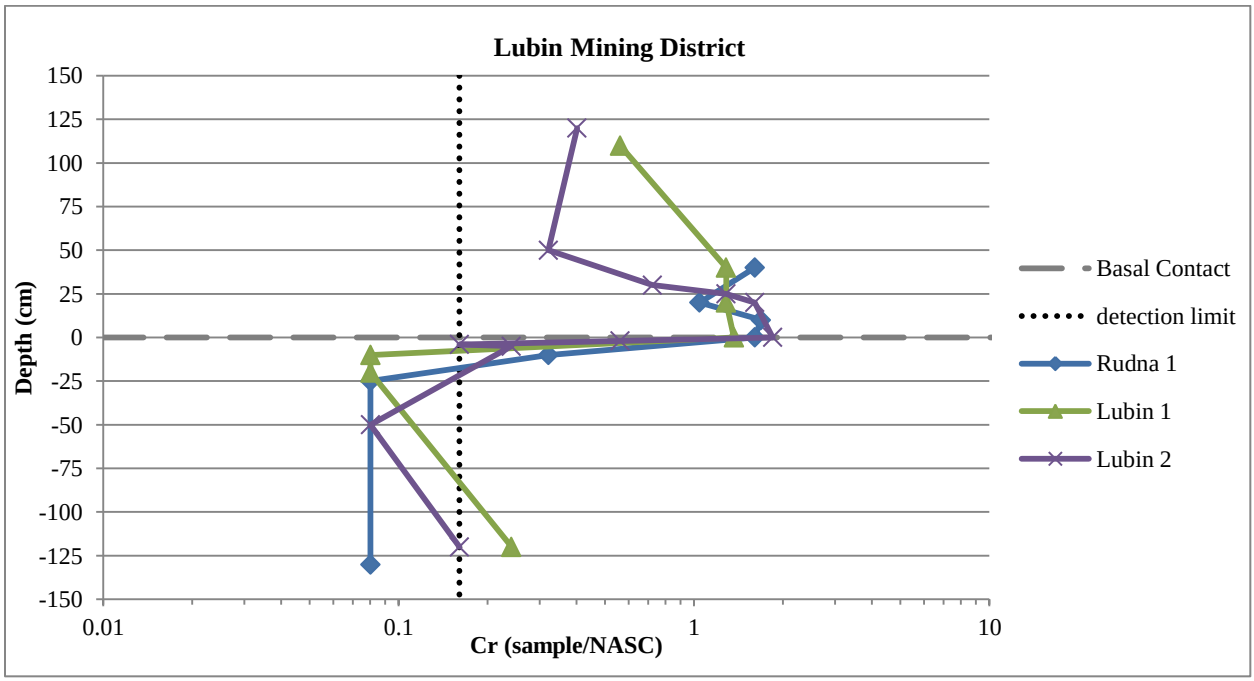


Figure 4.116: Chromium concentrations for Lubin mining district samples.

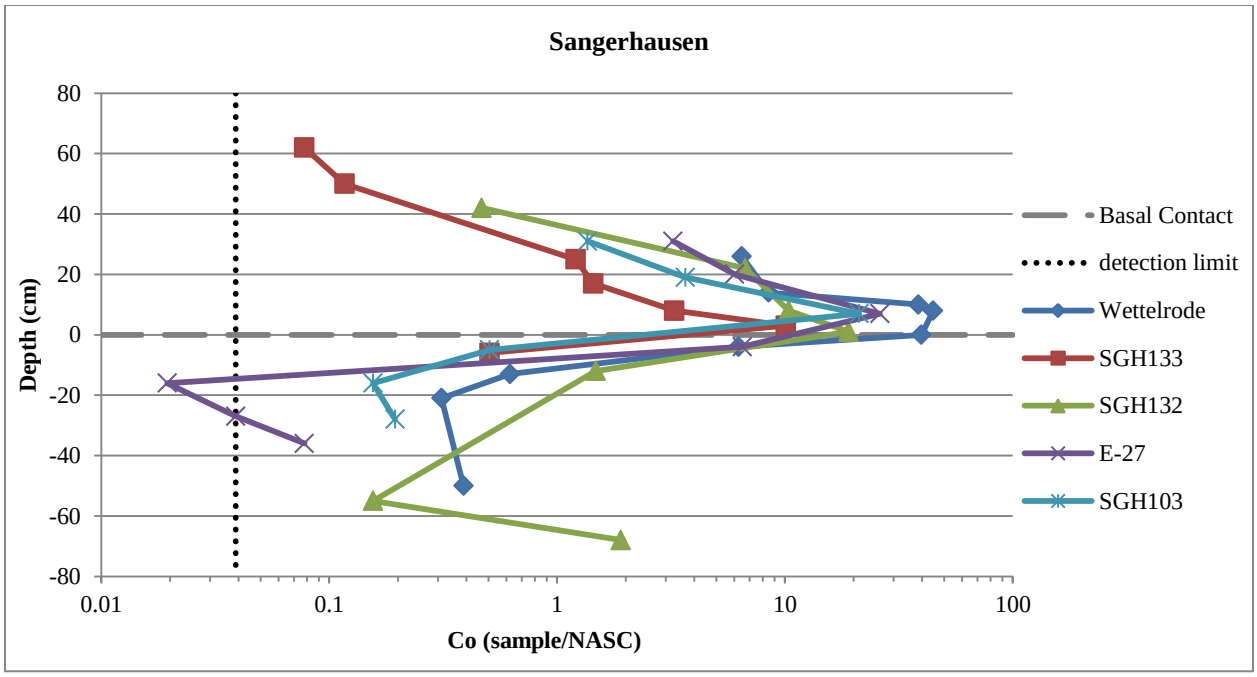


Figure 4.117: Cobalt concentrations for Sangerhausen Basin samples.

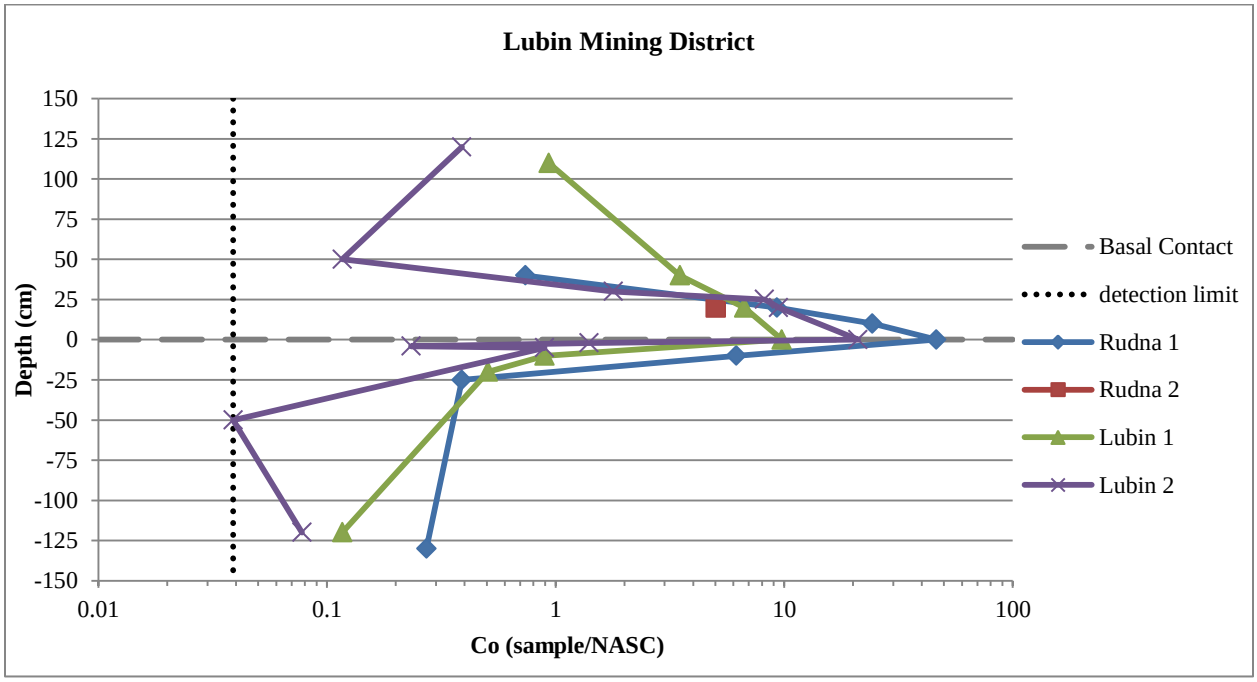


Figure 4.118: Cobalt concentrations for Lubin mining district samples.

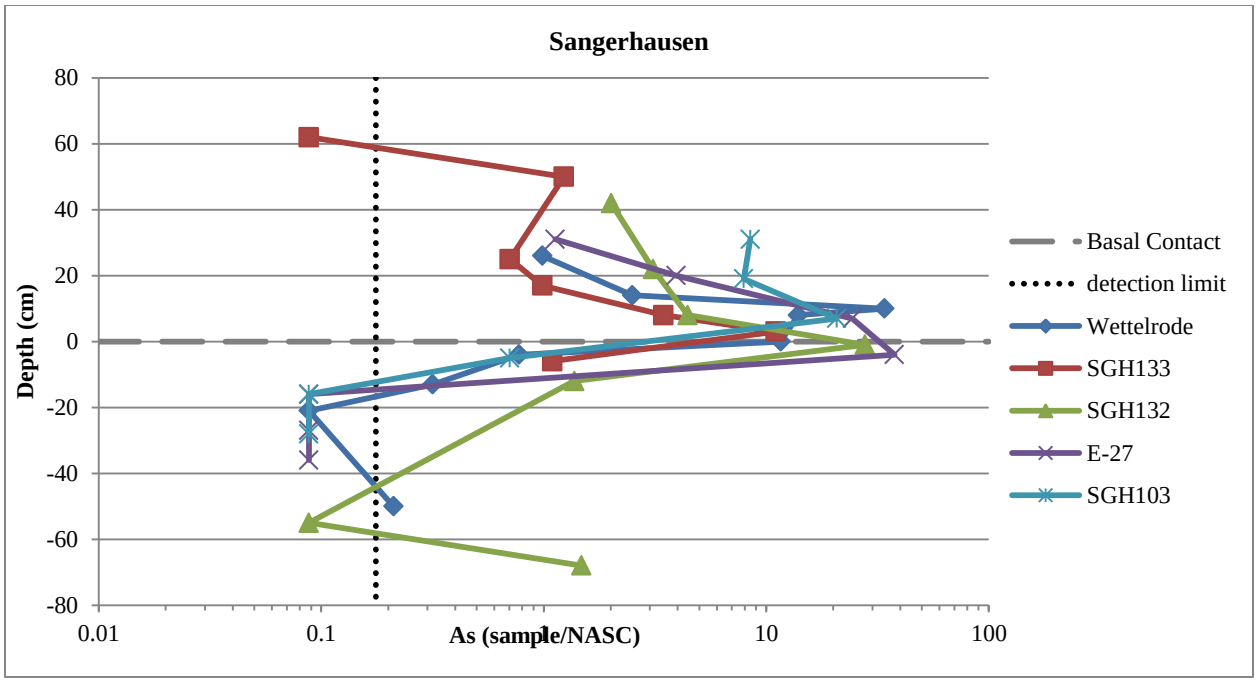


Figure 4.119: Arsenic concentrations for Sangerhausen Basin samples.

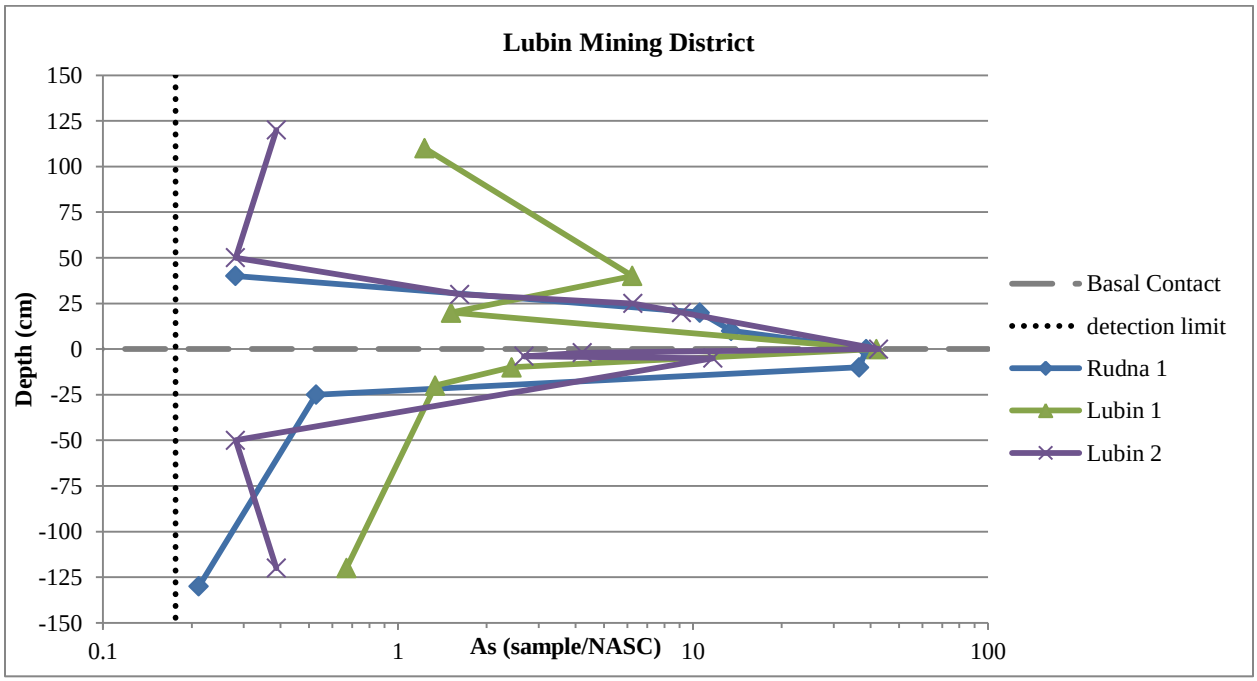


Figure 4.120: Arsenic concentrations for Lubin mining district samples.

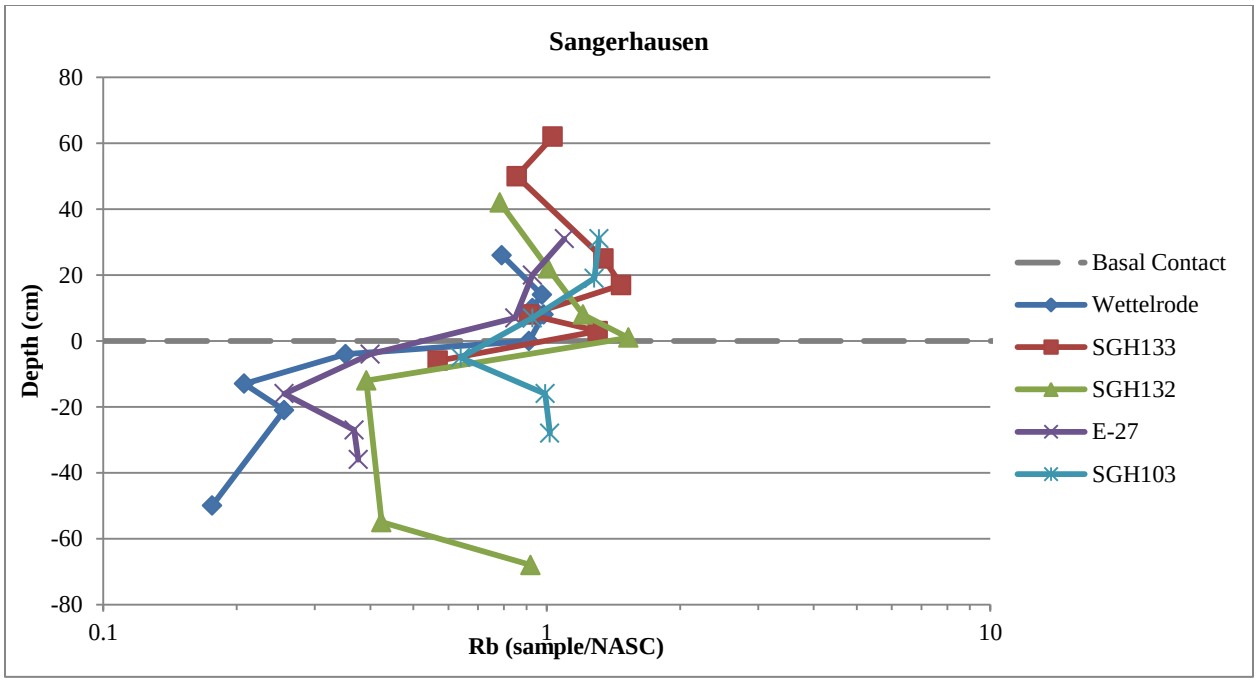


Figure 4.121: Rubidium concentrations for Sangerhausen Basin samples.

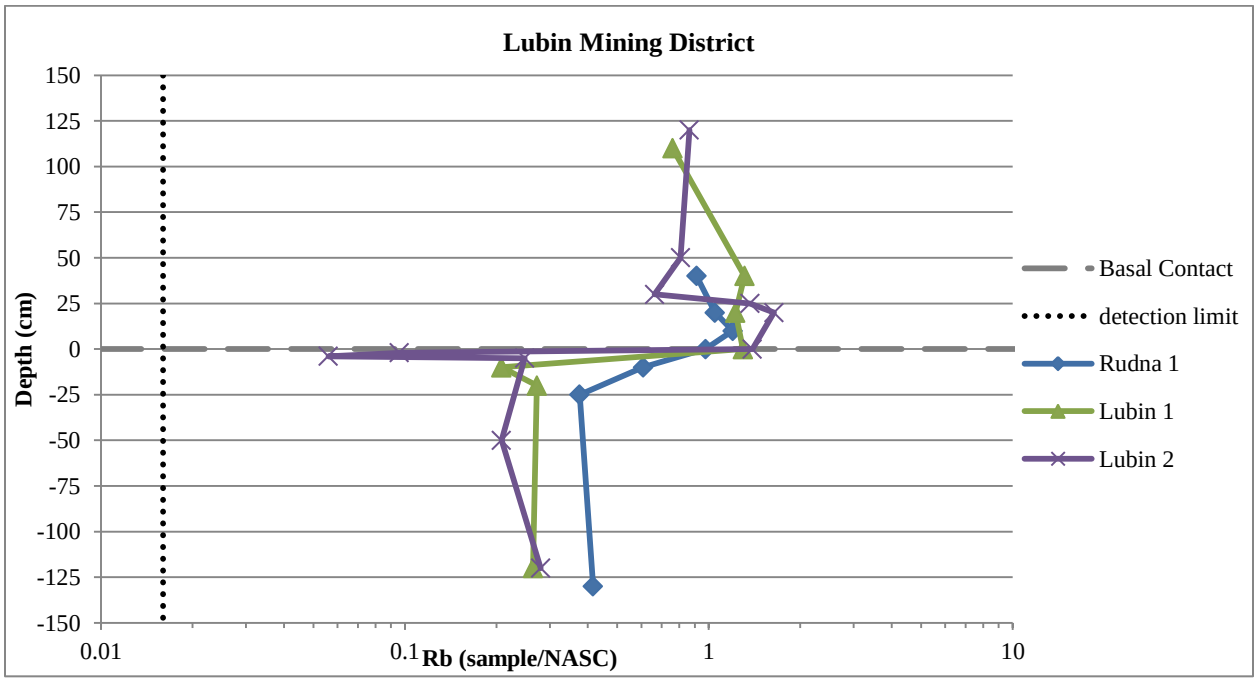


Figure 4.122: Rubidium concentrations for Lubin mining district samples.

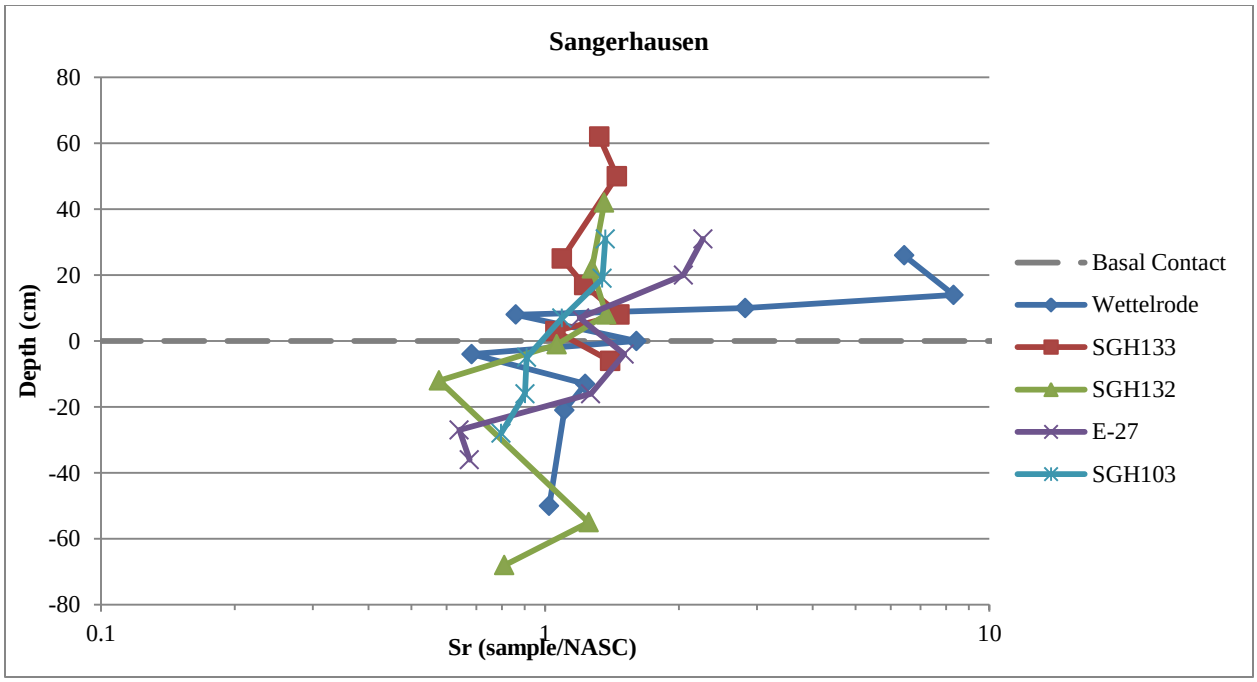


Figure 4.123: Strontium concentrations for Sangerhausen Basin samples.

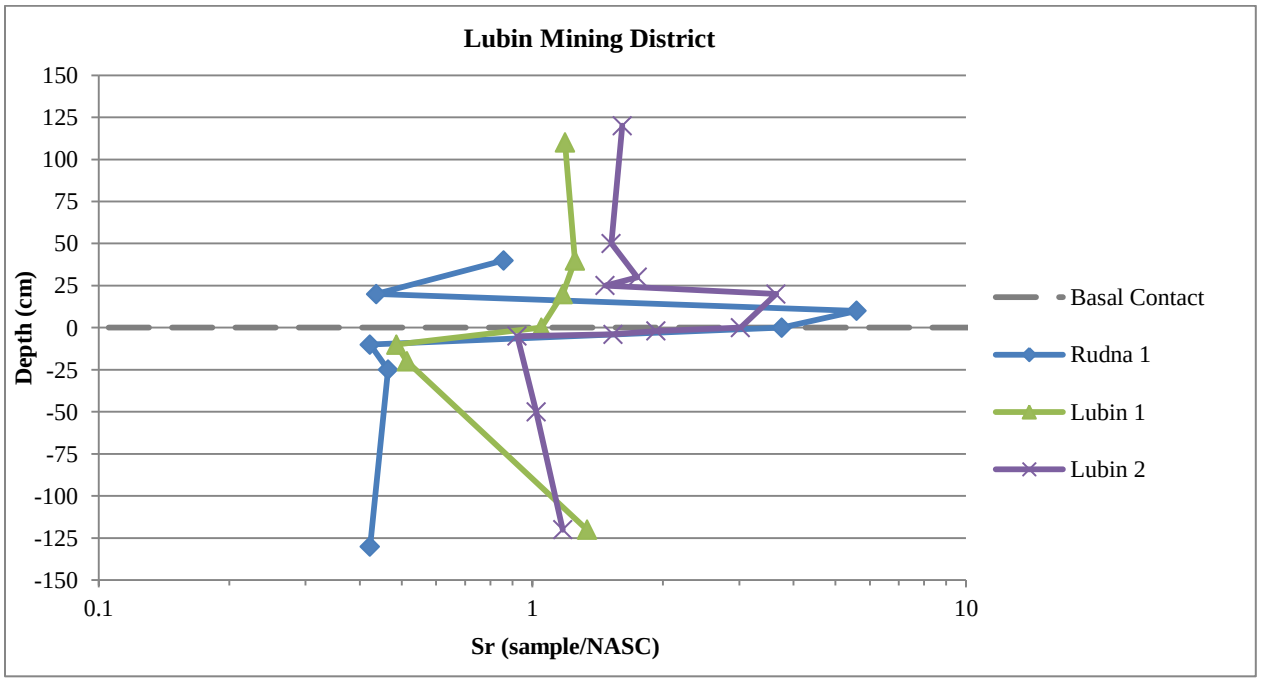


Figure 4.124: Strontium concentrations for Lubin mining district samples.

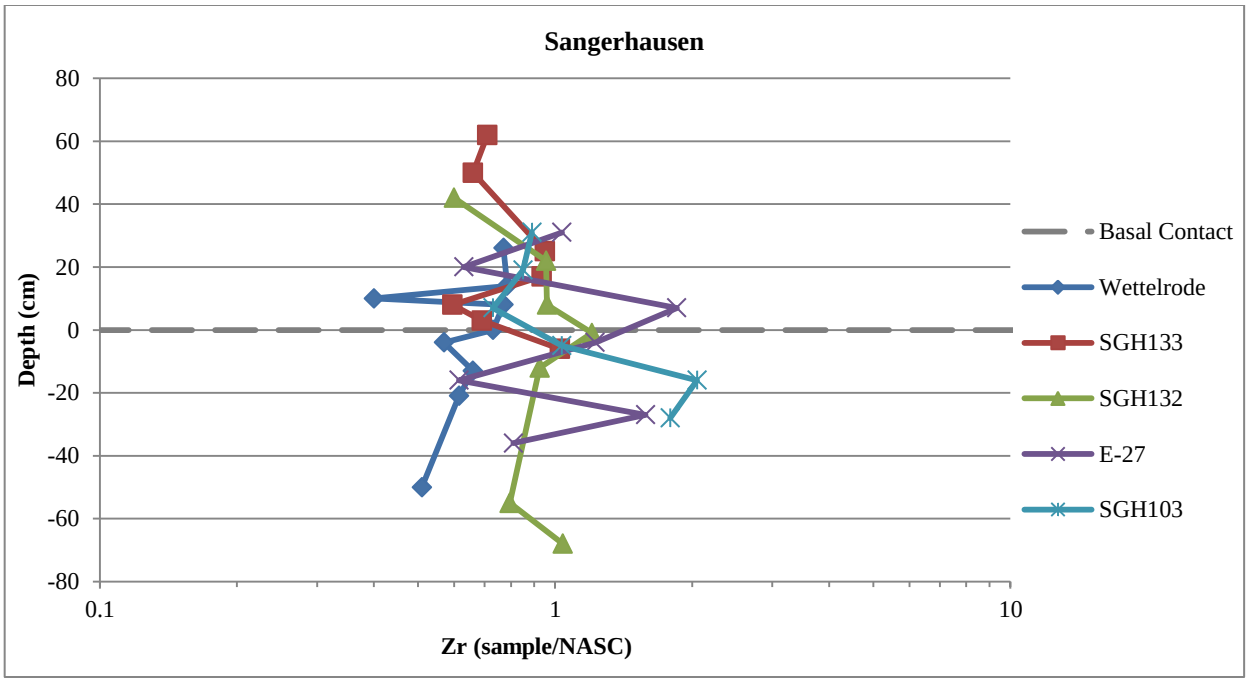


Figure 4.125: Zirconium concentrations for Sangerhausen Basin samples.

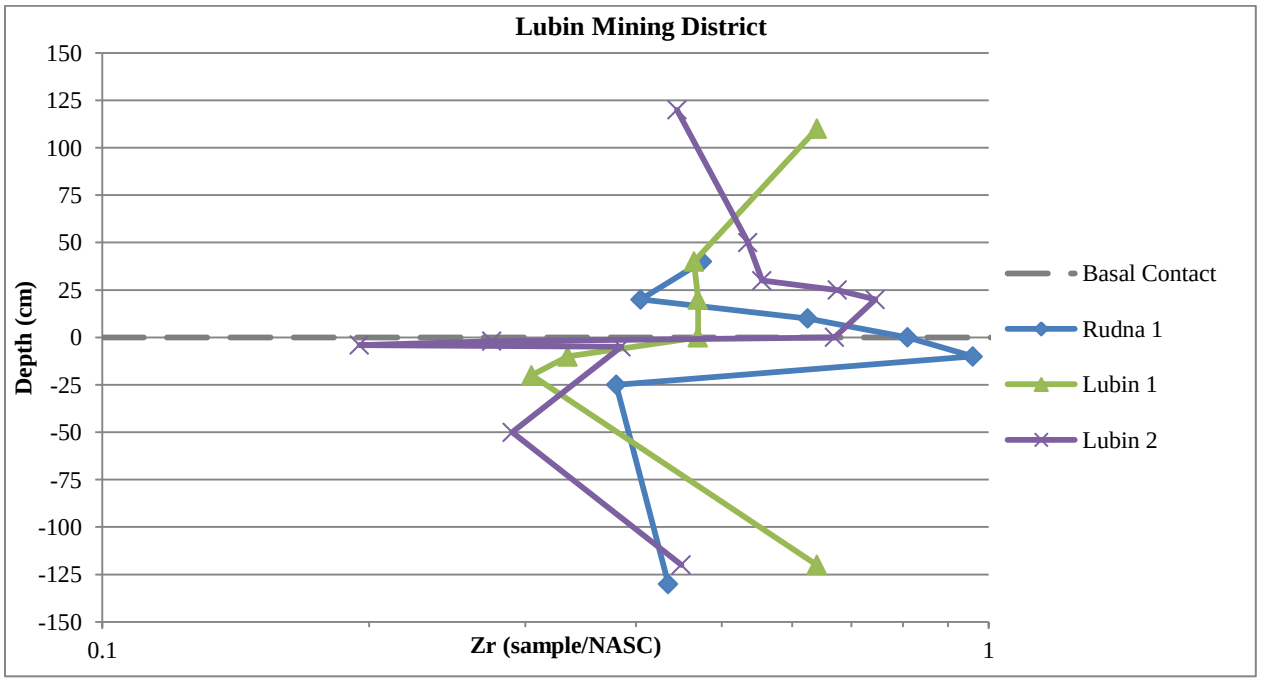


Figure 4.126: Zirconium concentrations for Lubin mining district samples.

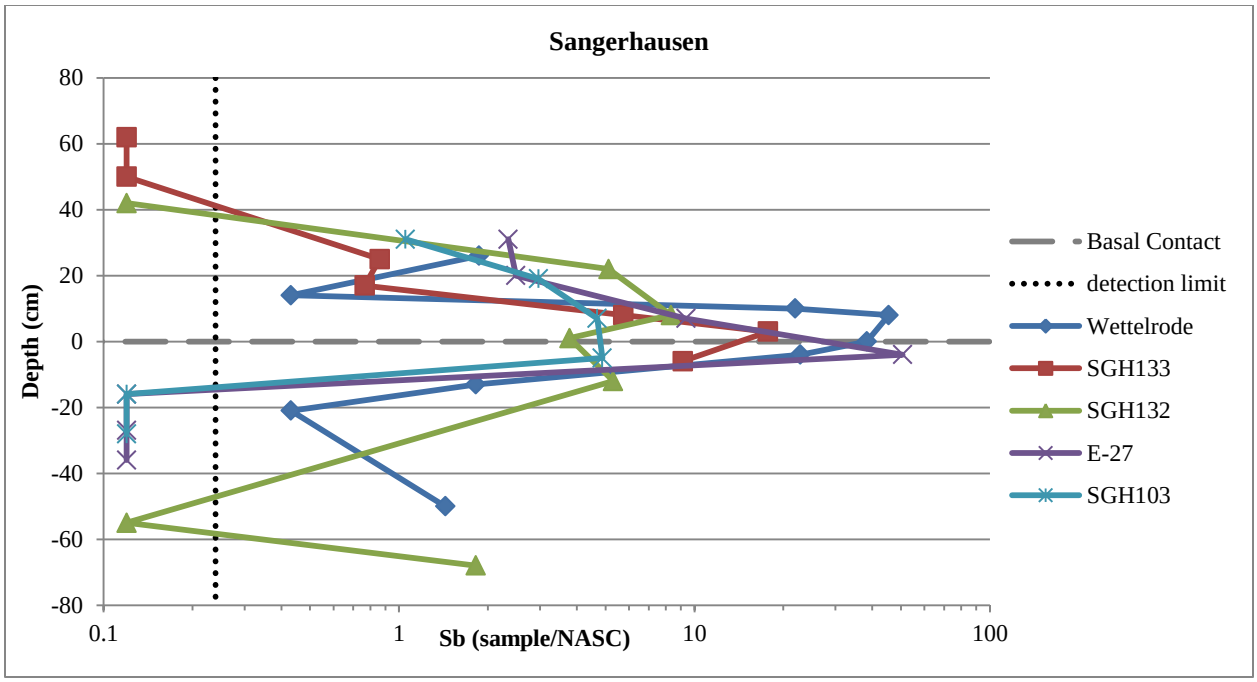


Figure 4.127: Antimony concentrations for Sangerhausen Basin samples.

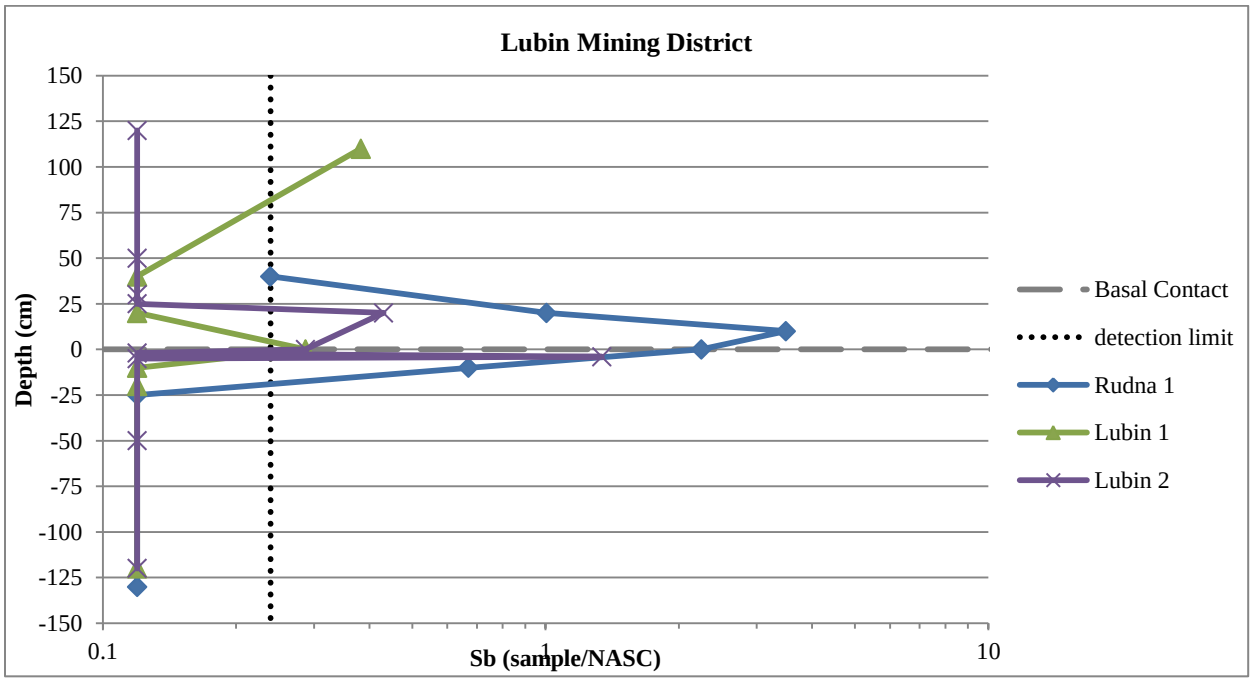


Figure 4.128: Antimony concentrations for Lubin mining district samples.

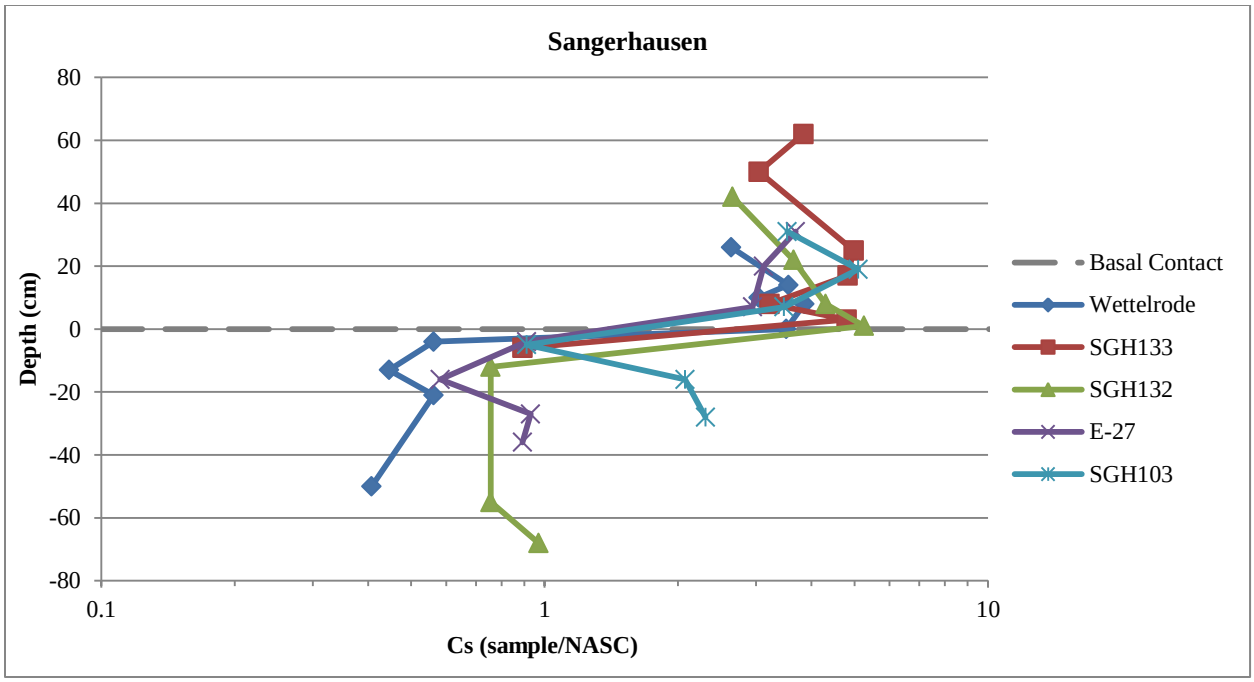


Figure 4.129: Cesium concentrations for Sangerhausen Basin samples.

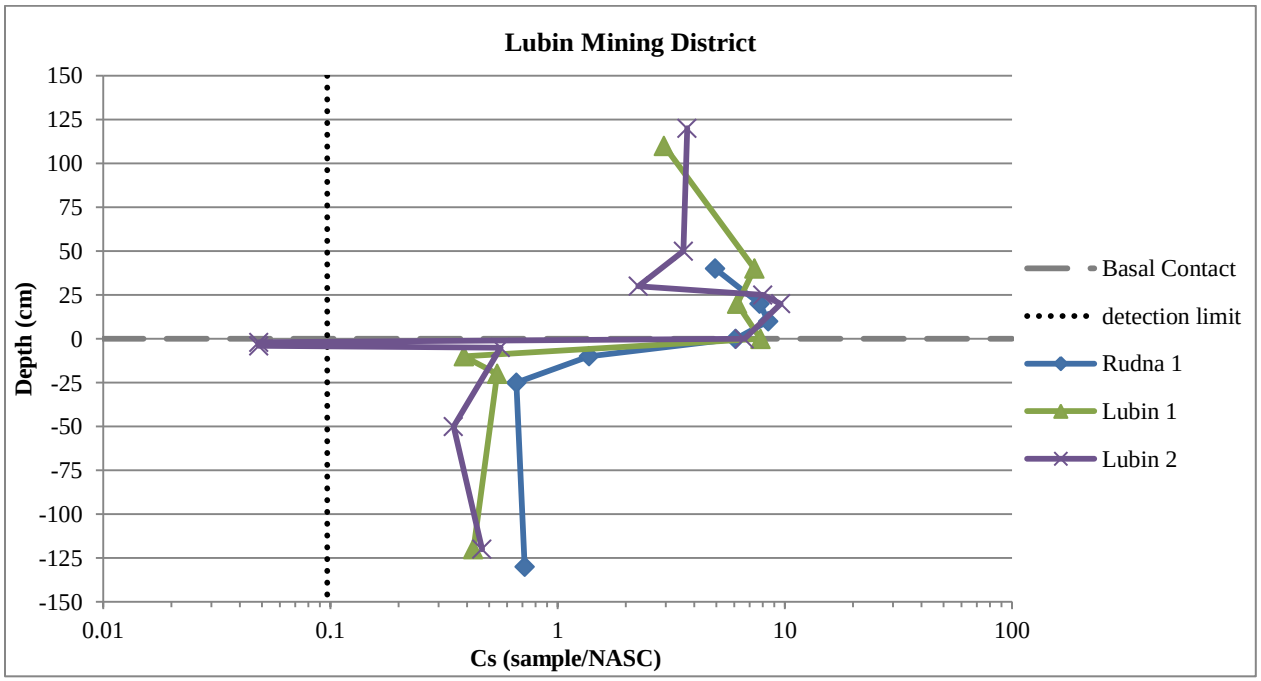


Figure 4.130: Cesium concentrations for Lubin mining district samples.

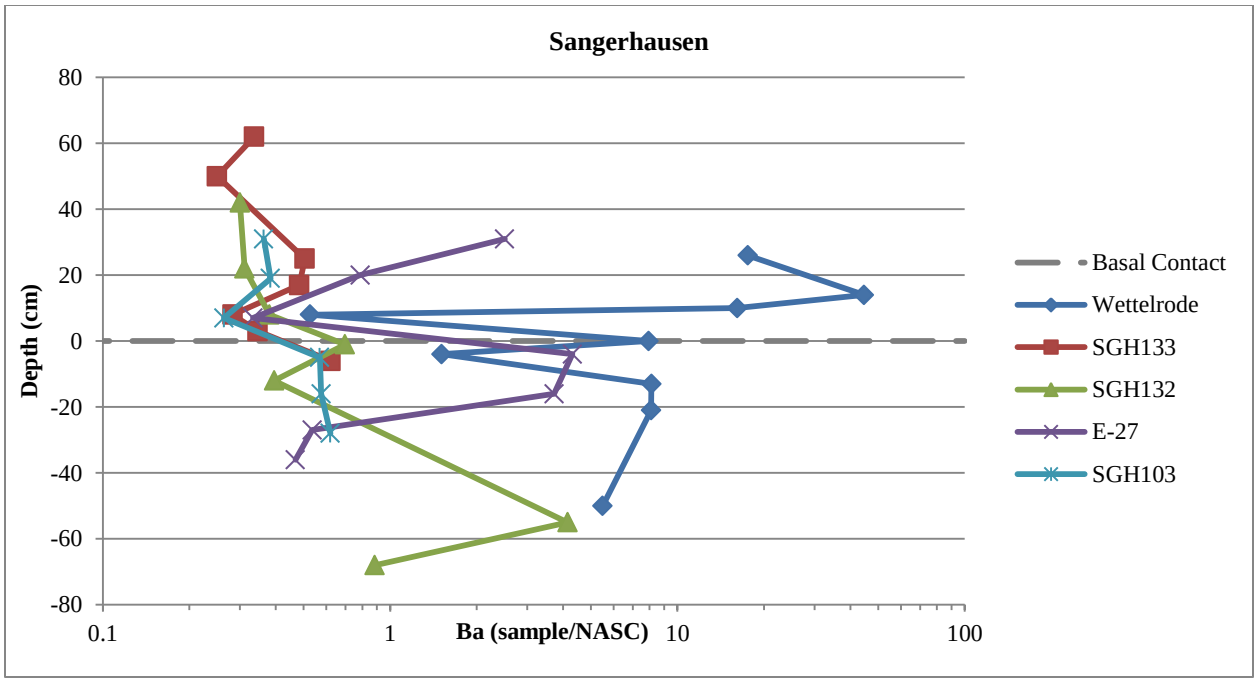


Figure 4.131: Barium concentrations for Sangerhausen Basin samples.

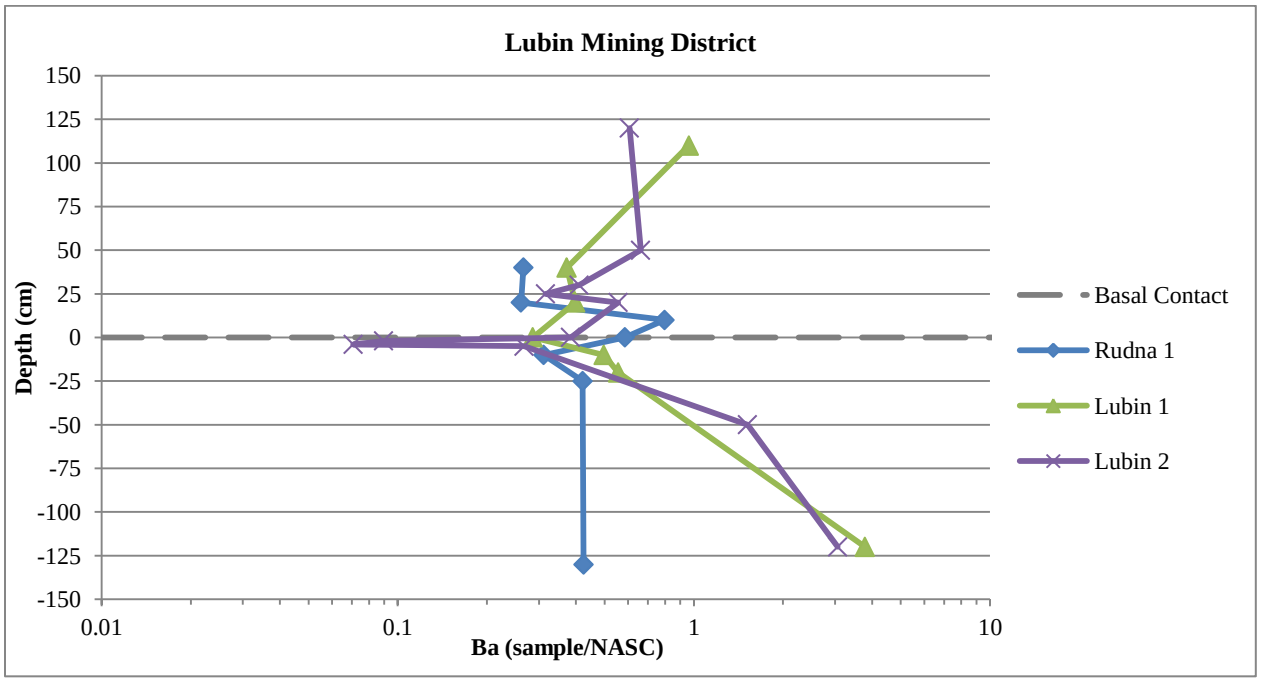


Figure 4.132: Barium concentrations for Lubin mining district samples.

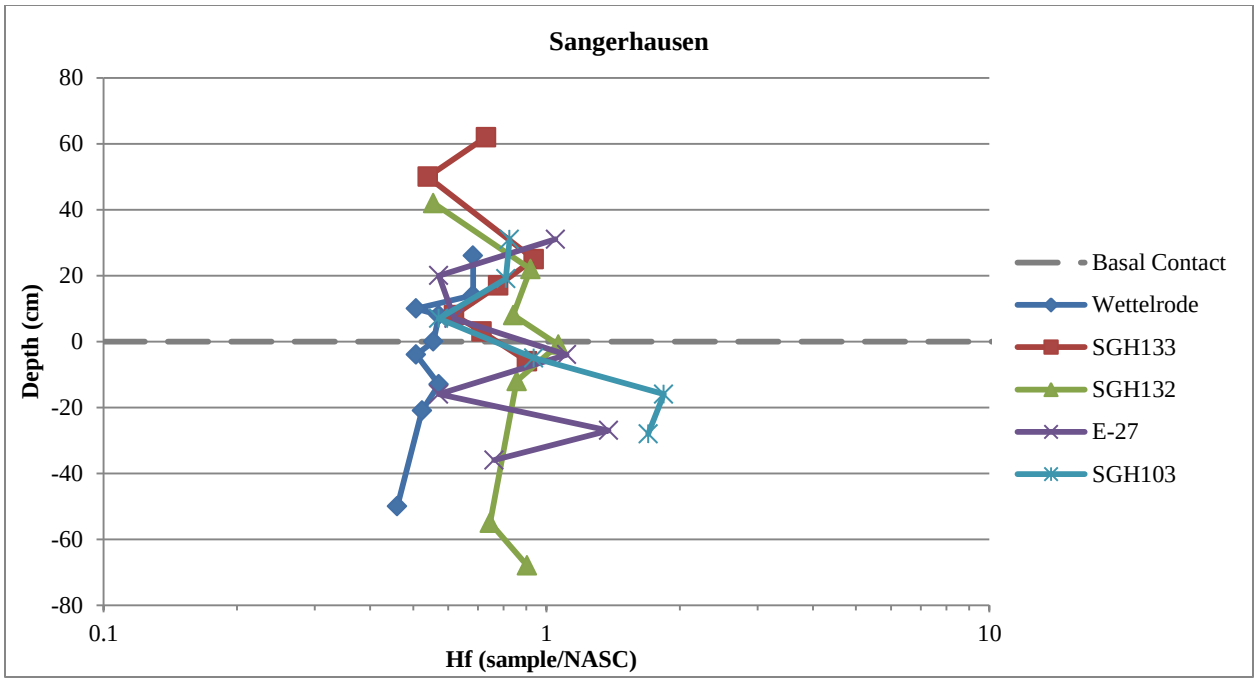


Figure 4.133: Hafnium concentrations for Sangerhausen Basin samples.

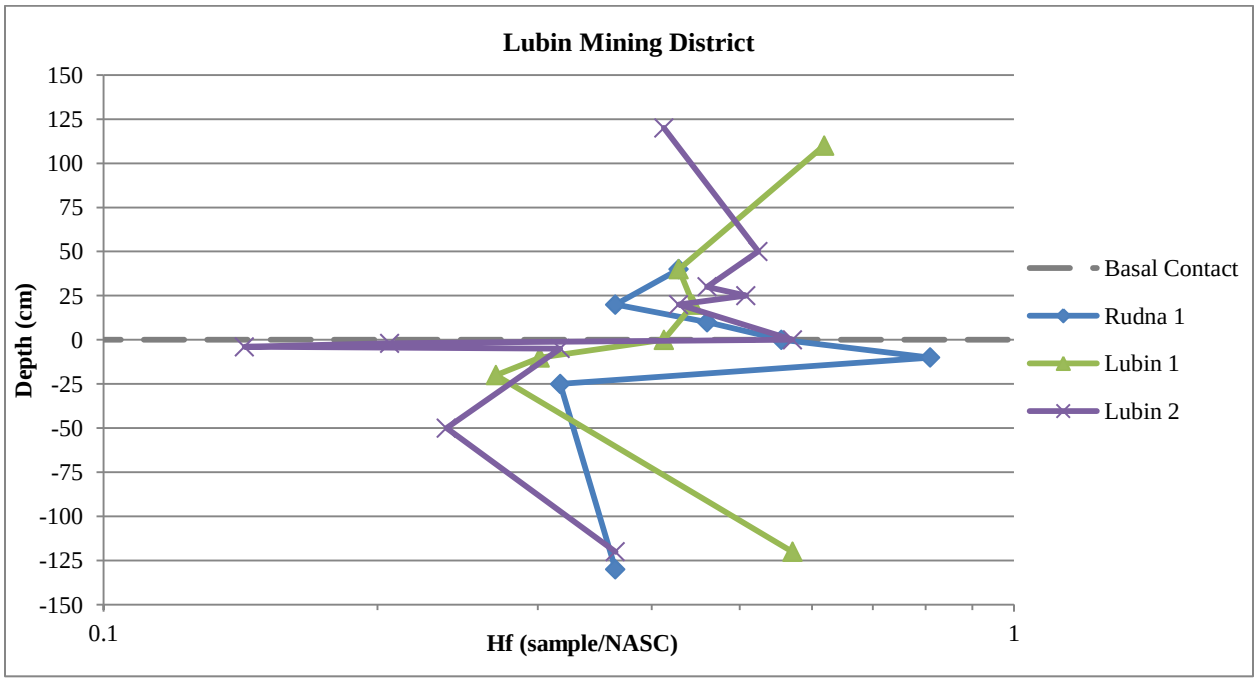


Figure 4.134: Hafnium concentrations for Lubin mining district samples.

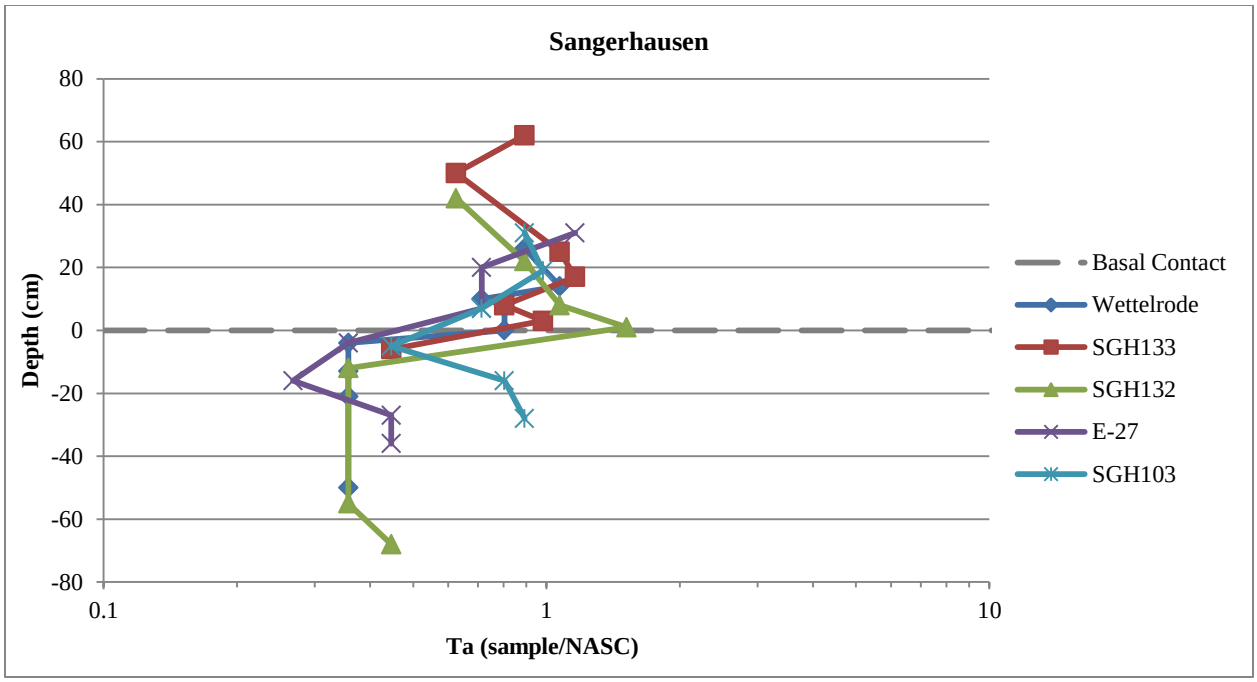


Figure 4.135: Tantalum concentrations for Sangerhausen Basin samples.

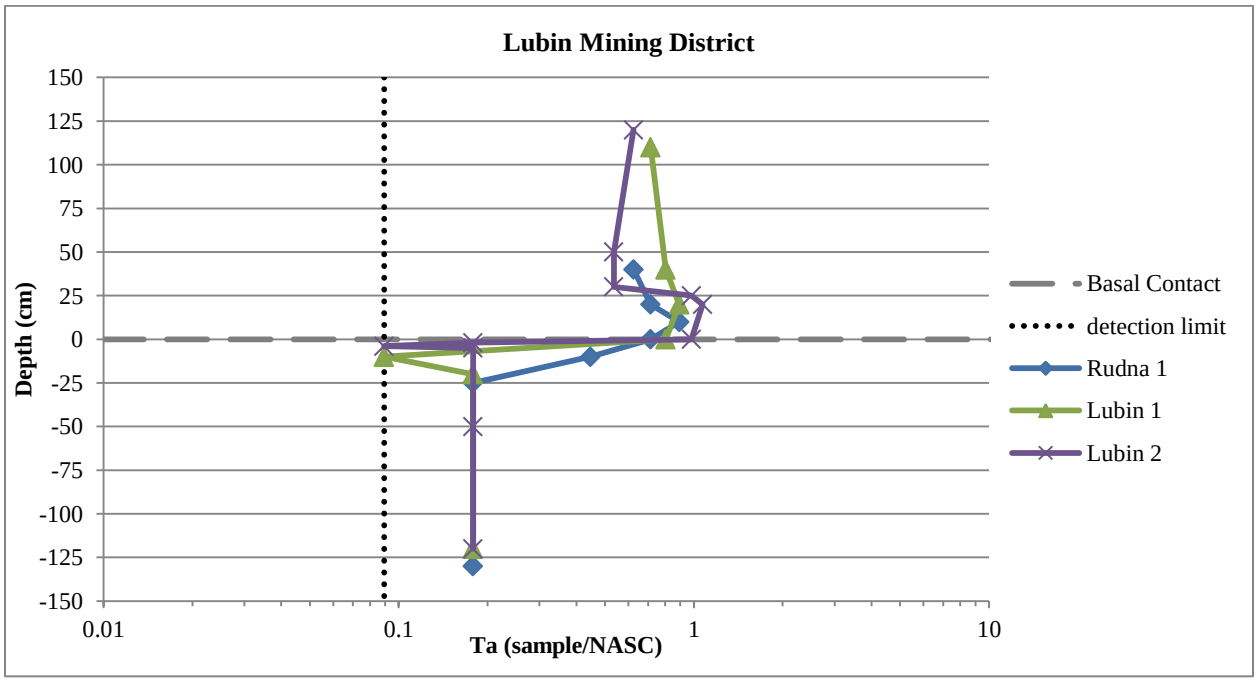


Figure 4.136: Tantalum concentrations for Lubin mining district samples.

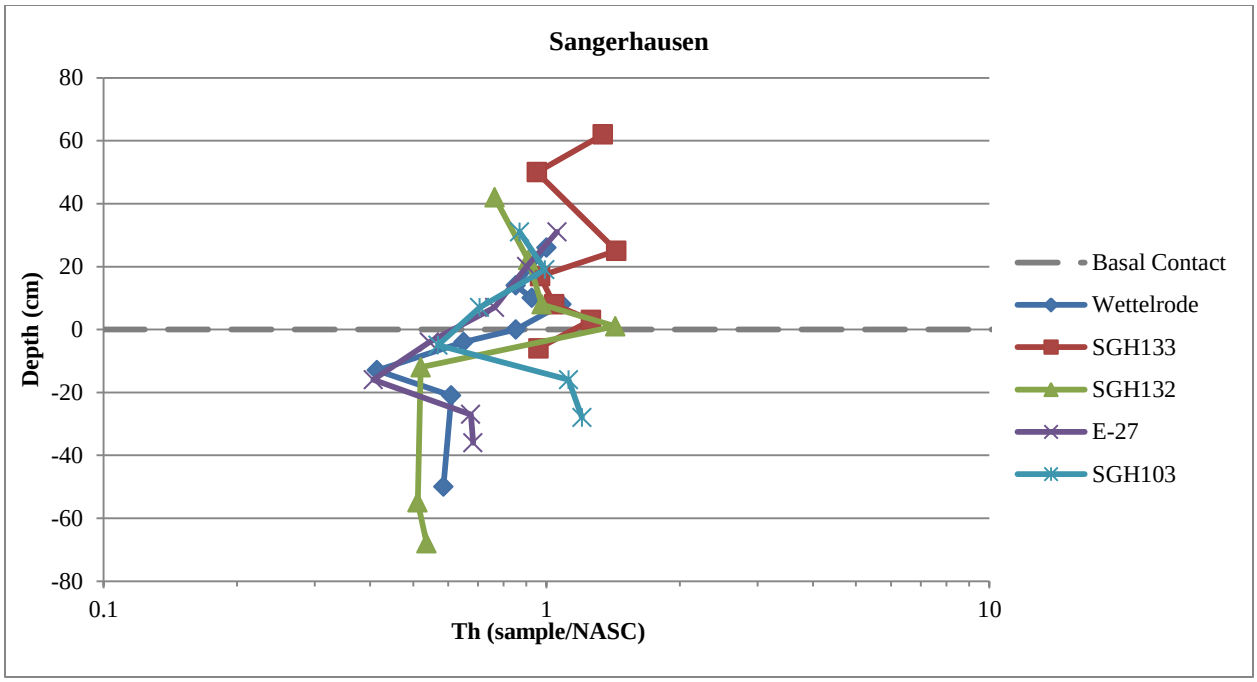


Figure 4.137: Thorium concentrations for Sangerhausen Basin samples.

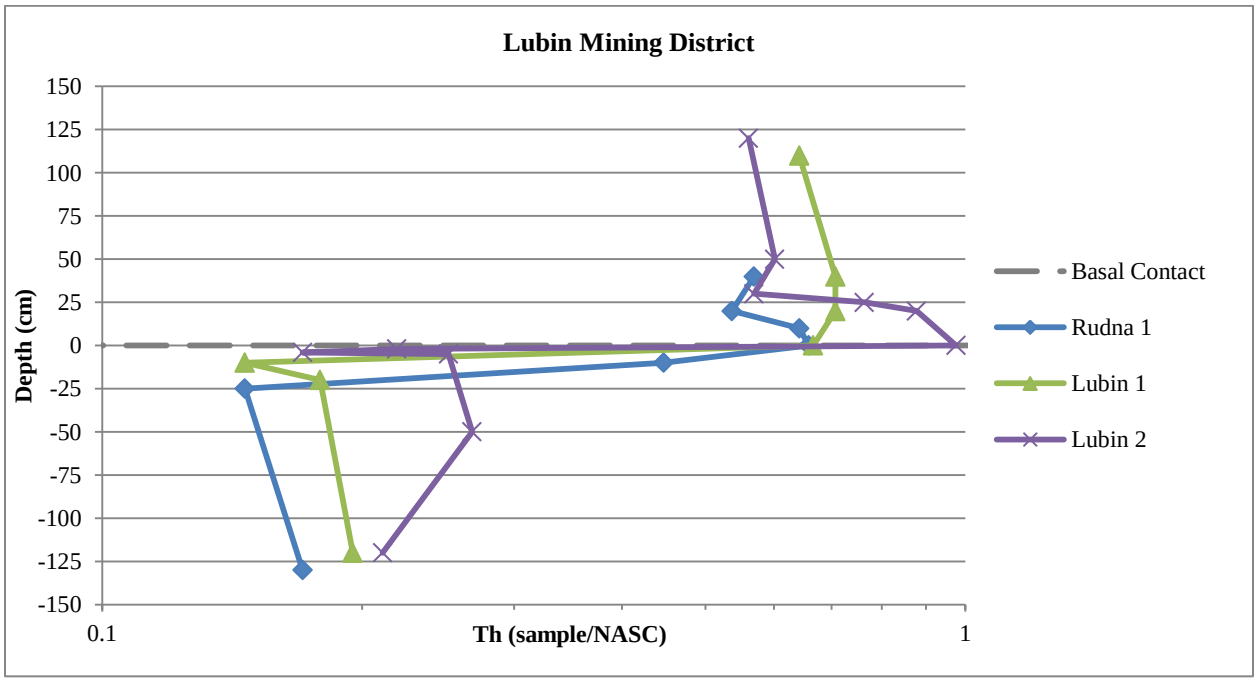


Figure 4.138: Thorium concentrations for Lubin mining district samples.

### 4.3.4 Rare Earth Elements

The rare earth elements include lanthanum (La), cerium (Ce), praseodymium (Pr), neodymium (Nd), samarium (Sm), europium (Eu), gadolinium (Gd), terbium (Tb), dysprosium (Dy), holmium (Ho), erbium (Er), thulium (Tm), ytterbium (Yb), and lutetium (Lu). For the purposes of this thesis, light rare earth elements (LREE) refer to La and Ce, middle rare earth elements (MREE) refer to Nd, Sm, Gd, and Tb, and heavy rare earth elements (HREE) refer to Dy, Ho, Er, Tm, Yb, and Lu. Europium (Eu) is excluded from the MREE sum due to its tendency of exhibiting positive and negative anomalies; this could artificially affect the sum middle rare earth elements and complicate comparisons of geochemical data. Data listed in Table 4.11 and Table 4.12.

In considering the data sources for the North American Shale Composite (NASC) and the Post Archean Average Shale (PAAS), it was decided that the PAAS would serve as a better baseline to compare the Kupferschiefer data to as opposed to the NASC. Thus the rare earth element data is normalized to the PAAS instead of the NASC, as the other trace elements were. One of the most noticeable patterns that emerges when the rare earth element data are compared to the PAAS data, is that samples from both the Sangerhausen Basin and Lubin mining district data sets show an enrichment in middle rare earth elements compared to concentrations of light and heavy REEs. This pattern is not exhibited by every sample, but where it is present, the highest levels of enrichment are found in samples taken 5 to 20 cm above the contact in the Sangerhausen , and below the contact in Weissliegend samples in the Lubin mining district.

#### 4.3.4.1 Sangerhausen Basin Patterns

**Wettelrode mine** (Figure 4.139): The strongest MREE enrichment of both Sangerhausen Basin and Lubin mining district samples is exhibited in the sample from 10 cm above the contact. Note that the samples from below the contact show slight MREE enrichment, while samples from 14, 8 and 0 cm above the contact show a relatively stronger MREE enrichment. The sample from 26 cm above the contact lacks a MREE enrichment altogether. Weissliegend samples and the sample from 28 cm above the contact exhibit lower REE values compared to the other samples.

**SGH133** (Figure 4.140): These samples do not show the same degree of MREE enrichment as found in the Wettelrode samples. The strongest MREE enrichment is found in samples from 3 and 8 cm above the contact. The other samples from above the basal contact do not show a MREE enrichment, though the pattern is found in the sample taken below the contact.

**SGH132** (Figure 4.141): The samples from above the contact show little or no MREE enrichment. The sample from 12 cm below shows the contact strongest enrichment of MREE from this location; the samples from 55 and 68 cm below the contact exhibit decreasing enrichments in MREE compared to the light and heavy rare earth elements. The sample taken 1 cm above the contact has a REE pattern such that the light and heavy elements are more enriched than the middle elements; this is the only sample from both the Sangerhausen Basin and Lubin mining district that shows an enrichment in LREE and HREE over MREE.

**E-27** (Figure 4.142): The sample taken 7 cm above the contact exhibits a strong MREE enrichment, the third highest of the Sangerhausen Basin samples, after the samples taken 10 cm above the contact in Wettelrode and 7 cm above the contact in SGH103. The samples from 20 and 31 cm above the contact do not show any enrichment of REEs. The Weissliegend samples show relatively low light REE concentration compared to middle and heavy rare earth elements, with the concentration of the middle elements slightly higher than that of the heavy elements.

**SGH103** (Figure 4.143): The sample from 7 cm above the contact shows the second greatest enrichment in MREE of the Sangerhausen samples, after the sample from 10 cm above the contact in Wettelrode. The Kupferschiefer samples from 19 and 31 cm above the contact do not exhibit an enrichment in any group of the rare earth elements over any other. The sample from 5 cm below the contact exhibits a slight MREE enrichment; the samples from 16 and 28 cm below the contact do not show any particular enrichment patterns.

#### 4.3.4.2 Lubin Mining District Patterns

The single geochemical sample from Rudna 2 has been omitted from the graphs, but the values are listed in Table 4.12 along with the other data from the Lubin mining district.

**Rudna 1** (Figure 4.144): The strongest MREE enrichment is observed in the sample taken 25 cm below the contact. The samples from 20, 10, and 0 cm above the contact, and 10 cm below the contact show an enrichment in MREE. The samples from 40 cm above the contact and 130 cm below the contact exhibit little or no MREE enrichment.

**Lubin 1** (Figure 4.145): The samples from 10 and 20 cm below the contact exhibit the strongest MREE enrichment of the Lubin mining district samples. Samples taken above the contact and 120 cm below the contact exhibit little or no MREE enrichment relative to the other rare earth elements.

**Lubin 2** (Figure 4.146): Samples from 50, 30, and 0 cm above the contact exhibit MREE enrichment, while samples from 120, 25, and 20 cm above the contact are enriched in LREE compared to the other rare earth elements. All of the Weissliegend samples from Lubin 2 exhibit some degree of MREE enrichment. The strongest enrichment is in the samples from 50 and 5 cm below the contact, followed by samples from 2 and 4 cm below the contact. The sample from 120 cm below the contact shows the weakest MREE enrichment.

#### 4.3.4.3 REEs By Depth

To better view any changes in rare earth element concentrations within each sampling location without the complication of a log scale or the disruption of Eu anomalies, the sum of middle REEs was divided by the total REE (TREE) sum and plotted by depth; this was also done for light REEs and heavy REEs. The absolute value (as opposed to PAAS-normalized value) was used for all calculations. The light/total ratio is a near mirror pattern of the middle/total ratio. In all locations, the light/total values (~0.6) are higher than the middle/total values (~0.3); the heavy/total ratio is the lowest (~0.1). PAAS-normalized Eu anomalies for each location are included in these plots.

**Sangerhausen Basin, Wettelrode**: The middle/total ratio shows the highest value at 10 cm above the contact; along with a slight increase in concentration between the contact and 20 cm below the contact, these peaks interrupt a trend that otherwise gradually decreases in middle/total value with decreasing depth (Figure 4.147). **SGH133**: The ratio of middle/total stays relatively steady in this core. There is a slight peak in the ratio value at the contact and 8 cm above it (Figure 4.148). **SGH132**: The

highest middle/total ratio values are found 12 and 55 cm below the contact (Figure 4.149). There is a decrease in the ratio value near the contact; for the three samples 8+ cm above the contact, the ratio appears to remain somewhat steady near ~0.25. **E-27**: It is difficult to discern a clear pattern from these samples, as the light and middle/total ratios zigzag between higher and lower values (Figure 4.150). There appears to be a general decrease in middle/total ratio with decreasing depth; if this is the case, then the samples from 7 cm above and 16 cm below the contact show relatively increased middle/total ratio values. **SGH103**: The samples from this core show a decreasing middle/total ratio value with decreasing depth from 28 cm below the contact to 31 cm above the contact, with the exception of the samples taken 7 cm above and 5 cm below the contact, which show slightly increased middle/total ratios (Figure 4.151).

**Lubin mining district, Rudna 1 and 2**: Ratio values in Rudna 1 are relatively steady, with the exception of 25 cm below the contact, where middle/total ratio increases and the light/total decreases (Figure 4.152). **Lubin 1**: The middle/total ratio exhibits the highest value at 10 and 20 cm below the contact (0.4+); for the other depths, the ratio is approximately 0.25 (Figure 4.153). **Lubin 2**: The middle/total ratio appears to gradually decrease with decreasing depth from ~0.36 to ~0.24, with the exception of a sudden decrease in value at the contact to about 25 cm above the contact (Figure 4.154).

Table 4.11: Geochemical data for Sangerhausen Basin samples, rare earth elements. Data in the following graphs are normalized to the Post Archaean Average Shale data listed.

| Sangerhausen Basin | Analyte Symbol | La | Ce | Pr | Nd | Sm | Eu | Gd | Tb | Dy | Ho | Er | Tm | Yb | Lu |
|---|---|---|---|---|---|---|---|---|---|---|---|---|---|---|---|
| | Unit Symbol | ppm | ppm | ppm | ppm | ppm | ppm | ppm | ppm | ppm | ppm | ppm | ppm | ppm | ppm |
| | Detection Limit | 0.1 | 0.1 | 0.05 | 0.1 | 0.1 | 0.05 | 0.1 | 0.1 | 0.1 | 0.1 | 0.1 | 0.05 | 0.1 | 0.04 |
| | Analysis Method | FUS-MS | FUS-MS | FUS-MS | FUS-MS | FUS-MS | FUS-MS | FUS-MS | FUS-MS | FUS-MS | FUS-MS | FUS-MS | FUS-MS | FUS-MS | FUS-MS |
| | PAAS (McLennan) | 38.2 | 79.6 | 8.83 | 33.9 | 5.55 | 1.08 | 4.66 | 0.774 | 4.68 | 0.991 | 2.85 | 0.405 | 2.82 | 0.433 |
| | Sample Number | | | | | | | | | | | | | | |
| Wettelrode | K2+26 | 35.9 | 62.9 | 6.78 | 21.5 | 4.1 | 0.8 | 3.5 | 0.6 | 3.3 | 0.7 | 1.9 | 0.29 | 2 | 0.29 |
| | K05+14 | 41.2 | 78.8 | 10.1 | 42.9 | 10.4 | 1.53 | 9 | 1.3 | 7.1 | 1.3 | 3.4 | 0.48 | 2.9 | 0.44 |
| | K6+10 | 60.7 | 164 | 25.7 | 119 | 36.8 | 6.87 | 37.7 | 5.4 | 26.1 | 4 | 8.8 | 0.92 | 4.4 | 0.55 |
| | K7+8 | 47.6 | 88.1 | 10.9 | 38.3 | 8.3 | 1.71 | 8.3 | 1.5 | 8.7 | 1.7 | 4.3 | 0.55 | 3.1 | 0.4 |
| | K8-0 | 42.1 | 83.6 | 10.6 | 38.2 | 8.7 | 1.61 | 7.6 | 1.1 | 6.1 | 1.1 | 2.8 | 0.37 | 2.1 | 0.29 |
| | K9-4 | 16.8 | 35.7 | 4.75 | 19.3 | 5.1 | 1.02 | 4.7 | 0.7 | 4 | 0.7 | 1.9 | 0.27 | 1.7 | 0.24 |
| | K10-13 | 12.5 | 23.8 | 3.19 | 15 | 3.9 | 0.65 | 3.7 | 0.6 | 3.3 | 0.6 | 1.7 | 0.23 | 1.4 | 0.2 |
| | K11-21 | 20.8 | 36.5 | 4.79 | 21 | 4.7 | 0.85 | 4.4 | 0.7 | 3.8 | 0.7 | 1.9 | 0.26 | 1.6 | 0.23 |
| | K15-50 | 17.5 | 36.7 | 5.06 | 23.4 | 5.7 | 1.12 | 5.4 | 0.8 | 4.7 | 0.8 | 2.2 | 0.32 | 1.9 | 0.28 |
| SGH133 | K32+62 | 38 | 71.6 | 7.78 | 31.2 | 6 | 1.18 | 5.2 | 0.9 | 4.7 | 0.9 | 2.6 | 0.41 | 2.6 | 0.39 |
| | K29+50 | 31.1 | 64.6 | 7.08 | 24.6 | 5 | 0.93 | 4.2 | 0.7 | 3.8 | 0.8 | 2.2 | 0.34 | 2.2 | 0.31 |
| | K22+25 | 43.7 | 79.1 | 8.3 | 32.6 | 6 | 1.08 | 4.8 | 0.7 | 4 | 0.8 | 2.3 | 0.38 | 2.5 | 0.36 |
| | K21+17 | 35.5 | 64 | 7.62 | 27.4 | 5.3 | 0.85 | 4.2 | 0.7 | 3.9 | 0.8 | 2.5 | 0.4 | 2.6 | 0.39 |
| | K20+8 | 40.5 | 87.9 | 11.8 | 46.4 | 9.1 | 1.76 | 8 | 1.1 | 5.8 | 1 | 2.8 | 0.4 | 2.5 | 0.37 |
| | K19+3 | 46.7 | 95.9 | 12.3 | 48 | 10.4 | 1.83 | 9 | 1.3 | 6.7 | 1.2 | 3.2 | 0.43 | 2.7 | 0.37 |
| | K17-6 | 23.1 | 44.5 | 5.12 | 21.5 | 4.2 | 0.75 | 3.4 | 0.5 | 2.9 | 0.6 | 1.6 | 0.25 | 1.6 | 0.24 |
| SGH132 | K43+42 | 30 | 58.8 | 6.56 | 22.9 | 4.6 | 0.86 | 3.9 | 0.6 | 3.5 | 0.7 | 2 | 0.29 | 1.8 | 0.27 |
| | K41+22 | 33.7 | 63 | 7.01 | 29.2 | 5.7 | 0.98 | 4.9 | 0.8 | 4.4 | 0.9 | 2.6 | 0.4 | 2.6 | 0.37 |
| | K40+8 | 46.1 | 83.9 | 9.6 | 35.9 | 7.5 | 1.22 | 6.1 | 1.1 | 6.3 | 1.2 | 3.5 | 0.49 | 3.1 | 0.51 |
| | K39+1 | 82.2 | 124 | 12.2 | 34.9 | 5.4 | 0.96 | 4.6 | 0.8 | 5 | 1 | 3.2 | 0.5 | 3.3 | 0.49 |
| | K38-12 | 22.8 | 46.8 | 6.18 | 28.3 | 6.1 | 1.09 | 5.2 | 0.8 | 4.1 | 0.7 | 2.1 | 0.3 | 1.8 | 0.25 |
| | K35-55 | 21.4 | 40 | 5.04 | 21.8 | 4.7 | 0.83 | 4.1 | 0.6 | 3.2 | 0.6 | 1.6 | 0.24 | 1.5 | 0.2 |
| | K34-68 | 20.3 | 36.2 | 4.22 | 16.9 | 3.3 | 0.72 | 2.8 | 0.4 | 2.4 | 0.5 | 1.3 | 0.21 | 1.3 | 0.19 |
| E-27 | K54+31 | 35.3 | 67.2 | 7.46 | 30.4 | 5.5 | 0.88 | 4.8 | 0.8 | 4.5 | 0.9 | 2.6 | 0.41 | 2.7 | 0.38 |
| | K53+20 | 33 | 68.8 | 7.01 | 24 | 4.7 | 0.87 | 3.9 | 0.6 | 3.7 | 0.7 | 2 | 0.3 | 1.9 | 0.28 |
| | K52+7 | 38.2 | 87.5 | 11.6 | 50.3 | 13.6 | 2.47 | 13.1 | 2.1 | 10.9 | 1.9 | 4.9 | 0.61 | 3.4 | 0.44 |
| | K51-4 | 20 | 43.1 | 5.33 | 20 | 4.6 | 0.68 | 4.1 | 0.6 | 3.6 | 0.7 | 1.8 | 0.26 | 1.6 | 0.25 |
| | K50-16 | 15.5 | 37.2 | 5.45 | 25.8 | 6.4 | 1.07 | 5.8 | 1 | 5.2 | 0.9 | 2.5 | 0.35 | 2.1 | 0.3 |
| | K49-27 | 22.5 | 49.2 | 5.73 | 25.1 | 5.6 | 0.9 | 5.4 | 0.8 | 4.6 | 0.8 | 2.5 | 0.36 | 2.2 | 0.31 |
| | K48-36 | 18.5 | 42.3 | 4.68 | 20.4 | 4.5 | 0.76 | 4.3 | 0.7 | 4 | 0.8 | 2.2 | 0.32 | 2 | 0.29 |
| SGH103 | K61+31 | 35.1 | 68.6 | 7.26 | 24.8 | 4.8 | 0.8 | 3.7 | 0.6 | 3.7 | 0.7 | 2.2 | 0.34 | 2.2 | 0.33 |
| | K60+19 | 35.8 | 69.6 | 7.48 | 26.1 | 5 | 0.84 | 4.1 | 0.6 | 3.6 | 0.7 | 2.1 | 0.33 | 2.1 | 0.32 |
| | K59+7 | 37.5 | 74.5 | 10.2 | 39.1 | 11.8 | 1.91 | 13.9 | 2.3 | 13.1 | 2.3 | 5.5 | 0.66 | 3.4 | 0.44 |
| | K58-5 | 21.1 | 47.3 | 6.34 | 29.1 | 5.8 | 1.2 | 5 | 0.8 | 3.9 | 0.7 | 2.1 | 0.3 | 1.8 | 0.26 |
| | K57-16 | 33.8 | 69.6 | 8.04 | 35.5 | 6.9 | 0.99 | 5.6 | 0.8 | 4.6 | 0.9 | 2.7 | 0.43 | 2.8 | 0.42 |
| | K56-28 | 33.2 | 68.5 | 8.2 | 35.2 | 6.9 | 1.1 | 6.1 | 0.9 | 5.2 | 1 | 3 | 0.48 | 3.1 | 0.45 |

Table 4.12: Geochemical data for Lubin mining district samples, rare earth elements. Data in the following graphs are normalized to the Post Archaean Average Shale data listed.

| Lubin Mining District | Analyte Symbol | La | Ce | Pr | Nd | Sm | Eu | Gd | Tb | Dy | Ho | Er | Tm | Yb | Lu |
|---|---|---|---|---|---|---|---|---|---|---|---|---|---|---|---|
| | Unit Symbol | ppm | ppm | ppm | ppm | ppm | ppm | ppm | ppm | ppm | ppm | ppm | ppm | ppm | ppm |
| | Detection Limit | 0.1 | 0.1 | 0.05 | 0.1 | 0.1 | 0.05 | 0.1 | 0.1 | 0.1 | 0.1 | 0.1 | 0.05 | 0.1 | 0.04 |
| | Analysis Method | FUS-MS | FUS-MS | FUS-MS | FUS-MS | FUS-MS | FUS-MS | FUS-MS | FUS-MS | FUS-MS | FUS-MS | FUS-MS | FUS-MS | FUS-MS | FUS-MS |
| | PAAS (McLennan) | 38.2 | 79.6 | 8.83 | 33.9 | 5.55 | 1.08 | 4.66 | 0.774 | 4.68 | 0.991 | 2.85 | 0.405 | 2.82 | 0.433 |
| | Sample Number | | | | | | | | | | | | | | |
| Rudna 1 | K63+40 | 27.5 | 49.5 | 5.57 | 20.4 | 3.9 | 0.71 | 3.2 | 0.5 | 2.9 | 0.6 | 1.7 | 0.26 | 1.7 | 0.25 |
| | K65+20 | 25.9 | 49.9 | 6.09 | 22.3 | 4.5 | 0.9 | 3.7 | 0.6 | 3.2 | 0.6 | 1.7 | 0.25 | 1.5 | 0.22 |
| | K67+10 | 31.6 | 61 | 7.98 | 29.1 | 6.6 | 1.33 | 5.5 | 0.8 | 4.1 | 0.7 | 1.9 | 0.27 | 1.7 | 0.23 |
| | K66-0 | 34.9 | 62.6 | 7.67 | 26 | 5.4 | 1.11 | 4.5 | 0.7 | 3.7 | 0.7 | 1.9 | 0.27 | 1.6 | 0.23 |
| | K68-10 | 21.7 | 41.7 | 4.98 | 18.4 | 4 | 0.87 | 3.5 | 0.5 | 3 | 0.6 | 1.6 | 0.23 | 1.5 | 0.22 |
| | K69-25 | 20.8 | 33.9 | 5.1 | 26.6 | 7.2 | 1.83 | 6.3 | 0.9 | 4.3 | 0.7 | 1.7 | 0.23 | 1.3 | 0.18 |
| | K70-130 | 12.6 | 19.1 | 2.27 | 9.3 | 1.7 | 0.4 | 1.4 | 0.2 | 1.2 | 0.2 | 0.7 | 0.1 | 0.7 | 0.1 |
| Rudna 2 | K76+20 | 31.2 | 57.6 | 6.19 | 21.5 | 4.3 | 0.79 | 3.6 | 0.6 | 3.3 | 0.7 | 2 | 0.31 | 2 | 0.3 |
| Lubin 1 | K84+110 | 24.7 | 46.6 | 5.38 | 19.4 | 3.8 | 0.69 | 3 | 0.4 | 2.6 | 0.5 | 1.5 | 0.24 | 1.6 | 0.23 |
| | K88+40 | 26.2 | 51.1 | 5.71 | 20.1 | 4.2 | 0.79 | 3.6 | 0.6 | 3.1 | 0.6 | 1.8 | 0.27 | 1.7 | 0.24 |
| | K89+20 | 31.1 | 67.3 | 6.52 | 24 | 4.9 | 0.94 | 4.1 | 0.6 | 3.5 | 0.7 | 1.9 | 0.29 | 1.8 | 0.26 |
| | K91+0 | 31 | 60.7 | 6.84 | 24.2 | 5.2 | 1.09 | 4.5 | 0.7 | 3.7 | 0.7 | 1.9 | 0.28 | 1.7 | 0.24 |
| | K92-10 | 12.5 | 28.2 | 5.4 | 30.6 | 9.1 | 2.23 | 7.6 | 1 | 4.9 | 0.8 | 1.9 | 0.24 | 1.4 | 0.19 |
| | K93-20 | 14.5 | 31.3 | 5.25 | 28.5 | 8.1 | 1.95 | 6.7 | 0.9 | 4.4 | 0.7 | 1.8 | 0.24 | 1.4 | 0.18 |
| | K94-120 | 12.7 | 20 | 2.46 | 9.8 | 1.9 | 0.49 | 1.6 | 0.2 | 1.3 | 0.2 | 0.7 | 0.1 | 0.7 | 0.1 |
| Lubin 2 | K105+120 | 28.4 | 43.5 | 5.19 | 20 | 3.5 | 0.69 | 2.6 | 0.4 | 2.1 | 0.4 | 1.2 | 0.19 | 1.2 | 0.18 |
| | K104+50 | 21.9 | 42 | 4.87 | 21 | 4.1 | 0.88 | 3.3 | 0.5 | 2.8 | 0.5 | 1.5 | 0.23 | 1.5 | 0.22 |
| | K103+30 | 22.7 | 47.9 | 5.82 | 22.6 | 5.1 | 1.2 | 4.8 | 0.7 | 4 | 0.7 | 2.1 | 0.31 | 1.9 | 0.27 |
| | K102+25 | 29.7 | 49.7 | 5.42 | 17 | 3 | 0.58 | 2.4 | 0.4 | 2.3 | 0.4 | 1.3 | 0.21 | 1.3 | 0.2 |
| | K101+20 | 31 | 53.6 | 6.3 | 25 | 4.5 | 0.82 | 2.9 | 0.4 | 2.4 | 0.5 | 1.4 | 0.21 | 1.4 | 0.21 |
| | K100+0 | 47 | 91.4 | 10.5 | 38.4 | 8.3 | 1.75 | 6.7 | 1 | 5 | 0.9 | 2.4 | 0.35 | 2.1 | 0.3 |
| | K99-UBD | 24.6 | 51.5 | 6.2 | 25.5 | 6.4 | 1.39 | 5.4 | 0.7 | 3.6 | 0.6 | 1.6 | 0.2 | 1.2 | 0.17 |
| | K98-LBD | 20.8 | 43.2 | 4.82 | 19.5 | 4.7 | 1.05 | 4.1 | 0.6 | 2.9 | 0.5 | 1.3 | 0.16 | 0.9 | 0.12 |
| | K97-5 | 15.6 | 35.2 | 4.8 | 20.9 | 5.9 | 1.35 | 4.8 | 0.7 | 3.6 | 0.6 | 1.6 | 0.22 | 1.3 | 0.18 |
| | K96-50 | 16.2 | 28.8 | 4.37 | 21.6 | 6 | 1.58 | 5.1 | 0.7 | 3.4 | 0.6 | 1.4 | 0.2 | 1.1 | 0.17 |
| | K95-120 | 9.9 | 18.9 | 2.37 | 9 | 2.2 | 0.54 | 1.9 | 0.3 | 1.4 | 0.3 | 0.7 | 0.1 | 0.6 | 0.1 |

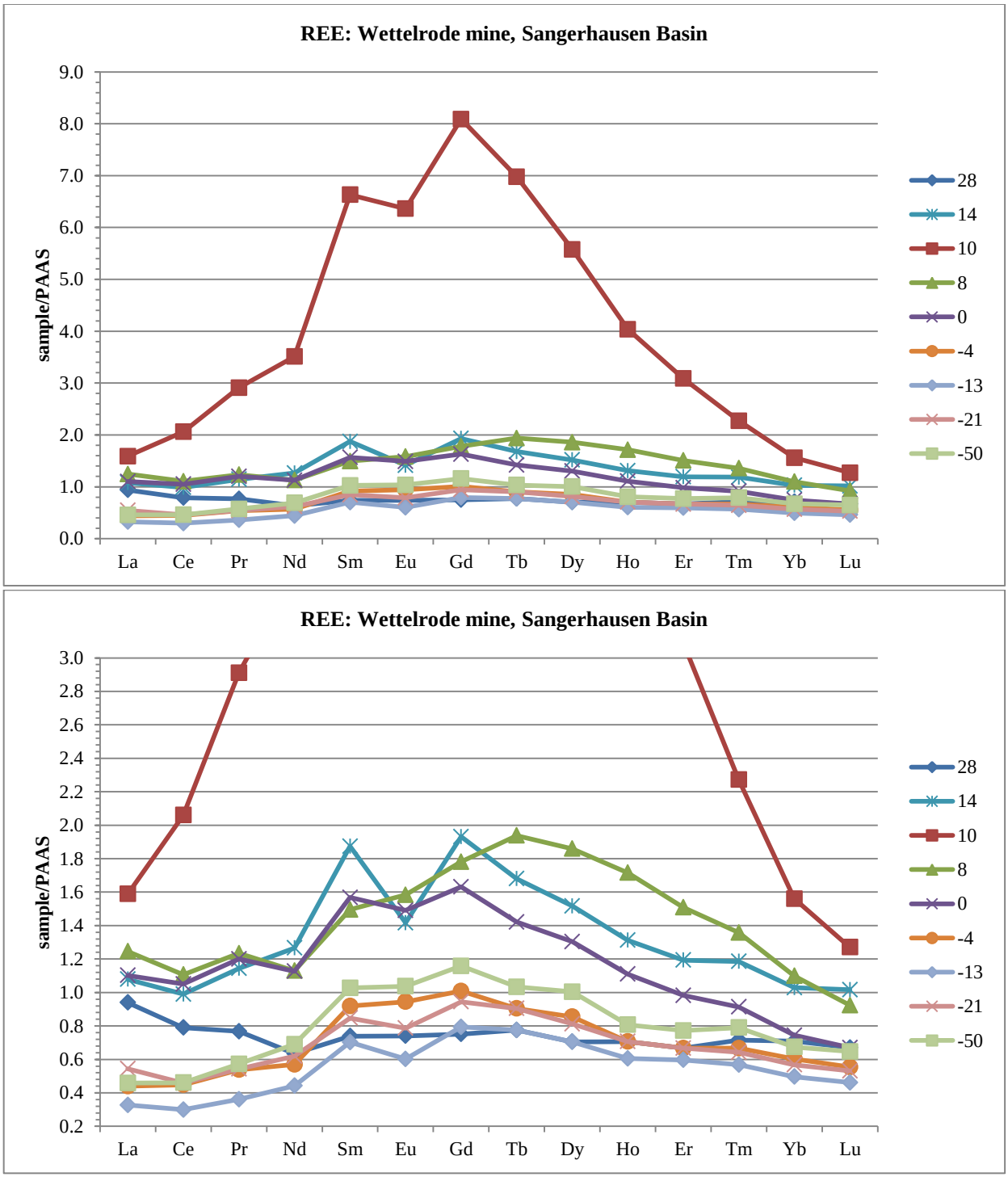


Figure 4.139: Rare earth element patterns for samples from Wettelrode Mine, Sangerhausen Basin, Germany. The numbers assigned to the lines of data represent the depth that the samples were taken from in relation to the basal contact of the Kupferschiefer.

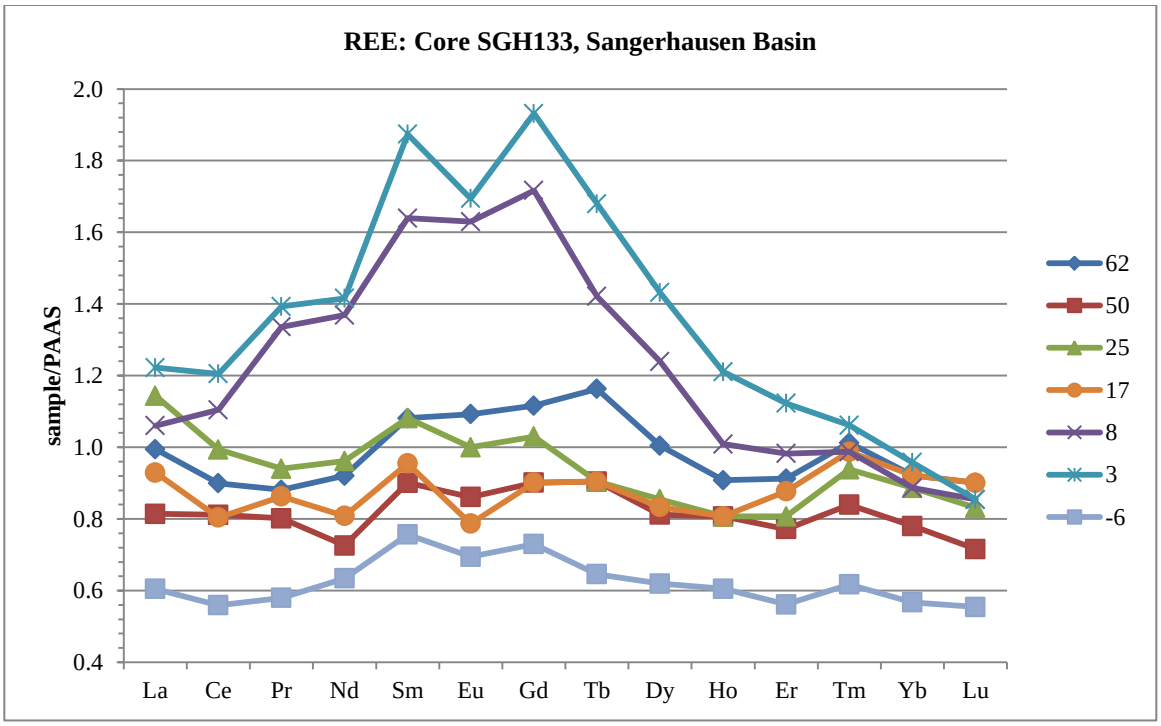


Figure 4.140: Rare earth element patterns for samples from core SGH133, Sangerhausen Basin, Germany. The numbers assigned to the lines of data represent the depth that the samples were taken from in relation to the basal contact of the Kupferschiefer.

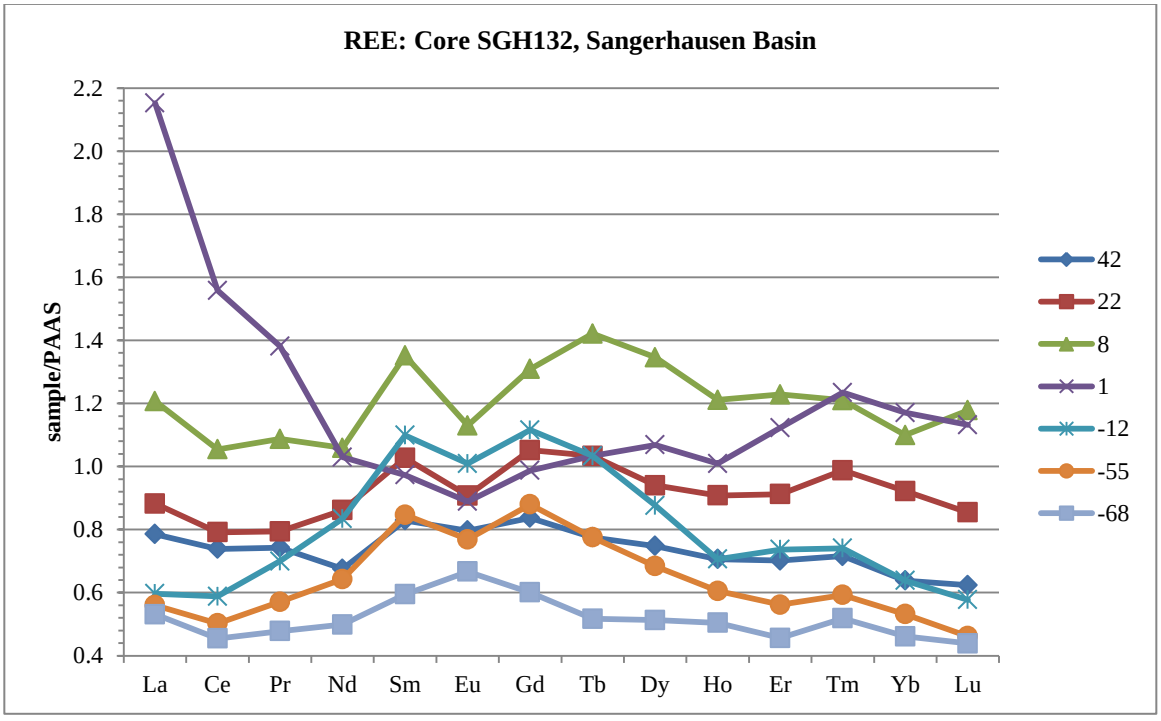


Figure 4.141: Rare earth element patterns for samples from core SGH132, Sangerhausen Basin, Germany. The numbers assigned to the lines of data represent the depth that the samples were taken from in relation to the basal contact of the Kupferschiefer.

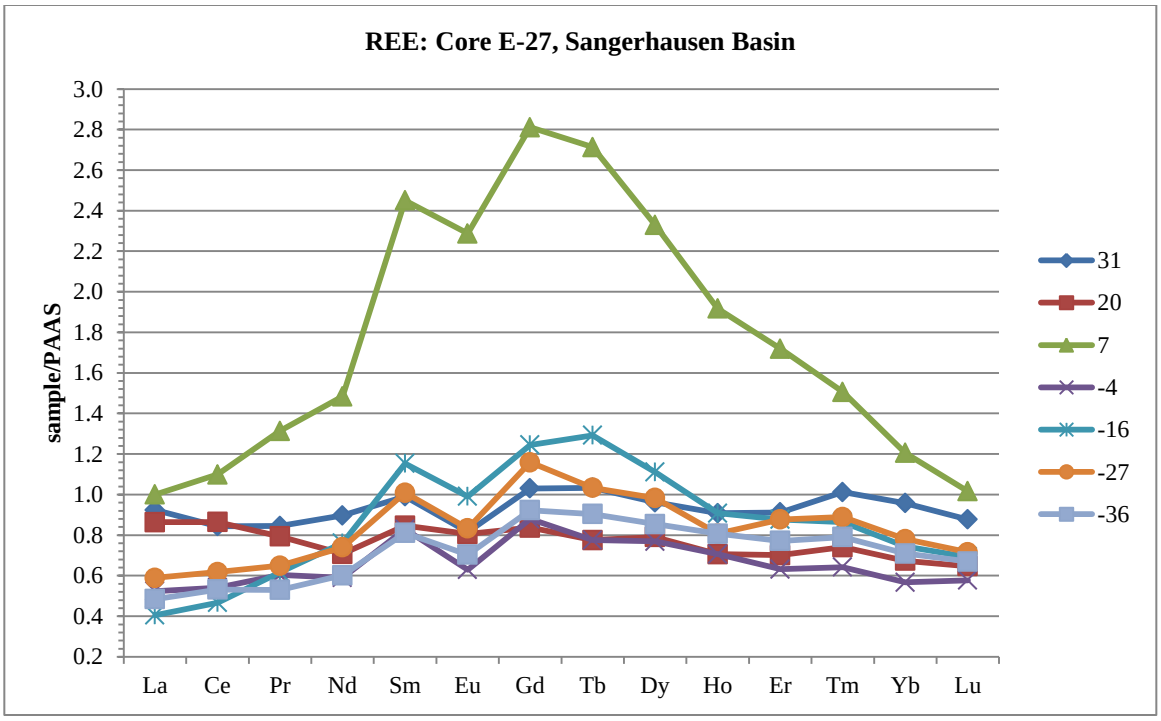


Figure 4.142: Rare earth element patterns for samples from core E-27, Sangerhausen Basin, Germany. The numbers assigned to the lines of data represent the depth that the samples were taken from in relation to the basal contact of the Kupferschiefer.

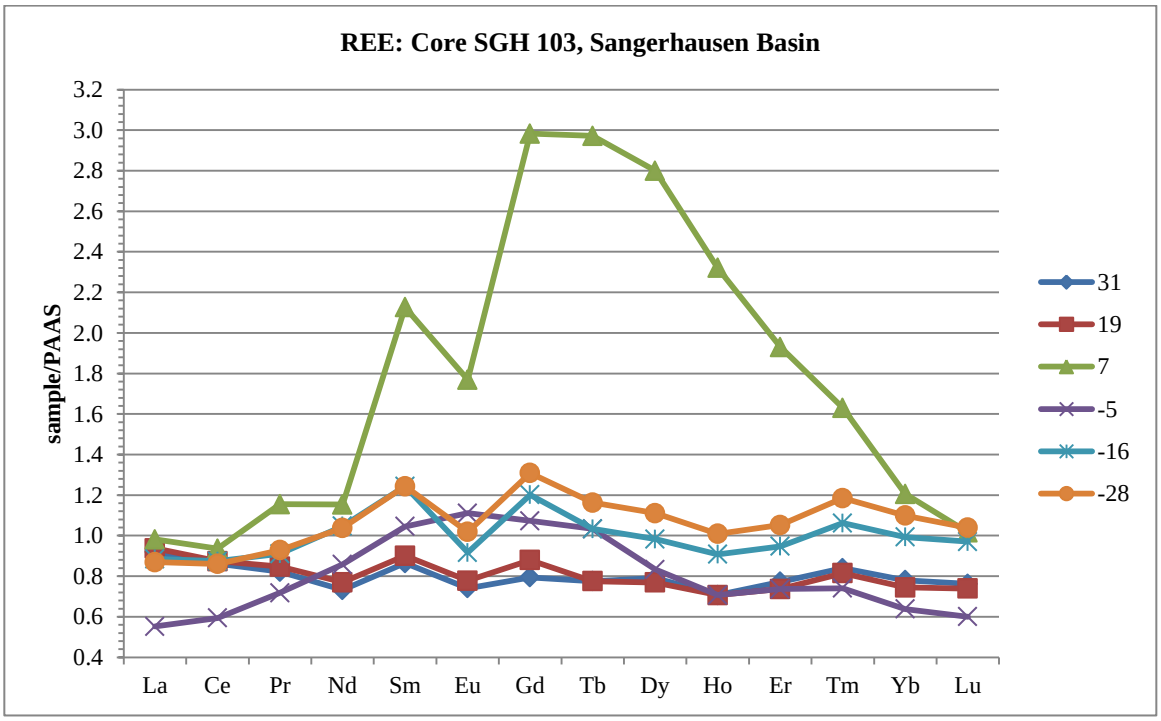


Figure 4.143: Rare earth element patterns for Weissliegend samples from core SGH103, Sangerhausen Basin, Germany. The numbers assigned to the lines of data represent the depth that the samples were taken from in relation to the basal contact of the Kupferschiefer.

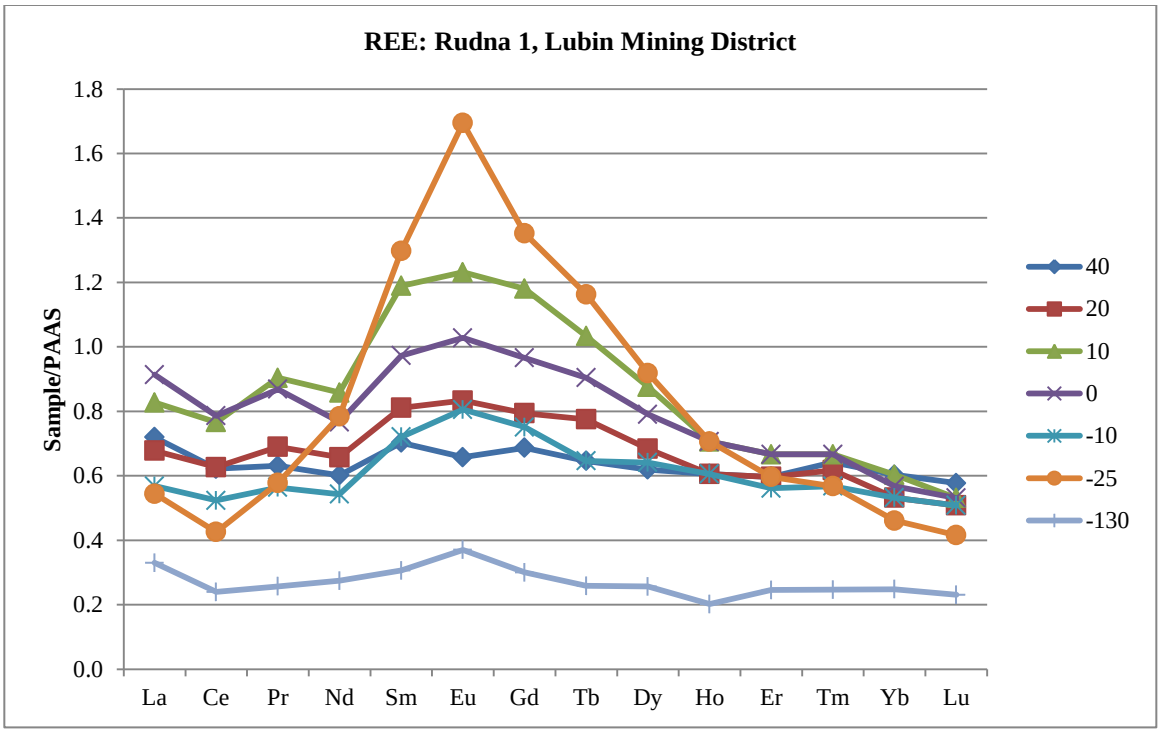


Figure 4.144: Rare earth element patterns for samples from Rudna 1, Lubin mining district, Poland. The numbers assigned to the lines of data represent the depth that the samples were taken from in relation to the basal contact of the Kupferschiefer.

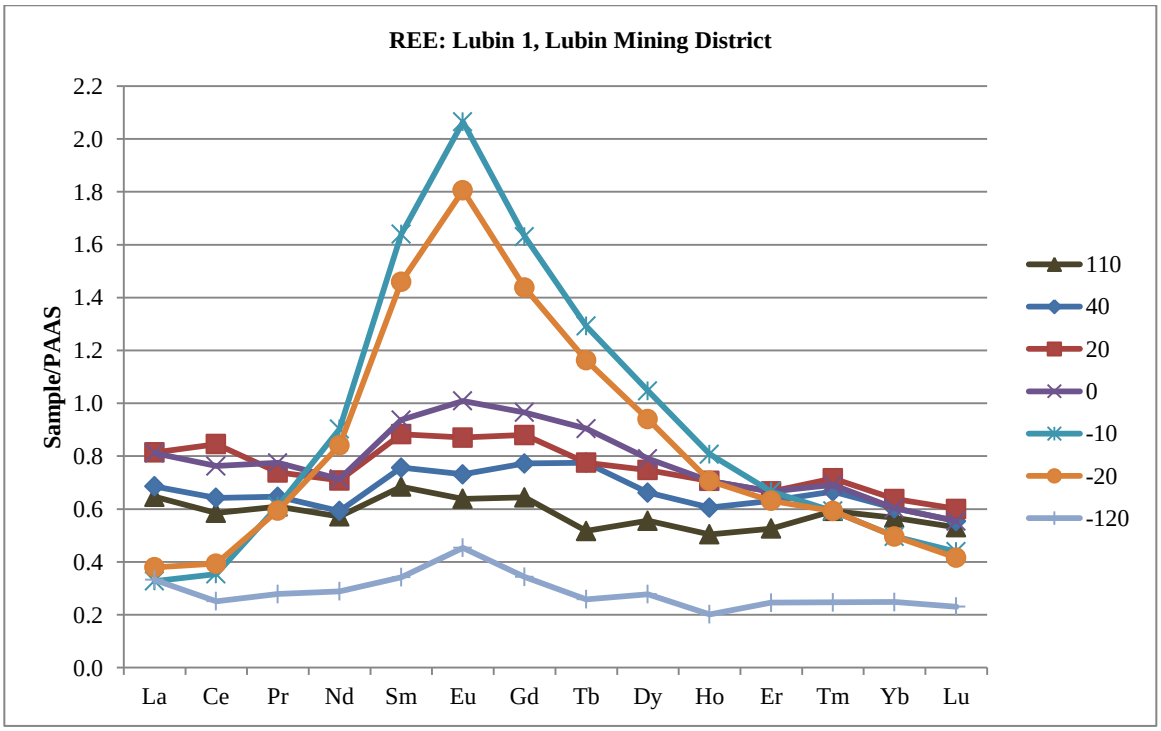


Figure 4.145: Rare earth element patterns for samples from Lubin 1, Lubin mining district, Poland. The numbers assigned to the lines of data represent the depth that the samples were taken from in relation to the basal contact of the Kupferschiefer.

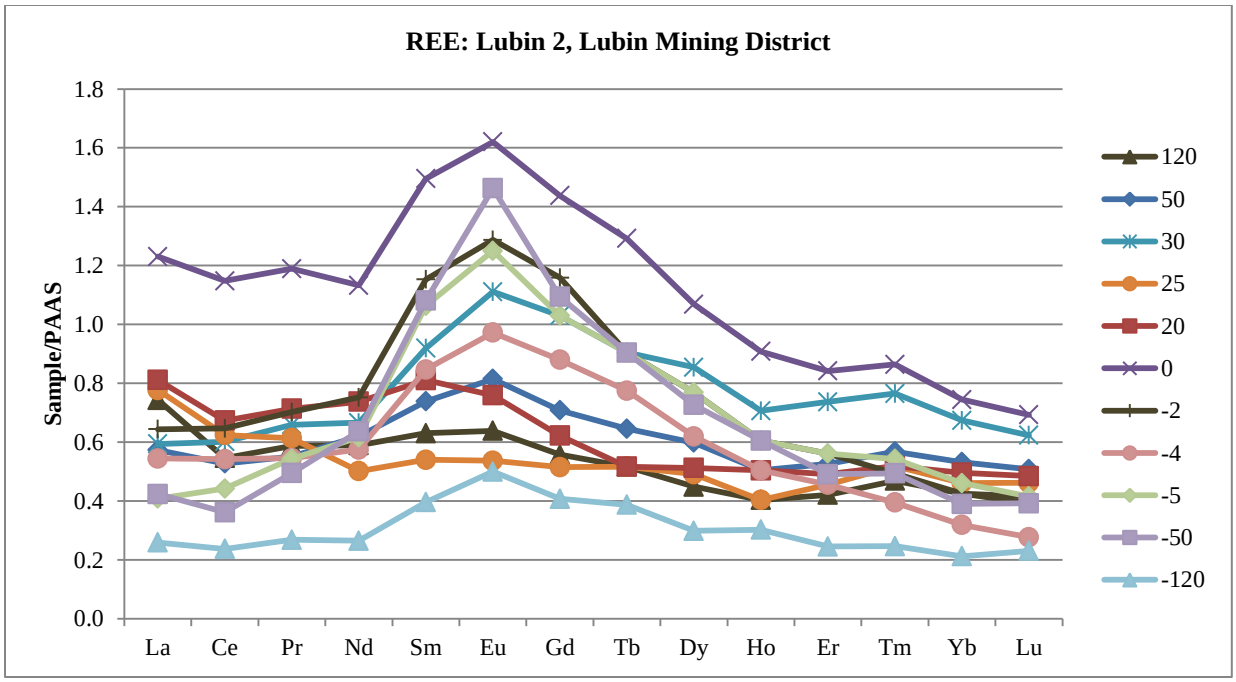


Figure 4.146: Rare earth element patterns for samples from Lubin 2, Lubin mining district, Poland. The numbers assigned to the lines of data represent the depth that the samples were taken from in relation to the basal contact of the Kupferschiefer.

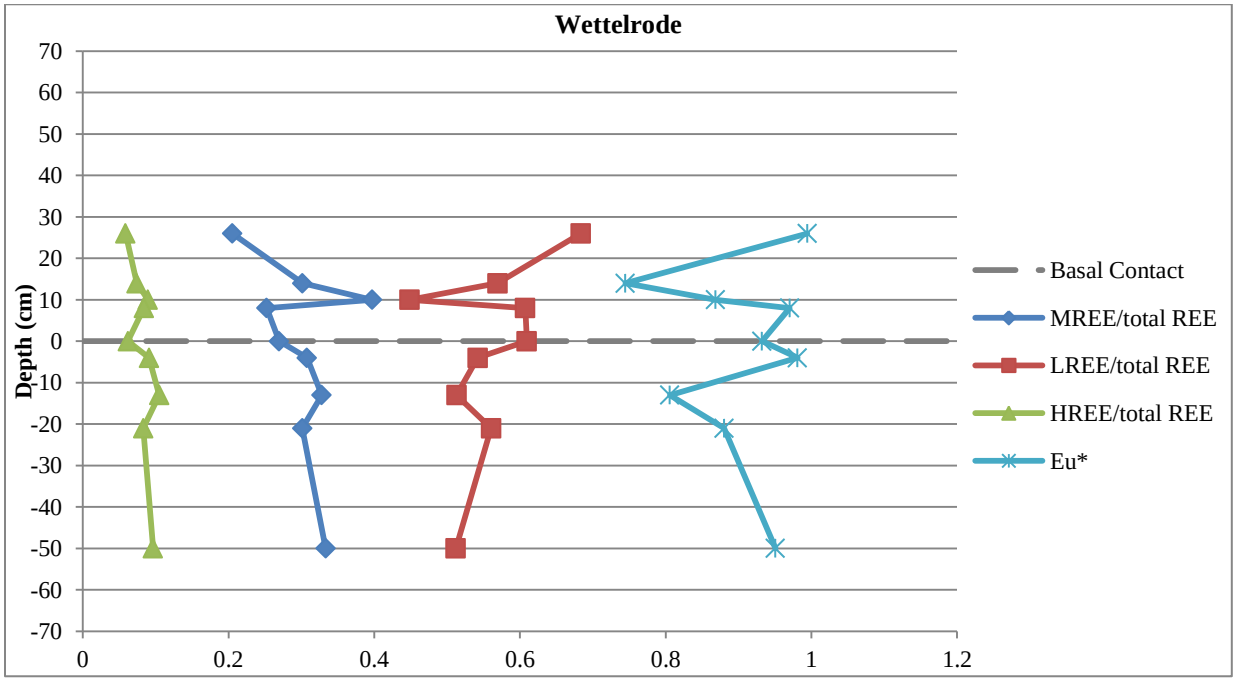


Figure 4.147: Light, middle, and heavy rare earth elements over total REE by depth for Wettelrode mine, Sangerhausen Basin (absolute REE values used). The Eu anomalies (Eu*) are also plotted (using PAAS-normalized data).

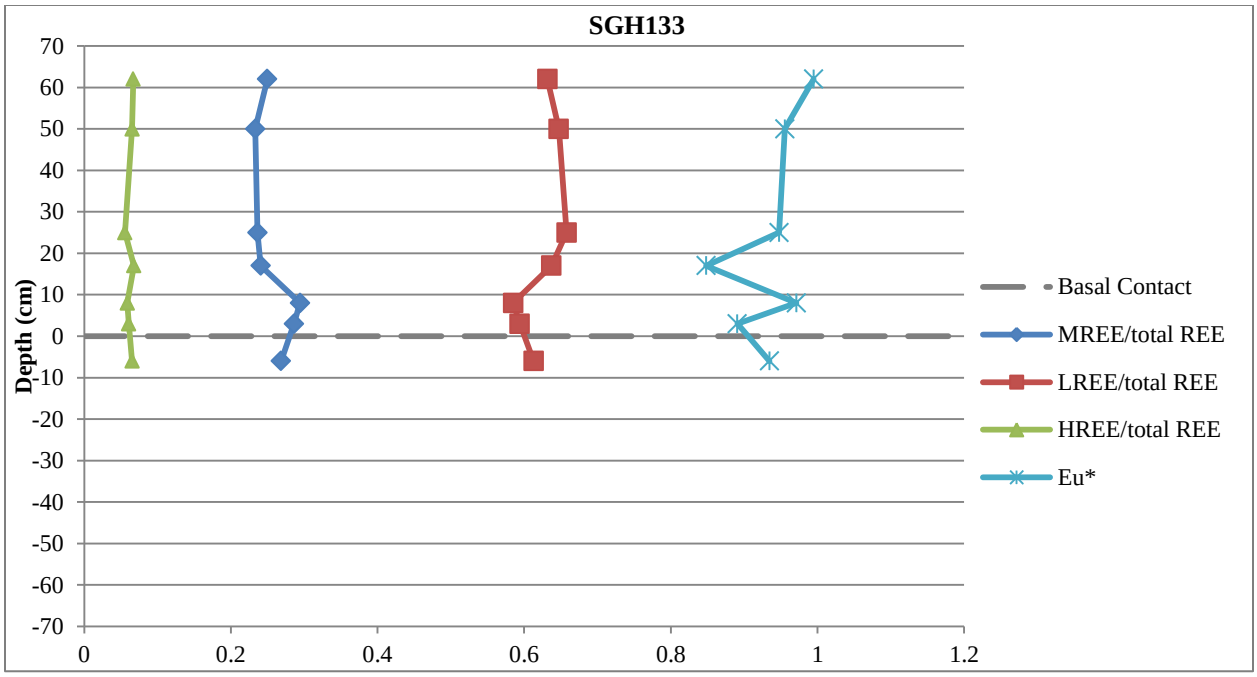


Figure 4.148: Light, middle, and heavy rare earth elements over total REE by depth for core SGH133, Sangerhausen Basin (absolute REE values used). The Eu anomalies (Eu*) are also plotted (using PAAS-normalized data).

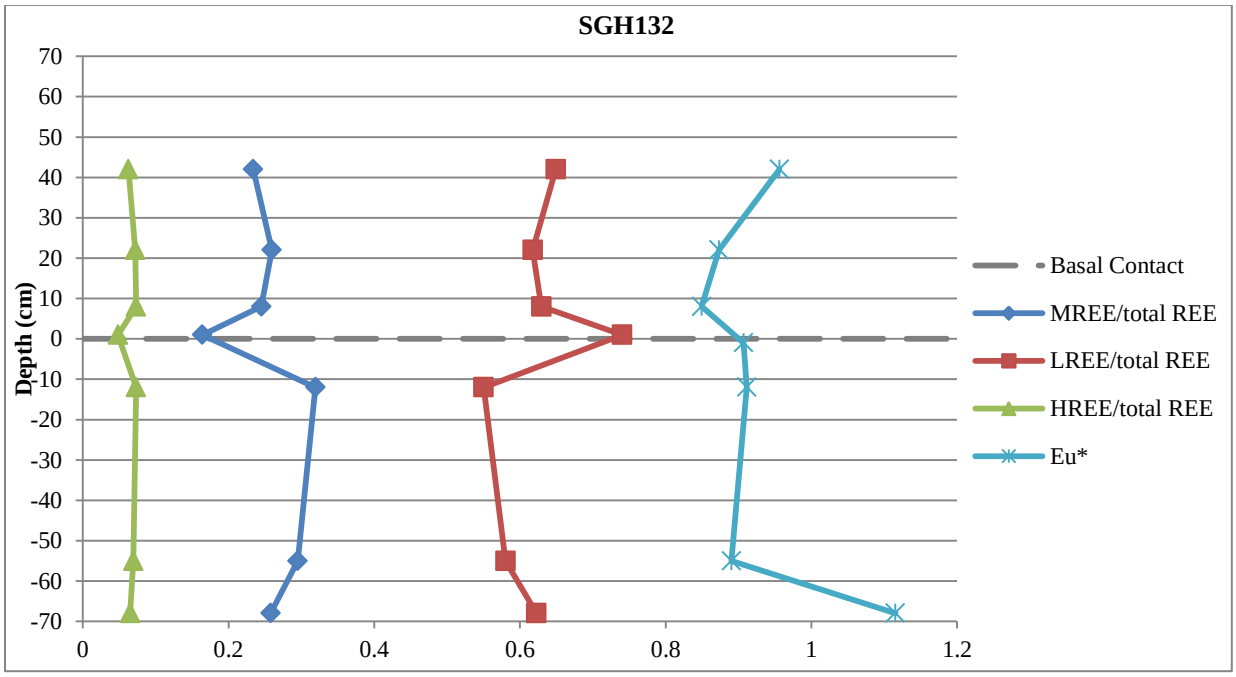


Figure 4.149: Light, middle, and heavy rare earth elements over total REE by depth for core SGH132, Sangerhausen Basin (absolute REE values used). The Eu anomalies (Eu*) are also plotted (using PAAS-normalized data).

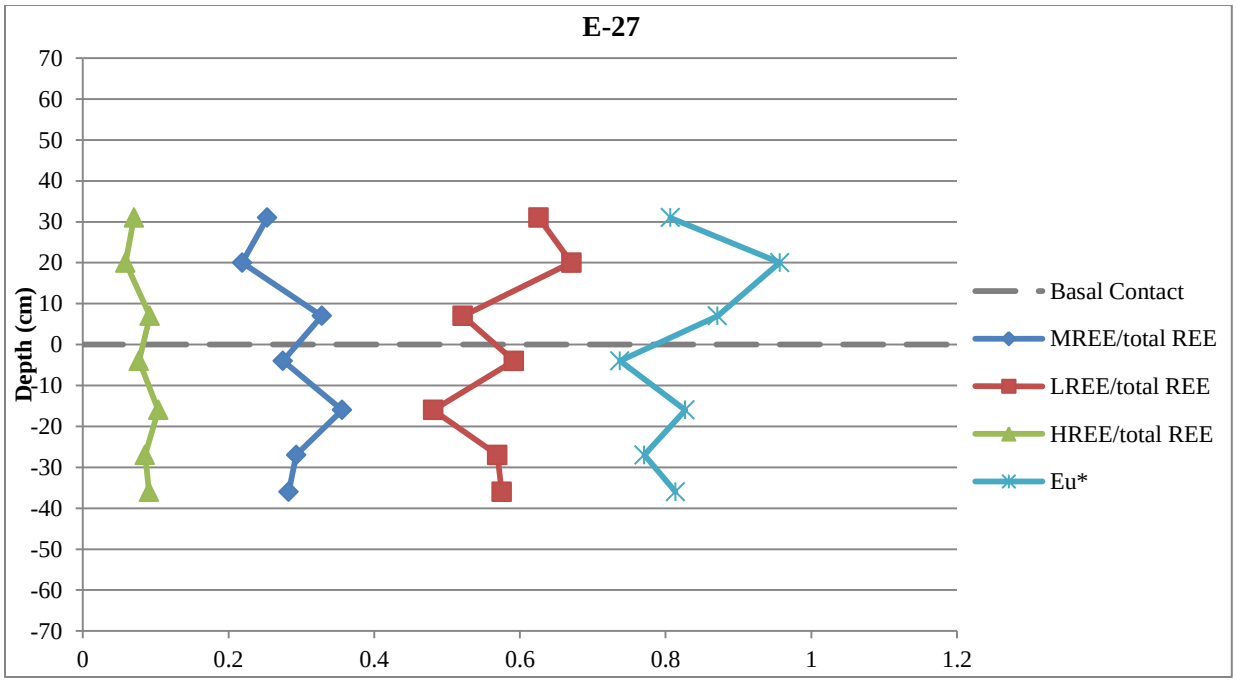


Figure 4.150: Light, middle, and heavy rare earth elements over total REE by depth for core E-27, Sangerhausen Basin (absolute REE values used). The Eu anomalies (Eu*) are also plotted (using PAAS-normalized data).

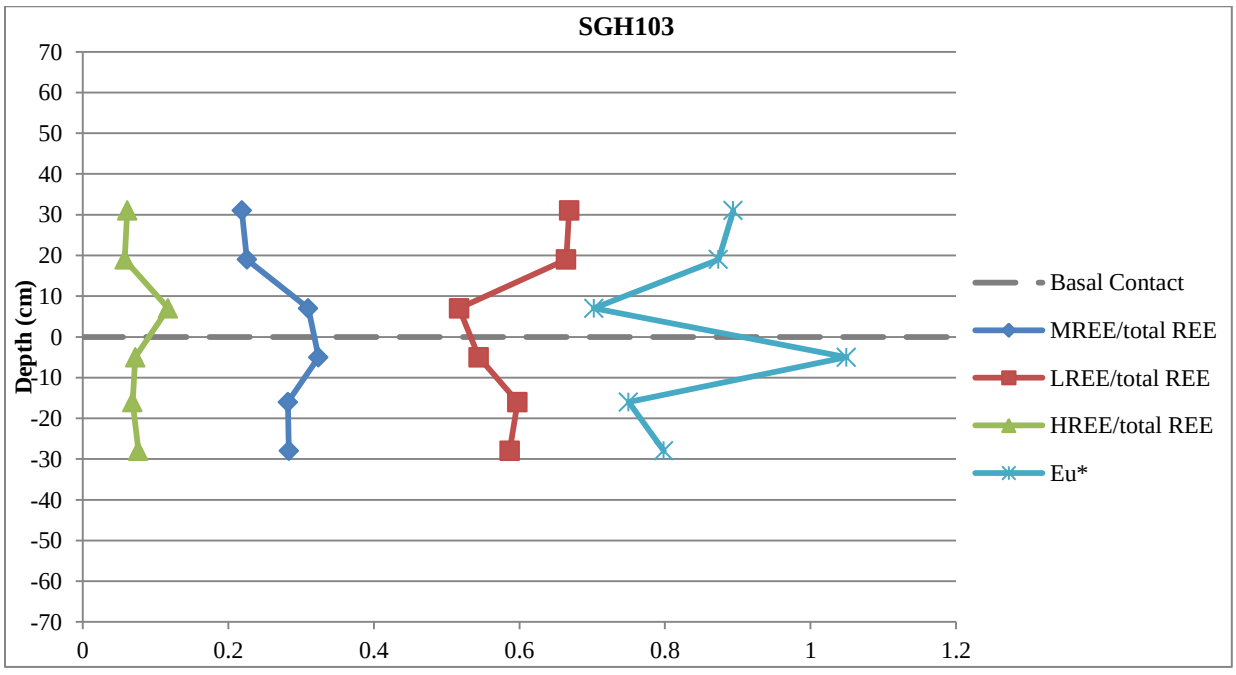


Figure 4.151: Light, middle, and heavy rare earth elements over total REE by depth for core SGH103, Sangerhausen Basin (absolute REE values used). The Eu anomalies (Eu*) are also plotted (using PAAS-normalized data).

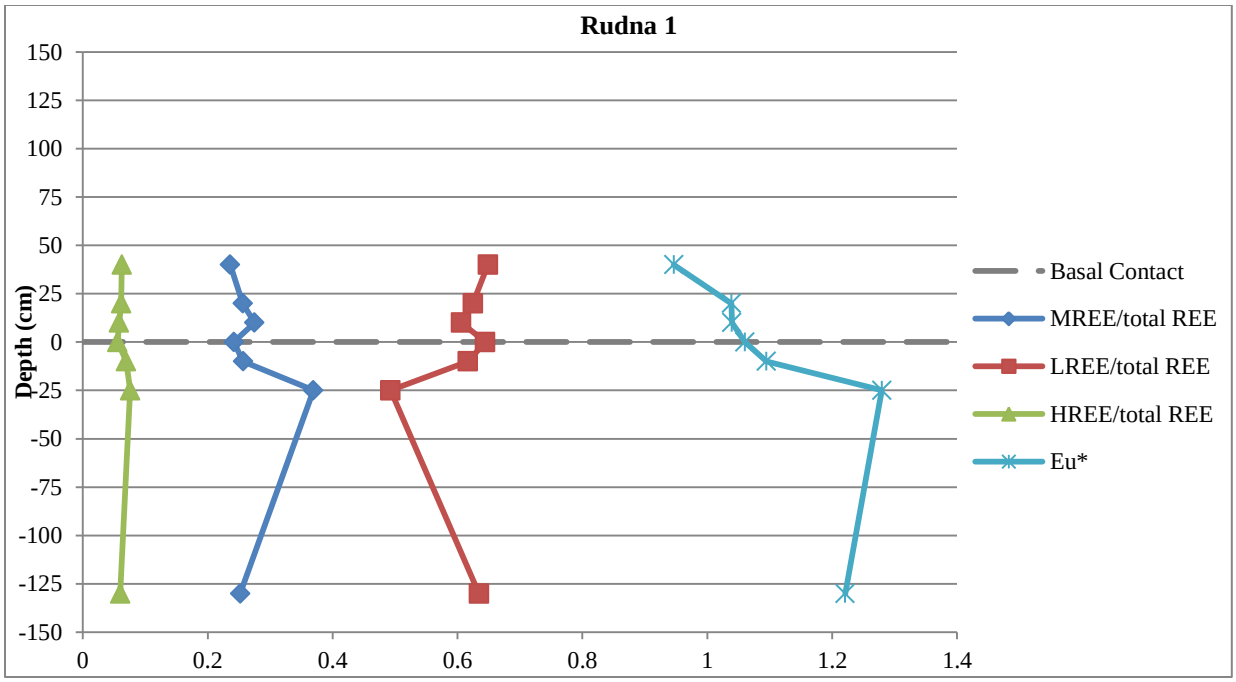


Figure 4.152: Light, middle, and heavy rare earth elements over total REE by depth for Rudna 1 and 2, Lubin mining district (absolute REE values used). The Eu anomalies (Eu*) are also plotted (using PAAS-normalized data).

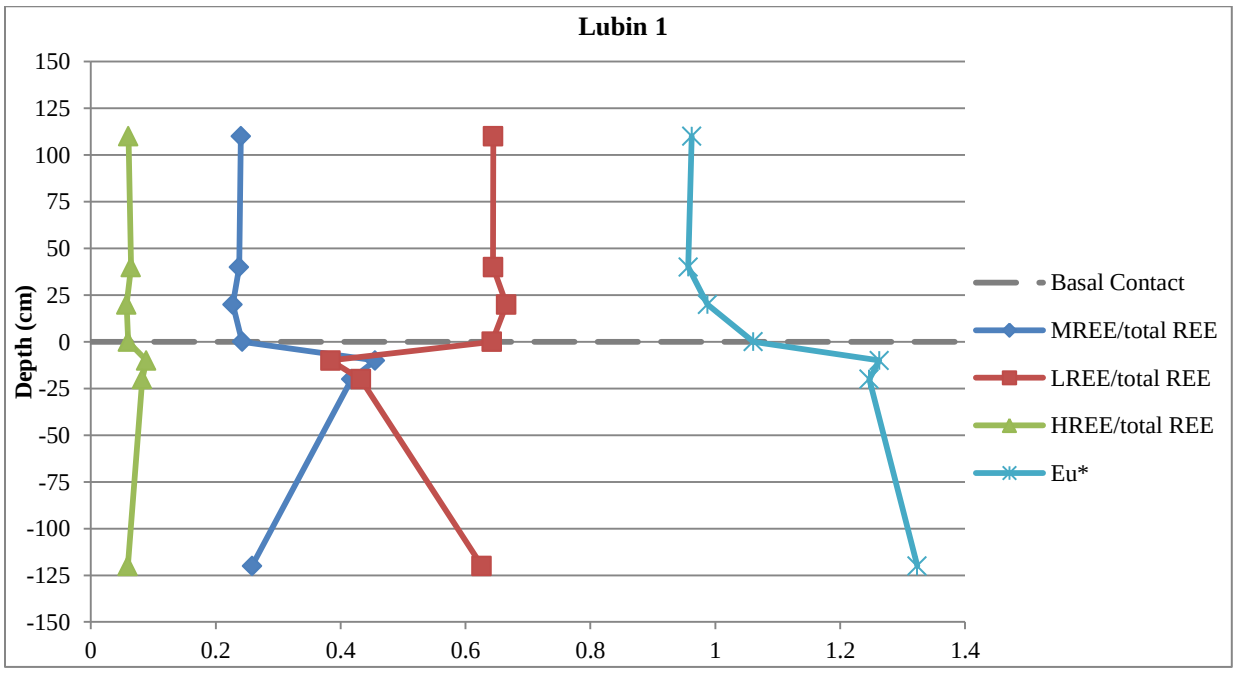


Figure 4.153: Light, middle, and heavy rare earth elements over total REE by depth for Lubin 1, Lubin mining district (absolute REE values used). The Eu anomalies (Eu*) are also plotted (using PAAS-normalized data).

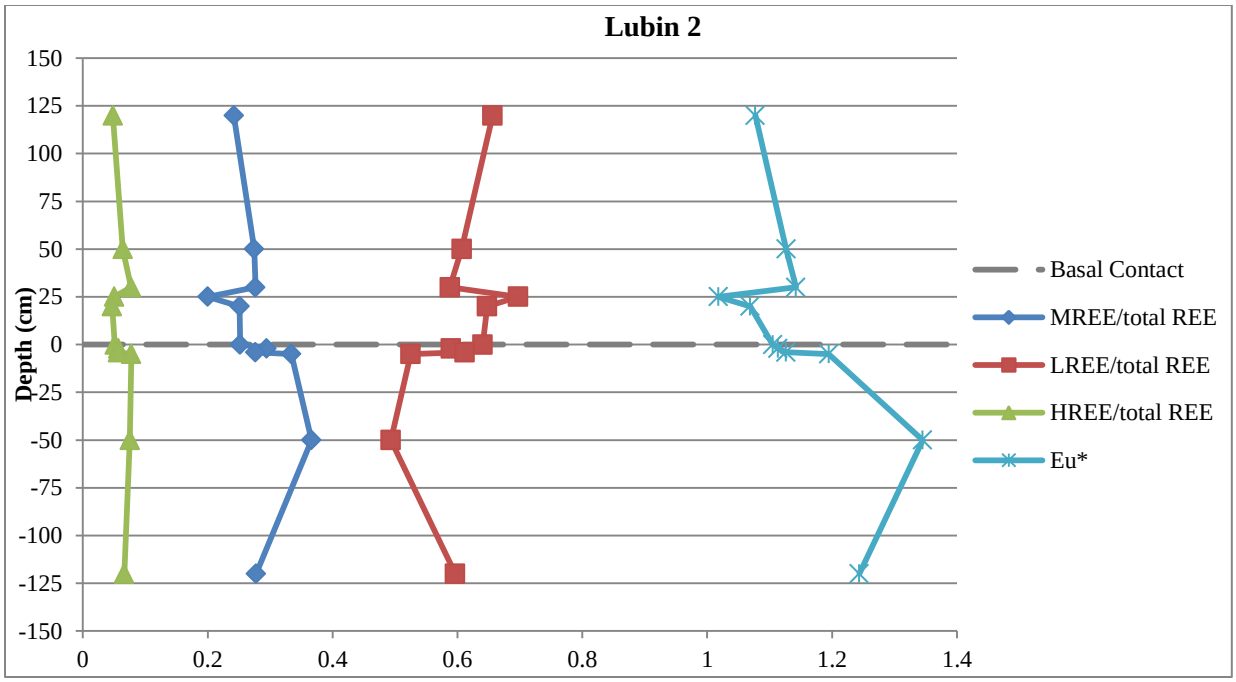


Figure 4.154: Light, middle, and heavy rare earth elements over total REE by depth for Lubin 2, Lubin mining district (absolute REE values used). The Eu anomalies (Eu*) are also plotted (using PAAS-normalized data).

#### 4.3.4.4 Eu Anomaly

Rare earth element patterns show that the samples exhibit a variation of Eu anomalies, both in whether they are positive or negative anomalies, and in how much the values differ from what would be expected using the equation $Eu^* = (Sm_N * Gd_N)^{0.5}$. Samples are assigned positive or negative Europium anomalies depending on the Eu/Eu* values: >1.05 is considered positive, while <0.95 is considered negative. Samples with values between 1.05 and 0.95 were not assigned an Eu anomaly ("none").

**Sangerhausen Basin** (PAAS): A majority of the samples from the Sangerhausen Basin show a negative Eu anomaly. Samples with no apparent anomaly include those from 4 cm below, and 8 and 26 cm above the contact in Wettelrode; 8, 50, and 62 cm above the contact in core SGH133; 22 and 42 cm above the contact in SGH132; and 20 cm above the contact E27 (Table 4.13). Only two samples, taken 68 cm below the contact in core SGH132 and 5 cm below the contact in core SGH103, exhibit positive Eu anomalies. The five Sangerhausen locations show no clear pattern when plotted by depth.

**Lubin mining district** (PAAS): Most of the samples from the Lubin mining district exhibit a positive Eu anomaly (Table 4.14). All of the samples at and below the contact in Rudna 1 are enriched in Eu; the samples from 10 and 20 cm above the contact lack an Eu anomaly, and the sample from 40 cm above the contact is depleted in Eu. The sample from Rudna 2, taken 20 cm above the contact, has a negative Eu anomaly (Figure 4.155). The samples taken at and below the contact in Lubin 1 exhibit a positive Eu anomaly; the samples taken above the contact exhibit a negative Eu anomaly. All of the samples from Lubin 2 exhibit a positive Eu anomaly, with the exception of the sample taken 25 cm above the contact, which lacks an Eu anomaly. When plotted by depth, the Eu anomalies clearly show higher values below the contact compared to samples from above the contact (Figure 4.156).

Table 4.13: Europium anomalies for Sangerhausen Basin samples. $Eu/Eu^* = Eu_N/(Sm_N*Gd_N)^{0.5}$. $Eu_N = Eu_{sample}/Eu_{PAAS}$.

| Location | Depth | Eu/Eu* (PAAS) | Present or Absent |
|---|---|---|---|
| Wettelrode | 26 | 0.9944 | none |
| | 14 | 0.7447 | negative |
| | 10 | 0.8685 | negative |
| | 8 | 0.9701 | none |
| | 0 | 0.9323 | negative |
| | -4 | 0.9810 | none |
| | -13 | 0.8057 | negative |
| | -21 | 0.8802 | negative |
| | -50 | 0.9506 | none |
| SGH133 | 62 | 0.9948 | none |
| | 50 | 0.9556 | none |
| | 25 | 0.9476 | negative |
| | 17 | 0.8483 | negative |
| | 8 | 0.9713 | none |
| | 3 | 0.8907 | negative |
| | -6 | 0.9346 | negative |
| SGH132 | 42 | 0.9561 | none |
| | 22 | 0.8732 | negative |
| | 8 | 0.8493 | negative |
| | 1 | 0.9070 | negative |
| | -12 | 0.9113 | negative |
| | -55 | 0.8903 | negative |
| | -68 | 1.1154 | positive |
| E-27 | 31 | 0.8065 | negative |
| | 20 | 0.9569 | none |
| | 7 | 0.8714 | negative |
| | -4 | 0.7373 | negative |
| | -16 | 0.8270 | negative |
| | -27 | 0.7707 | negative |
| | -36 | 0.8136 | negative |
| SGH103 | 31 | 0.8939 | negative |
| | 19 | 0.8736 | negative |
| | 7 | 0.7023 | negative |
| | -5 | 1.0493 | none |
| | -16 | 0.7500 | negative |
| | -28 | 0.7984 | negative |

Table 4.14: Europium anomalies for Lubin mining district samples. $Eu/Eu^* = Eu_N/(Sm_N*Gd_N)^{0.5}$. $Eu_N = Eu_{sample}/Eu_{PAAS}$.

| Location | Depth | Eu/Eu* (PAAS) | Present or Absent |
|---|---|---|---|
| Rudna 1 | 40 | 0.9464 | negative |
| | 20 | 1.0386 | none |
| | 10 | 1.0395 | none |
| | 0 | 1.0603 | positive |
| | -10 | 1.0949 | positive |
| | -25 | 1.2795 | positive |
| | -130 | 1.2209 | positive |
| Rudna 2 | 20 | 0.9455 | negative |
| Lubin 1 | 110 | 0.9623 | none |
| | 40 | 0.9567 | none |
| | 20 | 0.9875 | none |
| | 0 | 1.0610 | positive |
| | -10 | 1.2627 | positive |
| | -20 | 1.2464 | positive |
| | -120 | 1.3234 | positive |
| Lubin 2 | 120 | 1.0771 | positive |
| | 50 | 1.1265 | positive |
| | 30 | 1.1421 | positive |
| | 25 | 1.0178 | none |
| | 20 | 1.0689 | positive |
| | 0 | 1.1050 | positive |
| | -2 | 1.1134 | positive |
| | -4 | 1.1263 | positive |
| | -5 | 1.1945 | positive |
| | -50 | 1.3450 | positive |
| | -120 | 1.2437 | positive |

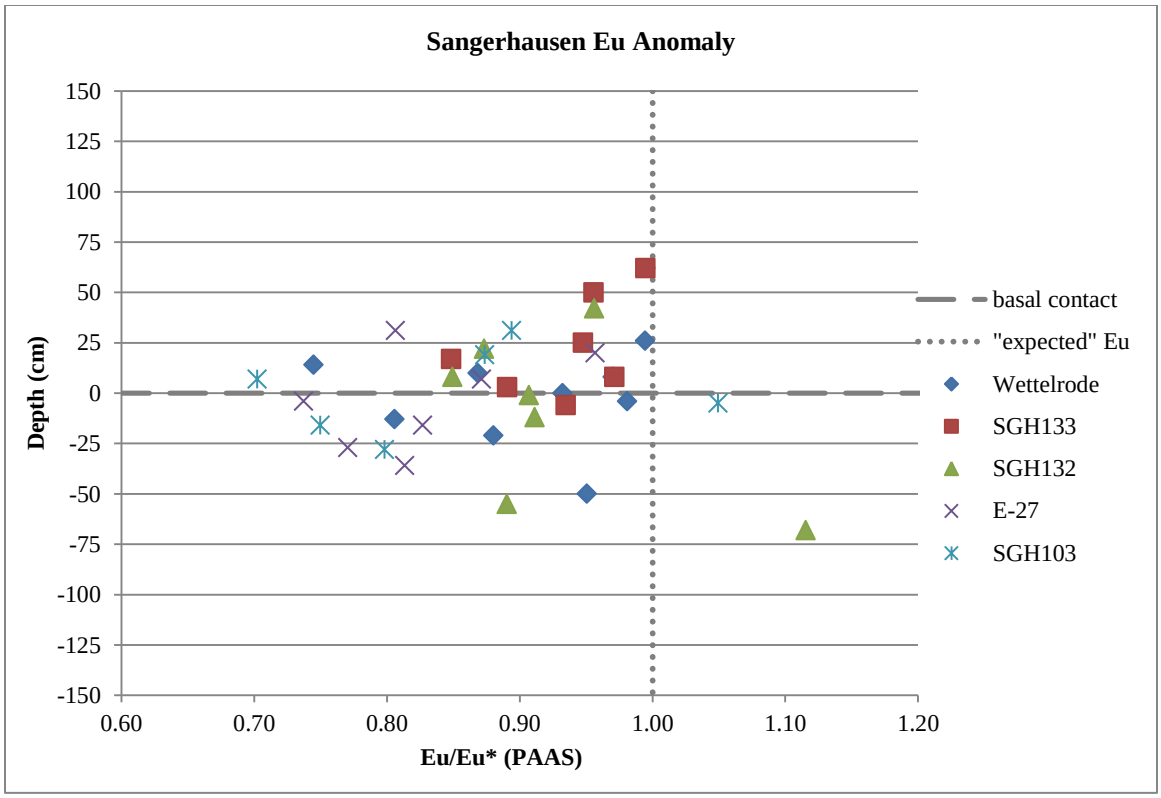


Figure 4.155: Illustration of the Eu anomaly data (Table 4.12) by depth for Sangerhausen Basin samples.

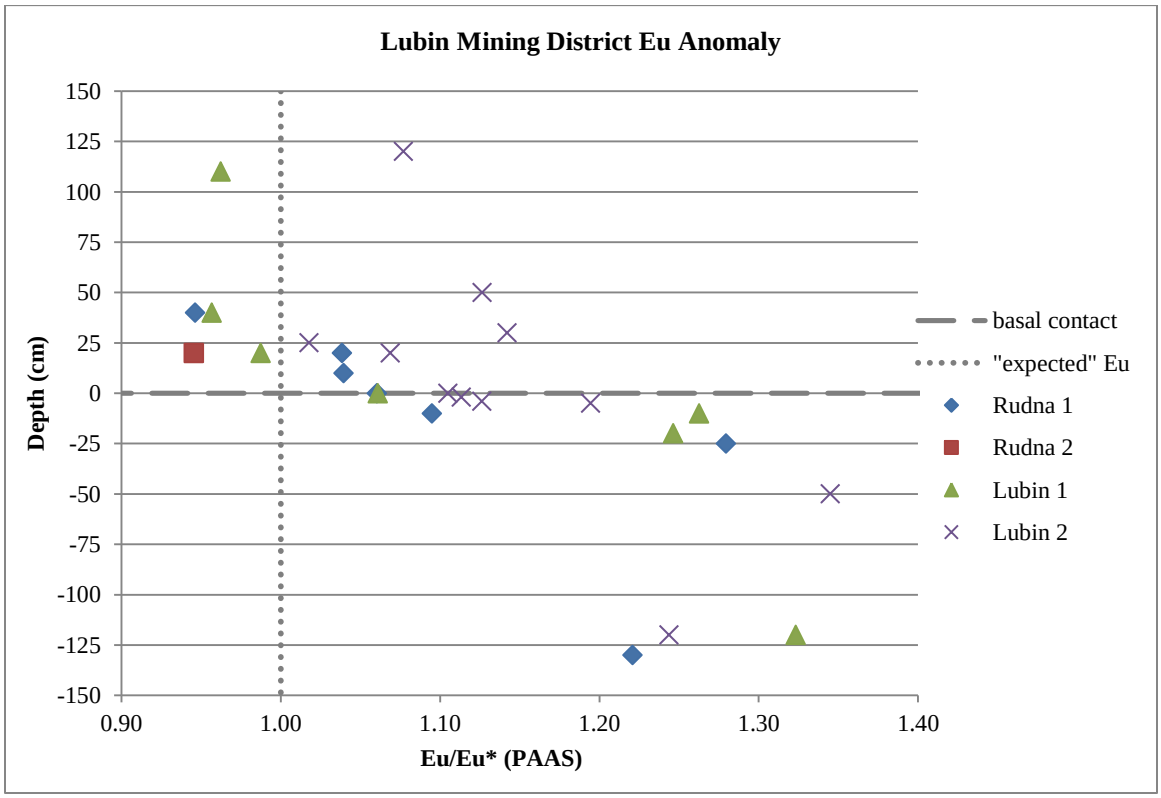


Figure 4.156: Illustration of the Eu anomaly data (Table 4.13) by depth for Lubin mining district samples.

# CHAPTER 5 - DISCUSSION

The mineralization and geochemistry documented in this study of the Kupferschiefer in the Sangerhausen Basin are broadly similar to those of the Kupferschiefer in the Lubin mining district, and to those reported in previous studies of the Kupferschiefer in both locations. Small but intriguing differences are present between the Sangerhausen Basin and Lubin mining district samples from this study, and in comparison to some of the other studies done at these locations. Some of these differences are illustrated in Table 5.1 at the end of the chapter.

## 5.1 Mineralization

Comparisons in macro- and micro-mineralization between the Sangerhausen Basin and Lubin mining district samples show that sulfide mineralization is more abundant in the Lubin mining district. Pyrite framboids in particular are much more common in the Lubin mining district than in the Sangerhausen samples. Most of macro-mineralization in Sangerhausen samples is the color of chalcopyrite, with only a few occurrences of chalcocite. Macro-mineralization in Lubin mining district samples is mostly chalcocite, with occasional occurrences of chalcopyrite, pyrite, and bornite. Another minor distinction between the Sangerhausen Basin and Lubin mining district is that the Sangerhausen exhibits macro-aggregate mineralization in almost every sample taken 7 or more cm above the basal contact of the Kupferschiefer, while the Lubin mining district exhibits almost exclusively macro-bleb and macro-disseminated mineralization, with only a few macro-aggregates. Thin, bedding-parallel horizons of mineralization are more common in the Sangerhausen as well.

The macro- and microscopic mineralization observed in Sangerhausen Basin and Lubin mining district samples, regardless of the abundance, is consistent with observations made in the Lubin mining district by Krouse *et al.* (2006) and Oszczepalski (1989). These authors noted that Kupferschiefer mineralization is generally in the form of micrometer-scale disseminated mineralization (up to ~80%), and rarely as small veins or more massive forms such as coarser grained aggregates and lenses. Mineralization in the form of blebs and disseminated spherules, as described in the samples of this study,

are similar to the granules, flasers, and lenses of mineralization described by Kucha and Pawlikowski (1986). The samples from this study exhibit almost every form of mineralization identified by Sawłowicz (1990): spherules, aggregates, clusters, large grains, framboids, dispersed mineralization, lenses, and irregular clusters. Features similar to laminae bending around sulfide grains, as recorded by Oszczepalski (1989), are observed in the samples from this study, for example carbonate grains that bend around sulfide mineralization 61 cm above the contact in core SGH103.

In addition to hematite ($Fe_2O_3$) and native copper (Cu), thirteen Cu- and Fe-sulfide minerals - chalcocite ($Cu_2S$), bornite ($Cu_5FeS_4$), chalcopyrite ($CuFeS_2$), covellite (CuS), digenite ($Cu_9S_5$), pyrite ($FeS_2$), galena (PbS), sphalerite ([Zn,Fe]S), djurleite ($Cu_{31}S_{16}$), anilite ($Cu_7S_4$), geerite ($Cu_8S_5$), spionkopite ($Cu_{1.4}S$), and yarrowite ($Cu_9S_8$) are reported by multiple authors (Rose, 1989; Large *et al*., 1995; Gablina and Lur'e, 2001). Eight of these sulfide minerals were recorded in the Sangerhausen and Lubin/Rudna samples studied in this thesis: chalcocite, bornite, chalcopyrite, covellite, digenite, pyrite, galena, sphalerite. Two of these, galena and sphalerite, were each only observed in one or two thin sections.

Pyrite framboids in the Lubin mining district samples occasionally show a bornite rim. The pyrite is most likely syndepositional/bacterial in nature, with the bornite rim resulting from later (syndiagenetic) alteration. These bornite rims may actually be a "cement," similar to the cobaltite "cement" observed around pyrite framboids by Large *et al.* (1999). It is possible that some of the disseminated or framboidal mineralization within the Kupferschiefer, that is not composed of pyrite, could be primary as well. Chalcocite framboids in the Nonesuch Shale of White Pine, Michigan, have been determined to be morphologically distinct from the pyrite framboids (Alyanak and Vogel, 1974). Sawłowicz (1990) noted that textures, chemistry, and features of the copper sulfides (digenite, chalcocite, and covellite in the form of disseminated spherules, framboids, aggregates, etc.) that differ from pyrite framboids suggest that the former are primary precipitates.

One of the differences between the Sangerhausen Basin and the Lubin mining district lies in the association, or lack thereof, between sulfide mineralization and quartz or carbonate features. For

example, sulfide mineralization is occasionally observed preferentially in association with lenses of relatively coarse quartz (and sometimes carbonate) grains within the Lubin mining district Kupferschiefer. This feature is not observed in the Sangerhausen Kupferschiefer, partially because of the lack of these coarser-grained lenses among the alternating lenses of carbonaceous and carbonate material within the samples.

In Sangerhausen Basin thin sections, sulfide mineralization is rarely associated with quartz or carbonate veins, whereas this characteristic is relatively common in Lubin mining district samples. This may be in part due to the lower abundance of quartz and carbonate veins in Sangerhausen samples. However, even when these features are present, the sulfide mineralization is rarely associated. In the thin section from 30 cm above the contact in Lubin 2, there are covellite-bornite-chalcopyrite ($CuS$-$Cu_5FeS_4$-$CuFeS_2$) blebs associated with a carbonate vein. At least 2 periods of growth (or alternating mineralization and calcite growth) can be discerned. The presence of covellite, bornite, and chalcopyrite in association with a carbonate vein differs only slightly from the sulfide mineralization observed by Large *et al.* (1995) in association with gypsum ($Ca(SO_4)\bullet 2H_2O$), anhydrite ($Ca(SO_4)$), and atacamite ($Cu_2Cl(OH)_3$) veins in that the samples from this study lacked the presence of yarrowite ($Cu_9S_8$). At the basal contact in Lubin 2, mineralization is mostly found along laminations and is relatively abundant alongside calcite veins and carbonate lenses, but more abundant within carbon/clay lenses than in carbonate. There is interstitial bornite with "flower" shaped blebs of chalcopyrite within, 100 cm below the contact in Rudna 2, possibly resulting from an incomplete replacement or alteration. Blebs showing zoned mineralization are more common in Lubin mining district samples than in Sangerhausen Basin samples. In Lubin mining district samples, blebs that show, from rim to center: chalcopyrite ($CuFeS_2$), bornite ($Cu_5FeS_4$), covellite ($CuS$), digenite ($Cu_9S_5$), are relatively common. Gablina and Lur'e (2001) found the sequence of replacement to be: pyrite ($FeS_2$) - chalcopyrite ($CuFeS_2$) - bornite ($Cu_5FeS_4$) - covellite ($CuS$) - digenite ($Cu_9S_5$) - (djurleite ($Cu_{31}S_{16}$), native copper ($Cu$)). This sequence requires impeded water exchange, since free water-exchange would result in the formation of unstable mineral associations (i.e. pyrite + djurleite, chalcopyrite + digenite) and disrupt the zonation as determined by

Gablina and Lur'e (2001). In Lubin and Rudna thin sections, covellite and digenite was observed, while in Sangerhausen thin sections replacement was only observed up to chalcopyrite and occasionally bornite.

Krouse *et al.* (2006) found polymineral veins in samples from the Lubin mine composed, from center to margin, of chalcocite-bornite-chalcopyrite ($Cu_2S$-$Cu_5FeS_4$-$CuFeS_2$). Some of these veins exhibit an irregular boundary between bornite and chalcocite, and signs of replacement of chalcocite by bornite. Some of the polymineral veins observed in the Lubin and Rudna samples studied in this thesis are composed of bornite with chalcopyrite margins; it is possible that these veins, like those observed by Krouse *et al.* (2006), originally had a chalcocite center that has since been completely replaced.

Hirst and Dunham (1963) note that there are mineralization lenses, independently oriented compared to any bedding plane within the Marl Slate, where sulfides are intergrown with carbonates in such a way as to suggest that an open space was present and later filled in with a carbonate lining and then sulfides. A feature similar to this is found in the thin section from 40 cm above the contact in Rudna 1, where sphalerite is surrounded by dolomite crystals, giving the appearance of sulfide mineralization within a carbonate dissolution cavity (Figure 5.1). Sulfide mineralization and carbonate are closely associated in the thin section from 31 cm above the contact in core SGH103 as well, where dolomite is surrounded by an aggregate of sulfide mineralization. Another instance of sulfide mineralization associated with carbonates is described by Jowett *et al*. (1987); the authors note that sulfide mineralization within the Weissliegend of the Lubin mining district occurs as disseminated spots or concretions, replacing calcite cement and quartz grains, and sometimes composed of chalcocite-bornite-chalcopyrite zones from inside to outside. Jowett *et al*. (1987) estimate that this sulfide mineralization is composed of up to 25-30% Cu.

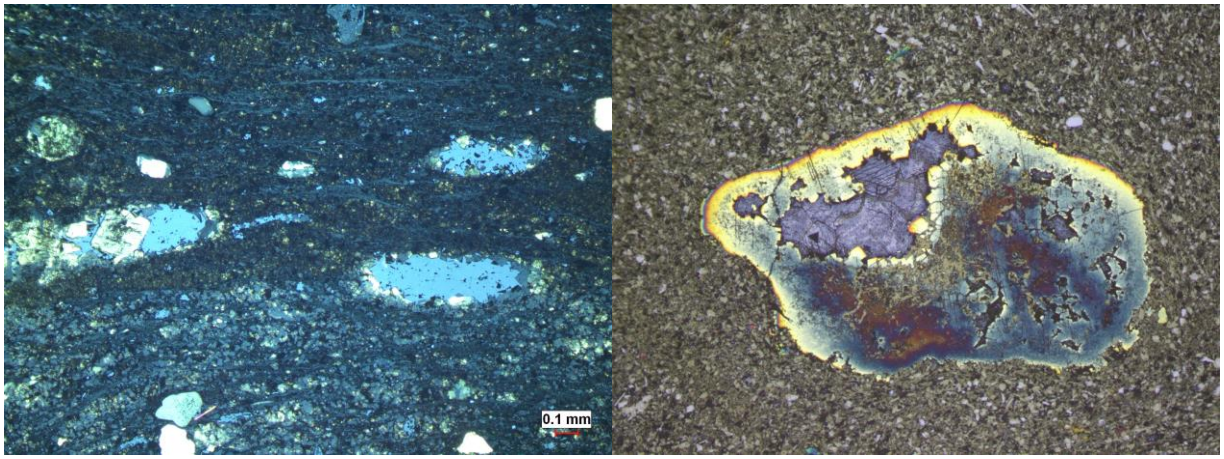

Figure 5.1: The photomicrograph on the left shows sphalerite in what appear to be dolomite dissolution cavities. The photomicrograph on the right shows dolomite surrounded by sulfide mineralization in sample K61+31 from core SGH103, Sangerhausen Basin; colors are distorted due to carbon coating and tarnish. Width of photomicrograph is ~2.5 mm. Note: both photomicrographs were taken under a combination of transmitted and reflected light.

The higher abundance of sulfides in the Lubin mining district samples correlates with higher copper concentrations compared to the Sangerhausen samples. The abundance of chalcocite ($Cu_2S$), and the very rare observation of galena (PbS) or sphalerite ([Zn,Fe]S), suggest that both the Sangerhausen Basin samples and the Lubin mining district samples are an intermediate distance from the Rote Fäule, within the Cu zone. The Kupferschiefer in these locations is not close enough to the redox boundary to be rich in Ag and Pt (PGE zone), nor is it distant enough to be within the Pb and Zn zones. Although petrographic observations suggest that the Sangerhausen Basin locations are not completely within the Pb and Zn zones, geochemical analyses show that Sangerhausen Basin samples exhibit higher concentrations of Pb and Zn, and lower concentrations of Cu, compared to the Lubin mining district samples. From these data, a comparative distance from the two basins to the Rote Fäule can be determined; i.e. the samples from the Sangerhausen Basin are comparatively distal to the Rote Fäule, and those from the Lubin mining district are comparatively proximal.

Weissliegend samples in both the Sangerhausen Basin and Lubin mining district exhibit chalcopyrite ($CuFeS_2$), chalcocite ($Cu_2S$), bornite ($Cu_5FeS_4$), and digenite ($Cu_9S_5$); the last two are more common in Lubin mining district samples. Sulfide bands, or "ore laminae" (Kucha and Pawlikowski,

1986), are observed in Weissliegend samples 50 cm below the contact in Wettelrode, 10 cm below contact in Rudna 1, and 120 cm below the contact in Lubin 1. Similar features, where sulfide laminations are proximal to conglomerate layers or associated with sulfide blebs are observed ~36 cm below the contact in E-27 and 120 cm below the contact in Lubin 2, respectively. The sample from 13 cm below the contact in Wettelrode exhibits macro-blebs of sulfide mineralization that are roughly aligned along bedding-parallel horizons. Similar to the description by Kucha and Pawlikowski (1986), the parallel bands or laminae are composed of cement-like chalcocite, separated on the order of centimeters by a layer of relatively barren white sandstone. The sulfide layers exhibit a sharp bottom boundary and a transitional top boundary. It is possible that the sulfide bands 120 cm below the contact in Lubin 2 indicate the presence of hematitic laminae traversing the chalcocite, resulting in the presence of chalcopyrite and bornite (Kucha and Pawlikowski, 1986). Alternatively, the chalcopyrite, bornite, and digenite may simply be the result of replacement.

**5.2 Sedimentary Lithology and Fabric**

The Kupferschiefer in the Sangerhausen Basin is broadly similar to the Kupferschiefer in the Lubin mining district. In both locations the lower portion of the Kupferschiefer exhibits alternating lenses of carbonaceous and carbonate material, grading upwards into a carbonate-rich matrix. These lenses at the base of the unit have also been noted by Oszczepalski and Rydzewski (1987). The authors describe the alternating lenses as discontinuous, alternating laminations of carbonate and organic material that may be flat, wavy, or lenticular in shape, and note that the light laminae are composed of a mix of clay and carbonate material, while the dark laminae are composed of clay, organics, and carbonates. The Sangerhausen and Lubin locations are different in that the alternating lenses are more clearly defined in the Sangerhausen Basin; it is not unusual for the carbonaceous lenses in the Lubin mining district to be obscured by fine carbonate or detrital quartz grains. In general, detrital quartz grains are much more abundant in Lubin mining district Kupferschiefer samples than in Sangerhausen Basin samples.

In cores SGH133, SGH132, E27, and SGH103, the alternating lenses are more rich in carbonate at and above approximately 20 cm above the contact. Geochemical analysis agrees with this observation,

as MgO shows higher concentrations in samples ≥20 cm above the contact. This change in sample composition and geochemistry indicates the transition from the carbon- and clay-rich section of the Kupferschiefer to the carbonate-rich section. Further increases in Mg and Ca concentrations, and the shift from alternating lenses to a matrix composed of carbonate material, indicate the gradation into the overlying Zechstein limestone.

The thicknesses of the alternating carbonaceous and carbonate lenses vary by depth, but also from lens to lens within each thin section. However, most of the carbonate pods between the contact and about 20 cm above the contact, before the samples become relatively carbonate-rich, are 0.1 to 0.2 mm thick (rare carbonate lenses are observed with thicknesses of up to 0.3 mm). Considering that these are the thicknesses post-compaction, and assuming the alternating pods of organic carbon and carbonates in the lower portion of the Kupferschiefer are the result of cyclical, possibly annual deposition as suggested by Hirst and Dunham (1963), perhaps the result of planktonic organism activity, I suggest that the rate of deposition was at the very least ≥0.1 mm/season during carbonate deposition (presumably summer, when planktonic organisms would be most active).

The presence of insect remains within mud lenses in at least two of the Sangerhausen Kupferschiefer samples (Figures 4.56 and 4.60) suggests a depositional environment other than the "shallow marine" environment generally attributed to the Kupferschiefer. The water depth would have needed to be shallow enough for the insects to get stuck in the substrate, or sink a very short distance to be buried and preserved within the substrate. This suggests a near-shore environment, perhaps similar to a modern day wetland. Oszczepalski (1989) notes that features associated with an extremely shallow marine environment, such as ripples, mud cracks, scours, burrows, etc., are absent from the Kupferschiefer, though localized bioturbation has been observed, and it is possible that some of the samples from this study exhibit ripple forms. It is nearly impossible to confirm that these alternating lenses are in the form of ripples (Figure 4.55) and not simply disturbed or wavy lenses. If these features are indeed ripples, however, it would suggest that the depositional environment was not perpetually stagnant, and that a sufficient current of water was present at one time to form the sedimentary structures.

Some features are only observed in a single sample; for example, the darker material inter-tonguing with white sandstone observed in the sample from 28 cm below the contact in core SGH103 is a feature unique to that sample (Figure 4.24). Geochemical analysis shows a slight increase in Al, K, Na, and Mn relative to the Weissliegend sample above it; little to no S is present in the sample, and under the reflecting light microscope interstitial chalcocite is only rarely observed. This suggests that the black "swirling" material is more likely to be carbonaceous or clay in composition than sulfide mineralization. Another unique feature is the ~1 mm patch of poikilotopic calcite cement in the sample from 10 cm below the contact in Rudna 1. This feature has been observed in previous studies of the Lubin mining district; Mayer and Piestrzyński (1990) noted that poikilotopic calcite can be abundant in the barren sandstone above sulfide bands. The cement is an early diagenetic feature, indicated by the uniform extinction and the increased compaction outside of the cement compared to the grains within the cement. This indicates that the calcite cement formed before the sandstone was compacted.

The Boundary Dolomite is only found between Kupferschiefer and Weissliegend samples from the Lubin mining district (Rudna 1, Lubin 1, and Lubin 2), which is consistent with previous studies that have only reported the Boundary Dolomite in the Lubin mining district (Kucha and Pawlikowski, 1986; Peryt, 1989; Jasinski, 1994; Rospondek *et al*., 1994; Large *et al*., 1995; Large and Gize, 1996; Large and Small, 2000; Pieczonka and Piestrzyński, 2011). In thin sections from Lubin 2 samples, the contact between the Boundary Dolomite and the Kupferschiefer is inter-tonguing. This contrasts with the sharp contact between the Kupferschiefer and the Weissliegend observed in locations that lack the Boundary Dolomite.

Aside from the differences in sulfide composition and abundance within the Sangerhausen Basin and Lubin mining district Weissliegend previously noted, there is also a difference in grain size and sorting. Weissliegend samples from the Lubin mining district are all composed of fine to very fine sandstone, while at least one Weissliegend sample from each of the 5 Sangerhausen Basin locations exhibit coarse sand grains, laminations of granules, and/or layers of conglomerate. In thin section, the Sangerhausen Weissliegend samples are much more likely to be moderately poorly to very poorly sorted,

while the Lubin mining district samples are more likely to be moderately well sorted. Furthermore, grains in the Lubin mining district Weissliegend are almost exclusively sub-rounded, while Sangerhausen Weissliegend grains are more likely to be sub-rounded to sub-angular and angular. These differences in grain character could simply be the result of different sampling techniques; almost all of the Sangerhausen locations represent a nearly continuous stratigraphic section, whereas Lubin and Rudna locations have large sections of the column unaccounted for. The differences could also be the result of different sources, or, as suggested by the disparity in sorting and roundness between the two basins, different energy levels at the time of deposition.

Further support for different sources comes from the actual composition of the Weissliegend grains. In both basins, the sandstone is composed mostly of quartz and feldspar (particularly orthosite). Volcanic clasts are much more common in the Sangerhausen Weissliegend, and relatively rare in the Lubin mining district Weissliegend. This suggests that there was a volcanic source (either active or being eroded) relatively close to the Sangerhausen Basin.

Grains are cemented with calcite, and rarely anhydrite; some samples also exhibit very small amounts of silica cement. Porosity differs by location and varies from sample to sample with no clear pattern in changes in porosity with depth. In the Sangerhausen Basin samples, porosity is more likely to be present in samples closer to the basal contact of the Kupferschiefer. Weissliegend samples from the Lubin mining district are more likely to show porosity in all samples to some degree, with the exception of a few samples close to the basal contact of the Kupferschiefer, which exhibit little to no porosity. These differences in cementation and porosity could have implications for fluid flow, but the temporal relationship between the cement and other petrographic features was not explored in this study, so no definite comment can be made on the influence of the cement on fluid migration, or the possible effect of fluid migration on cement.

### 5.3 Veining

Veins composed of quartz, carbonate, and/or sulfide mineralization are present in both the Sangerhausen and Lubin mining district basins, but veins in general are more abundant in samples from

the Lubin and Rudna locations. Quartz veins are slightly more abundant than carbonate veins in Sangerhausen samples, while carbonate veins are much more abundant than quartz veins in Lubin and Rudna samples. Bedding-parallel and -perpendicular fractures in samples from both locations are sometimes filled with carbonate precipitates.

Bedding-parallel horizons of mineralization observed in samples above the basal contact may be indications of preferential fluid flow, or perhaps a layer that was especially rich in organic matter, resulting in a stronger localized reducing environment, and thus preferential sulfide precipitation. Such features are observed in the lower 14 cm of the Kupferschiefer in each of the Sangerhausen locations. Mineralization oriented perpendicular, or at a high angle, to the bedding is more common further from the basal contact, at approximately 31 to 42 cm above the contact. A small bedding-perpendicular vein is present 8 cm above the contact in SGH133, but it is directly associated with a bedding-parallel mineralization horizon.

Other possible indicators of fluid flow include elongated blebs that are oriented nearly perpendicular to the bedding; these could be indicative of local bedding-perpendicular flow. A few samples, such as the one taken 1 cm above the contact in core SGH133, exhibit a mineralization horizon that occasionally "steps up" perpendicular to the bedding (<1 mm), which is likely evidence for a combination of bedding-parallel and -perpendicular flow. The hand sample taken from 7 cm above the contact in core E-27 exhibits approximately bedding-parallel carbonate material that "steps up" perpendicular to the bedding, as if the fluid has been forced upwards. Mineralization is present at the top of this carbonate vein; if the mineralization occurred after the carbonate was formed, it might have been following the pathway previously formed by the carbonate. In the sample from 20 cm above the contact in E-27, there are horizons of quartz, and a bedding-perpendicular plane (~1 cm tall and 0.5 cm thick) of disseminated dolomite; the bedding appears as though it has been disturbed in this area. It may be that fluid was forced upwards, since the main orientation of the vein is bedding-perpendicular, and appears to have irregular bedding-parallel spreading (Figure 5.2).


Figure 5.2: Sample K53+20 from core E-27; note the bedding-perpendicular vein with bedding-parallel spreading. Note that the photomicrograph was taken while the sample was dry.

The presence of a relatively thick (~1.5 cm), very disseminated bedding-parallel quartz "vein," 38 cm above the contact in core E-27 could indicate zones of slightly higher permeability, or be a primary sedimentary layer (Figure 4.19). In some cases, macro-aggregates of sulfide mineralization appear to be associated with quartz or carbonate veins, as in the sample from 29 cm above the contact in SGH133.

Mineralization of the Kupferschiefer is likely to have been aided by the presence of bedding-parallel and -perpendicular veins. However, using the presence of macro- and microscopic sulfide mineralization as an indication of paleo fluid flow through the Sangerhausen Kupferschiefer, it can be assumed that veins and fractures were not the sole manner of fluid transportation through the unit. The relative rarity of veins and the lack of association between the mineralization and veins within the Sangerhausen thin section suggests that, at least in this basin, the veins are not directly associated with the precipitation of sulfides.

Previous studies of the Kupferschiefer have noted bedding-parallel and -perpendicular veinlets composed of calcite and gypsum, associated with or independent of sulfides (Jowett, 1987; Warren, 2000; Schmidt Mumm and Wolfgramm, 2004; Krouse *et al.*, 2006). Jowett (1987) describes sulfide mineralization associated with bedding-parallel and -perpendicular carbonate veins, specifically of

chalcopyrite, chalcopyrite-bornite, chalcocite, or chalcopyrite-bornite-chalcocite with gypsum and calcite veins. Schmidt Mumm and Wolfgramm (2004) is one of the few studies that records the presence of quartz veins. Jowett (1987) notes that carbonate veins are not found in through-going fractures, but are of a limited extent, usually millimeter-scale in thickness and centimeter-scale in height and length. This corresponds to the observations made in this study.

### 5.4 Other Fabric Characteristics

As noted previously, localized bedding disruption is sometimes observed in the presence of sulfide mineralization. The alternating lenses or laminations of carbonate grains are bent around relatively large blebs or aggregates of sulfides. The presence of quartz and carbonate veins can also result in bedding disturbances. In the thin section from 26 cm above the contact from the Wettelrode mine, there is evidence of both bedding-parallel flow (a disseminated vein) and bedding-perpendicular flow (two bedding-perpendicular/high angle veins).

The sample from 35 cm above the contact in Rudna 2 has severely disrupted bedding (Figures 4.29 and 4.45) that is very likely to have affected, or have been affected by, fluid flow. The disruption of what appear to be bedding-parallel mineralization horizons in hand sample suggest that the disruption occurred after at least one phase of mineralization; chalcopyrite mineralization is present within the fractures between mud chips and disrupted bedding observed in thin section (Figure 5.3), suggesting that a second phase of mineralization occurred after the disruption of the sediment. It is also possible that there was only one phase of mineralization, and the disrupted macro-mineralization formed after the replacement of disrupted heavy minerals. Carbonate material present along the edges of "chunks" of bedding, visible in both hand sample and thin section, suggests that the carbonate was precipitated after the disruption of the sediment. The thin section from this sample also contains detrital quartz grains which exhibit micro-tectonic features, such as migrating boundaries and sub-grains (Figure 4.41). The features indicate a history of micro-tectonic stresses on the grains, or on the sediment as a whole; it is possible that the stresses occurred to the quartz grains previous to their deposition in the Kupferschiefer. The stress would have occurred after lithification, otherwise the bedding would not have fractured.

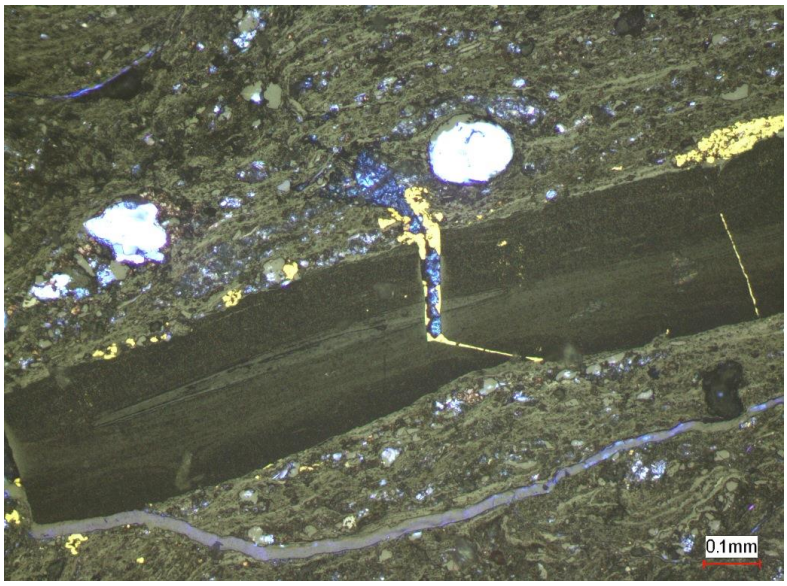

Figure 5.3: Sample K71+35, Rudna 2; sulfide mineralization (chalcopyrite) in fractured mud chips. Photomicrograph taken under reflected and transmitted (plain polar) light; the blue-white clasts are quartz grains.

### 5.5 Fluorescence and Hydrocarbons

In general, fluorescence is more abundant within Sangerhausen thin sections than the Lubin and Rudna thin sections, in samples from both above and below the basal contact of the Kupferschiefer. The sample taken 26 cm above the contact in the Wettelrode mine exhibits two different colors of fluorescence (Figures 4.58). Blue fluorescent inclusions are abundant within the carbonate vein and present in smaller amounts within the matrix; yellow fluorescence is present within the matrix adjacent to the vein and within the vein itself. Oil inclusions that fluoresce yellow indicate a lower maturation level of the oil compared to inclusions that fluoresce blue (Zhang *et al*., 2012). The presence of two maturation types suggests that there were at least two different pulses of oil, or oil from differing migration pathways, entering the Sangerhausen and Lubin mining district Kupferschiefer samples. For example, one pathway might have removed more of the asphaltic and aromatic compounds compared to the other, resulting in blue colored fluorescence as opposed to yellow. Another feature of interest within this thin section is that the most abundant fluorescence is found within the larger of the two carbonate veins present in the sample, which is oriented nearly perpendicular to the bedding. The amount of oil fluorescence within the matrix decreases with increasing distance from the vein, suggesting that the oil is

associated with the presence of the vein. It is likely that the oil was introduced by fluids whose migration was facilitated by the presence of the vein, and some of the oil managed to migrate a small distance into the surrounding matrix.

The presence of oil drops in all the Weissliegend samples from the Sangerhausen Basin and the Lubin mining district illustrates that the sandstone unit was porous and permeable. Zero to 4 cm below the contact in core E-27, interstitial oil decreases in fluorescent brightness as distance increases from the overlying Kupferschiefer. The change in brightness most likely indicates a decrease in the abundance of interstitial oil further from the basal contact of the Kupferschiefer. It is probable that the oil came from the overlying Kupferschiefer and migrated into the more porous and permeable Weissliegend. The presence of oil within the Boundary Dolomite, near the sandstone, suggests that fluids could travel into the dolomite from the overlying Kupferschiefer and/or the underlying Weissliegend.

Hydrocarbons and/or mineralization are present in the top few centimeters of some Weissliegend samples, immediately below the Kupferschiefer contact. Both cases may be the result of interaction between the Kupferschiefer and Weissliegend, where reduced fluids or hydrocarbons migrate downward from the shale into the interstitial pores of the sandstone. It is also possible that the contact with the less-permeable Kupferschiefer slowed the migration of the migrating fluids and resulted in the precipitation of the hydrocarbons and sulfide minerals.

The association of some fluorescent organic matter with sulfide mineralization, as in the sample from 10 cm below the contact in Rudna 2, supports the findings of previous studies of correlations between organic carbon/kerogen/bitumen/oil with sulfur/sulfide mineralization (ex: Poplavko *et al*., 1977; Bechtel and Püttmann, 1991; Sawłowicz, 1991). The presence of fluorescent opaque material within a few millimeters, and occasionally immediately adjacent to, reflective sulfide mineralization may be because of the reducing effect of the hydrocarbons, which could have facilitated sulfide precipitation. Not all oil is proximal to mineralization, and not all mineralization has corresponding organic matter, however. This is particularly clear in carbonate-rich samples that contain sulfide mineralization but where the only fluorescence comes from zoned carbonate grains. There are also samples, such as

K87+50 in Lubin 1, where fluorescent oil is associated with some of the sulfide mineralization within a carbonate-rich section, but not all of it.

### 5.6 Geochemistry

Most of the elements analyzed in this thesis (20 of the 33: CaO, $Fe_2O_3$, $P_2O_5$, $K_2O$, $Ti_2O$, S, Cu, Ag, U, Ni, V, Mo, Sc, Co, As, Rb, Sb, Cs, Ta, and Th) show a similar general stratigraphic trend in samples from both the Sangerhausen Basin and the Lubin mining district. Of these, $Fe_2O_3$, $P_2O_5$, $K_2O$, $Ti_2O$, S, Cu, Ag, U, Ni, V, Mo, Sc, Co, As, Sb, and Cs -in addition to Pb, Zn, Cd, and Cr- show an increased concentration within the lower ~25 cm of the Kupferschiefer in both the Sangerhausen Basin and Lubin mining district samples. The remaining elements show a decrease or no change in trend at this depth range.

#### 5.6.1 Bulk Geochemistry

Some of the geochemistry of the Sangerhausen Basin and Lubin mining district samples correlates clearly with transitions between the different units: Zechstein Limestone, carbonate- and carbon-rich Kupferschiefer, Boundary Dolomite (where present), and Weissliegend. For example, both Sangerhausen and Lubin samples show a sharp increase in Si concentrations below the contact compared to levels above the Kupferschiefer basal contact, correlating to the transition from sandstone to marly shale. This is the result of higher levels of quartz within the Weissliegend sandstone compared to the sparse detrital quartz found within the clay- and carbonate-rich Kupferschiefer. The sharp decrease in $SiO_2$ 2 and 4 cm below the contact in Lubin 2 reflects the local presence of the Boundary Dolomite between the Kupferschiefer and the Weissliegend.

Similarly related to the general makeup of the units, both Sangerhausen Basin and Lubin mining district samples show increased levels of Mg and Ca above the contact compared to below the contact, with increasing concentrations as depth decreases. This trend has also been observed in other studies (Jung and Knitzscheke, 1976), and illustrates the gradual transition between the lower section of the Kupferschiefer, which is clay-rich, and the upper section of the Kupferschiefer, which is carbonate-rich and grades into the overlying Zechstein limestone.

The samples from 50 and 62 cm above the contact in core SGH133, 42 cm above the contact in SGH132, and 20 cm above the contact in E-27 have relatively high Mg levels; these samples are most likely from the Zechstein Limestone. These samples are all relatively rich in carbonate grains (some of which exhibit zonation under fluorescent light, including carbonates within the lenses present in the sample 20 cm above the contact in E-27. The sample taken 26 cm above the contact in Wettelrode also exhibits relatively high Mg, though this most likely due to the presence of a relatively large carbonate vein. The samples taken 2 and 4 cm below the contact in Lubin 2 show relatively high concentrations of Mg and Ca, further evidence of the presence of the Boundary Dolomite.

A cross plot of $Al_2O_3$ versus $SiO_2$ yields two subgroups in the data from Sangerhausen Basin and Lubin mining district. In both locations, when the data are separated into groups according to their relation to the basal contact of the Kupferschiefer, samples from above the contact have a roughly positive correlation (Sangerhausen $R^2$=0.88246, Lubin mining district $R^2$=0.70918) where $Al_2O_3$ increases as $SiO_2$ increases (Figures 5.4 and 5.5). There is no corresponding correlation in samples below the basal contact (Sangerhausen $R^2$=0.01089, Lubin mining district $R^2$=0.19792). The positive correlation between $SiO_2$ and $Al_2O_3$ above the contact is likely the result of carbonate dilution.

A comparison of Al concentrations with K and Ti show that in Sangerhausen Basin samples, there is a strong positive correlation in samples from above the contact between Al and K ($R^2$=0.94148) (Figures 5.6 and 5.7) and between Al and Ti ($R^2$=0.97235) (Figures 5.8 and 5.9). This correlation is absent in samples from below the contact. In samples from the Lubin mining district, all samples show a positive correlation between Al and K ($R^2$=0.96063) and between Al and Ti ($R^2$=0.9699). When the data are separated by depth into samples from the Zechstein limestone, "above the contact" (i.e. Kupferschiefer), the Boundary Dolomite, and "below the contact" (i.e. Weissliegend), the data show that the lowest Al, K, and Ti values are in samples from the Boundary Dolomite, followed by the Weissliegend. The highest concentrations are in samples from the Kupferschiefer; samples from the Zechstein Limestone are among the lowest values for samples taken above the basal Kupferschiefer contact. The strong positive correlation of Al with K and Ti likely indicates that K and Ti are

incorporated in mainly clay minerals. The Al above the contact is mostly present within potassic clay material, while Al below the contact is within feldspars, including plagioclase.

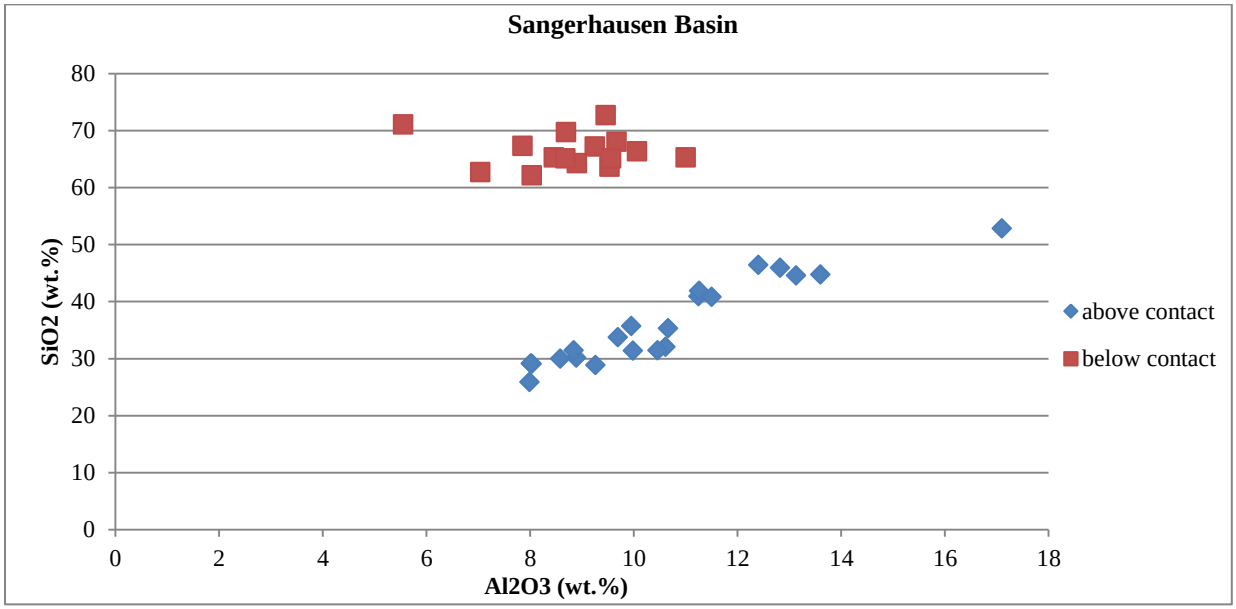


Figure 5.4: Sangerhausen data plotted according to sample position in relation to the basal contact of the Kupferschiefer. The $R^2$ value for above contact = 0.88246; $R^2$ for below contact = 0.01089

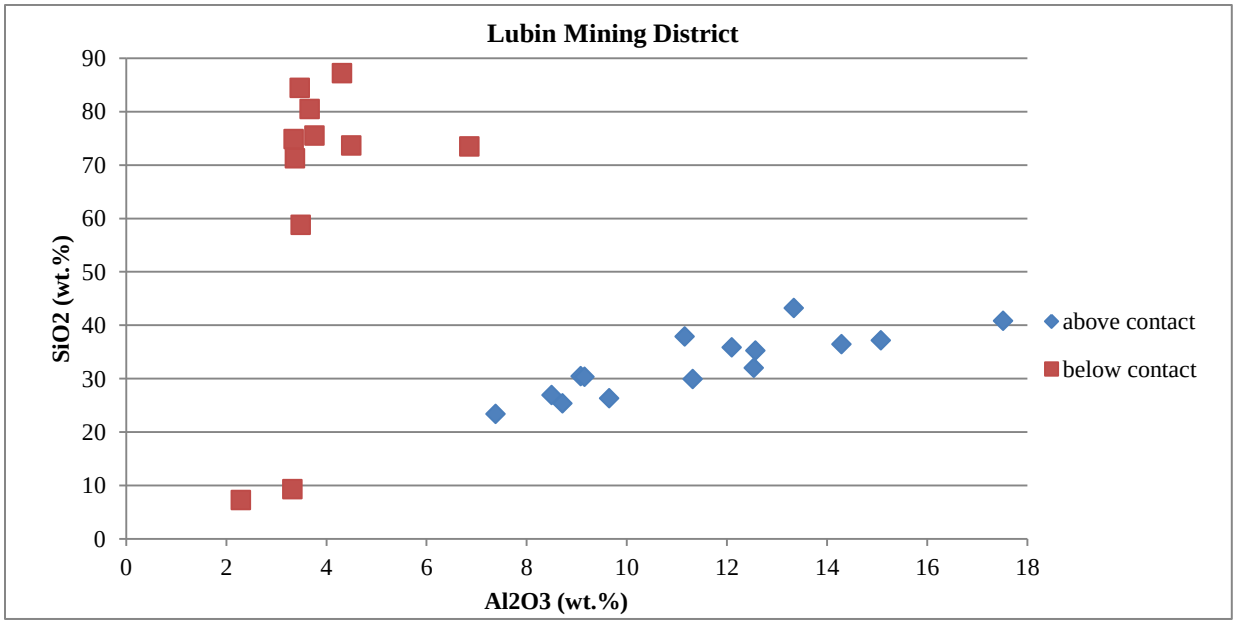


Figure 5.5: Lubin mining district data plotted according to sample position in relation to the basal contact of the Kupferschiefer. The $R^2$ for above contact: 0.70918; $R^2$ for below contact = 0.19792.

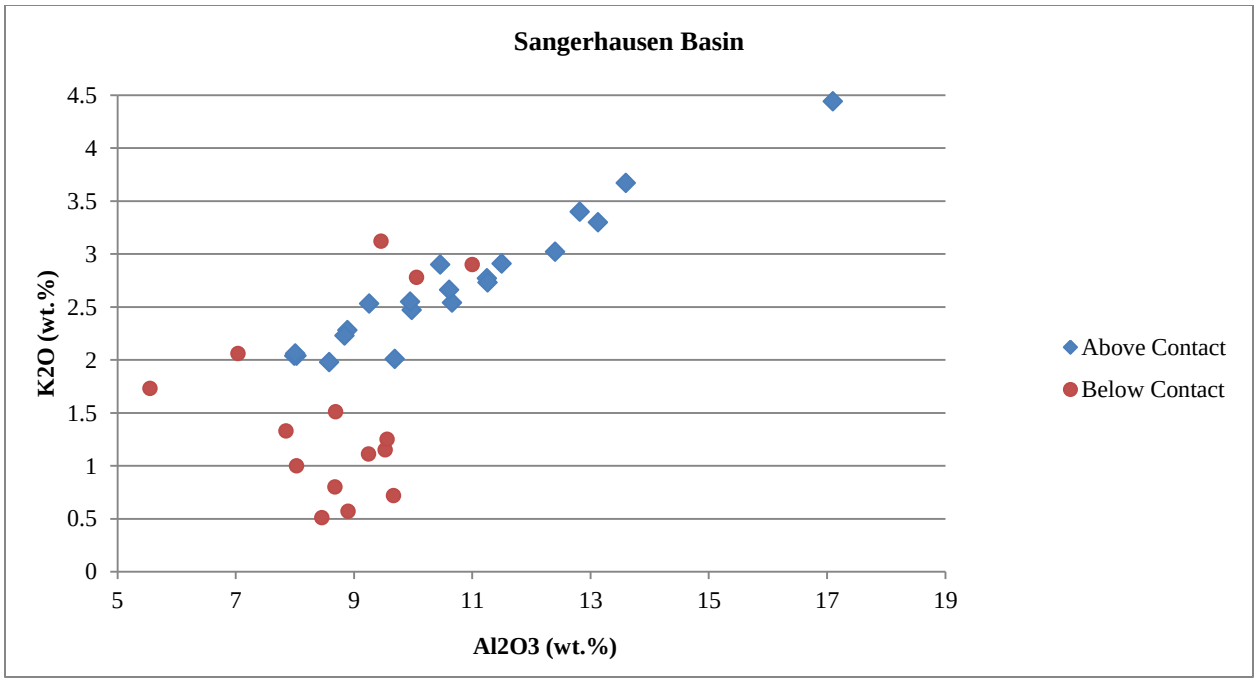


Figure 5.6: Sangerhausen samples above contact have a $R^2$ value of 0.94148; samples below contact have a $R^2$ value of 0.05278. The $R^2$ value for whole data set is 0.5372.

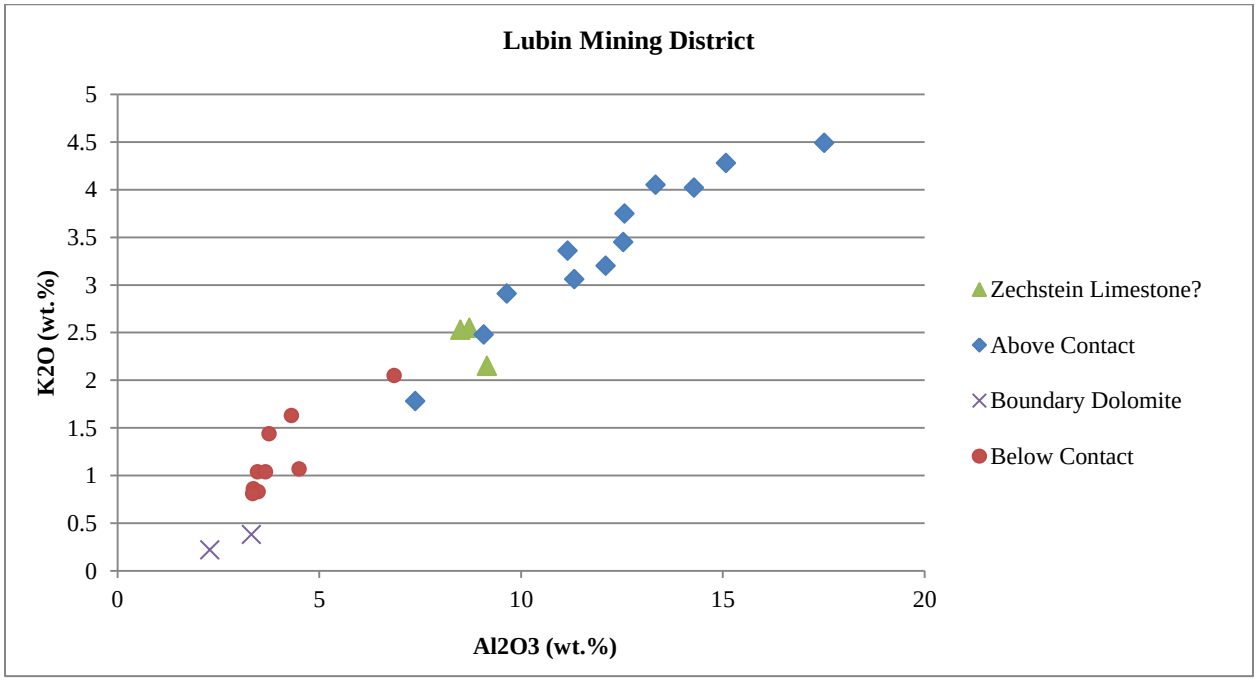


Figure 5.7: Lubin mining district samples above contact (including Zechstein Limestone) have a $R^2$ value of 0.91707; samples below contact (including the Boundary Dolomite) have a $R^2$ value of 0.74074. The $R^2$ value for whole data set is 0.96063.

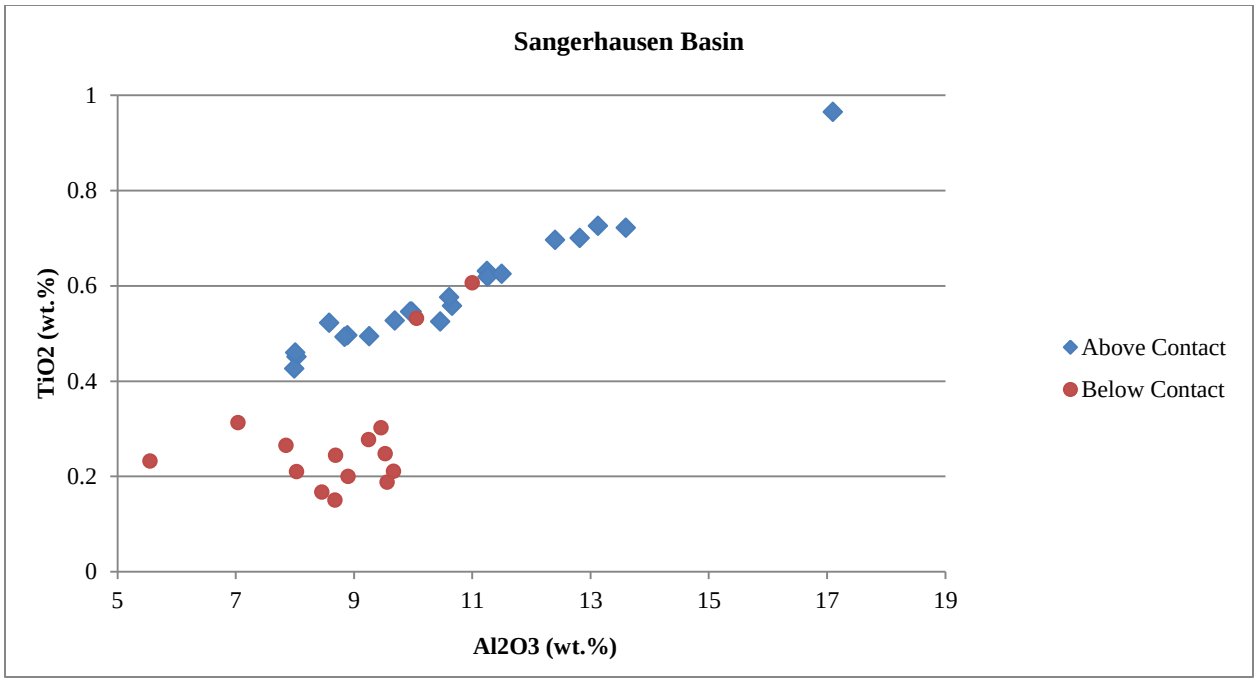


Figure 5.8: Sangerhausen samples above contact have a $R^2$ value of 0.97235; samples below contact have a $R^2$ value of 0.2207. The $R^2$ value for whole data set is 0.63956.

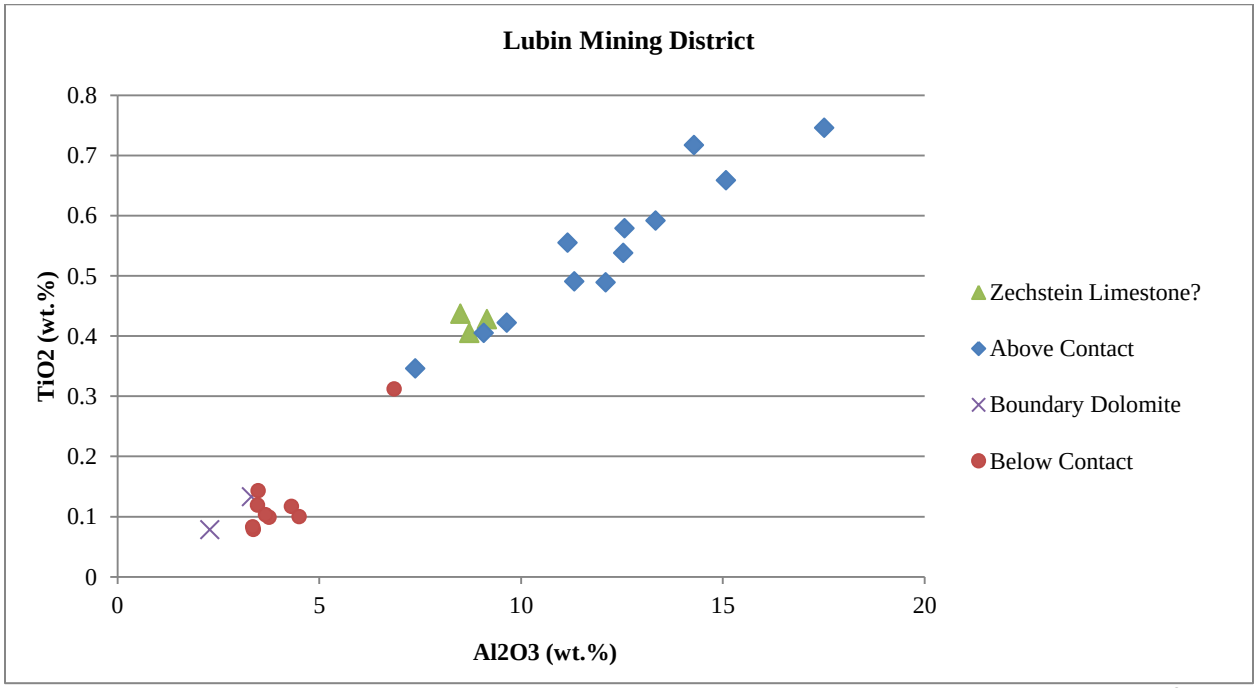


Figure 5.9: Lubin mining district samples above contact (including Zechstein Limestone) have a $R^2$ value of 0.91873; samples below contact (including Boundary Dolomite samples) have a $R^2$ value of 0.75514. The $R^2$ value for whole data set is 0.9699.

Sawłowicz (2013) notes that the Lubin mining district Kupferschiefer $P_2O_5$ values (0.16%) from is study are comparable to an average shale (listed as 0.16%). These values are slightly greater than the average $P_2O_5$ values for the Lubin mining district Kupferschiefer samples in this study (0.13%), but much lower than the average $P_2O_5$ values for the Sangerhausen Basin Kupferschiefer samples in this study (0.26%). It is suggested that some of the $P_2O_5$ observed in the Sangerhausen Kupferschiefer is syndepositional and/or biogenic in origin. It is also possible that this relative enrichment in $P_2O_5$ played a part in the enrichment of REEs in the Sangerhausen Basin, particularly the MREEs.

### 5.6.2 Metals

All of the ore metals (Cu, Ag, Pb, Zn, U) exhibit increased concentrations in the lower ~25 cm of the Kupferschiefer. The Lubin mining district has higher concentrations of Cu and Ag compared to the Sangerhausen Basin samples. The highest Pb concentration is present in the sample 20 cm above the contact in Rudna 1, but otherwise Sangerhausen samples have higher concentrations of Pb (generally ~one order of magnitude). Sangerhausen samples have higher concentrations of Zn (one order of magnitude) and U (one to two orders of magnitude) as well. As mentioned previously, the higher concentrations of Pb and Zn within the Sangerhausen Basin samples could be an indication that the Sangerhausen locations are more distal, and the Lubin mining district locations more proximal, to the Rote Fäule. The higher concentrations of U in Sangerhausen samples compared to Lubin mining district samples may reflect a correlation between U and REE enrichment within phosphates. It is also possible for U to be remobilized within sediments if an oxidant penetrates to a depth where authigenic U has accumulated; the U will reprecipitate at another location or depth, where conditions are reducing (Tribovillard *et al*., 2006). This suggests that the higher enrichment of U within the Sangerhausen samples may be the result of comparatively higher U concentrations in the underlying Weissliegend or Rotliegend, and the movement of the redox front allowed for enrichment of U within the Kupferschiefer. The increase in V concentrations in the lower 25 cm of the Kupferschiefer in both the Sangerhausen Basin and the Lubin mining district may be because V(III) substituted for Al in authigenic clay minerals (Tribovillard *et al*., 2006).

### 5.6.3 Rare Earth Elements

Some of the samples from the Sangerhausen Basin have greater concentrations of shale-normalized REEs than those seen in the Lubin mining district. Many of the samples taken above and below the basal contact of the Kupferschiefer exhibit an enrichment of MREE with respect to light and heavy REEs. The strongest MREE enrichments in the Sangerhausen Basin samples are most commonly observed in samples taken in the lower ~15 cm of the Kupferschiefer. The strongest MREE enrichments in the Lubin mining district are observed in the top ~10 to 20 cm of the Weissliegend. This discrepancy may be due to differences in redox conditions within the two basins. The correlation between MREE enrichment and the increased concentrations of other elements, as noted previously, in the lower ~25 cm of the Sangerhausen Kupferschiefer suggests that there may be an association between the REEs and the metals carried by the mineralizing fluids. Bechtel, Ghazi, *et al.* (2001) and Sawłowicz (2013) also suggest that REEs may have been carried by the migrating fluids, and REE enrichments may therefore be used as an indication of proposed fluid movement in the Kupferschiefer. If the REEs were carried along with the mineralizing fluids, then the lack of close similarity between the REE patterns (Figure 5.10) for samples taken 7 or 8 cm above the contact from locations within the Sangerhausen Basin may serve as an indication that the reactions associated with the migration and interaction of the fluids did not occur at the same stratigraphic depth across all locations. The carbonate-rich half of the Kupferschiefer is characterized by a matrix composed of "inter-tonguing grays;" this feature starts in the Sangerhausen samples between 30 and 40 cm above the contact. It appears that mineralization and element enrichment is not only concentrated within the Kupferschiefer, but specifically within the carbon-rich lower portion of the Kupferschiefer. This could be the result of the mineralizing fluid petering out, perhaps because most of the redox-sensitive elements precipitated when the fluid came into contact with the reduced Kupferschiefer, or because the volume of mineralizing fluids that passed through the units decreased with decreasing depth.

The sample from 10 cm above the contact in Wettelrode shows the highest REE concentration and the strongest MREE enrichment of all the samples in this study. This particular sample also contains

the highest concentration of Co and $P_2O_5$ of all samples, and the highest Pb (4.86%) in all the Sangerhausen samples; the only higher concentration of Pb (11.6%) is in the sample from 20 cm above the contact in Rudna 1. The correlation between high REE and $P_2O_5$ concentrations is most likely the result of REEs present within phosphate minerals.

A comparison of shale-normalized REE patterns from common phosphate minerals indicates that biogenic and authigenic phosphate exhibit a MREE enrichment, whereas apatite does not (Hannigan and Sholkovitz, 2001). Rare earth elements may also be concentrated through the diagenesis of phosphate minerals such as monazite, florencite, crandallite, gorceixite, goyazite, apatite, and xenotime (Rasmussen *et al*., 1998). Studying these minerals is made difficult by the low concentration, minute crystal size (<0.1 to 10 μm), and difficultly in performing geochemical analysis. Some of these minerals likely play a role in the MREE enrichment observed in the Kupferschiefer and Weissliegend samples examined in this thesis, as illustrated by the rough correlation between $P_2O_5$ and MREE in samples from the Sangerhausen Basin (Figure 5.11). A strong association between REEs and phosphates has been observed in other studies, as well (Byrne *et al*., 1996; Sawłowicz, 2013). The REE-$P_2O_5$ correlation is not as strong in the Lubin mining district samples (Figure 5.12). Further support for this connection is the relatively high concentration of both REE and $P_2O_5$ present in the sample from 10 cm above the contact in the Wettelrode mine from Sangerhausen Basin.

The Eu anomalies in Sangerhausen samples are almost exclusively negative anomalies, while Eu anomalies in Lubin mining district samples are almost all positive. This difference could be the result of differences in redox conditions or some other condition. Sawłowicz (2013) suggests that Eu anomalies in the Kupferschiefer, and the differences in Eu anomalies between different sections, are likely the result of the reducing conditions present during deposition and early diagenesis. It is also possible that, under highly reducing conditions, $Eu^{2+}$ migrated and re-precipitated in sections where conditions were relatively less reducing. Sawłowicz (2013) also notes that Eu anomalies that result from Eh conditions during deposition can be "eliminated" by prolonged oxidation (i.e. the presence of oxidizing fluids from the formation of the Rote Fäule).

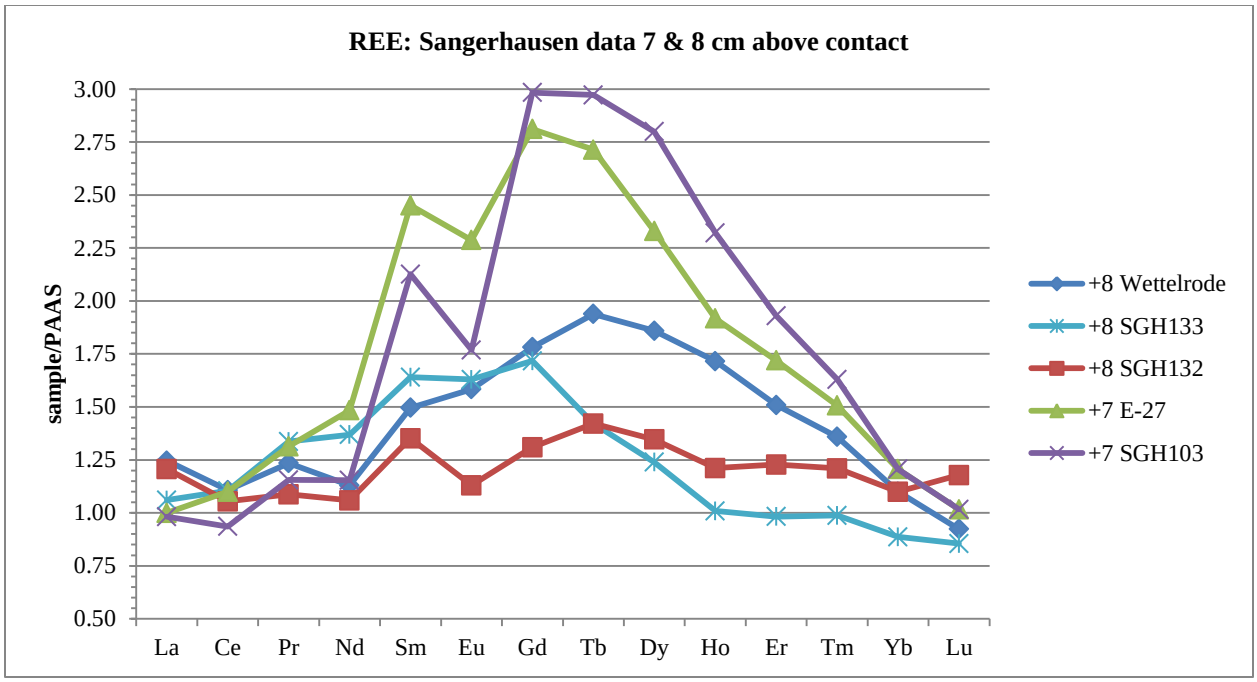


Figure 5.10: Comparison of REE data for samples taken 7 or 8 cm above the basal contact from the 5 Sangerhausen locations. Note the differences in MREE enrichment.

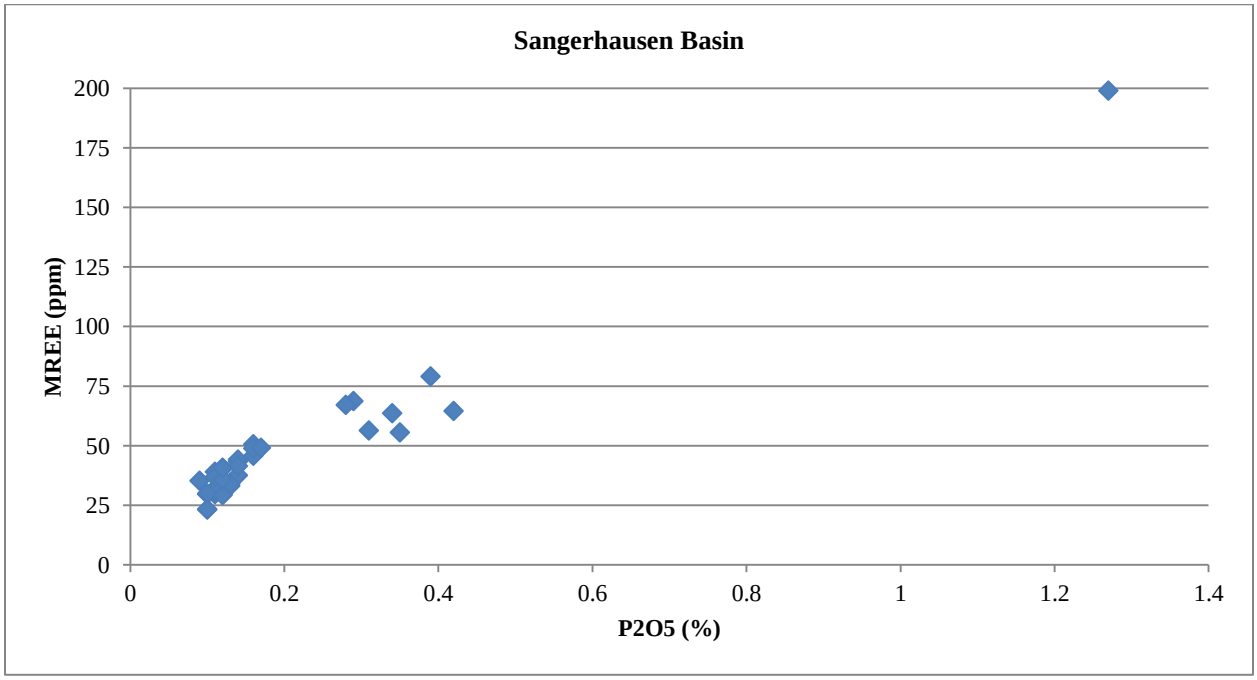


Figure 5.11: MREE versus $P_2O_5$ for Sangerhausen Basin samples; $R^2$ value = 0.95642. Excluding the data for Wettelrode +10 (198.9 MREE and 1.27 $P_2O_5$), the $R^2$ value drops to 0.79724.

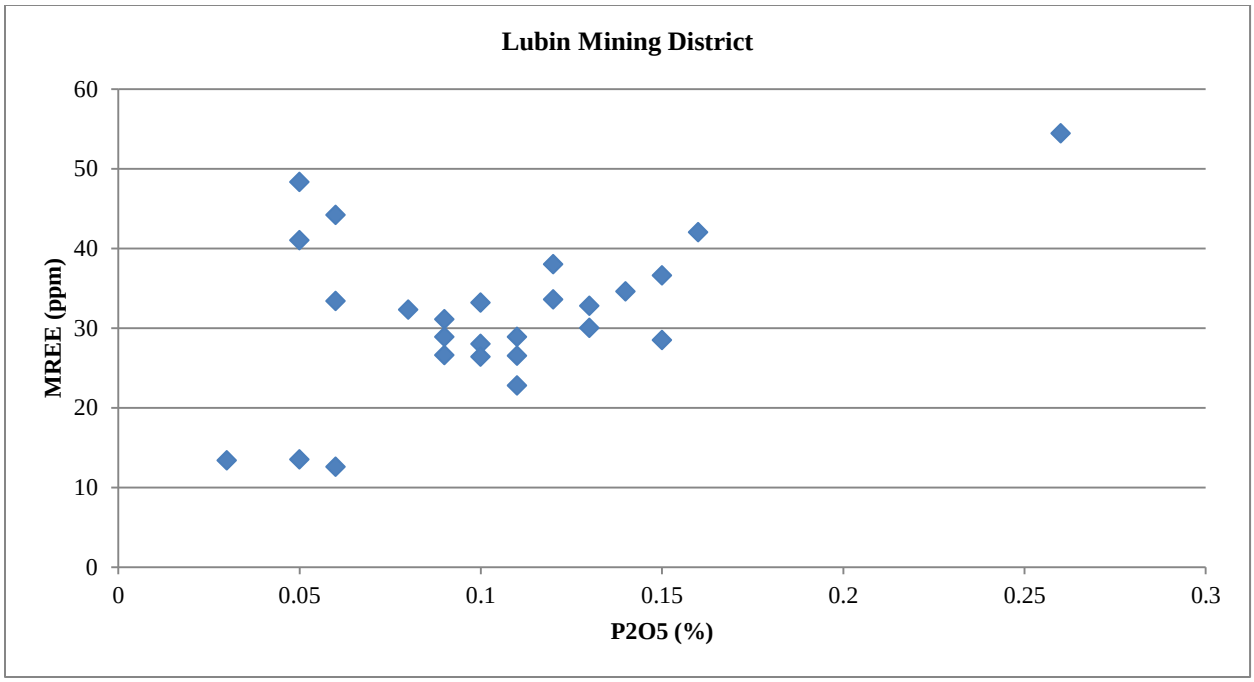

Figure 5.12: MREE versus $P_2O_5$ for Lubin mining district samples; $R^2$value = 0.22738.

Transfer of REEs from water to sediment is achieved through REE adsorption to particulate surfaces, especially those with organic coatings, and through advective transport (Elderfield *et al*., 1988). A study of pore waters from the upper ~25 cm of modern marine sediments found that REE concentrations are higher within the sediments than in the overlying sea water, and that there are systematic variations in the concentration and normalized pattern down core (Haley *et al*., 2004). Some of the cores studied by Haley *et al*. (2004) exhibit MREE enrichment patterns similar to what is seen in the Kupferschiefer samples examined in this study; the similarity includes a slight increase in HREE concentration over LREE in some cores. The authors propose that the MREE enrichment, found in cores with zones of dissolved Fe production, is the result of an Fe-bearing mineral scavenging REE from the water column. Reducing conditions are needed in the pore waters for solid Fe-oxides to release the REEs they scavenged (Haley *et al*., 2004). The influence of Fe might account for some of the MREE in the Kupferschiefer samples. When MREE (Nd+Sm+Gd+Tb) is plotted against $Fe_2O_3$, there is little to no correlation (Figure 5.13 and 5.14), but this may simply be because the reducing environment that released the REEs also resulted in Fe-oxides going into solution and thus being mobilized.

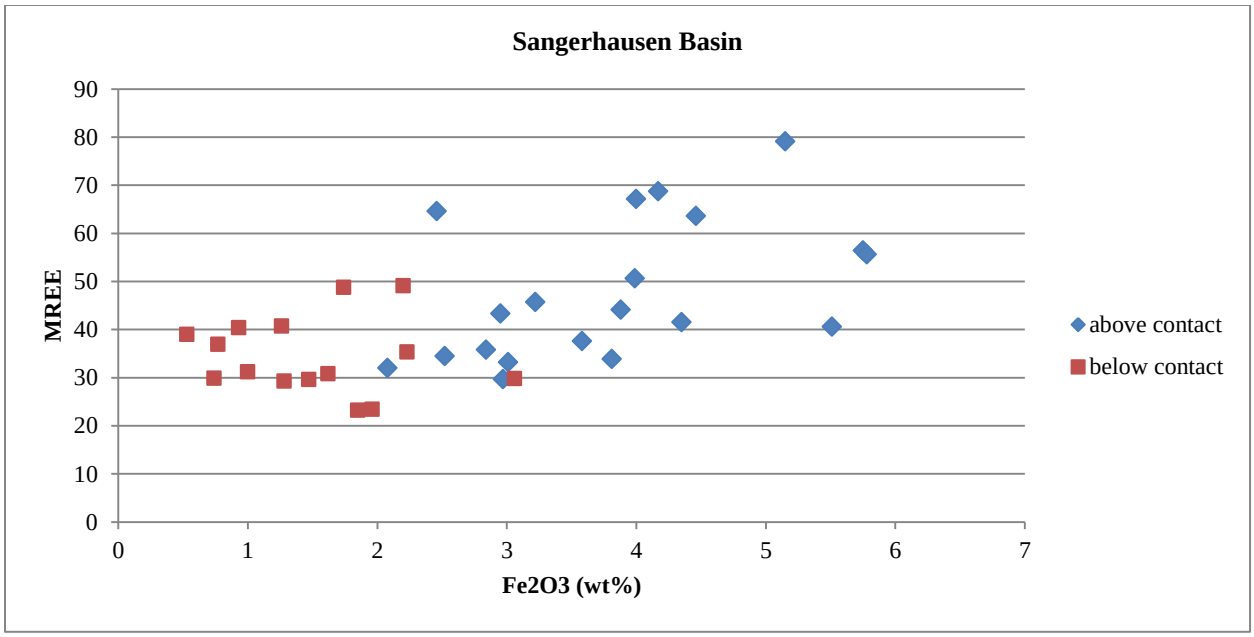


Figure 5.13: MREE versus Fe plot for Sangerhausen Basin data. NOTE: data for the sample taken 10 cm above the contact in Wettelrode, Sangerhausen was removed due to its uniquely high MREE concentration, to better view the pattern of the other samples.

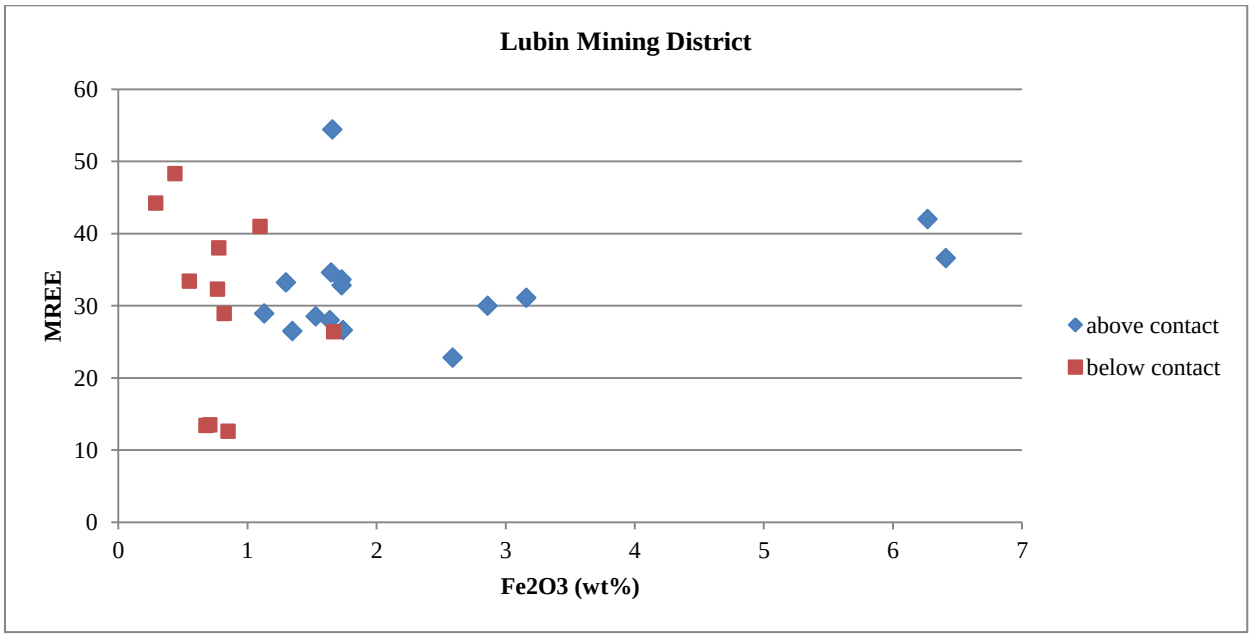


Figure 5.14: MREE versus Fe plot for Lubin mining district data.

Kupferschiefer data from Hammer *et al*. (1990), Bechtel, Ghazi, *et al*. (2001), and Lewan *et al*. (2008) show a slight MREE enrichment when normalized to PAAS (Figure 5.15). Kupferschiefer samples studied by Muller *et al*. (2008) from Mansfeld, Germany, include two slag piles and a pile of

barren rock; all three exhibit varying degrees of MREE enrichment when normalized to PAAS (Figure 5.16). In a study by Mayer *et al*. (1992), samples from the Lubin, Gomunice, and Bialogard areas show "weak but distinct" negative Ce anomalies, suggesting oxic depositional conditions. These samples show a higher sum of LREE than HREE in the Kupferschiefer, and strong negative Eu anomalies in dolomite samples. Their (patchy) data [La, Ce, Nd, Sm, Eu, Tb, Yb] hint that there might be MREE enrichment in some samples.

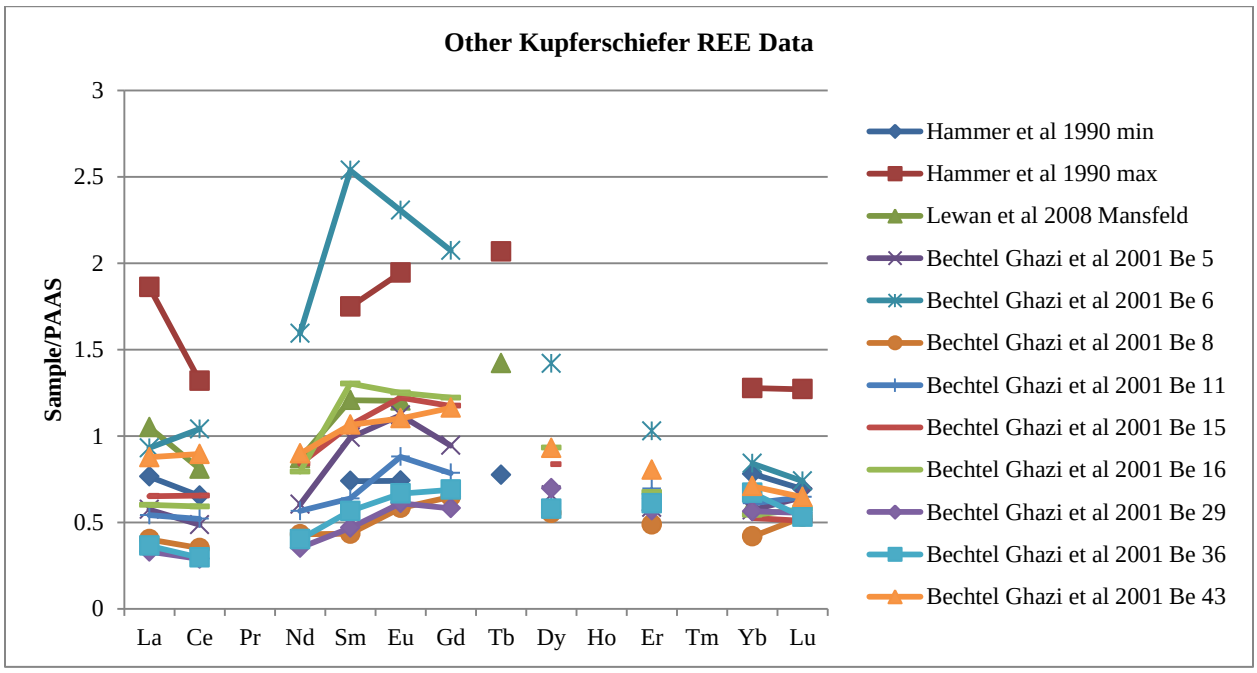


Figure 5.15: PAAS-normalized REE data from Hammer *et al*. (1990), Bechtel, Ghazi, *et al*. (2001), and Lewan *et al*. (2008).

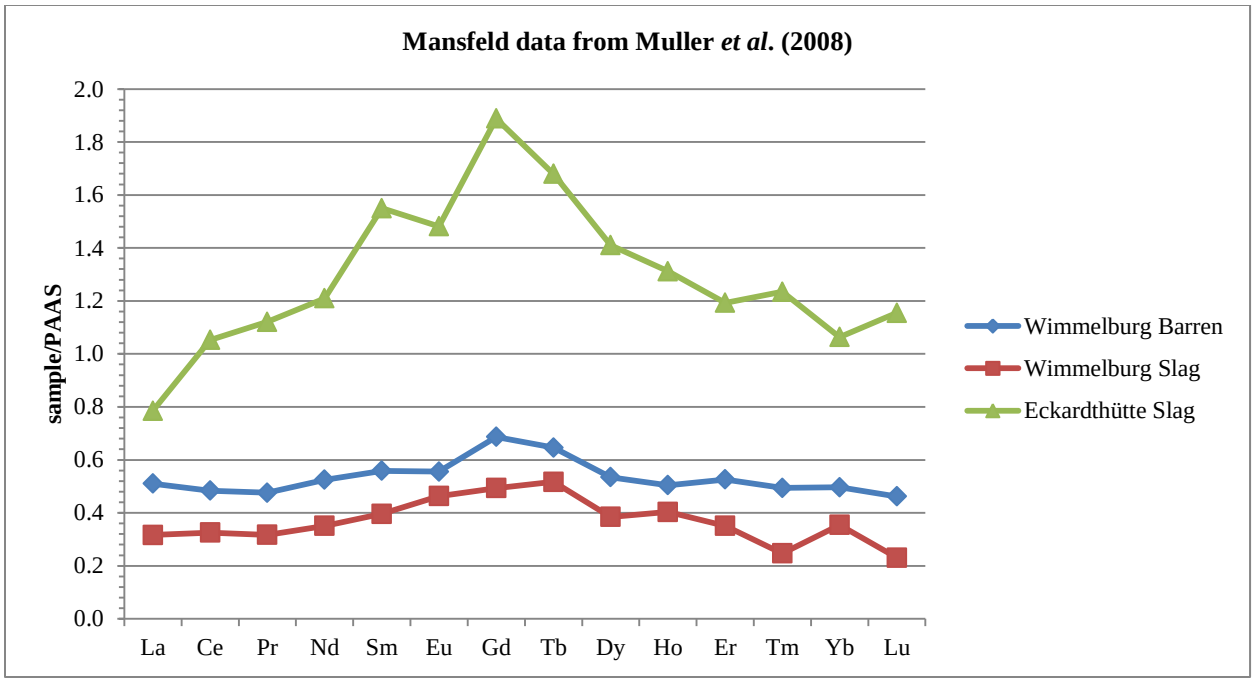


Figure 5.16: PAAS-normalized REE data from Muller *et al*. (2008). Note the slight MREE enrichments, similar to the pattern seen in the Kupferschiefer samples from this study.

### 5.7 Implications for fluid migration pathways

The migration direction of paleo-fluids, as indicated by the strata-form nature of the Kupferschiefer deposits, was mostly bedding-parallel on a large scale. The orientation of sulfide mineralization, carbonate veins, and quartz veins indicate that localized fluid flow was probably mostly bedding-parallel in nature as well, though some cross-stratal flow was also present. It is also possible that these small-scale features are simply the result of available pore space within the Kupferschiefer, which opened up between the alternating lenses of carbonaceous and carbonate material. Bedding-parallel horizons of mineralization could also be explained by the presence of syndepositional features, such as organic-rich laminations, that promoted precipitation of sulfide minerals. Veins were not the sole means of fluid flow, as illustrated by the presence of macro- and microscopic mineralization present in samples that do not exhibit quartz or carbonate veins.

The prevalence of bedding-parallel veins and aggregates in the lower section of the Kupferschiefer, and the increase in abundance of bedding-perpendicular mineralization more than 30 cm above the basal contact, suggests there was a change in preferential fluid flow. The alternating lenses

common in the lower, carbon-rich half of the Kupferschiefer may have impeded bedding-perpendicular flow compared to bedding-parallel flow because of their largely horizontal alignment. The absence of these lenses higher in the section may have removed the obstruction to bedding-perpendicular flow, allowing for a change in preferential flow direction. Alternatively, the upward increase in carbonate and decrease in clay may have made the host rock more brittle and thus prone to forming fractures perpendicular to the bedding.

Weissliegend samples may also show evidence for preferential horizontal fluid flow, in the form of laminations of lighter sand grains or dark sulfides. Alternatively, these laminations may reflect depositional layering that controlled the later precipitation of sulfides. The sorting and composition of the Weissliegend samples also have important implications for fluid flow. The predominantly well sorted nature of the Lubin mining district Weissliegend samples could have resulted in relatively greater permeability compared to the poorly sorted Sangerhausen samples. This in turn could have resulted in greater volumes of fluid flow through the Lubin mining district Weissliegend, and thus greater amounts of sulfide mineralization.

### 5.8 Implications for multiple fluid flow events

At least 2 periods of sulfide mineralization can be discerned in samples from the Lubin and Rudna mines. The evidence is present in the form of the two edges of sulfide mineralization in the carbonate vein 30 cm above the contact in Lubin 2, and in the disrupted fabric 35 cm above the contact in Rudna 2, where there is disruption of horizontal macro-mineralization as well as the presence of micro-mineralization in mud chip cracks.

There is no clear evidence for more than one pulse of mineralizing fluid flow in the Sangerhausen samples, though this does not necessarily rule out multiple pulses. There were at least two pulses of hydrocarbon migration, however, as illustrated by the presence of blue and yellow fluorescence in some of the Sangerhausen samples.

The process of mineralization would have also affected fluid flow through time. As sulfides were precipitated, pore space would have decreased, resulting in a decrease in permeability and thus the volume of fluid that would be able to infiltrate the unit during the next pulse of fluid flow.

Table 5.1: Summary of petrographic, mineralogical, and geochemical differences between the Sangerhausen Basin and Lubin mining district.

| Features | Sangerhausen Basin | Lubin Mining District |
|---|---|---|
| **Petrography** | | |
| Carbonate veins/ Quartz veins | <1 | >1 |
| Veins "disseminated" in character | more common | less common |
| Coarse lenses of quartz/carbonate | no | yes, may be mineralized |
| Kupferschiefer: detrital quartz | less | more |
| Boundary Dolomite | no | yes |
| Weissliegend: grain size | variable (fine sand to conglomerate) | fine sand (in samples studied) |
| Weissliegend: porosity | more abundant closer to contact | more abundant further from contact |
| Weissliegend: grain roundness | mostly sub-round to sub-angular | mostly round to sub-round |
| Weissliegend:sorting | mostly moderate to poor | very well to moderate |
| Weissliegend: volcanic clasts | more common | less common |
| Fluorescence | more | less |
| **Mineralization** | | |
| Mineralization associated with carbonate/quartz veins | very rare | common |
| Zoned mineralized blebs | less common | more common |
| Mineral replacement sequence | shorter | longer |
| Sulfides | less | more |
| Mineralization: bedding-parallel horizons | more | less |
| Mineralization: macro-aggregates | more common | less common |
| Weissliegend: sulfide banding | not observed | observed |
| Bornite & digenite: Kupferschiefer | rarely observed | observed |
| Bornite & digenite: Weissliegend | less | more |
| **Geochemistry** | | |
| Cu | lower | higher |
| Ag | lower | higher |
| Pb | higher | lower (with 1 exception) |
| Zn | higher | lower |
| U | higher | lower |
| maximum MREE | higher | lower |
| greatest MREE enrichments | lower 20 cm of Kupferschiefer | within Weissliegend |
| Eu anomalies | mostly negative | mostly positive |
| Weissliegend Eu anomalies | <1.0 (with 2 exceptions) | ≥1.1 |

# CHAPTER 6 - CONCLUSIONS

## 6.1 Summary

With regards to textural, geochemical, and mineralization characteristics, the Kupferschiefer unit is broadly similar in the Sangerhausen Basin and Lubin mining district locations, with a few distinct and intriguing differences.

- Both basins exhibit sulfide mineralization in the form of disseminated spherules, blebs, aggregates, framboids, and bedding-parallel and -perpendicular veins on macro- and microscopic scales.
- Chalcocite is the most abundant sulfide mineral in both locations, followed by chalcopyrite.
- Sulfide mineralization is commonly associated with the presence of quartz and carbonate veins in Lubin mining district samples; mineralization is rarely associated with these veins in Sangerhausen Basin samples.
- Both locations show similar stratigraphic geochemical trends in many, but not all, elements.
- The enrichment of $P_2O_5$ (averaging 0.26 wt.%) in the Sangerhausen Basin Kupferschiefer relative to the Lubin mining district Kupferschiefer and average shale values suggests that the enrichment could be the result of biogenic and/or syndepositional processes.
- The lower ~25 cm of the Kupferschiefer is enriched in ore metals (Cu, Ag, Pb, Zn, and U), and in the Sangerhausen Basin, in middle REEs as well.
- Geochemical patterns suggest the mineralizing reactions resulting from the interaction of fluids migrating from the underlying Weissliegend and overlying Zechstein evaporites occurred mostly within the lower 20 cm of the Kupferschiefer.
- Rare earth element enrichments in the Sangerhausen Kupferschiefer could be the result of syndepositional enrichment due to biogenic activity, or the result of the migrating fluids having carried both the REEs and the elements required for sulfide mineralization.

- Assuming that REEs were carried in migrating fluids, differences in REE patterns from Sangerhausen samples taken 7 and 8 cm above the basal contact of the Kupferschiefer suggest that, even within a single basin, the reactions did not occur at the same stratigraphic level at all locations.
- Higher Pb and Zn concentrations in Sangerhausen samples, and higher Cu concentrations in Lubin mining district samples, suggest that the Sangerhausen locations were more distal to the Rote Fäule compared to the Lubin and Rudna locations.
- Localized migration of paleo-fluids through the Kupferschiefer appears to have been preferentially, but not exclusively, bedding-parallel in the lower 20 to 30 cm of the unit, as illustrated by the orientation of mineralization features.
- The more well-sorted nature of the Lubin mining district Weissliegend likely resulted in greater permeability compared to the poorly sorted Sangerhausen Weissliegend.
- Increasing sulfide mineralization likely led to decreasing the volume of fluid able to infiltrate the units, as the process of sulfide mineralization decreased porosity, and thus permeability, of the units through time.
- It is likely that the Lubin mining district experienced at least two pulses of fluid flow, as illustrated by the presence of veins that exhibit alternating carbonate and sulfide mineralization; similar features were not observed in the Sangerhausen Basin samples.
- The presence of both yellow and blue fluorescence in Sangerhausen samples suggests there were at least two pulses of hydrocarbon migration.
- Fluorescence resulting from the presence of hydrocarbons is observed in association with sulfide mineralization in some samples; fluorescence is generally more common in samples from the Sangerhausen Basin than the Lubin mining district.
- The Boundary Dolomite is present between the Kupferschiefer and the Weissliegend in Rudna 1, Lubin 1, and Lubin 2; it is not observed in Sangerhausen samples.

- The presence of insect remains in at least two of the Sangerhausen Kupferschiefer samples suggests that the depositional environment was not exclusively shallow marine; it was likely shallower in some areas, similar to a wetland environment.

The differences in mineralization, geochemical, and textural characteristics between the Sangerhausen Basin and the Lubin mining district are likely the result of variations in basement faulting and hydrothermal activity, the number or volume of mineralizing fluid pulses, and source material for the Kupferschiefer.

### 6.2 Unresolved Questions / Further Work

Questions that remain at the conclusion of this study, to be addressed by further work, include: what is the cause of the differences in Eu anomalies observed in the Sangerhausen Basin and Lubin mining district samples? and what minerals contain the MREEs that cause the enrichment seen in some samples? It is suggested that future work includes scanning electron microscopy, to tease out more information regarding pathways for fluid migration and for the possibility of sub-microscopic petrologic indicators of paleo-fluid migration, such as dissolution cavities. The temporal relationship of cement and mineralization is another subject of interest, to better determine the influence of cement on fluid flow, or vice versa.

# REFERENCES CITED


Alyanak, N., and Vogel, T.A., 1974, Framboidal Chalcocite from White Pine, Michigan: Economic Geology, v. 69, p. 697–703.

Asael, D., Matthews, A., Oszczepalski, S., Bar-Matthews, M., and Halicz, L., 2009, Fluid speciation controls of low temperature copper isotope fractionation applied to the Kupferschiefer and Timna ore deposits: Chemical Geology, v. 262, no. 3-4, p. 147–158, doi: 10.1016/j.chemgeo.2009.01.015.

Bechtel, A., Elliott, W.C., and Oszczepalski, S., 1996, Indirect Age Determination of Kupferschiefer-Type Mineralization in the Polish Basin by K/Ar Dating of Illite: Preliminary Results: Economic Geology, v. 91, p. 1310–1319.

Bechtel, A., Ghazi, A.M., Elliott, W.C., and Oszczepalski, S., 2001, The occurrences of the rare earth elements and the platinum group elements in relation to base metal zoning in the vicinity of Rote Fäule in the Kupferschiefer of Poland: Applied Geochemistry, v. 16, no. 3, p. 375–386, doi: 10.1016/S0883-2927(00)00035-4.

Bechtel, A., Gratzer, R., Püttmann, W., and Oszczepalski, S., 2002, Geochemical characteristics across the oxic/anoxic interface (Rote Fäule front) within the Kupferschiefer of the Lubin-Sieroszowice mining district (SW Poland): Chemical Geology, v. 185, no. 1-2, p. 9–31, doi: 10.1016/S0009-2541(01)00395-3.

Bechtel, A., and Püttmann, W., 1997, Palaeoceanography of the early Zechstein Sea during Kupferschiefer deposition in the Lower Rhine Basin (Germany): A reappraisal from stable isotope and organic geochemical investigations: Palaeogeography, Palaeoclimatology, Palaeoecology, v. 136, p. 331–358.

Bechtel, A., and Püttmann, W., 1991, The origin of the Kupferschiefer-type mineralization in the Richelsdorf Hills, Germany, as deduced from stable isotope and organic geochemical studies: Chemical Geology, v. 91, p. 1–18.

Bechtel, A., Püttmann, W., and Hoernes, S., 1995, Reconstruction of the thermal history of the Kupferschiefer within the Zechstein basin of Central Europe: A stable isotope and organic geochemical approach: Ore Geology Reviews, v. 9, no. 5, p. 371–389, doi: 10.1016/0169-1368(94)00020-O.

Bechtel, A., Shieh, Y.-N., Elliott, W.C., Oszczepalski, S., and Hoernes, S., 2000, Mineralogy, crystallinity and stable isotopic composition of illitic clays within the Polish Zechstein basin: implications for the genesis of Kupferschiefer mineralization: Chemical Geology, v. 163, no. 1-4, p. 189–205, doi: 10.1016/S0009-2541(99)00112-6.

Bechtel, A., Sun, Y., Püttmann, W., Hoernes, S., and Hoefs, J., 2001, Isotopic evidence for multi-stage base metal enrichment in the Kupferschiefer from the Sangerhausen Basin, Germany: Chemical Geology, v. 176, no. 1-4, p. 31–49, doi: 10.1016/S0009-2541(00)00336-3.

Blakey, R., 2011, Paleogeography Illustrations: Colorado Plateau Geosystems, Inc,.

Blundell, D.J., Karnkowski, P.H., Alderton, D.H.M., Oszczepalski, S., and Kucha, H., 2003, Copper Mineralization of the Polish Kupferschiefer: A Proposed Basement Fault-Fracture System of Fluid Flow: Economic Geology, v. 98, p. 1487–1495.

Borg, G., Frotzscher, M., and Ehling, B., 2002, Metal content and spatial distribution of Au and PGE in the Kupferschiefer of the Mansfeld/Sangerhausen mining district, Germany, *in* Mao, J. and Bierlein, F.P. eds., Mineral Deposit Research: Meeting the Global Challenge. Proceedings of the Eighth Biennial SGA Meeting Beijing, China, 18–21 August 2005, Springer Berlin Heidelberg, Berlin, p. 885–888.

Byrne, R.H., Liu, X., and Schijf, J., 1996, The influence of phosphate coprecipitation on rare earth distributions in natural waters: Geochimica et Cosmochimica Acta, v. 60, no. 17, p. 3341–3346.

Cathles III, L.M., Oszczepalski, S., and Jowett, E.C., 1993, Mass Balance Evaluation of the Late Diagenetic Hypothesis for Kupferschiefer Cu Mineralization in the Lubin Basin of Southwestern Poland: Economic Geology, v. 88, p. 948–956.

Chang, Y.-J., and Huang, W.-L., 2008, Simulation of the fluorescence evolution of "live" oils from kerogens in a diamond anvil cell: Application to inclusion oils in terms of maturity and source: Geochimica et Cosmochimica Acta, v. 72, no. 15, p. 3771–3787, doi: 10.1016/j.gca.2008.05.041.

Dickson, J.A.D., 1965, A Modified Staining Technique for Carbonates in Thin Section: Nature, v. 205, no. 4971, p. 587, doi: 10.1038/205587a0.

Dill, H., 1984, Digenetic sulfide mineralization in the Lower Zechstein beds from N Bavaria: Neues Jahrbuch fur Mineralogie Monatshefte, v. 1984, no. 3, p. 118–124.

Elderfield, H., Whitfield, M., Burton, J.D., Bacon, M.P., and Liss, P.S., 1988, The Oceanic Chemistry of the Rare-Earth Elements [and Discussion]: Philosophical Transactions of the Royal Society A: Mathematical, Physical and Engineering Sciences, v. 325, no. 1583, p. 105–126, doi: 10.1098/rsta.1988.0046.

Flügel, E., 2004, Microfacies of Carbonate Rocks: Analysis, Interpretation and Application: Springer.

Gablina, I.F., and Lur'e, A.M., 2001, Formation and alteration of the stratiform copper deposits, *in* Piestrzyński et al. ed., Mineral Deposits at the Beginning of the 21st Century, Swets & Zeitlinger Publishers Lisse, p. 231–234.

Glennie, K.W., 1989, Some effects of the Late Permian Zechstein transgression in northwestern Europe, *in* Sediment-hosted Stratiform Copper Deposits: Geological Association of Canada, Special Paper 36, p. 557–565.

Haley, B.A., Klinkhammer, G.P., and McManus, J., 2004, Rare earth elements in pore waters of marine sediments: Geochimica et Cosmochimica Acta, v. 68, no. 6, p. 1265–1279, doi: 10.1016/j.gca.2003.09.012.

Hammer, J., Junge, F., Rösler, H.J., Niese, S., Gleisberg, B., and Stiehl, G., 1990, Element and isotope geochemical investigations of the Kupferschiefer in the vicinity of "Rote Fäule", indicating copper

mineralization (Sangerhausen basin, G.D.R.): Chemical Geology, v. 85, no. 3-4, p. 345–360, doi: 10.1016/0009-2541(90)90012-V.

Hannigan, R.E., and Sholkovitz, E.R., 2001, The development of middle rare earth element enrichments in freshwaters: weathering of phosphate minerals: Chemical Geology, v. 175, p. 495–508.

Hirst, D.M., and Dunham, K.C., 1963, Chemistry and petrography of the Marl Slate of S.E. Durham, England: Economic Geology, v. 58, p. 912–940.

Hitzman, M.W., Selley, D., and Bull, S., 2010, Formation of Sedimentary Rock-Hosted Stratiform Copper Deposits through Earth History: Economic Geology, v. 105, no. 3, p. 627–639, doi: 10.2113/gsecongeo.105.3.627.

Jasinski, A., 1994, The formation of copper-bismuth sulphosalts in sedimentary copper deposits: The Fore-Sudetic Copper Deposit, Poland as an example: Ore Geology Reviews, v. 9, no. 3, p. 209–217, doi: 10.1016/0169-1368(94)90006-X.

Jowett, E.C., 1987, Formation of Sulfide-Calcite Veinlets in the Kupferschiefer Cu-Ag Deposits in Poland by Natural Hydrofracturing During Basin Subsidence: The Journal of Geology, v. 95, no. 4, p. 513–526.

Jowett, E.C., 1986, Genesis of Kupferschiefer Cu-Ag Deposits by Convective Flow of Rotliegende Brines during Triassic Rifting Zechstein: Economic Geology, v. 81, no. 8, p. 1823–1837.

Jowett, E.C., 1992, Role of organics and methane in sulfide ore formation, exemplified by Kupferschiefer Cu-Ag deposits, Poland: Chemical Geology, v. 99, no. 1987, p. 51–63.

Jowett, E.C., Rydzewski, A., and Jowett, R.J., 1987, The Kupferschiefer Cu-Ag ore deposits in Poland: a re-appraisal of the evidence of their origin and presentation of a new genetic model: Canadian Journal of Earth Sciences, v. 24, p. 2016–2037.

Jung, W., and Knitzscheke, G., 1976, Chapter 7: Kupferschiefer in the German Democratic Republic (GDR) with special reference to the Kupferschiefer deposit in the southeastern Harz Foreland, *in* Wolf, K.H. ed., Handbook of Stratabound and Stratiform Ore Deposits; II. Regional Studies and Specific Deposits; Volume 6: Cu, Zn, Pb, and Ag Deposits, Elsevier Scientific Publishing Company, p. 353–406.

Konhauser, K., 2007, Introduction to Geomicrobiology (M. Malden, Ed.): Blackwell Publishing.

Kotarba, M.J., Peryt, T.M., Kosakowski, P., and Wieclaw, D., 2006, Organic geochemistry, depositional history and hydrocarbon generation modelling of the Upper Permian Kupferschiefer and Zechstein Limestone strata in south–west Poland: Marine and Petroleum Geology, v. 23, no. 3, p. 371–386, doi: 10.1016/j.marpetgeo.2005.10.003.

Krouse, H.R., Parafiniuk, J., Nowak, J., and Halas, S., 2006, Millimeter scale variations in the isotopic composition of vein sulphide minerals in the Kupferschiefer deposits, Lubin area, SW Poland.: Isotopes in environmental and health studies, v. 42, no. 4, p. 327–333, doi: 10.1080/10256010600990963.

Kucha, H., 1990, Geochemistry of the Kupferschiefer, Poland: Geologische Rundschau, v. 79, no. 2, p. 387–399, doi: 10.1007/BF01830634.

Kucha, H., and Pawlikowski, M., 1986, Two-brine model of the genesis of strata-bound Zechstein deposits (Kupferschiefer type), Poland: Mineralium Deposita, v. 21, p. 70–80.

Kucha, H., and Przybyłowicz, W., 1999, Noble Metals in Organic Matter and Clay-Organic Matrices, Kupferschiefer, Poland: Economic Geology, v. 94, p. 1137–1162.

Large, D.J., and Gize, A.P., 1996, Pristane/phytane ratios in the mineralized Kupferschiefer of the Fore-Sudetic Monocline, southwest Poland: Ore Geology Reviews, v. 11, no. 1-3, p. 89–103, doi: 10.1016/0169-1368(95)00017-8.

Large, D.J., MacQuaker, J., Vaughan, D.J., Sawłowicz, Z., and Gize, A.P., 1995, Evidence for Low-Temperature Alteration of Sulfides in the Kupferschiefer Copper Deposits of Southwestern Poland: Economic Geology, v. 90, p. 2143–2155.

Large, D.J., Sawłowicz, Z., and Spratt, J., 1999, A cobaltite-framboidal pyrite association from the Kupferschiefer: possible implications for trace element behaviour during the earliest stages of diagenesis: Mineralogical Magazine, v. 63, no. 3, p. 353–361.

Large, D.J., and Small, J.S., 2000, Diffusion and Reaction-Controlled Cu-Pb-Zn Ore Mineral Precipitation in a Reducing System: A Model Applied to the Pattern of Ore Mineral Precipitation in the Kupferschiefer and Other Black Shales: Economic Geology, v. 95, no. 3, p. 577–586, doi: 10.2113/95.3.577.

Legler, B., Gebhardt, U., and Schneider, J.W., 2005, Late Permian non-marine–marine transitional profiles in the central Southern Permian Basin, northern Germany: International Journal of Earth Sciences, v. 94, no. 5-6, p. 851–862, doi: 10.1007/s00531-005-0002-5.

Malinovsky, Y., and Gablina, I., 2008, Periodicity of formation of red bed copper deposits and phosphorites: International Geological Congress, Abstracts, v. 33.

Matlakowska, R., and Sklodowska, A., 2010, Uptake and degradation of copper and cobalt porphyrins by indigenous microorganisms of Kupferschiefer (Fore-Sudetic Monocline, Poland): Hydrometallurgy, v. 104, no. 3-4, p. 501–505, doi: 10.1016/j.hydromet.2010.03.030.

Mayer, W., and Piestrzyński, A., 1990, Sulphide banding in the mineralized Weissliegend sandstones from the Lubin copper district, SW Poland: Mineralogia Polonica, v. 21, no. 1-2, p. 15–22.

Michalik, M., 1997, Chlorine containing illites, copper chlorides and other chlorine bearing minerals in the Fore-Sudetic copper deposit (Poland), *in* Papunen, H. ed., Mineral Deposits: research and exploration, where do they meet?: proceedings of the 4th Biennial SGA Meeting, Turku, Finland, 11-13 August 1997, p. 543–546.

Michalik, M., and Sawłowicz, Z., 2001, Multi-stage and long-term origin of the Kupferschiefer copper deposits in Poland, *in* Piestrzyński A. et al. ed., Mineral Deposits at the Beginning of the 21st Century, Swets & Zeitlinger Publishers Lisse, p. 235–238.

Nemec, W., and Porębski, S.J., 1977a, Weissliegendes sandstones: A transition from fluvial-aeolian to shallow-marine sedimentation (Permian of the Fore-Sudetic Monocline) 1. Sedimentary structures and textural differentiation: Rocznik Polskiego Towarzystwa Geologicznego, Annales De La Société Géologique De Pologne, v. 47, no. 3, p. 387–418.

Nemec, W., and Porębski, S.J., 1977b, Weissliegendes sandstones: A transition from fluvial-aeolian to shallow-marine sedimentation (Permian of the Fore-Sudetic Monocline) 2. A study in significance of rock coloration: Rocznik Polskiego Towarzystwa Geologicznego, Annales De La Société Géologique De Pologne, v. 47, no. 4, p. 513–544.

Nowak, G.J., 2007, Comparative studies of organic matter petrography of the late palaeozoic black shales from Southwestern Poland: International Journal of Coal Geology, v. 71, no. 4, p. 568–585, doi: 10.1016/j.coal.2007.01.004.

Oszczepalski, S., 1989, Kupferschiefer in southwestern Poland; sedimentary environments, metal zoning, and ore controls, *in* Boyle, R.W., Brown, A.C., Jefferson, C.W., Jowett, E.C., and Kirkham, R.V. eds., Sediment-hosted Stratiform Copper Deposits: Geological Association of Canada, Special Paper 36, p. 571–600.

Oszczepalski, S., 1999, Origin of the Kupferschiefer polymetallic mineralization in Poland: Mineralium Deposita, v. 34, no. 5-6, p. 599–613, doi: 10.1007/s001260050222.

Oszczepalski, S., Nowak, G.J., Bechtel, A., and Zák, K., 2002, Evidence of oxidation of the Kupferschiefer in the Lubin-Sieroszowice deposit, Poland: implications for Cu-Ag and Au-Pt-Pd mineralisation: Geological Quarterly, v. 46, no. 1, p. 1–23.

Oszczepalski, S., Nowak, G.J., Bechtel, A., and Zák, K., 2001, Oxidation of the Kupferschiefer in the Lubin-Sieroszowice deposit, SW Poland: Evidence from petrographic and geochemical studies, *in* Piestrzyński, A. and Al, E. eds., Mineral Deposits at the Beginning of the 21st Century, Swets & Zeitlinger Publishers Lisse, p. 239–242.

Oszczepalski, S., and Rydzewski, A., 1987, Palaeogeography and Sedimentary Model of the Kupferschiefer in Poland, *in* Bhattacharji, S., Friedman, G.M., Neugebauer, H.J., Seilacher, A., and Peryt, T.M. eds., Lecture Notes in Earth Sciences: Vol. 10, The Zechstein Facies in Europe, Springer-Verlag Berlin Heidelberg, p. 189–205.

Pancost, R.D., Crawford, N., and Maxwell, J.R., 2002, Molecular evidence for basin-scale photic zone euxinia in the Permian Zechstein Sea: Chemical Geology, v. 188, p. 217–227.

Pašava, J., Oszczepalski, S., and Du, A., 2010, Re–Os age of non-mineralized black shale from the Kupferschiefer, Poland, and implications for metal enrichment: Mineralium Deposita, v. 45, no. 2, p. 189–199, doi: 10.1007/s00126-009-0269-8.

Passchier, C.W., and Trouw, R.A.J., 2005, Micro-tectonics: Springer.

Paul, J., 1982, Types of stratification in the Kupferschiefer, *in* Cyclic and event stratification, Springer Berlin Heidelberg, p. 476–481.

Peryt, T.M., 1989, Basal Zechstein in southwestern Poland; sedimentation, diagenesis, and gas accumulation, *in* Sediment-hosted Stratiform Copper Deposits: Geological Association of Canada, Special Paper 36, p. 601–625.

Pieczonka, J., and Piestrzyński, A., 2011, Gold and other precious metals in copper deposit, Lubin-Sieroszowice district, SW Poland: Gold in Poland, v. AM Monogra, no. 2, p. 135–152.

Poplavko, E.M., Ivanov, V.V., Serkies, Y.T., Tarkhov, Y.A., Orekhov, V.S., Bydyanskiy, D.A., Miller, A.D., Scrdobova, L.I., Bol'shakova, N.A., and Kosharovskaya, G.D., 1977, Geochemical Characteristics and Conditions of Formation of Cupriferous Sandstones and Shales: Geochemistry International, v. 14, p. 156–171.

Rasmussen, B., Buick, R., and Taylor, W.R., 1998, Removal of oceanic REE by authigenic precipitation of phosphatic minerals: Earth and Planetary Science Letters, v. 164, p. 135–149.

Rentzsch, J., 1974, The Kupferschiefer in Comparison with the Deposits of the Zambian Copperbelt, *in* Bartholome, P. ed., Gisements Stratiformes et Provinces Cupriferes, p. 395–418.

Riecker, R., 1962, Hydrocarbon fluorescence and migration of petroleum: Bulletin of the American Association of Petroleum Geologists, v. 46, no. 1, p. 60–75.

Rose, A., 1989, Mobility of copper and other heavy metals in sedimentary environments, *in* Sediment-hosted Stratiform Copper Deposits: Geological Association of Canada, Special Paper 36, p. 97–110.

Rospondek, M.J., De Leeuw, J.W., Baas, M., Van Bergen, P.F., and Leereveld, H., 1994, The role of organically bound sulphur in stratiform ore sulphide deposits: Organic Geochemistry, v. 21, no. 12, p. 1181–1191.

Rudnick, R.L., and Gao, S., 2003, Composition of the Continental Crust, *in* Treatise On Geochemistry, Elsevier Ltd., p. 1–64.

Ryka, W., 1989, Rotliegendes volcanics, sediment lithologies and paleoenvironments, and Polish basin history; an overview, *in* Sediment-hosted Stratiform Copper Deposits: Geological Association of Canada, Special Paper 36, p. 627–633.

Sawłowicz, Z., 1989, On the origin of copper mineralization in the Kupferschiefer: a sulphur isotope study: Terra Nova, v. 1, no. 4, p. 339–343.

Sawłowicz, Z., 1990, Primary copper sulphides from the Kupferschiefer, Poland: Mineralium Deposita, v. 25, p. 262–271.

Sawłowicz, Z., 2013, REE and their relevance to the development of the Kupferschiefer copper deposit in Poland: Ore Geology Reviews, v. in press, p. 11, doi: 10.1016/j.oregeorev.2013.06.006.

Sawłowicz, Z., 1991, The relationship between copper mineralization and organic matter in the Polish Kupferschiefer, *in* Pagel, M. and Leroy, J.L. eds., Source, transport and deposition of metals: proceedings of the 25 years SGA anniversary meeting, Nancy, 30 August-3 September 1991, p. 589–592.

Sawłowicz, Z., and Kosacz, R., 1995, On the origin of high-grade copper ores in the Weissliegendes elevations from the Polish Kupferschiefer deposits, *in* Pašava, Knbek, and Zak eds., Mineral deposits: from their origin to their environmental impacts: proceedings of the Third Biennial SGA Meeting, Prague, Czech Republic, 28-31 Aug, p. 977–980.

Sawłowicz, Z., and Wedepohl, K.H., 1992, The origin of rhythmic sulphide bands from the Permian sandstones (Weissliegendes) in the footwall of the Fore-Sudetic "Kupferschiefer" (Poland): Mineralium Deposita, v. 27, p. 242–248.

Schmidt Mumm, A., and Wolfgramm, M., 2004, Fluid systems and mineralization in the north German and Polish basin: Geofluids, v. 4, p. 315–328, doi: 10.1111/j.1468-8123.2004.00090.x.

Speczik, S., 1995, The Kupferschiefer mineralization of Central Europe: New aspects and major areas of future research: Ore Geology Reviews, v. 9, p. 411–426.

Sun, Y., 1998, Influences of secondary oxidation and sulfide formation on several maturity parameters in Kupferschiefer: Organic Geochemistry, v. 29, no. 5, p. 1419–1429.

Sun, Y., and Püttmann, W., 1997, Metal accumulation during and after deposition of the Kupferschiefer from the Sangerhausen Basin, Germany: Applied Geochemistry, v. 12, no. 5, p. 577–592, doi: 10.1016/S0883-2927(97)00015-2.

Sun, Y., and Püttmann, W., 2000, The role of organic matter during copper enrichment in Kupferschiefer from the Sangerhausen basin, Germany: Organic Geochemistry, v. 31, no. 11, p. 1143–1161, doi: 10.1016/S0146-6380(00)00117-0.

Sun, Y., Püttmann, W., and Speczik, S., 1995, Differences in the depositional environment of basal Zechstein in southwest Poland: implication for base metal mineralization: Organic Geochemistry, v. 23, no. 9, p. 819–835.

Sverjensky, D.A., 1989, Chemical evolution of basinal brines that formed sediment-hosted Cu-Pb-Zn deposits, *in* Sediment-hosted Stratiform Copper Deposits: Geological Association of Canada, Special Paper 36, p. 127–134.

Symons, D.T.A., Kawasaki, K., Walther, S., and Borg, G., 2011, Paleomagnetism of the Cu–Zn–Pb-bearing Kupferschiefer black shale (Upper Permian) at Sangerhausen, Germany: Mineralium Deposita, v. 46, no. 2, p. 137–152, doi: 10.1007/s00126-010-0319-2.

Tribovillard, N., Algeo, T.J., Lyons, T., and Riboulleau, A., 2006, Trace metals as paleoredox and paleoproductivity proxies: An update: Chemical Geology, v. 232, p. 12–32, doi: 10.1016/j.chemgeo.2006.02.012.

Turner, P., Vaughan, D.J., and Whitehouse, K.I., 1978, Dolomitization and the Mineralization of the Marl Slate (N.E. England): Mineralium Deposita, v. 13, p. 245–258.

Vaughan, D.J., Sweeney, M., Friedrich, G., Diedel, R., and Haranczyk, C., 1989, The Kupferschiefer: An Overview with an Appraisal of the Different Types of Mineralization: Economic Geology, v. 84, p. 1003–1027.

Wagner, T., Okrusch, M., Weyer, S., Lorenz, J., Lahaye, Y., Taubald, H., and Schmitt, R.T., 2010, The role of the Kupferschiefer in the formation of hydrothermal base metal mineralization in the Spessart ore district, Germany: insight from detailed sulfur isotope studies: Mineralium Deposita, v. 45, no. 3, p. 217–239, doi: 10.1007/s00126-009-0270-2.

Walker, T.R., 1989, Application of diagenetic alteration in redbeds to the originof copper in stratiform copper deposits, *in* Sediment-hosted Stratiform Copper Deposits: Geological Association of Canada, Special Paper 36, p. 85–96.

Walther, S., and Borg, G., 2010, Special Aspects of Kupferschiefer Mineralization in Germany Compared to Common Black Shale Mineralization, *in* GeoDarmstadt 2010, p. 586–587.

Warren, J.K., 2000, Evaporites, brines and base metals: Low- temperature ore emplacement controlled by evaporite diagenesis: Australian Journal of Earth Sciences, v. 47, no. 2, p. 179–208, doi: 10.1046/j.1440-0952.2000.00781.x.

Wedepohl, K.H., 1994, Composition and origin of the Kupferschiefer bed: Geological Quarterly, v. 38, no. 4, p. 623–638.

Wedepohl, K.H., 1965, "Kupferschiefer" and the problem of syngenetic ore deposition: Geological Society of America, Special Papers, v. 82, p. 219–220.

Wedepohl, K.H., 1980, The Geochemistry of the Kupferschiefer bed in Central Europe: Special Publication of the Society for Geology Applied to Mineral Deposits, v. 1, p. 129–135.

Wedepohl, K.H., Delevaux, M.H., and Doe, B.R., 1978, The potential source of lead in the Permian Kupferschiefer bed of Europe and some selected Paleozoic mineral deposits in the Federal Republic of Germany: Contributions to Mineralogy and Petrology, v. 65, no. 3, p. 273–281, doi: 10.1007/BF00375513.

Wedepohl, K.H., and Rentzsch, J., 2006, The composition of brines in the early diagenetic mineralization of the Permian Kupferschiefer in Germany: Contributions to Mineralogy and Petrology, v. 152, no. 3, p. 323–333, doi: 10.1007/s00410-006-0105-4.

Zhang, Z., Greenwood, P., Zhang, Q., Rao, D., and Shi, W., 2012, Laser ablation GC–MS analysis of oil-bearing fluid inclusions in petroleum reservoir rocks: Organic Geochemistry, v. 43, p. 20–25, doi: 10.1016/j.orggeochem.2011.11.005.

Ziegler, P.A., 1990, 5. Permo-Triassic Development of Pangaea, *in* Glennie, K.W., Hoorn, B. van, and Haug, G.M.W. eds., Geological Atlas of Western and Central Europe, p. 68–79.